Structure and Bonding 171
Series Editor: D.M.P. Mingos

D. Michael P. Mingos *Editor*

The Chemical Bond III

100 Years Old and Getting Stronger

Springer

171
Structure and Bonding

Aims and Scope

The series *Structure and Bonding* publishes critical reviews on topics of research concerned with chemical structure and bonding. The scope of the series spans the entire Periodic Table and addresses structure and bonding issues associated with all of the elements. It also focuses attention on new and developing areas of modern structural and theoretical chemistry such as nanostructures, molecular electronics, designed molecular solids, surfaces, metal clusters and supramolecular structures. Physical and spectroscopic techniques used to determine, examine and model structures fall within the purview of *Structure and Bonding* to the extent that the focus is on the scientific results obtained and not on specialist information concerning the techniques themselves. Issues associated with the development of bonding models and generalizations that illuminate the reactivity pathways and rates of chemical processes are also relevant.

The individual volumes in the series are thematic. The goal of each volume is to give the reader, whether at a university or in industry, a comprehensive overview of an area where new insights are emerging that are of interest to a larger scientific audience. Thus each review within the volume critically surveys one aspect of that topic and places it within the context of the volume as a whole. The most significant developments of the last 5 to 10 years should be presented using selected examples to illustrate the principles discussed. A description of the physical basis of the experimental techniques that have been used to provide the primary data may also be appropriate, if it has not been covered in detail elsewhere. The coverage need not be exhaustive in data, but should rather be conceptual, concentrating on the new principles being developed that will allow the reader, who is not a specialist in the area covered, to understand the data presented. Discussion of possible future research directions in the area is welcomed.

Review articles for the individual volumes are invited by the volume editors.

In references *Structure and Bonding* is abbreviated *Struct Bond* and is cited as a journal.

More information about this series at http://www.springer.com/series/430

D. Michael P. Mingos
Editor

The Chemical Bond III

100 Years Old and Getting Stronger

With contributions by

G. Bouhadir · D. Bourissou · C.B. Caputo · R.H. Crabtree · M.L.H. Green · N.J. Long · P.W. Miller · G. Parkin · A. Phanopoulos · D.W. Stephan

Springer

Editor
D. Michael P. Mingos
Inorganic Chemistry Laboratory
University of Oxford
Oxford, United Kingdom

ISSN 0081-5993 ISSN 1616-8550 (electronic)
Structure and Bonding
ISBN 978-3-319-35145-2 ISBN 978-3-319-35146-9 (eBook)
DOI 10.1007/978-3-319-35146-9

Library of Congress Control Number: 2016952286

Printed on acid-free paper

This Springer imprint is published by Springer Nature
The registered company is Springer International Publishing AG Switzerland

Preface

These three volumes of *Structure and Bonding* celebrate the 100th anniversary of the seminal papers by Lewis and Kossel. These papers, which formed the basis of the current view of the chemical bond, were published independently in 1916 and have greatly influenced the development of theoretical chemistry during the last century. Their essential ideas, which were initially formulated within classical Newtonian framework, have withstood many experimental tests and proved to be sufficiently flexible to incorporate the newer quantum mechanical ideas, which emerged in the 1920s and 1930s. Most importantly, Lewis' description of the covalent bond provided a graphical notation and a language for experimental chemists, which enabled generations of chemists to constructively discuss and predict the structures of molecules and graphically represent the course of chemical reactions. The Lewis and Kossel descriptions of chemical bonding are cornerstones of the undergraduate curriculum. They have achieved this pre-eminent distinction by evolving and incorporating a flexible view of chemical bonding, based on the symmetry characteristics and radial distribution functions of atomic orbitals. The development of a universally accepted notation for representing the bonds in inorganic and organic molecules has been particularly significant. Spectroscopic and structural results, which emerged as chemistry incorporated quantum mechanical concepts, provided detailed information concerning the structures of molecules not only in the solid state but also in the liquid and gas phases. These have provided increasingly rigorous tests of the bonding models, which emerged from the quantum mechanical description of the chemical bond.

The idea to celebrate this important anniversary in chemical evolution struck a chord with leading figures in the area of theoretical chemistry and resulted in the submission of 18 chapters, and it became necessary to produce three separate volumes of *Structure and Bonding* to satisfactorily account for the enormous influence Lewis and Kossel's seminal ideas had on modern chemistry. Following a historical introduction by myself, Volume 1 contains chapters by Dietar Stalke, Zhenyang Lin, Gernot Frenking, Jean-Francois Halet, Jen-Yves Saillard, José M. Goicoechea, John McGrady and Michael Hall covering a variety of

experimental and theoretical studies of topical chemical bonding issues. Examples include the implications of experimentally determined electron densities on Lewis bond structures, the Lewis description of lone pairs in transition metal complexes, dative Lewis bonds, the bonding patterns in large metal clusters and the role of carbonyl ligands in stabilising such clusters and the electronic properties of endohedral metal clusters.

Volume 2 starts with a detailed account of Lewis and Kossel's legacy in defining the bonding in ionic and covalent compounds of main group elements and addresses the thermochemical and bond length implications of the Lewis and Kossel models. The subsequent chapters by Paul Poppelier, Miroslav Kohout, Sason Shaik, Philippe Hiberty and Bernard Silvi use highly accurate theoretical calculations to address and explore the fundamental nature of the covalent bond. Discussions of quantum chemical topology, the definition of electron pairs in positional space, provide a deeper insight into the nature of the chemical bond and the relevance of the ELF topological approach to the Lewis bond model and the evolution of electron pair bonding in covalent, ionic and charge shift bonds. The Lewis description of the chemical bond was limited to single, double and triple bonds, but in recent years compounds with bond orders greater than three have become commonplace, and the final chapter by Santiago Alvarez compares the electronic characteristics of Cr–Cr quadruple and quintuple bonds.

In Volume 3, the implications of the Lewis bonding ideas for modern inorganic, organic and organometallic chemistry are discussed by Douglas Stephen, Philip Miller, Robert Crabtree, Malcolm Green, Ged Parkin, Didier Bourissou and Ghenwa Bouhadir. These fascinating articles demonstrate how non-conventional Lewis acids and bases have been used to develop new chemistry based on frustrated Lewis pairs and describe the modern coordination chemistry of triphosphine ligands and its catalytic implications. Lewis developed the concept that bases function by donating non-bonding electron pairs, but Crabtree recounts how this view has had to be modified by the discovery of complexes where π-bonds and σ-bonds act as donors. Green and Parkin extend the basic Lewis concepts to organometallic complexes with three-center two-electron bonds. Bourissou and Bouhadir describe compounds where the lone pairs on transition metals are able to function as Lewis bases – a field which has grown enormously in recent years.

This brief summary provides an indication of how the basic ideas introduced by Lewis and Kossel have blossomed over the last century as a result of the nourishment provided by quantum theory and the love and attention bestowed on them by successive generations of chemists. We hope that the quality and depth of the many contributions in these three volumes will convince the reader that the sentiment expressed in the title of this series "The Chemical Bond 100 Years Old and Getting Stronger" is appropriate.

Oxford, UK
April 2016

D. Michael P. Mingos

Contents

Struct Bond (2017) 171: 1–30
DOI: 10.1007/430_2015_177

Published online: 29 July 2015

Non-conventional Lewis Acids and Bases in Frustrated Lewis Pair Chemistry

Christopher B. Caputo and Douglas W. Stephan

Abstract The discovery of frustrated Lewis pairs (FLPs) was based on the reactions of combinations of sterically demanding phosphine donors and electrophilic boranes with dihydrogen. Since these early findings, the range of species that exhibit FLP chemistry has broadened dramatically to include a series of Lewis acids and bases. In this review, we describe a variety of such systems and the corresponding reactivity of FLPs derived from group 13–16 species.

Keywords Activation of small molecules • Catalysis • Frustrated Lewis pairs • Lewis acids • Lewis bases

Contents

Abbreviations

9-BBN Borabicyclo(3.3.1)nonane
DIBAL Diisobutylaluminium hydride

C.B. Caputo and D.W. Stephan (✉)
Department of Chemistry, University of Toronto, Toronto, ON, Canada M5S3H6
e-mail: dstephan@chem.utoronto.ca

EPR	Electron paramagnetic resonance
FLP	Frustrated Lewis pair
FRP	Frustrated radical pair
IDipp	1,3-Bis(2,6-diisopropylphenyl)imidazol-2-ylidene
Imid	1,3,4,5-Tetramethylimidazol-2-ylidene
I*t*Bu	1,3-Di-*tert*-butylimidazol-2-ylidene
MBL	α-Methylene-γ-butyrolactone
MMA	Methyl methacrylate
MMBL	γ-Methyl-α-methylene-γ-butyrolactone
NHC	*N*-Heterocyclic carbene
NMR	Nuclear magnetic resonance
OTf	Trifluoromethanesulfonate
Pin	Pinacolato
SIMes	1,3-Bis(2,4,6-trimethylphenyl)-4,5-dihydroimidazol-2-ylidene
THF	Tetrahydrofuran
TIBAL	Triisobutylaluminum
TMS	Trimethylsilyl

1 Introduction

It was nearly a century ago that Gilbert Lewis published his seminal work entitled *The Atom and the Molecule*. In it, he distinguishes between molecules that can donate a pair of electrons and molecules which can accept a pair of electrons. These classes of molecules subsequently became known as *Lewis bases and acids*, respectively (Scheme 1) [1, 2]. The reactions of Lewis acids with Lewis bases have been well documented to yield a *classical Lewis acid/base adduct* (Scheme 1). Lewis acids have found numerous applications in synthesis and catalysis, including the well-known Friedel–Crafts alkylation and acylation reactions [3, 4]. On the other hand, Lewis bases or donor molecules are exploited as ligands in transition metal catalysis [5, 6] and more recently in organocatalysis [7].

The first evidence that some Lewis acid/base combinations do not yield classical adducts came in a 1942 report [8]. In it, H.C. Brown described the absence of reactivity between 2,6-dimethylpyridine (lutidine) and BMe_3, while in contrast, lutidine and the Lewis acid BF_3 formed a classical adduct. This result was attributed to the steric conflict between the methyl substituents on the boron and those on lutidine, thus preventing adduct formation. Subsequently in 1950, Wittig and coworkers observed a ring-opening reaction of THF when bound to BPh_3 in the presence of a bulky trityl anion, instead of the anticipated solvent displacement and classical adduct formation [9]. A further report described that PPh_3 and BPh_3 do not form a classical adduct in the presence of benzyne, rather P/B addition across the C–C triple bond results in the formation of an *ortho*-disposed phosphonium borate zwitterion (**1**, Scheme 2) [10]. In related work, Tochtermann [11] in 1966 described that the reactions of trityl anion with Lewis acids (BPh_3, $AlPh_3$, $BePh_2$, and $MgPh_2$)

Scheme 1 Depiction of classic Lewis pair reactivity

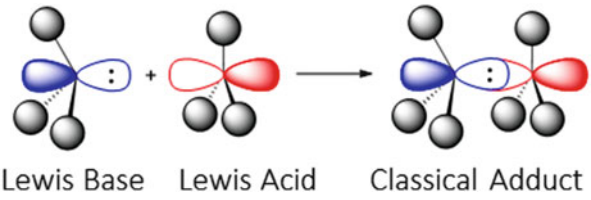

Scheme 2 Exceptions to classical Lewis acid and base reactivity

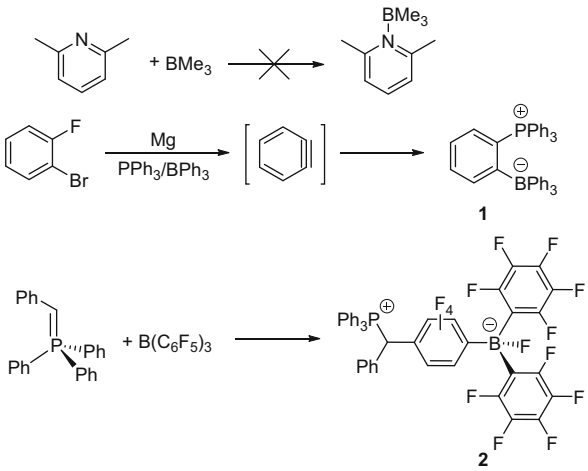

in the presence of butadiene gave similar addition of the Lewis acid and base across the olefin. This stood in contrast to the expected initiation of anionic polymerization of the diene. This result prompted Tochtermann to name these combinations "antagonistisches Paar" or antagonistic pairs. Unconventional reactivity of Lewis acid/base combinations was also observed in the 1990s when Erker and coworkers reported that the phosphorus ylide adduct of $B(C_6F_5)_3$ dissociates under thermal duress and results in Lewis base attack of the pentafluorophenyl ring in the *para*-position, yielding a linked phosphonium fluoroborate salt (**2**, Scheme 2) [12]. Similar or analogous reactivity was subsequently observed with a number of phosphine Lewis bases with $B(C_6F_5)_3$ [13] and $[Ph_3C][B(C_6F_5)_4]$ [14].

These examples of "nonclassical" behavior for combination of Lewis acids and bases were viewed as anomalies until 2006. An altered view resulted from the finding that bulky secondary phosphines react with $B(C_6F_5)_3$ yielding the product of nucleophilic aromatic substitution, $R_2PH(C_6F_4)BF(C_6F_5)_2$. Removal of the HF yields a non-interacting intramolecular phosphino-borane $R_2P(C_6F_4)B(C_6F_5)_2$ (**3**). Remarkably, these systems were found to react with H_2, heterolytically cleaving the H–H bond, resulting in the formation of a zwitterionic phosphonium hydridoborate salt $R_2PH(C_6F_4)BH(C_6F_5)_2$ (**4**) [15]. This salt liberates H_2 with heating, reforming the phosphino-borane (Scheme 3). This was the first example of reversible metal-free dihydrogen activation, and it demonstrates that unquenched Lewis acidity and basicity can be exploited for the activation of H_2. Shortly thereafter, it was found

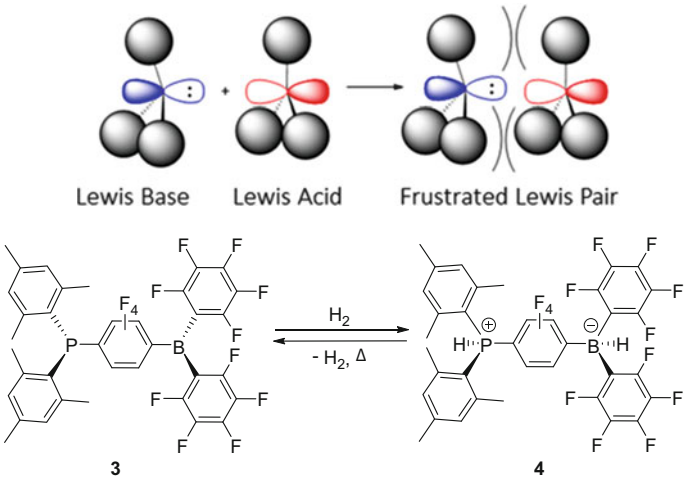

Scheme 3 Hydrogen activation with an intramolecular phosphino-borane FLP

that such reactivity was not limited to these rather esoteric intramolecular systems. Indeed simple combinations of bulky intermolecular phosphines (tBu$_3$P or Mes$_3$P) and B(C$_6$F$_5$)$_3$ do not form adducts but effects heterolytic cleavage of H_2 yielding phosphonium hydridoborate salts [16]. These findings have led to the development of these and related systems for applications in metal-free hydrogenation chemistry. Such developments have been thoroughly reviewed [17–20].

The ability to use intermolecular systems opened the door to investigations of a range of Lewis bases and acids. However, phosphines [21–23] and amines [24–28] of varying steric encumbrance have been predominately explored in FLP chemistry. In addition, variations of the Lewis acid component have drawn lesser attention as the majority of FLP systems studied to date have exploited electrophilic perfluoroaryl-substituted boranes [17, 18]. Such FLP systems have led to the burgeoning range of reactivity studies of FLPs with a wide range of small-molecule substrates. In pushing the boundaries of FLP chemistry, our group and others have begun to investigate alternative Lewis acids and bases targeting systems that could offer ready access, greater stability, as well as novel reactivity. This chapter will discuss the recent advances in developing alternative Lewis acids and bases in FLP chemistry.

2 Alternative Lewis Acids and Bases: Boron

Cationic, three-coordinate boron species are known as borenium cations, and these have recently been shown to be effective Lewis acids in FLP chemistry. The cationic charge generates increased Lewis acidity without the prerequisite of strongly electron-withdrawing substituents on the boron atom. This allows for a highly modular synthesis to access a variety of unique borenium cations [29].

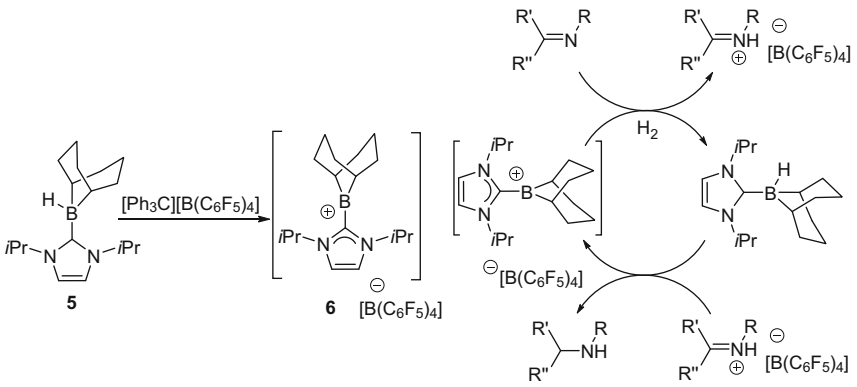

Scheme 4 H_2 activation with borenium Lewis acids

Our initial report described the synthesis of the I*i*Pr$_2$-stabilized borenium cations, derived from the NHC adduct of 9-BBN (**5**). This classical Lewis acid/base adduct can be converted to a potent borenium Lewis acid by hydride abstraction with $[Ph_3C][B(C_6F_5)_4]$ (**6**, Scheme 4). Compound (**6**) in the presence of a Lewis base (e.g., *t*Bu$_3$P) generates an FLP which can activate H_2 under ambient conditions. This finding prompted studies as a hydrogenation catalyst. Indeed (**6**) is a competent catalyst at loadings of 1–5 mol% for the hydrogenation of imines, enamines, and to a lesser extent *N*-heterocycles. In contrast to $B(C_6F_5)_3$, (**6**) exhibited greater functional group tolerance. Mechanistically this hydrogenation is believed to occur in a similar fashion to that previously reported for FLP hydrogenations of imines [30, 31]. Thus, initial H_2 activation occurs between the Lewis acid and the imine Lewis base, generating an iminium $[B(C_6F_5)_4]$ salt. Subsequent hydride transfer from the NHC–borane adduct results in amine formation and borenium cation regeneration (Scheme 4, right).

As mentioned earlier, the syntheses of these borenium cations are quite modular allowing the study of the impact of the steric and electronic attributes on reactivity and optimization for catalytic activity [32]. After a screening process of a number of variants, it was found that sterically unencumbered NHCs bearing electron-withdrawing substituents in the backbone proved to provide the most active hydrogenation catalysts. In contrast, replacement of the 9-BBN moiety with $HB(C_6F_5)_2$ as in (I*t*Bu)$HB(C_6F_5)_2$ (**7**, Scheme 5) precluded hydride abstraction with reagents such as $[Ph_3C][B(C_6F_5)_4]$, TMSOTf, and HOTf, and thus the corresponding borenium cation was not accessible. However, reaction with $HNTf_2$ at 100°C for 4 days seemed to generate the anticipated borenium cation transiently; however, subsequent C–H activation of a *t*Bu substituent occurred, resulting in the observed product $(CHN)_2(tBu)(CMe_2CH_2)CB(C_6F_5)_2$ (**8**, Scheme 5).

Shortly after our reports, Crudden and coworkers reported the synthesis of mesoionic carbene-stabilized borenium cations [33]. It was reasoned that a triazole-derived mesoionic carbene coordinated to a borane yields a more hydridic B–H fragment than the related NHC derivatives [34] and thus a more effective

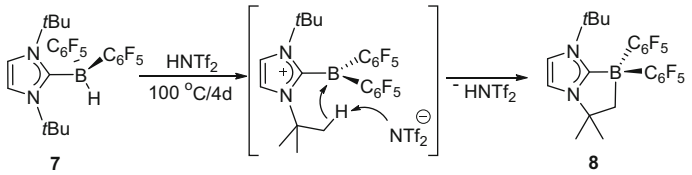

Scheme 5 C–H activation by a borenium Lewis acid

hydrogenation catalyst. Synthesis of these triazolium mesoionic carbenes was achieved through a simple Huisgen cycloaddition [35] of an alkyne to an azide, affording access to a variety of highly effective borenium hydrogenation catalysts for the reduction of imines under 1 atm of H_2. In addition, these triazolium-based borenium cations effectively hydrogenated a number of *N*-heterocycles.

Borenium cation-derived FLPs have also found applications in electrochemistry. The electrochemical oxidation of H_2 to $2H^+$ and $2e^-$ requires a large oxidative voltage, and therefore electrocatalysts are required. Typically these are Pt or Pt-group metals; however, Ashley, Wildgoose, and coworkers have utilized borenium-based FLPs as alternate catalysts (Scheme 6) [36]. The authors show that using a borenium cation instead of $B(C_6F_5)_3$ as the Lewis acid decreases the voltage required to oxidize H_2 by nearly one volt. Furthermore, they note that the borenium Lewis acids are more resistant to proteolytic side reactions.

Piers and coworkers have developed a pentaarylborole (**9**) which has shown exceptional Lewis acidity [37]. The extreme Lewis acidity was attributed to the electron-withdrawing pentafluorophenyl substituents and the antiaromaticity of the 4-electron π-system found in the borole ring. This compound rapidly activates H_2, without the addition of a Lewis base, resulting in the formation of *cis* (**10a**) and *trans* (**10b**) isomers of a boracyclopent-3-ene product, where two hydrogen atoms are installed on the carbons alpha to boron (Scheme 7, top) [38]. This reactivity implies that a boron-H_2 complex must be initially generated. This notion was further supported by recent work in which Piers and coworkers isolated a related borole that was shown to form an isolable adduct with Et_3SiH, resulting in a complex which is thought to be analogous to the proposed H_2 adduct (Scheme 7, bottom) [39].

Wang and coworkers [40] have developed a unique boryl/borate system which acts as a Lewis base and can promote FLP chemistry with $B(C_6F_5)_3$. Reaction of B_2Pin_2 with PhLi results in the formation of a phenyl-substituted boryl–borate salt Li[pinBB(Ph)pin] (**11**). This compound does not show any interaction with $B(C_6F_5)_3$ in solution; however, exposure to an atmosphere of H_2 results in FLP activation of H_2, yielding a mixture of the products Li[$HB(C_6F_5)_3$] (**12**), PhBPin (**13**), and B_2Pin_2. The formation of B_2Pin_2 was unexpected; however, under these reaction conditions, the authors report that the expected product HBPin undergoes dehydrocoupling reaction. This FLP combination was also shown to react with ethylene, resulting in the formation of the lithium (2-boroethyl)borate addition product (**14**, Scheme 8). Computational mechanistic studies indicated that the

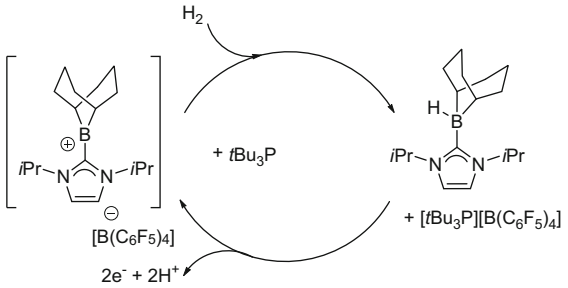

Scheme 6 Electrochemical H_2 oxidation cycle using borenium-based FLPs

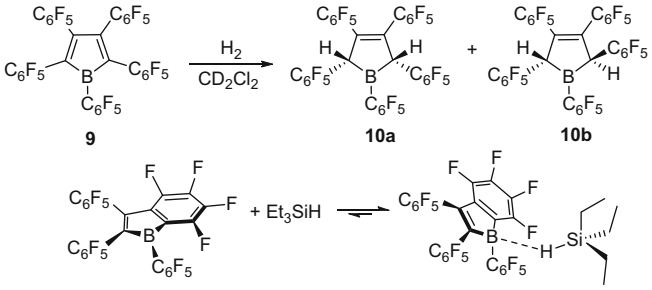

Scheme 7 H_2 activation with perfluorinated pentaphenylborole and 1,2,3-tris(pentafluorophenyl)-4,5,6,7-tetrafluoro-1-boraindene

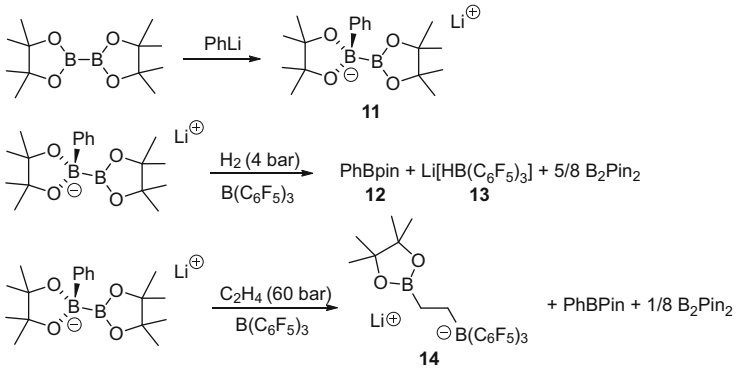

Scheme 8 Using a boryl Lewis base in FLP chemistry

mechanisms for H_2 and ethylene activation differ. The authors specify that the oxygen in pinacol functions as the Lewis base in the activation of H_2, followed by a rearrangement step. In contrast, olefin activation is believed to proceed via initial ethylene coordination to $B(C_6F_5)_3$ with cleavage of the π-bond occurring via attack from the nucleophilic boryl moiety.

3 Alternative Lewis Acids: Aluminum

The investigation of aluminum-based Lewis acids in FLP chemistry seems an obvious extension from boron. However, in some cases aluminum Lewis acids in FLP chemistry act in an analogous fashion to the boron analogues and in other it behalves drastically different. Initial reports of using aluminum Lewis acids in FLP chemistry came in 2009 and utilized the Lewis acid $Al(C_6F_5)_3$. This is a strong Lewis acid, coordinating toluene in the solid state. $Al(C_6F_5)_3$ acts as a potent Lewis acid for the activation of terminal alkynes [41, 42] prompting reaction with 1 equiv. of a bulky phosphine. The nature of the product depending on the phosphine utilized. With tBu$_3$P, deprotonation of the terminal alkyne occurred and a phosphonium alkynylaluminate [tBu$_3$PH][RCCAl$(C_6F_5)_3$] (**15**) was produced. Alternatively, using the less basic phosphine, Mes$_3$P, results in a 1,2-addition reaction across the alkyne forming the zwitterionic product Mes$_3$P(R)C=CHAl$(C_6F_5)_3$ (**16**, Scheme 9). The mechanism for these reactions is thought to occur via electrophilic attack of the Lewis acid on the alkyne (Scheme 9). This intermediate can then react with a phosphine and, depending on the basicity, result in either the deprotonation of the alkyne forming the phosphonium alkynylaluminate or nucleophilic attack resulting in the addition product.

$Al(C_6F_5)_3$ in combination with PR_3 in a 2:1 ratio also activates H_2 resulting in the product $[R_3PH][(\mu\text{-}H)(Al(C_6F_5)_3)_2]$ (**17**) [43]. Unlike the borane congener, the hydride bridges between the two Lewis acidic centers. Attempts to generate the 1:1 species or to liberate H_2 gas were unsuccessful, presumably a result of the nucleophilicity of the $[HAl(C_6F_5)_3]^-$ anion and the Lewis acidity of $Al(C_6F_5)_3$. In an attempt to hydrogenate unsaturated substrates, ethylene was added to (**17**) affording products including $[R_3PH][Al(C_6F_5)_4]$ and $EtAl(C_6F_5)_2$. These are believed to result from the disproportionation of the bridging aluminate anion to $[HAl(C_6F_5)_3]^-$ and $Al(C_6F_5)_3$, olefin coordination to the Lewis acid, and subsequent attack by the hydride generating an alkylaluminate anion which undergoes redistribution to the observed products (Scheme 10, top). This mechanism is supported by the formation of crystallographically characterized cyclohexene adduct of $Al(C_6F_5)_3$.

While the salt (**17**) was inactive for hydrogenation catalysis, aluminum Lewis acids have been applied in hydrogenation of unsaturated substrates. Both DIBAL and TIBAL have been found to hydrogenate a number of imines through a hydroalumination of the imine double bond, followed by hydrogenolysis of the resulting Al–N bond (Scheme 10, bottom) [44].

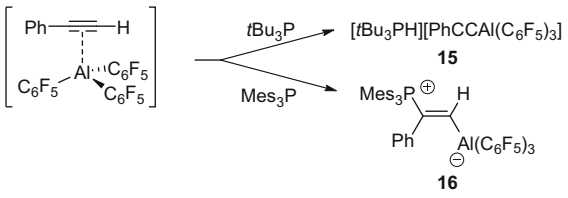

Scheme 9 Alkyne activation using $Al(C_6F_5)_3$ as a Lewis acid

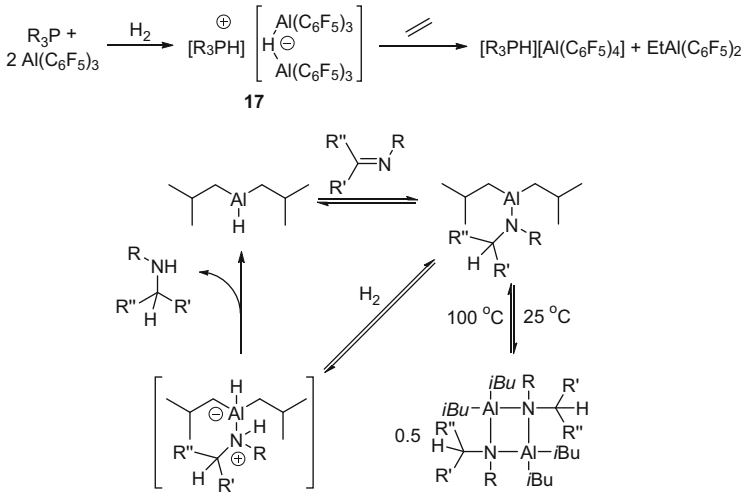

Scheme 10 Hydrogenation reactions using aluminum Lewis acids

Simple aluminum halides are sufficiently Lewis acidic to participate in FLP chemistry. Indeed, despite the fact that combinations of the Lewis base Mes_3P and the Lewis acid AlX_3 (X = Cl, Br) form an adduct at room temperature, this combination generates an FLP and which can be exploited to capture CO_2 forming the product $Mes_3P(CO_2)(AlX_3)_2$ (**18**, Scheme 11) [45]. Following isolation, these complexes were found to be remarkably robust, remaining intact even after heating to 80°C under vacuum. Nonetheless, these complexes were found to react stoichiometrically with ammonia borane resulting in the formation of Al methoxides which gave methanol on hydrolysis.

In addition, these species also provided an alternative pathway to reduction of CO_2 to CO. The analogous compound $Mes_3P(CO_2)(AlI_3)_2$ can be readily synthesized; however, when this complex is allowed to stir under an atmosphere of CO_2, new products were observed. These products were identified as the salts $[Mes_3PI][AlI_4]$ and $Mes_3P(C(OAlI_2)_2O)(AlI_3)$ (**19**) which contain a six-membered ring comprised of a CO_2 fragment linked to an $I_2AlOAlO_2$ moiety (Scheme 12) [46]. The capture of this oxide species in the Al–O–Al fragment insinuates the reduction of CO_2 to CO. Indeed CO was confirmed as a product via a number of spectroscopic methods and capture in a Ru complex. The mechanism of this reaction was studied in detail and found to involve multiple equilibria. The equilibrium governing adduct formation between Mes_3P and AlI_3 was determined to have a K_{eq} of 0.0372 at 25°C. Upon exposure to CO_2, the formation of the kinetic product (**18**) was observed. Nonetheless, equilibrium with the starting materials allow slow generation of the Lewis acid dimer which can react with CO_2 promoting CO elimination resulting in the observed thermodynamic products $[Mes_3PI][AlI_4]$ and $Mes_3P(C(OAlI_2)_2O)(AlI_3)$ (**19**) (Scheme 12) [47].

Scheme 11 CO_2 activation by aluminum halides

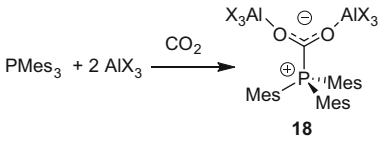

Scheme 12 CO_2 reduction to CO using a P/Al FLP system

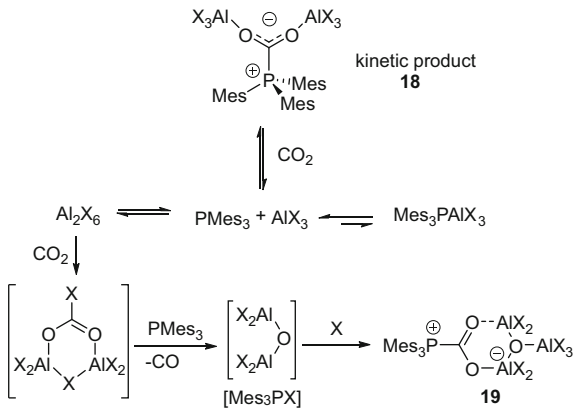

N_2O, a gas best known for its anesthetic properties, is also a potent greenhouse gas. Boron-based FLPs have been shown to readily capture it forming the product tBu$_3$PN$_2$OB(C$_6$F$_5$)$_3$ [48]. Careful control of the stoichiometry of Al(C$_6$F$_5$)$_3$ as the Lewis acid results in the analogous product tBu$_3$PN$_2$OAl(C$_6$F$_5$)$_3$ (**20**) in good yields. As expected, the O–Al bond length is significantly longer than the corresponding O–B distance in the boron analogue [49]. Interestingly, 2 equiv. of the Lewis acid affects the outcome of the reaction, resulting in C–H bond activation of the tBu substituent yielding the salt [tBu$_2$PMe(C(CH$_2$)Me][(μ-OH)(Al(C$_6$F$_5$)$_3$)$_2$] (**21**, Scheme 13). Alternatively, this product can be readily generated via the addition of Al(C$_6$F$_5$)$_3$ to **20**. The corresponding reaction using Mes$_3$P, N_2O, and 2 equiv. of alane resulted in immediate discoloration of the solution to deep purple. The multinuclear NMR analysis indicated the formation of the bridging hydroxyl anion [(μ-OH)(Al(C$_6$F$_5$)$_3$)$_2$]$^-$; however, the resonances attributed to the phosphine moiety were absent in the ^{1}H and ^{31}P NMR spectra indicating the formation of a phosphoniumyl radical cation. With subsequent EPR, UV–vis, and X-ray crystallographic studies, the product was confirmed as the radical cation salt [Mes$_3$P·][(μ-OH)(Al(C$_6$F$_5$)$_3$)$_2$]. The larger phosphine, (Nap)$_3$P, was found to undergo similar reactivity, but the isolated products were attributed to hydrogen atom abstraction from the solvent (toluene or bromobenzene) resulting in the alkylated phosphonium salts [(Nap)$_3$PC$_6$H$_4$X][(μ-OH)(Al(C$_6$F$_5$)$_3$)$_2$] (X = H, Br) (**22**, Scheme 13). This C–H activation is believed to proceed via a radical mechanism involving a transient "frustrated radical pairs (FRPs)." This result is reminiscent of the activation of NO by FLPs as described by Erker and coworkers that yield the FLP–NO radical which can also activate C–H bonds [50].

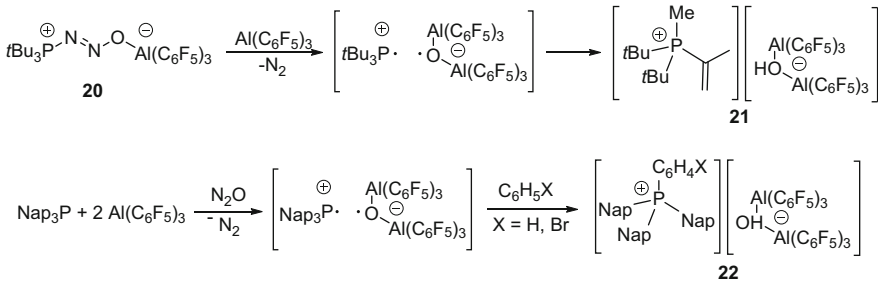

Scheme 13 Frustrated radical pair formation

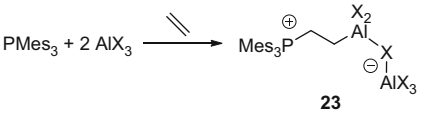

Scheme 14 Ethylene activation with a P/Al FLP

The reactivity of ethylene, propylene, and isobutylene with aluminum FLPs shows contrasting behavior to the analogous boron reactions [51–54]. The reaction of ethylene with Mes_3P and aluminum halides (AlX_3) resulted in the 1,2-addition product in which 2 equiv. of AlX_3 is incorporated to give $Mes_3PCH_2CH_2AlX_2(\mu\text{-}X)AlX_3$) **23** (Scheme 14).

In contrast, the reaction of propylene with P/Al FLPs does not give an addition product, rather ^{31}P NMR data indicated the formation of the phosphonium cation, $[Mes_3PH]^+$, while the ^{27}Al NMR spectrum is consistent with formation of the anion AlI_4^- and a product subsequently identified as $CH_2{=}CHCH_2C(Me)HCH_2AlI_2$. In the latter case, the pendant olefin is bound to the aluminum center (**24**, Scheme 15) [54]. This reaction is thought to proceed via initial deprotonation of propylene, resulting in an allyl intermediate followed by insertion of another equivalent of propylene (Scheme 15). Support for this allyl intermediate came from the analogous reaction of tBu_3P and $Al(C_6F_5)_3$ with isobutylene, where the bridging allyl intermediate, $[tBu_3PH]$ $[(C_6F_5)_3AlCH_2C(Me)CH_2Al(C_6F_5)_3]$ (**25**), was isolated and crystallographically characterized [53].

These interactions with olefins have not gone unnoticed, and other research groups have investigated the propensity of aluminum-based FLPs to act as polymerization catalysts. This field has been spearheaded by the group of Eugene Chen, who initially reported the polymerization of functionalized olefins with classical and FLP systems [55]. For example, using $Al(C_6F_5)_3$ in combination with a number of Lewis bases (tBu_3P, Ph_3P, ^{Mes}NHC, and ^{tBu}NHC) resulted in rapid polymerization of MMA, MBL, and MMBL. Mechanistic studies were undertaken using MMA as the substrate indicated that the polymerization reaction proceeds through the formation of a phosphonium enolaluminate species $(tBu)_3PCH_2C(Me){=}C(OMe)OAl(C_6F_5)_3$ (**26**, Scheme 16). Addition of monomer to this product led to

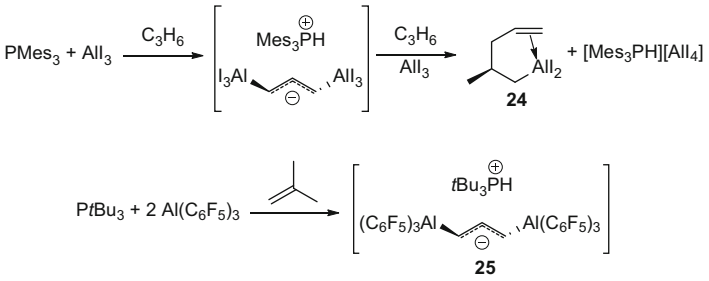

Scheme 15 Propylene activation with P/Al FLPs

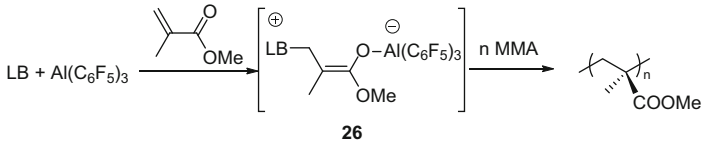

Scheme 16 Polymerization of MMA using FLPs

rapid polymerization. It is interesting that while Ph_3P forms an adduct with $Al(C_6F_5)_3$, it still behaves as an FLP effecting polymerization. Surprisingly, the FLP combination of Mes_3P and $Al(C_6F_5)_3$ is not active in polymerization catalysis. This lack of reactivity has been attributed to the poor nucleophilicity of Mes_3P, precluding formation of the active intermediate species. This reaction was shown to be highly dependent on the Lewis acid used as replacing $Al(C_6F_5)_3$ with $B(C_6F_5)_3$, $AlMe_3$, or $MeAl(2,6\text{-}tBu_2\text{-}4\text{-}Me\text{-}C_6H_2O)_2$ did not result in any detectable polymerization except in special cases [56]. This chemistry has subsequently been applied to a number of monomers, including pyridine and oxazoline vinyl derivatives [57] in addition to a number of polarized olefins. A more detailed account of this reactivity has appeared recently in *Topics in Current Chemistry* [58].

Uhl and coworkers have developed an elegant synthesis of a geminal intramolecular P/Al FLP using hydroalumination of an alkynylphosphine affording $R_2AlC(=CHPh)PMes_2$ (**27**, Scheme 17) [59]. Unlike some of the intramolecular P/B FLP systems, there does not appear to be any dative P–Al interaction in the solid state. The reaction of this FLP (**27**) with phenylacetylene at room temperature resulted in two distinct products in a 3:1 ratio, a phosphonium alkynylaluminate (**28**) formed by the deprotonation of the alkyne by the phosphine and a second product formed by the addition of the FLP across the alkyne (**29**). This reaction can be pushed to give exclusively **29** by gently heating the reaction to 70°C. This geminal FLP was also shown to activate CO_2, resulting in the formation of a 5-membered heterocycle (**30**). The addition of CO_2 was found to be reversible at 135°C, which is in contrast to the P/B intramolecular systems which rapidly lose CO_2 [60].

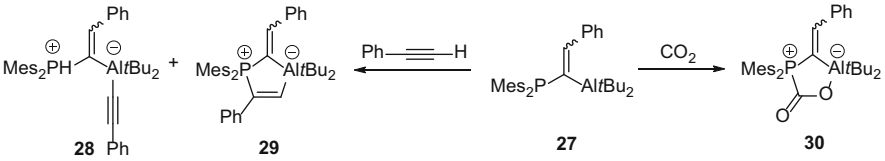

Scheme 17 Reactivity of an intramolecular P/Al FLP

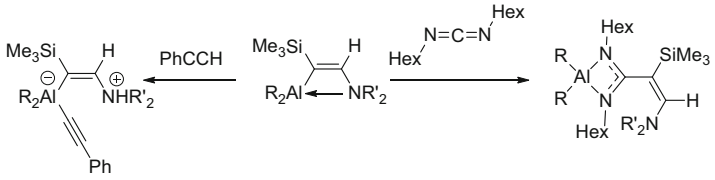

Scheme 18 Alkyne and carbodiimide activation with an Al/N FLP

This system has subsequently been found to form Lewis acid/base adducts with ammonia and borane independently. Moreover, **27** acts as a dehydrocoupling catalyst for ammonia borane [61].

Uhl and coworkers [62] have also shown that hydroalumination of dialkynylphosphine occurs to form heterocycles which bear dative P–Al bonds. Despite this dative interaction, these bonds are labile and can activate small molecules including CO_2 and isocyanates [62]. In an unprecedented result, they reported the hydroalumination of an ynamine to give a N/Al FLP system [63]. This compound was also found to contain a weak dative bond, and thus it activated alkynes and carbodiimides (Scheme 18). In addition this molecule was found to be an effective catalyst for the oligomerization of cyanamides [64].

4 Alternative Lewis Acids and Bases: Carbon

Carbon-based Lewis bases, in the form of carbenes, constitute a very important class of donor molecules [65, 66]. Shortly after the report of the initial FLP systems, Bertrand et al. discovered that (alkyl)(amino)carbenes are capable of activating H_2 and NH_3 [67]. They described this reactivity as resulting from the strong nucleophilicity and accepting capabilities of the carbene. Thus, in some sense, one can view this reactivity as that of an FLP in which the donor and acceptor sites are located on the same atom. It is important to note that the *N*-heterocyclic carbenes (NHCs) do not undergo analogous reactivity, presumably the result of the diminished acceptor capacity. In simultaneous studies, our group [68] and that of Tamm [69] investigated the reactivity of NHCs with $B(C_6F_5)_3$ in FLP chemistry. The NHC IDipp forms a strong adduct with $B(C_6F_5)_3$, but I*t*Bu did not form an adduct at low

Scheme 19 Carbene Lewis bases in FLP chemistry

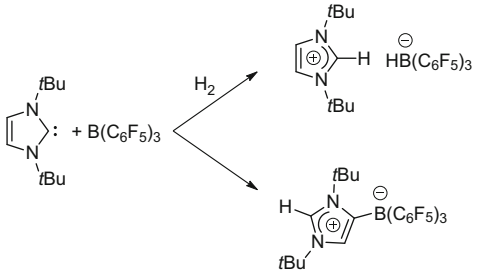

Scheme 20 Examples of carbodiphosphorane Lewis base FLP reactivity

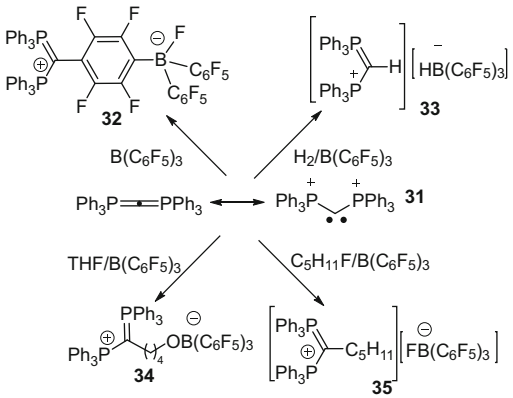

temperatures (−60°C). The latter FLP is capable of activating H_2 to give the corresponding imidazolium hydridoborate salt (Scheme 19). In the absence of H_2, this combination forms an abnormal carbene adduct with $B(C_6F_5)_3$ on warming to room temperature. Tamm et al. have further extended this chemistry to the Lewis acid $B(3,5\text{-}(CF_3)_2C_6H_3)_3$ [70].

Alcarazo and coworkers [71] investigated the use of carbon(0) compounds as Lewis bases in FLP chemistry. Using the carbodiphosphorane, Ph_3PCPPh_3 (**31**), in combination with $B(C_6F_5)_3$ at room temperature, nucleophilic aromatic substitution was observed to give the *para*-substituted zwitterionic product $(Ph_3P)CC_6F_4BF(C_6F_5)_2$ (**32**). However, this reaction is prevented if the combination is cooled to −78°C which allowed this system to act as an FLP. Indeed, this system was shown to activate H_2 affording **33**, THF to give **34**, and fluoroalkanes yielding **35** (Scheme 20). The reactivity of this FLP with esters, carbonates, phenylacetylene, and silanes was explored and described.

Transition metal centers are known to impart nucleophilic character to the β-carbon of acetylide fragments, and our group exploited this to generate a novel carbon Lewis base for FLP chemistry [72, 73]. The compound [(indenyl)Ru $(PPh_3)_2(CCPh)$] was reacted with $B(C_6F_5)_3$ at 110°C for 16 h, resulting in nucleophilic attack of the β-carbon from the acetylide fragment on a pentafluorophenyl ring, yielding the product [(indenyl)Ru$(PPh_3)_2$(=C=C(Ph)

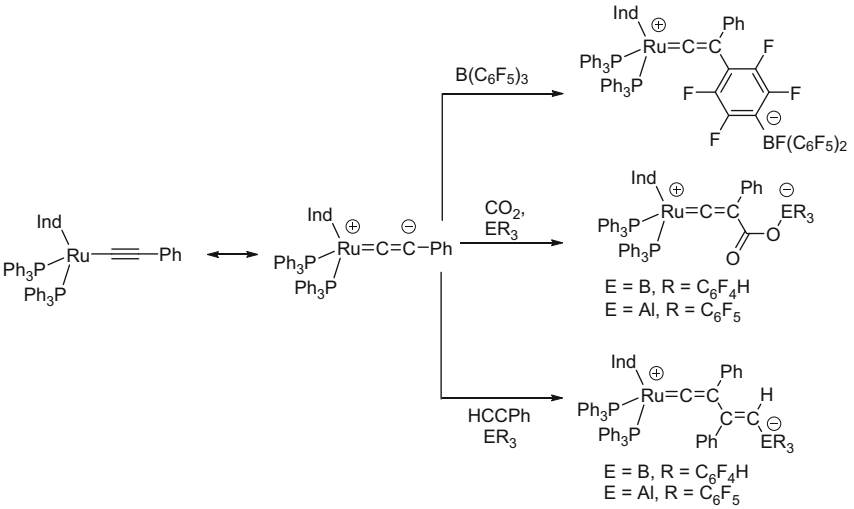

Scheme 21 Ruthenium acetylide Lewis base in FLP chemistry

$(C_6F_4)BF(C_6F_5)_2$] (Scheme 21). To frustrate this substitution, use of Lewis acids that do not undergo nucleophilic aromatic substitution reactions, such as B(*p*-$C_6F_4H)_3$ and $Al(C_6F_5)_3$, was employed. These combinations of this ruthenium acetylene with Lewis acids were shown to effectively activate CO_2 and benzaldehyde (Scheme 19). Furthermore, reactivity with phenylacetylene was observed to give 1,2 addition [(indenyl)$Ru(PPh_3)_2$(C(=CPh)(Ph)C=CH(ER_3)] (E = B(*p*-$C_6F_4H)_3$, $Al(C_6F_5)_3$).

Some group 14 compounds can also act as Lewis acids. For example, triphenylmethyl cation $[Ph_3C]^+$ which is isoelectronic with $B(C_6F_5)_3$ is an inherently strong Lewis acid due to the empty *p*-orbital at the central carbon, as well as the positive charge. Initial attempts to generate an FLP using trityl borate as a Lewis acid [14] with small Lewis bases, such as Me_3P or pyridine, resulted in the classical adducts, while sterically encumbered Lewis bases initiate nucleophilic aromatic substitution reactions on an arene ring of trityl resulting in the formation of the product $[R_3P(C_6H_4)CHPh_2][B(C_6F_5)_4]$ (Scheme 22, top). The latter result illustrates the delocalization of the positive charge on to the ring enhancing the electrophilic character of the *para*-carbons.

Nonetheless, it is possible to incorporate trityl as a Lewis acid component in FLP-derived species. For example, reaction of [*t*$Bu_3PN_2OB(p$-$C_6H_4F)_3$] with $[Ph_3C][B(C_6F_5)_4]$ resulted in the exchange of the weaker Lewis acid and affording [*t*$Bu_3PN_2OCPh_3][B(C_6F_5)_4]$ (Scheme 22, middle) [74]. More recently, Arduengo and coworkers have developed an all-carbogenic FLP by utilizing the sterically encumbered carbene (I*t*Bu) with $[Ph_3C][BF_4]$. At −60°C this combination was shown to activate H_2, generating the imidazolium tetrafluoroborate salt and triphenylmethane (Scheme 22, bottom) [75].

Alcarazo and coworkers took a unique approach developing carbon-based Lewis acids designing an allene-derived Lewis acid which can delocalize negative charge

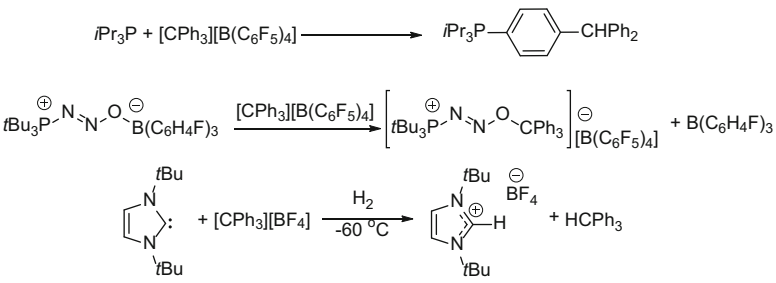

Scheme 22 Reactions using trityl cation as a Lewis acid

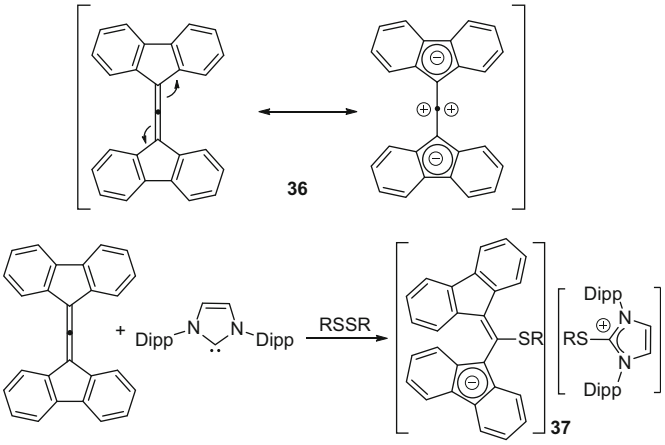

Scheme 23 All carbogenic allene/carbene FLP system

onto fluorene rings, generating an electrophilic central carbon atom (**36**, Scheme 23) [76]. The Lewis acidity of this compound was quantified using the Child's method [77] and shown to be less Lewis acidic than perfluorinated boranes, but similar to B $(OPh)_3$. This allene Lewis acid (**36**) binds sterically unencumbered NHCs. Conversely, IDipp generates an all-carbogenic FLP which activates disulfides effecting heterolytic cleave of the S–S bond to give the salt **37** (Scheme 23). Additionally, this research group also reported a number of allene derivatives that incorporate electron-withdrawing CF_3 substituents. These species also effected disulfide activation [78].

Our group has pursued a different approach to the generation of a carbon Lewis acid [79, 80]. We have exploited the electron-withdrawing power of the coordination of a metal center to an aromatic ring to increase Lewis acidity. Thus, the complex $[((Ph_2PC_6H_4)_2B(\eta^6\text{-}Ph))RuCl][B(C_6F_5)_4]$ (**38**) was prepared by the reaction of the PBP ligand with $(Ph_3P)_3RuCl_2$ with subsequent chloride abstraction. Surprisingly, the three-coordinate boron center was not the center of Lewis acidity in this species. Rather, the η^6-bound aromatic ring was shown to be susceptible to

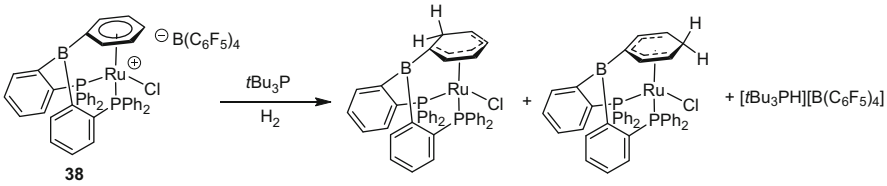

Scheme 24 H_2 activation using an η^6-bound aromatic ring as a Lewis acid

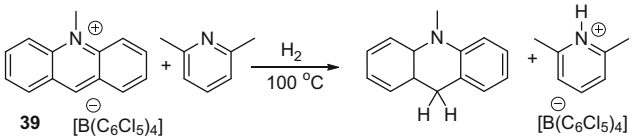

Scheme 25 H_2 activation with a methylated acridine derivative

nucleophilic attack at both the *ortho*- and *para*-positions with sterically unencumbered phosphines, such as PCy_3. Interestingly, more sterically demanding phosphines such as $PMes_3$ and $PtBu_3$ did not attack the aromatic ring, yielding instead an FLP. Such unique combinations were able to heterolytically cleave H_2 between the P Lewis base and the aromatic C Lewis acid (Scheme 24). Interestingly, the metal complex does not independently react with H_2, indicating that the H_2 activation proceed through an FLP route. This arene-based Lewis acid was also found to act as a competent hydrogenation catalyst for imines, with catalyst loadings as low as 1 mol%.

Ingleson and coworkers [81] have investigated the use of acridine derivatives as carbon-based Lewis acids. Initially, the borenium-bound acridine, [(acridine)BCl_2]$^+$, was shown to act as both a boron and carbon-based Lewis acid. Calculations indicated that the hydride ion affinity of the C9 carbon center was 14 kcal/mol more favorable than the borenium cation, inferring higher Lewis acidity at the carbon. Ingleson et al. subsequently developed a related FLP by the simple methylation of acridine (**39**). The resonance form in which the positive charge is localized on the C9 carbon generates an air- and moisture-stable, yet potent cationic Lewis acid. Heating this Lewis acid with 2,6-lutidine to 100°C for 23 h in the presence of 4 atm of H_2 yielded the products of H_2 cleavage (Scheme 25). Moreover, this Lewis acid catalytically hydrosilylates a number of imines and in addition effects the dehydrocoupling of alcohols with silanes [82].

5 Alternative Lewis Acids and Bases: Silicon

The removal of a substituent from four-coordinate silicon (usually a hydride) generates silylium cations which are some of the strongest Lewis acids known [83–87]. While such species are particularly sensitive, researchers have overcome

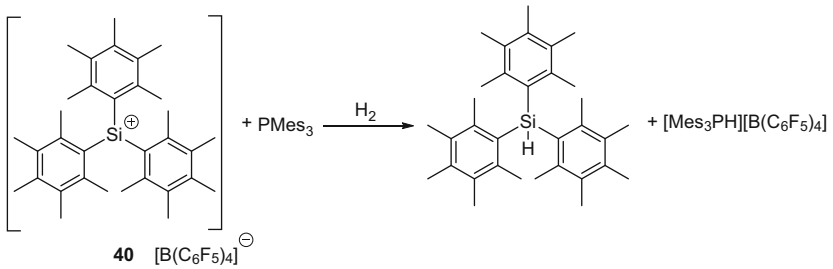

Scheme 26 H_2 activation with a permethylated silylium cation

these barriers and have begun to investigate the reactivity of silylium Lewis acids in FLP chemistry. Such work has been initiated by the group of Müller who has shown that the reaction between a permethylated-triphenylsilylium cation (**40**) and Mes_3P under an atmosphere of hydrogen results in H_2 activation, forming the silane and phosphonium borate salt (Scheme 26) [88]. These large steric demands are necessary to frustrate silylium-based adduct formation.

Subsequently, the Müller group [89] extended the scope of reactivity of this system to probe H_2 activation with a large variety of phosphines, and the use of several sterically encumbered phosphines resulted in activation of H_2, as well as the capture of CO_2. Interestingly the incorporation of extremely bulky TIPP substituents prevented such activation. In this latter case, computational insight showed that the required encounter complex for H_2 activation is not accessible as the distances between the Lewis acid and base are simply too far to promote small-molecule activation.

Silicon compounds have also been employed as bases, and thus Müller and coworkers have developed a silylene/silylium FLP which effects H_2 cleavage [90]. Neither silicon species react with H_2 independently, and indeed activation of H_2 is only observed in the presence of both moieties. Unexpectedly, the protonated silylene undergoes a rearrangement reaction, resulting in a hydrogen-bridged disilyl cation (**41**, Scheme 27). More recently, Ashley and coworkers have overcome the requirement for extremely bulky silylium cations describing that silylium–phosphine adducts can in fact activate H_2 under elevated temperatures. This indicates that even though they are strong Lewis acids, dissociation provides access to the corresponding FLP [91].

More recently, a series of N-geminal phosphorus/silicon Lewis pairs have been reported [92]. These compounds, of the form $Ph_2PN(Ar)SiCl_{3-n}Me_n$ (where Ar = 2,4,6-$Me_3C_6H_2$ or 2,6-iPr$_2$C$_6$H$_3$, $n = 0,1,2,3$), were found to react with methyl propiolate and dimethyl acetylenedicarboxylate to give zwitterionic heterocycles (Scheme 28). Interestingly, the stability of these heterocycles decreases as the number of methyl substituents on silicon increases. When $n = 3$, a ring-opening reaction occurs and the Si–N bond is cleaved in the heterocycle with simultaneous P=N bond formation (Scheme 28).

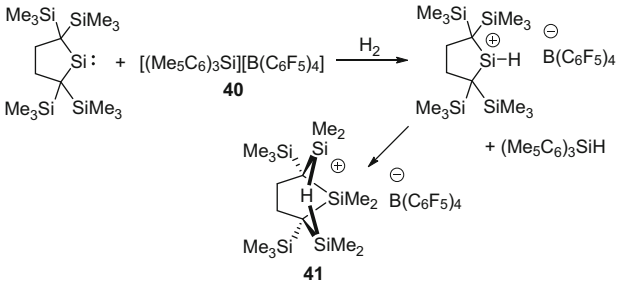

Scheme 27 H_2 activation with an all-Si FLP system

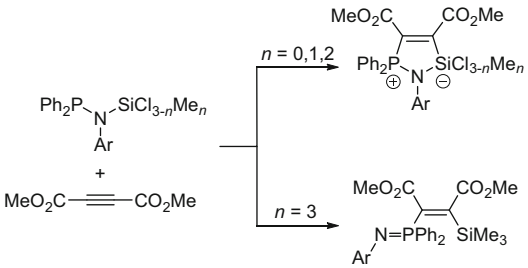

Scheme 28 N-geminal phosphorus/silicon FLP addition to alkynes

6 Alternative Lewis Acids: Phosphorus

Phosphines have a lone pair of electrons and phosphorus compounds typically act as an electron donor. However, phosphenium cations possess both a lone pair and a vacant *p*-orbital. The latter infers Lewis acidic character [93]. To the best of our knowledge, FLP chemistry with phosphenium cations has yet to be achieved. In related reactivity, however, we have recently described the reaction of the aromatic triphosphabenzene (**42**) with H_2 [94]. This compound has a resonance structure which generates a positive charge at a phosphorus atom (phosphenium cation) and negative charge on the *para*-carbon atom. This combination can act as an intramolecular FLP reacting with H_2. The resulting transient species undergoes a suprafacial hydride shift yielding the [3.1.0]bicycle reduction product **43** (Scheme 29).

Phosphonium cations are a different class of Lewis acids in that their Lewis acidity is derived from a vacant σ^* orbital. While others have utilized chelating oxygen substituents [95] and simple alkylation to generate moderately acidity [96], generally these systems are not strongly Lewis acidic as this σ^* orbital is generally too high in energy. However, we have installed electron-withdrawing substituents on phosphorus and thus lowered the energy of the σ^* orbital. To the end, our first efforts targeted intramolecular FLPs which incorporated both a phosphonium

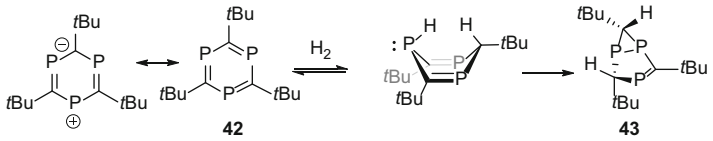

Scheme 29 H_2 activation with a triphosphabenzene derivative

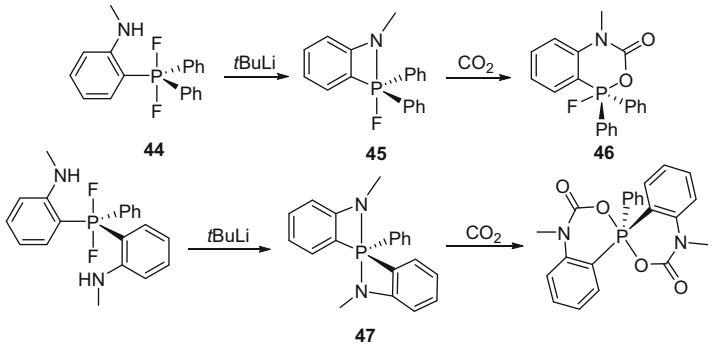

Scheme 30 CO_2 activation with amidofluorophosphoranes

Lewis acid and an amide Lewis base for the sequestration of CO_2 [97]. The phosphinoaniline, $Ph_2P(o\text{-}C_6H_4N(H)Me)$, was oxidized with XeF_2 to give the difluorophosphorane (**44**). Fluoride ion abstraction with trimethylsilyl triflate resulted in the formation of the corresponding fluorophosphonium triflate salt. While this species does not react with CO_2, deprotonation of the amine using *t*BuLi generates the amidofluorophosphorane (**45**) which does react rapidly with CO_2 to form the 6-membered carbamatofluorophosphorane (**46**). This reactivity can be extended to capture 2 equiv. of CO_2, via generation of a diamidophosphorane (**47**, Scheme 30) from the corresponding phosphine. Experimental and computational [98] studies revealed that the CO_2 is activated via an open form of the corresponding N/P FLPs. The reactivity of these systems is reminiscent of those described by Cavell where CO_2 can be inserted into P–N bonds of amidophosphoranes [99–101], although in the present systems, the reaction rates are significantly increased due to the ring strain of the 4-membered ring.

Targeting increased Lewis acidity, the compound $[Ph_2(C_6F_5)PF][FB(C_6F_5)_3]$ (**48**) was generated from the reaction of the difluorophosphorane, $Ph_2(C_6F_5)PF_2$, with $B(C_6F_5)_3$ [102]. This compound shows interesting behavior in solution as variable temperature NMR experiments indicated that an equilibrium existed between the difluorophosphorane and free borane, implying that the cation is of similar Lewis acidity to $B(C_6F_5)_3$. Compound **48** does not form adducts with phosphine Lewis bases, but rather undergoes nucleophilic aromatic substitution reactions, yielding *para*-attack products (**49**, Scheme 31). This reactivity can be

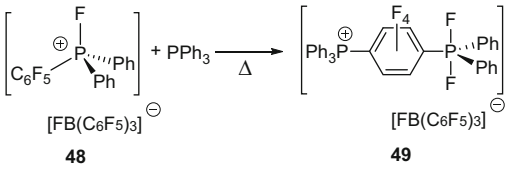

Scheme 31 Nucleophilic aromatic substitution of phosphonium Lewis acids

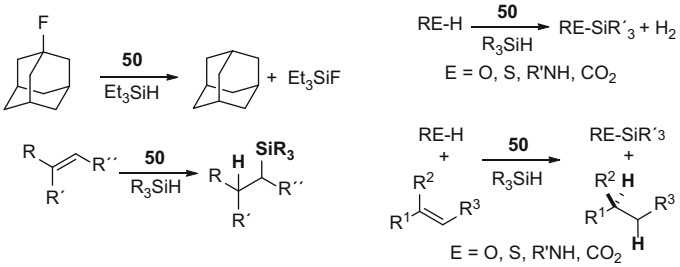

Scheme 32 Reactions catalyzed by the phosphonium Lewis acid $[(C_6F_5)_3PF][B(C_6F_5)_4]$ (**50**)

prevented by replacing the *para*-fluorine atom with a hydrogen atom [103, 104]. However, the Lewis acidity of **48** was not sufficient enough to incite small-molecule activation.

Increasing the electron-withdrawing substituents enhances the Lewis acidity. Thus, the compound $[(C_6F_5)_3PF][B(C_6F_5)_4]$ **50** was exploited for the catalytic activation of C–F bonds yielding hydrodefluorination of fluoroalkanes (Scheme 32) [105]. In addition, **50** was found to be a highly effective catalyst for the hydrosilylation of olefins, alkynes, ketones, imines, and nitriles (Scheme 32) [106, 107] as well as the dehydrocoupling of amines, alcohols, thiols, and carboxylic acids with silanes. In these latter reactions, the hydrogen generated from these reactions can also be captured in a tandem transfer hydrogenation reaction, affording simultaneous dehydrocoupling and hydrogenation of a number of 1,1 disubstituted olefins (Scheme 32) [108].

Mechanistically the hydrosilylation and dehydrocoupling reactions are thought to proceed via a mechanism analogous to the FLP mechanism involving the hydrosilylation of ketones by $B(C_6F_5)_3$ (Scheme 33) [109, 110].

The above strategy to electrophilic phosphonium cations is limited to those with electron-withdrawing substituents. One strategy to access a broader range of potential P-based Lewis acid catalysts is to generate dicationic species. To this end, the reaction of Ph_2PCl and SIMes and $[Et_3Si][B(C_6F_5)_4]$ results in a phosphonium cation $[(SIMes)PPh_2][B(C_6F_5)_4]$ (**51**). This cationic compound was then oxidized with XeF_2 yielding the cationic difluorophosphorane (**52**), while subsequent fluoride abstraction with an additional equivalent of $[Et_3Si][B(C_6F_5)_4]$ results in the formation of the dicationic phosphonium salt $[(SIMes)PFPh_2][B(C_6F_5)_4]$

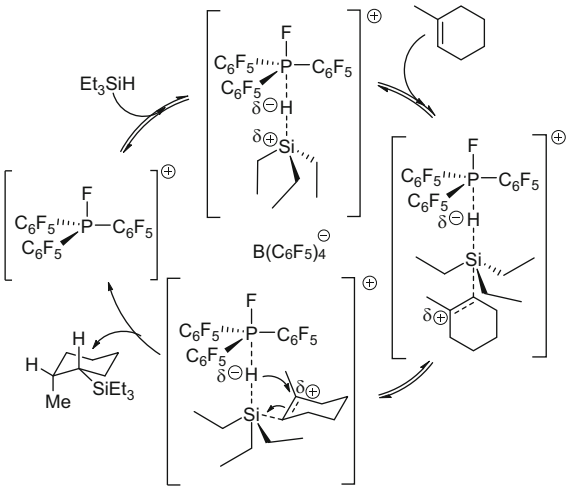

Scheme 33 Proposed mechanism for phosphonium Lewis acid-catalyzed hydrosilylation

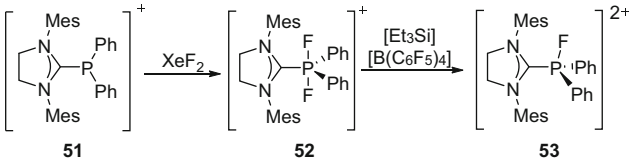

Scheme 34 Lewis acidic dicationic fluorophosphonium cations. $[B(C_6F_5)_4]^-$ omitted for clarity

(**53**, Scheme 34) [111]. This dicationic species exhibits comparable Lewis acidity to the monocationic $[(C_6F_5)_3PF]$ without the need for strongly electron-withdrawing pentafluorophenyl rings. Indeed, **53** acts as catalyst for hydrodefluorination and hydrosilylation reactions. This finding opens the door to a range of new Lewis acids as variation in both the P-substituents and the carbene is readily accessible.

A strategy involving the incorporation of proximal Lewis acid centers has been previously exploited for B-based Lewis acids [112, 113]. Applying a similar strategy to phosphonium cations was readily accomplished by the oxidation of 1,8-bis(diphenylphosphino)naphthalene by XeF_2 and fluoride abstraction to generated the bis-fluorophosphonium dicationic salt **54** (Scheme 35). This species is significantly more Lewis acidic than the analogous triphenylfluorophosphonium cation [114]. In a similar fashion, the corresponding derivative of $(Ph_2P)_2CH_2$ is also an effect Lewis acid (**55**). This strategy provides ready access to Lewis acids from readily and commercially available Lewis bases. These species are also effective catalysts for hydrosilylations of a variety of substrates and hydrodefluorination of C–F bonds.

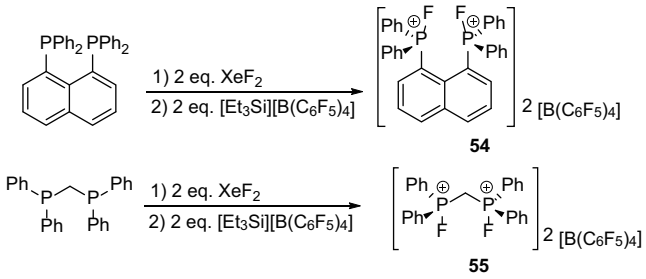

Scheme 35 Enhanced Lewis acidity using proximity of two Lewis acidic phosphonium cations

7 Alternative Lewis Bases: Group 16 Oxygen, Sulfur, and Tellurium

Oxygen donors were implicated when mechanistic studies indicated that H_2 activation between a rotaxane Lewis base and $B(C_6F_5)_3$ proceeded via activation between an O center and the borane, followed by proton transfer to the amine Lewis base (Scheme 36, top) [115]. Shortly thereafter in studying the reduction of CO with H_2 using the FLP comprised of a 1:2 mixture of tBu$_3$P and $B(C_6F_5)_3$, it was recognized that the epoxy borate salt $[t\text{Bu}_3\text{PH}][(C_6F_5)_2\text{BCH}(C_6F_5)\text{OB}(C_6F_5)_3]$ (**56**) reacts with H_2, yielding the borane/borate salt $[t\text{Bu}_3\text{PH}][(C_6F_5)\text{BCH}_2(C_6F_5)\text{OB}(C_6F_5)_3]$ (**57**, Scheme 36, bottom) [116]. This result implied H_2 activation between the boron Lewis acid and the oxygen Lewis base when the classical B–O adduct opens, allowing the two atoms to cooperatively activate H_2.

These results led to the investigation of the FLP derived from diethyl ether and $B(C_6F_5)_3$ [117]. Initially a mixture in a 2:1 ratio of Et_2O to $B(C_6F_5)_3$ appeared to have no interaction by ^{1}H NMR spectroscopy. However, cooling the reaction mixture indicated that rapid exchange was occurring between the ether molecules at the borane. The highly reversible Lewis acid base adduct was exposed to 4 atm of HD gas, and the formation of H_2 was immediately observed, indicating that this combination can act as an FLP to reversibly activate H_2. This combination was also found to be an effective catalyst for the hydrogenation of 1,1-diphenylethylene under mild conditions. This mechanism proceeded via initial H_2 activation between the oxygen and the borane, and computational analysis indicated that additional ether molecules led to stabilization of the $[Et_2OH]$ cation. This highly acidic cation could then protonate the olefin, generating a transient carbocation which is quenched by delivery of hydride from $[HB(C_6F_5)_3]^-$, yielding the alkane and regenerating the catalyst.

Attempts to catalytically reduce carbonyl functional groups with $B(C_6F_5)_3$ and H_2 in toluene at 100°C resulted in protonolysis of the B–C bond, yielding $ROB(C_6F_5)_2$ and HC_6F_5 [118, 119]. These results indicate that the protonated ketone is too acidic and leads to catalyst decomposition. However, in a simultaneous effort, our group [120] and the group of Ashley [121] realized that ethereal Lewis bases

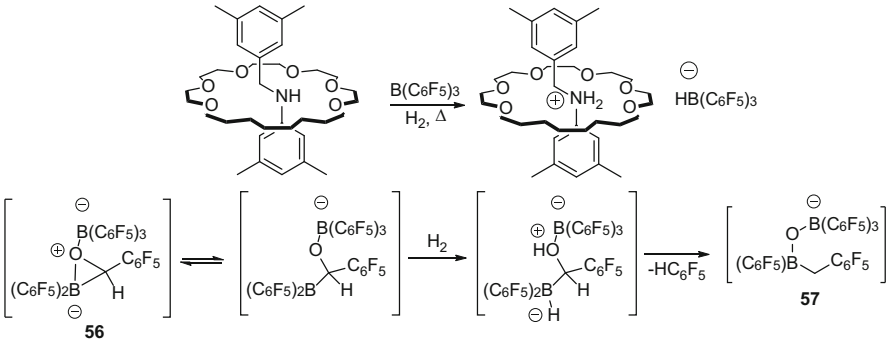

Scheme 36 H_2 activation with an epoxy borate $[t\mathrm{Bu_3PH}]^+$ was omitted for clarity

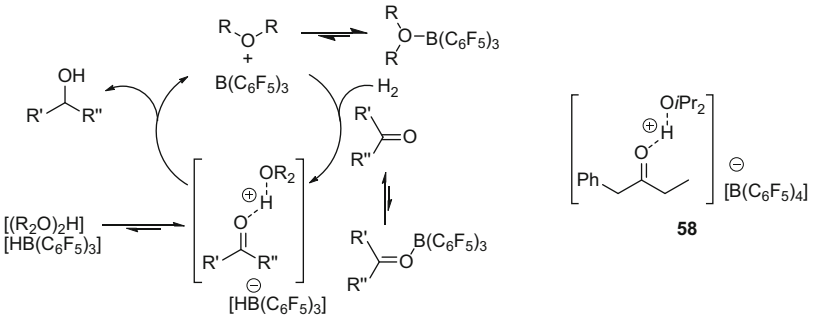

Scheme 37 Catalytic ketone hydrogenation with an ether/$B(C_6F_5)_3$ FLP

can stabilize highly acidic intermediates. Thus, we utilized diethyl ether as solvent, while Ashley's group used 1,4-dioxane. Regardless, using a catalytic amount of $B(C_6F_5)_3$ in an ethereal solvent under 4–60 atm of H_2 at slightly elevated temperatures resulted in the effective hydrogenation of a number of carbonyl functionalities. The proposed mechanism for both catalytic processes (Scheme 37, left) involves initial H_2 activation between the ethereal oxygen and the borane. The protonated ether then forms a hydrogen bonding complex with the carbonyl functionality, polarizing the C–O double bond and allowing for hydride delivery from $[HB(C_6F_5)_3]^-$. Strong evidence for this mechanism was provided when a stoichiometric amount of Jutzi's acid, $[(Et_2O)_2H][B(C_6F_5)_4]$ [122], was reacted with 1-phenyl-2-butanone and $i\mathrm{Pr_2O}$. This yielded the hydrogen bonding complex $[(i\mathrm{Pr_2O})H(OC(CH_2Ph)CH_2CH_3][B(C_6F_5)_4]$ (**58**, Scheme 37, right) which was unambiguously characterized using X-ray crystallography. This cation demonstrated the role of hydrogen bonding proposed in the mechanism.

Sulfur-based Lewis donors have found limited applications in FLP chemistry. Nonetheless, the methylene-linked thioether borane, $PhSCH_2B(C_6F_5)_2$ (**59**), was prepared [123] and shown to be to be a dimer in the solid state. It does dissociate in solution, providing an open S/B FLP. The addition of simple donors, such as $t\mathrm{Bu_3P}$

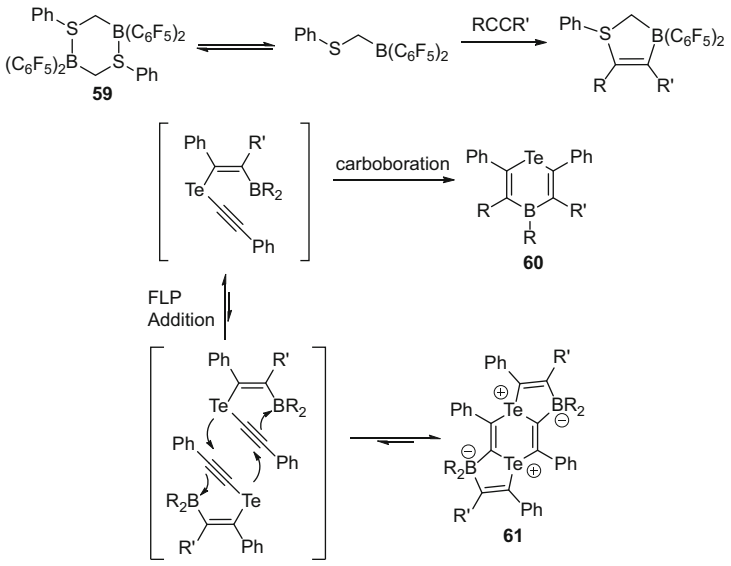

Scheme 38 S and Te Lewis bases in FLP chemistry

or Et_3PO, resulted in adduct formation with the borane. However, intramolecular FLP addition to terminal and internal alkynes was observed, yielding 5-membered S/B heterocycles (Scheme 38).

More recently our group has investigated the use of heavier group 16 congeners, in particular tellurium. The synthesis of a 6-membered Te/B heterocycle (**60**) was reported via a dialkynyltellurium species undergoing two subsequent carboboration reactions [124, 125]. Interestingly, in some cases another product derived from initial carboboration reaction followed by an FLP addition to the alkyne fragment of a second Te/B species was obtained. This was shown to be the unusual dizwitterionic species **61** (Scheme 33). This product could be isolated in several cases, but this is believed to be the kinetic product as heating in solution affords the thermodynamic bis-carboborated heterocycle **60**.

8 Conclusions and Outlook

Although studies generalizing the notion of FLP systems are in its infancy, it is clear that this concept for designing reactivity is not limited to the main group combination of electrophilic boranes and tradition P/N donors. This review has described a variety of seemingly unconventional main group combinations that give rise to a range of FLP chemistry. Such studies provide new understanding and serve to demonstrate the generality of the concept for developing new synthetic strategies, developing new reactivity and uncovering new metal-free catalysts.

Moreover, some the work described herein also suggests that the concept of FLP has a broadening field of influence. This rapid diversification of the field since 2006 makes it an area with increasing impact that undoubtedly foreshadows a future filled with new and exciting developments.

References

1. Lewis GN (1916) J Am Chem Soc 38:762–785
2. Lewis GN (1923) Valence and the structure of atoms and molecules. Chemical Catalogue , New York
3. Groves JK (1972) Chem Soc Rev 1:73–97
4. Rueping M, Nachtsheim BJ (2010) Beilstein J Org Chem 6:6
5. Tolman CA (1977) Chem Rev 77:313–348
6. Tang W, Zhang X (2003) Chem Rev 103:3029–3069
7. Denmark SE, Beutner GL (2008) Angew Chem Int Ed 47:1560–1638
8. Brown HC, Schlesinger HI, Cardon SZ (1942) J Am Chem Soc 64:325–329
9. Wittig G, Ruckert A (1950) Ann Chem Just Lieb 566:101–113
10. Wittig G, Benz E (1959) Chem Ber 92:1999–2013
11. Tochtermann W (1966) Angew Chem Int Ed 5:351–371
12. Doering S, Erker G, Fröhlich R, Meyer O, Bergander K (1998) Organometallics 17:2183–2187
13. Welch GC, Cabrera L, Chase PA, Hollink E, Masuda JD, Wei PR, Stephan DW (2007) Dalton Trans 3407–3414
14. Cabrera L, Welch GC, Masuda JD, Wei PR, Stephan DW (2006) Inorg Chim Acta 359:3066–3071
15. Welch GC, Juan RRS, Masuda JD, Stephan DW (2006) Science 314:1124–1126
16. Welch GC, Stephan DW (2007) J Am Chem Soc 129:1880–1881
17. Stephan DW, Erker G (2010) Angew Chem Int Ed 49:46–76
18. Stephan DW, Erker G (2015) Angew Chem Int Ed 54:6400–6441
19. Stephan DW, Erker G (2013) Top Curr Chem 332:85–110
20. Stephan DW, Erker G (eds) (2013) Frustrated Lewis Pairs II, expanding the scope, vol 334. Springer, Berlin
21. Greb L, Oña-Burgos P, Schirmer B, Grimme S, Stephan DW, Paradies J (2012) Angew Chem Int Ed 51:10164–10168
22. Spies P, Erker G, Kehr G, Bergander K, Fröhlich R, Grimme S, Stephan DW (2007) Chem Commun 5072–5074
23. Greb L, Tussing S, Schirmer B, Oña-Burgos P, Kaupmees K, Lõkov M, Leito I, Grimme S, Paradies J (2013) Chem Sci 4:2788–2796
24. Geier SJ, Stephan DW (2009) J Am Chem Soc 131:3476–3477
25. Sumerin V, Schulz F, Nieger M, Leskelä M, Repo T, Rieger B (2009) Angew Chem 121:10023–10027
26. Sumerin V, Schulz F, Nieger M, Leskelä M, Repo T, Rieger B (2008) Angew Chem 47:6001–6003
27. Chernichenko K, Madarász Á, Pápai I, Nieger M, Leskelä M, Repo T (2013) Nat Chem 5:718–723
28. Caputo CB, Geier SJ, Winkelhaus D, Mitzel NW, Vukotic VN, Loeb SJ, Stephan DW (2012) Dalton Trans 41:2131–2139
29. Farrell JM, Hatnean JA, Stephan DW (2012) J Am Chem Soc 134:15728–15731
30. Chase PA, Welch GC, Jurca T, Stephan DW (2007) Angew Chem Int Ed 46:8050–8053
31. Chase PA, Jurca T, Stephan DW (2008) Chem Commun 1701–1703

32. Farrell JM, Posaratnanathan RT, Stephan DW (2015) Chem Sci 6:2010–2015
33. Eisenberger P, Bestvater BP, Keske EC, Crudden CM (2015) Angew Chem Int Ed 54:2467–2471
34. de Oliveira Freitas LB, Eisenberger P, Crudden CM (2013) Organometallics 32:6635–6638
35. Huisgen R (1961) Proc Chem Soc 357–396
36. Lawrence EJ, Oganesyan VS, Hughes DL, Ashley AE, Wildgoose GG (2014) J Am Chem Soc 136:6031–6036
37. Fan C, Piers WE, Parvez M (2009) Angew Chem Int Ed 48:2955–2958
38. Fan C, Mercier LG, Piers WE, Tuononen HM, Parvez M (2010) J Am Chem Soc 132:9604–9606
39. Houghton AY, Hurmalainen J, Mansikkamäki A, Piers WE, Tuononen HM (2014) Nat Chem 983–988
40. Zheng J, Wang Y, Li ZH, Wang H (2015) Chem Commun 51:5505–5508
41. Dureen MA, Stephan DW (2009) J Am Chem Soc 131:8396–8397
42. Dureen MA, Brown CC, Stephan DW (2010) Organometallics 29:6594–6607
43. Ménard G, Stephan DW (2012) Angew Chem Int Ed 51:8272–8275
44. Hatnean JA, Thomson JW, Chase PA, Stephan DW (2014) Chem Commun 50:301–303
45. Ménard G, Stephan DW (2010) J Am Chem Soc 132:1796–1797
46. Ménard G, Stephan DW (2011) Angew Chem Int Ed 50:8396–8399
47. Ménard G, Gilbert TM, Hatnean JA, Kraft A, Krossing I, Stephan DW (2013) Organometallics 32:4416–4422
48. Otten E, Neu RC, Stephan DW (2009) J Am Chem Soc 131:9918–9919
49. Ménard G, Hatnean JA, Cowley HJ, Lough AJ, Rawson JM, Stephan DW (2013) J Am Chem Soc 135:6446–6449
50. Sajid M, Stute A, Cardenas AJP, Culotta BJ, Hepperle JAM, Warren TH, Schirmer B, Grimme S, Studer A, Daniliuc CG, Fröhlich R, Petersen JL, Kehr G, Erker G (2012) J Am Chem Soc 134:10156–10168
51. McCahill JSJ, Welch GC, Stephan DW (2009) Angew Chem 121:10023–10027
52. McCahill JSJ, Welch GC, Stephan DW (2009) Angew Chem 46:4968–4971
53. Ménard G, Stephan DW (2012) Angew Chem Int Ed 51:4409–4412
54. Ménard G, Tran L, McCahill JSJ, Lough AJ, Stephan DW (2013) Organometallics 32:6759–6763
55. Zhang YT, Miyake GM, Chen EYX (2010) Angew Chem Int Ed 49:10158–10162
56. Xu T, Chen EY (2014) J Am Chem Soc 136:1774–1777
57. He JH, Zhang YT, Chen EYX (2014) Synlett 25:1534–1538
58. Chen EX (2013) In: Erker G, Stephan DW (eds) Frustrated Lewis Pairs II, vol 334. Springer, Berlin, p 239
59. Appelt C, Westenberg H, Bertini F, Ehlers AW, Slootweg JC, Lammertsma K, Uhl W (2011) Angew Chem Int Ed 50:3925–3928
60. Mömming CM, Otten E, Kehr G, Fröhlich R, Grimme S, Stephan DW, Erker G (2009) Angew Chem Int Ed 48:6643–6646
61. Appelt C, Slootweg JC, Lammertsma K, Uhl W (2013) Angew Chem Int Ed 52:4256–4259
62. Roters S, Appelt C, Westenberg H, Hepp A, Slootweg J, Lammertsma K, Uhl W (2012) Dalton Trans 41:9033–9045
63. Holtrichter-Rossmann T, Isermann J, Rosener C, Cramer B, Daniliuc CG, Kosters J, Letzel M, Wurthwein EU, Uhl W (2013) Angew Chem Int Ed 52:7135–7138
64. Holtrichter-Rossmann T, Rosener C, Hellmann J, Uhl W, Wurthwein EU, Frohlich R, Wibbeling B (2012) Organometallics 31:3272–3283
65. Bourissou D, Guerret O, Gabbaï FP, Bertrand G (2000) Chem Rev 100:39–92
66. Hopkinson MN, Richter C, Schedler M, Glorius F (2014) Nature 510:485–496
67. Frey GD, Lavallo V, Donnadieu B, Schoeller WW, Bertrand G (2007) Science 316:439–441
68. Chase PA, Stephan DW (2008) Angew Chem Int Ed 47:7433–7437

69. Holschumacher D, Bannenberg T, Hrib CG, Jones PG, Tamm M (2008) Angew Chem Int Ed 47:7428–7432
70. Kolychev EL, Bannenberg T, Freytag M, Daniliuc CG, Jones PG, Tamm M (2012) Chem Eur J 18:16938–16946
71. Alcarazo M, Gomez C, Holle S, Goddard R (2010) Angew Chem Int Ed 49:5788–5791
72. Boone MP, Stephan DW (2011) Organometallics 30:5537–5542
73. Boone MP, Stephan DW (2014) Organometallics 33:387–393
74. Neu RC, Otten E, Lough A, Stephan DW (2011) Chem Sci 2:170–176
75. Runyon JW, Steinhof O, Dias HVR, Calabrese JC, Marshall WJ, Arduengo AJ (2011) Aust J Chem 64:1165–1172
76. Inés B, Holle S, Goddard R, Alcarazo M (2010) Angew Chem Int Ed 49:8389–8391
77. Childs RF, Mulholland DL, Nixon A (1982) Can J Chem 60:801–808
78. Palomas D, Holle S, Ines B, Bruns H, Goddard R, Alcarazo M (2012) Dalton Trans 41:9073–9082
79. Boone MP, Stephan DW (2013) J Am Chem Soc 135:8508–8511
80. Boone MP, Stephan DW (2014) Chem Eur J 20:3333–3341
81. Clark ER, Ingleson MJ (2013) Organometallics 32:6712–6717
82. Clark ER, Ingleson MJ (2014) Angew Chem Int Ed 53:11306–11309
83. Lambert JB, Zhang S, Ciro SM (1994) Organometallics 13:2430–2443
84. Lambert JB, Zhang S, Stern CL, Huffman JC (1993) Science 260:1917–1918
85. Reed CA, Xie Z, Bau R, Benesi A (1993) Science 262:402–404
86. Gusev DG, Ozerov OV (2011) Chem Eur J 17:634–640
87. Nava M, Reed CA (2011) Organometallics 30:4798–4800
88. Schafer A, Reissmann M, Schafer A, Saak W, Haase D, Muller T (2011) Angew Chem Int Ed 50:12636–12638
89. Reißmann M, Schäfer A, Jung S, Müller T (2013) Organometallics 32:6736–6744
90. Schafer A, Reissmann M, Schafer A, Schmidtmann M, Muller T (2014) Chem Eur J 20:9381–9386
91. Herrington TJ, Ward BJ, Doyle LR, McDermott J, White AJP, Hunt PA, Ashley AE (2014) Chem Commun 50:12753–12756
92. Li J, Li Y, Purushothaman I, De S, Li B, Zhu H, Parameswaran P, Ye Q, Liu W (2015) Organometallics 150420110250005
93. Burford N, Ragogna PJ (2002) Dalton Trans 4307–4315
94. Longobardi LE, Russell CA, Green M, Townsend NS, Wang K, Holmes AJ, Duckett SB, McGrady JE, Stephan DW (2014) J Am Chem Soc 136:13453–13457
95. Terada M, Kouchi M (2006) Tetrahedron 62:401–409
96. Werner T (2009) Adv Synth Catal 351:1469–1481
97. Hounjet LJ, Caputo CB, Stephan DW (2012) Angew Chem Int Ed 51:4714–4717
98. Zhu J, An K (2013) Chem Asian J 8:3147
99. Cavell RG, The KI, Griend LV (1981) Inorg Chem 20:3813–3818
100. Cavell RG, Vandegriend L (1983) Inorg Chem 22:2066–2070
101. Cavell RG, Vandegriend L (1986) Inorg Chem 25:4699–4704
102. Hounjet LJ, Caputo CB, Stephan DW (2013) Dalton Trans 42:2629–2635
103. Ullrich M, Lough AJ, Stephan DW (2009) J Am Chem Soc 131:52–53
104. Caputo CB, Winkelhaus D, Dobrovetsky R, Hounjet LJ, Stephan DW (2015) Dalton Trans 44. doi:10.1039/C1035DT00217F
105. Caputo CB, Hounjet LJ, Dobrovetsky R, Stephan DW (2013) Science 341:1374–1377
106. Perez M, Hounjet LJ, Caputo CB, Dobrovetsky R, Stephan DW (2013) J Am Chem Soc 135:18308–18310
107. Perez M, Qu ZW, Caputo CB, Podgorny V, Hounjet LJ, Hansen A, Dobrovetsky R, Grimme S, Stephan DW (2015) Chem Eur J 21:6491–6500
108. Perez M, Caputo CB, Dobrovetsky R, Stephan DW (2014) Proc Natl Acad Sci U S A 111:10917–10921

109. Parks DJ, Blackwell JM, Piers WE (2000) J Org Chem 65:3090–3098
110. Rendler S, Oestreich M (2008) Angew Chem Int Ed 47:5997–6000
111. Holthausen MH, Mehta M, Stephan DW (2014) Angew Chem Int Ed 53:6538–6541
112. Jiang C, Blacque O, Berke H (2009) Chem Commun 5518–5520
113. Piers WE, Irvine GJ, Williams VC (2000) Eur J Inorg Chem 2131–2142
114. Holthausen MH, Hiranandani RR, Stephan DW (2015) Chem Sci 6:2016–2021
115. Caputo CB, Zhu KL, Vukotic VN, Loeb SJ, Stephan DW (2013) Angew Chem Int Ed 52:960–963
116. Dobrovetsky R, Stephan DW (2013) J Am Chem Soc 135:4974–4977
117. Hounjet LJ, Bannwarth C, Garon CN, Caputo CB, Grimme S, Stephan DW (2013) Angew Chem Int Ed 52:7492–7495
118. Longobardi LE, Tang C, Stephan DW (2014) Dalton Trans 43:15723–15726
119. Lindqvist M, Sarnela N, Sumerin V, Chernichenko K, Leskelä M, Repo T (2012) Dalton Trans 41:4310–4312
120. Mahdi T, Stephan DW (2014) J Am Chem Soc 136:15809–15812
121. Scott DJ, Fuchter MJ, Ashley AE (2014) J Am Chem Soc 136:15813–15816
122. Jutzi P, Müller C, Stammler A, Stammler HG (2000) Organometallics 19:1442–1444
123. Tanur CA, Stephan DW (2011) Organometallics 30:3652–3657
124. Tsao FA, Lough AJ, Stephan DW (2015) Chem Commun 51:4287–4289
125. Tsao FA, Stephan DW (2015) Dalton Trans 44:71–74

Struct Bond (2017) 171: 31–62
DOI: 10.1007/430_2015_211

Published online: 23 February 2016

Triphosphine Ligands: Coordination Chemistry and Recent Catalytic Applications

Andreas Phanopoulos, Nicholas J. Long, and Philip W. Miller

Abstract Phosphines are a long established class of ligand that are known to form a vast array of transition metal complexes. They behave as neutral electron pair donors, or Lewis bases, that alter the solubility and stereoelectronic properties of the metal centre. A key motivation for their continued development is for homogeneous catalysis. For over five decades, transition metal–phosphine complexes have been used for catalytic reactions, mainly exploiting monodentate or bidentate phosphine ligands. Multidentate phosphines by comparison have received much less attention in part because they tend to form more stable complexes with a saturated coordination environment around the metal centre. Recent developments in the areas of catalytic reduction of carboxylic acid derivatives using molecular hydrogen and in the field of biomass up-conversion have exploited catalysts based on tridentate phosphines. This chapter highlights the use of these multidentate phosphines for synthesis of coordination complexes and discusses some of their recent applications in homogeneous catalysis.

Keywords Homogeneous catalysis · Hydrogenation · Multidentate · Phosphine · Polyphosphine · Transition metal complex · Tridentate

Contents

A. Phanopoulos, N.J. Long, and P.W. Miller (✉)
Department of Chemistry, Imperial College London, South Kensington, London SW7 2AZ, UK
e-mail: philip.miller@imperial.ac.uk

Abbreviations

acac	Acetylacetone
Ad	Adamantyl
BINAP	2,2′-bis(Diphenylphosphino)-1,1′-binaphthyl
^{t}Bu	*tert*-Butyl
^{n}Bu	*n*-Butyl
Bz	Benzyl
cod	Cyclooctadiene
DMO	Dimethyl oxalate
DOTA	1,4,7,10-Tetraazacyclododecane-1,4,7,10-tetraacetic acid
dppf	1,1′-bis(Diphenylphosphanyl) ferrocene
dppe	Ethane-1,2-diylbis(diphenylphosphane)
dpmp	bis[(Diphenylphosphino)methyl]phenylphosphine
dppm	Methylenebis(diphenylphosphane)
dppp	Propane-1,3-diylbis(diphenylphosphane)
EDTA	2-({2-[bis(Carboxymethyl)amino]ethyl}(carboxymethyl)amino) acetic acid
EG	Ethylene glycol
Et	Ethyl
etp	bis[2-(Diphenylphosphino)ethyl]phenylphosphine
fac	Facial
$HNTf_2$	bis(Triflimide)
2-MTHF	2-Methyltetrahydrofuran
LA	Levulinic acid
Me	Methyl
$MeC^{Et}P_3{}^{Ph}$	$MeC(CH_2CH_2PPh_2)_3$
mer	Meridional
MG	Methyl glycolate
MSA	Methanesulfonic acid
$N^{Et}P_3{}^{Ph}$	$N(CH_2CH_2PPh_2)_3$
o-	*ortho*-
p-	*para*-
p-TsOH	*para*-Toluenesulfonic acid
$P^{Et}P_3{}^{Ph}$	$P(CH_2CH_2PPh_2)_3$
Ph	Phenyl

1,4-PDO	1,4-Pentanediol
$R'EP_3$	$R'E(CH_2PR_2)_3$ (E = C B, P, Si, Sn, N)
Tf	Triflate
THF	Tetrahydrofuran
tmm	Trimethylenemethane
TON	Turnover numbers
$TriSulf^{Bu}$	$MeC(CH_2S^nBu)_3$
Ttp	bis[3-(Diphenylphosphino)propyl]phenylphosphine
v	Stretching frequency
Xantphos	4,5-bis(Diphenylphosphino)-9,9-dimethylxanthene
γVL	γ-Valerolactone

1 Introduction

A century ago, building on the concept of valency, Lewis introduced the idea that a covalent bond is composed of a pair of electrons that are shared equally between two atoms in a molecule. At the same time, Kossel independently introduced the concepts of ionic chemical bonding and the octet rule. These ideas on chemical bonding were further refined and extended by Langmuir who also introduced the 18-electron rule, the importance of which is understood by anyone studying transition metal coordination or organometallic chemistry. A short time later, Lewis presented his electron pair theory of acid–base reactions where the now commonly used terms 'Lewis base' for an electron pair donor and 'Lewis acid' for an electron pair acceptor originate. The description of many ligands as Lewis bases and the observation that numerous transition metal complexes follow the 18-electron rule is testament to the longevity and influence of these concepts.

Today the legacies of Lewis, Kossel and Langmuir still endure in field of coordination chemistry and are used to guide transition metal complex formation via reaction with Lewis base ligands. There are many classes of ligand that form well-defined metal–ligand bonds; some of the more common include halides, amines, imines, pyridyls, ketones, carbon monoxide, alkenes, cyclopentadienes, N-heterocyclic carbenes and phosphines. Of these ligands, tertiary phosphines (PR_3) are arguably one of the most important classes used to modify the properties of transition metals. The sheer diversity of this ligand set and their wide applicability in coordination chemistry and transition metal catalysis is unparalleled. The development of new phosphine ligands that impart greater stereoelectronic control at the metal continues apace, while the array of commercially available ligands is evidence to their industrial importance, especially for homogenous catalysis. Despite the increasing complexity of newer phosphine ligands that contain stereocentres and/or more elaborate appended R groups, the basic premise of bonding to the metal centre is the same and can be distilled into two components: a phosphine which acts as a neutral 'L-type' electron pair donor Lewis base and metal centre which is electron an pair acceptor or Lewis acid.

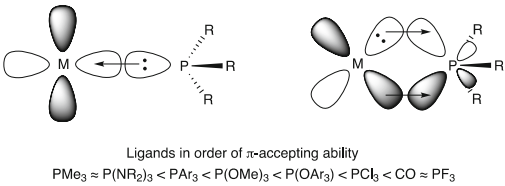

Fig. 1 The bonding motifs observed upon coordination of tertiary phosphines to metal centres

It is now well established that the formal σ-bond, formed by the lone pair on the phosphorus atom donating into an empty metal d-orbital, is also complemented by π-back donation that occurs from the metal into the σ* orbital of the P–R bond and the phosphorus dπ component (Fig. 1). The electronics of R groups bonded to the phosphorous dictate the strengths of both σ and π bonding components to the metal centre. Varying the attached R groups is one of the key ways to 'tune' the electronics of the phosphine ligand and resultant metal complexes. For example, more electronegative R groups result in a lowering in energy of the P–R σ* orbital, making it more accessible to back bonding from the metal. The PF_3 ligand with its electron-withdrawing fluorine atoms has a similar π-acceptor character to CO, while at the other end of the spectrum, PMe_3 is a relatively weak π-acceptor but is a strong σ-donor.

Phosphines have been so widely used for complex formation because their steric and electronic properties can be judiciously controlled by varying the nature of the attached R groups. These stereoelectronic parameters significantly influence the reactivity of the metal centre. The steric bulk and electron-donor ability of a ligand are however difficult to quantify and cannot be easily decoupled. For instance, as the steric bulk of the R groups in a tertiary phosphine of type PR_3 are increased, the intervalence angles around the phosphorus centre will similarly increase. These structural changes will lead to a reduction in *s*-character of the phosphorus lone pair orbital, making the ligand more Lewis basic. As the steric bulk and electronic description of phosphines are so closely interlocked, satisfactory quantification of either becomes very problematic.

The use of diphosphine ligands that contain two donor P atoms is well established and has been very successfully employed mainly in the area of homogenous catalysis and especially for C–C, C–N and C–O cross coupling and for asymmetric reactions [1]. In many cases, bidentate ligands display superior qualities to analogous monodentate species because of their ability to chelate and stabilise the metal centre. Common diphosphine ligands, such as ethane-1,2-diylbis(diphenylphosphine) (dppe), propane-1,3-diylbis(diphenylphosphine) (dppp), 1,1′-bis(diphenylphosphinyl)ferrocene (dppf), BINAP and xantphos, contain terminal disubstituted phosphine moieties that are separated by a hydrocarbon chain or other structural feature to ensure that the phosphines are able to chelate in a cis arrangement (Fig. 2). The formation of a chelate complex adds extra stability and thus reduces the ligand dissociation, which is common for monodentate phosphine ligands. The internal angle P–M–P bond of these chelate complexes is known as the 'bite angle' and has been proven to impart an extra degree of control at

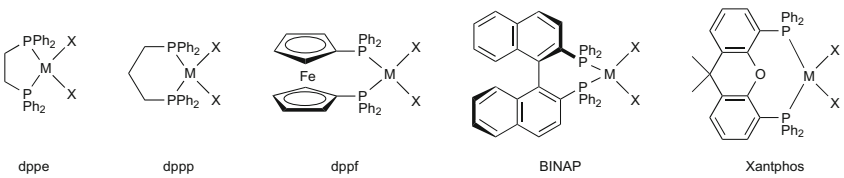

Fig. 2 Arrangement of diphosphine ligands upon metal coordination

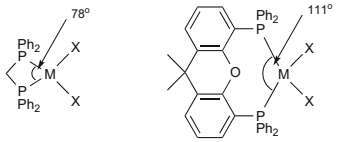

Fig. 3 Bite angles of dppm and xantphos

the metal ion that can have a profound influence on catalytic reactions in terms of rates and selectivities [1]. The bite angle of the diphosphine depends almost exclusively on the linking backbone of the ligand and can have a wide degree of variation in angle ranging from a narrow 72° for dppm to a wide 111° angle seen for xantphos (Fig. 3).

Multidentate phosphine ligands with three or more P-donor atoms have, in comparison to bidentate ligands, received less attention. Nevertheless a large number of linear and branched tridentate, tetradendtate, pentadentate and hexadentate polyphosphines have been synthesised and complexed to transition metals [2], forming a wide variety of coordination complexes. The thermodynamic stability of complexes featuring multidentate ligands enables the generation of robust complexes. These complexes can be used to stabilise unusual oxidation states at the metal centre, to form multimetallic clusters and to sequester metals that do not generally form complexes with monodentate ligands.

2 Stereoelectronic Considerations of Phosphines

One of the earliest quantifications of phosphine ligand sterics was made by Tolman who proposed using a geometrical parameter, the so-called Tolman cone angle [3, 4], as a measure of steric bulk. For phosphines of type PR_3, the cone angle is defined as the apex of a cylindrical cone, centred 2.28 Å from the centre of the phosphorus atom, which radiates out towards the R groups and just touches the van der Waals radii of the outermost atoms (Fig. 4). The value of 2.28 Å represents an intermediate length for M–P bonds. In cases where the R groups contain internal degrees of freedom, the Tolman cone is taken to be the minimum angle in which the R groups remain completely contained within it [5].

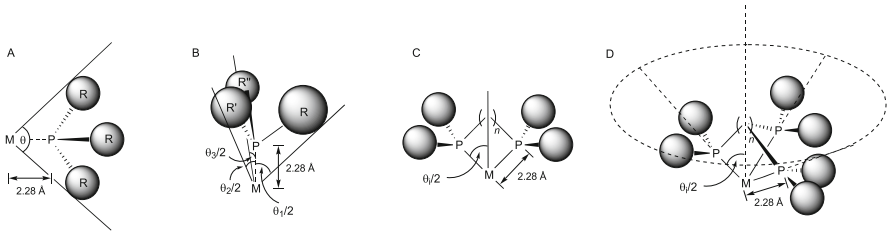

Fig. 4 Graphical representation of (**a**) the Tolman cone angle of a symmetrical monodentate phosphine ligand, (**b**) $\theta_i/2$ values of unsymmetrical monodentate phosphine ligands, (**c**) chelating diphosphine ligands and (**d**) *fac*-chelating triphosphines

Although the cone angles are found to be reliable in describing steric arrangements around symmetrical monodentate phosphine ligands [4], a similarly quantitative evaluation for more exotic ligands such as unsymmetrical phosphines or chelating multidentate phosphines is also desirable. Tolman's cone angles can be similarly applied to unsymmetrical ligands of type PRR′R″ using a model to minimise the sum of half angles shown graphically in Fig. 4b. In the case of bidentate diphosphine ligands, the angle between one M–P bond and the bisector of the P–M–P angle is used to represent the third substituent on phosphorus (Fig. 4c) [5]. Tridentate ligands that coordinate in a *fac* arrangement can also be quantified in a similar manner, using the angle between the central bisector of the cone originating from the metal that just encompasses all three phosphorus atoms instead of the P–M–P bisector used for bidentate ligands (Fig. 4d).

Analysis of X-ray crystallographic data suggests that the actual cone angle of coordinated phosphine ligands is smaller than predicted [1] as the values reported by Tolman were derived using space filling models and did not accurately predict the 'intermeshing' of R substituents [3–5]. A more accurate analysis of cone angles from real systems was undertaken by Mingos and co-workers, who analysed thousands of structures obtained from the Cambridge Crystallographic Database [6]. A general algorithm was developed that allowed the same geometrical description of Tolman's cones to be applied to crystal structures. This involved measurement of the distance, *d*, from a metal centred 2.28 Å from the phosphine, to each of the hydrogen (or halide) atoms on the first organic substituent on the phosphine, as well as the angle, α, between the phosphorus centre, metal atom and hydrogen/halide (Fig. 5).

For chelating multidentate phosphines, the length of the bridging backbone and its degree of flexibility influence the steric parameters at the metal centre by altering the bite angle. Under various coordination geometries, there exists a stable 'metal-preferred' geometry [1]; however in practice, a range of bite angles that will be thermally accessible is influenced by ligand flexibility.

To quantify the electron-donor ability of phosphine ligands, Tolman proposed that the A_1 carbonyl stretching frequency of monosubstituted nickel complexes in CH_2Cl_2 could be used as a measure [7]. The greater the electron-donor ability of the

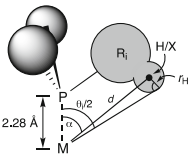

Fig. 5 Graphical definition proposed by Mingos and co-workers [6] of the van der Waals surface for phosphine ligands which results in the calculation of the Tolman cone angle directly from crystallographic data

Table 1 $^{1}J_{P,Se}$-coupling constants for various phosphorus selenides

PR_3	$^{1}J_{P,Se}$ (Hz)
P(*p*-$MeOC_6H_4)_3$	708
PPh_2(*o*-Tol)	730
PPh_3	732
PPh_2(*m*-$CF_3C_6H_4$)	766

phosphine, the larger the degree of back donation into the CO π* orbitals, resulting in a lower bond order and consequently a decrease in ν_{CO} to lower wave numbers. Conversely a relatively weaker Lewis basic phosphine would have the opposite effect and increase the ν_{CO}. The nickel complexes under investigation were easily prepared and gave well-resolved carbonyl stretching peaks; however, their associated toxicity and occasional high volatility and/or air-sensitive nature make this methodology less universally applicable [8].

Alternatively, Allen and Taylor demonstrated that the $^{1}J_{P,Se}$-coupling constant obtained from ^{77}Se satellites in ^{31}P NMR spectra of phosphorus selenides can be used to measure the Lewis basicity of the parent phosphine [9]. An increase in the magnitude of the $^{1}J_{P,Se}$-coupling constant has been shown to correspond to an increase in *s*-character of the phosphorus lone pair (as *s*-electrons are most penetrating and consequently contribute most to the Fermi contact between nuclear magnetic moments), reducing p-orbital contribution and consequently reducing the Lewis basicity (Table 1) [10, 11].

3 Multidentate Ligand Coordination

Multidentate ligands most commonly contain three to six donor atoms, with each additional donor increasing the complex stability in a step-wise fashion. Hexacoordinate ligands are some of the best known compounds for stabilising potentially reactive or toxic metal ions, for example, the hexadentate aminopolycarboxylic acid, EDTA, is widely used as a metal sequestering agent because it forms highly stable complexes with good solubility. The potentially octadentate ligand 1,4,7,10-tetraazacyclododecane-1,4,7,10-tetraacetic acid (DOTA) is widely applied in imaging sciences to form stable complexes with radiometals or toxic Gd^{3+} ions. Complexes can then be safely used in vivo for human imaging studies.

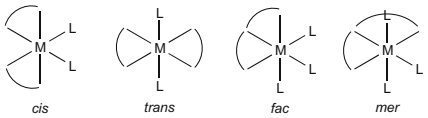

Fig. 6 Comparison of coordination modes of bi- and tridentate ligands in an octahedral coordination environment

There are various geometric arrangements that multidentate ligands can adopt around metal centres; it is useful to briefly categorise these motifs here. In an octahedral coordination environment, the coordination of two bidentate ligands and two monodentate ligands can be arranged with the monodentate ligands either trans or cis; however, tridentate ligands cannot be similarly described. Instead, the coordination of tridentate ligands can either occupy the face of the octahedron (*fac*) or three points of the equatorial plane (*mer*). All these motifs are visualised in Fig. 6. Moving from tridentate to tetradentate ligands, the arrangements can again be described by trans and cis, as this now describes the remaining ligands around the octahedron.

Multidentate ligands do not necessarily coordinate to the same metal centre through all potential donor atoms. In some cases one or more donors remain pendent, and these can now coordinate to a separate metal centre, forming multimetallic species. If two (or more) different metals coordinate to the same multidentate ligand, these species are known as hetero-multimetallic complexes.

4 Triphosphine Ligands

Tridentate ligands can be generally divided into two major categories: linear and branched (tripodal). This division is simply based on the arrangement of the three phosphorous atoms and as such results in different coordination behaviours. Linear triphosphines are typically prepared via the free radical reaction of a secondary phosphine with the vinyl groups on tertiary phosphine. The various coordination modes that are seen for linear triphosphines depend on (1) the metal centre and oxidation state, (2) substituents at the phosphorus atoms and (3) the length of the carbon backbone spacer. Three classic linear triphosphines are shown below (Fig. 7), with the general formula $(Ph_2P(CH_2)_n)_2PPh$ ($n = 1$, dpmp; $n = 2$, etp; $n = 3$, ttp) [12]. Although other variations with different R groups on the P atoms have been reported, they are more difficult to prepare and have not been as widely investigated [13–16].

Linear triphosphines that contain methyl linkages (e.g. dpmp) typically coordinate in a bidentate mode, forming either four- or six-membered metallocycles, for example, $[Mo(CO)_4\{(^tBu_2PCH_2)_2PMe\}]$ or $[PdCl_2(dpmp)]$ (Fig. 8a and b, respectively) [12]. This leaves a free phosphorus atom that can be used to coordinate to a second metal ion to give mixed bimetallic complexes. Additionally, mixed

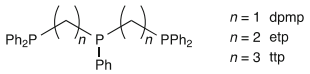

Fig. 7 The most common linear triphosphines with various length carbon spacers between phosphorus atoms

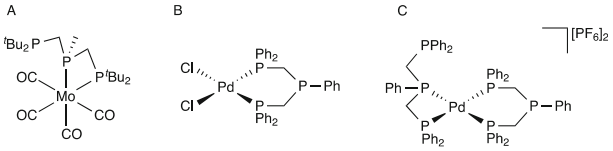

Fig. 8 Geometries of some monometallic complexes obtained via coordination of linear triphosphines with methylene spacers, forming either four- or six-membered metallocycles

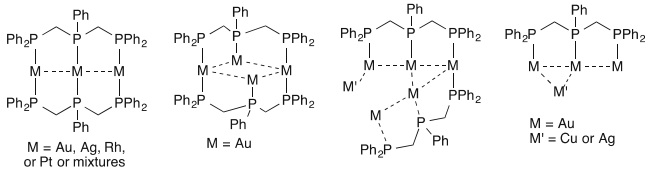

Fig. 9 Examples of the dpmp ligand acting as a bridging unit supporting the formation of multimetallic complexes; counter ions and solvent ligands have been removed for clarity

structures can be isolated with a four- and a six-membered ring (Fig. 8c). It is thought that this is largely due to steric encumbrance, as the presence of two six-membered rings results in significant crowding around the metal centre [17]. Such linear triphosphines have also been used to form polymetallic structures by bridging between metal centres and coordinating in an η^1 fashion. A number of examples of copper [18, 19], silver [20], gold [21–24], platinum [25–27] and rhodium [28–36] complexes, as well as mixed metal species [21, 37–40], have been reported for the dpmp ligand (Fig. 9). This ligand motif has also been used as a support for the synthesis of more elaborate mixed gold and silver clusters that have shown interesting photophysical properties [41].

The etp ($Ph_2P(CH_2CH_2)_2PPh$) ligand is the most widely used ligand of this class. The ethylene groups in its backbone give greater conformational flexibility that typically results in the formation of tridentate complexes. Bridging between metal centres is also common for this ligand, and multimetallic complexes can also form. The exact coordination geometry, of course, depends on the metal centre, oxidation state and other ligands that may be coordinated. In an octahedral environment, the etp ligand can either form *fac* or *mer* coordination complexes (Fig. 10), the *fac* isomer being more common. Complexes of the etp ligand (Fig. 11) have been used in the subsequent synthesis of metallic clusters [42–46], dinitrogen activation [47], generating low-valent complexes [48–50], CO_2-ethylene coupling [16] and for a range of catalytic reactions including lignin depolymerisation [51], alkene

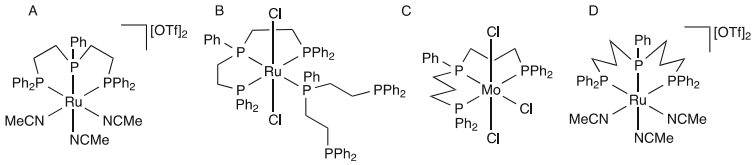

Fig. 10 The coordination geometries adopted upon coordination of etp and ttp ligands showing either *fac* or *mer* geometries in each case

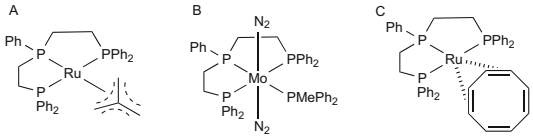

Fig. 11 (**a**) [Ru(etp)(tmm)] complex that is an active catalyst for the C–O bond cleavage of lignin model compounds, (**b**) dinitrogen-activated complex $[Mo(N_2)_2(etp)(PMePh_2)]$ and (**c**) the low-valent η^4-iron etp complex $[Fe(etp)(\eta^4\text{-COT})]$

hydrogenation [52], ester hydrogenation [53], hydroamination [54], alkyne reduction [55], hydroformylation [56], aldehyde decarbonylation [57], CO_2 reduction [13] C–C coupling [58] and electrophilic fluorination [59]. In comparison, the ttp ligand $(Ph_2P(CH_2CH_2CH_2)_2PPh$ which contains more flexible propylene backbones is much less commonly used, probably because it is more difficult to synthesise. This ligand has been found to favour the meridional coordination mode in an octahedral environment (Fig. 10c) although *fac* geometries have also been observed (Fig. 10d) [12]. There are few catalytic applications of complexes of this ligand, with most reports making comparisons to the etp ligand.

5 Coordination Chemistry of Triphos-Type Ligands

There are many structural variations possible with branched triphosphines, e.g. length of spacers between phosphines, substituents on phosphorus, mixed donor atoms, etc. Figure 12 shows three phosphine moieties (PR_2) situated on 'arms' of various lengths that originate from an apical atom or group (R′E), resulting in ligands with the general formula $R'E\{(CH_2)_nPR_2\}_3$ ($n = 0$–3; E = C, B, P, Si, Sn, N; R′ = Me, Et, Ph, Bz, etc.). Depending on the identity of the apical atom, an ancillary group may be present (R′) that does not participate in metal binding.

The smallest branched triphosphine $HC(PPh_2)_3$ forms either metal clusters [21, 60–63] or bidentate complexes [64–66] since the P atoms are not able to coordinate in a tridentate fashion (Fig. 13). Increasing the arm length between the apical moiety and phosphine groups to ethylene linkers $(CH_3C(CH_2CH_2PPh_2)_3$, $MeC^{Et}P_3{}^{Ph}$) adds a great deal of flexibility, enabling mono-, bi- or tridentate

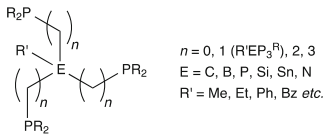

Fig. 12 Branched triphosphines with various 'arm' lengths between the apical moiety and phosphine groups

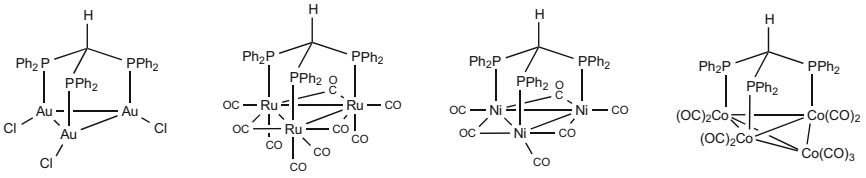

Fig. 13 Transition metal cluster complexes containing $HC(PPh_2)_3$ [67]

coordination mode [68–70]. Although only a few reports exist, the stability of complexes featuring the $MeC^{Et}P_3{}^{Ph}$ ligand appears to become increasingly unstable as more phosphines coordinate to a single metal centre. This is likely due to the generation of unfavourable eight-membered metallocycles upon multidentate coordination [68]. The reaction of $MeC^{Et}P_3{}^{Ph}$ with nickel(II) dichloride give a novel trimetallic complex $[Ni_3Cl_6(\kappa^1{:}\eta^3\text{-}MeC^{Et}P_3{}^{Ph})_2]$, where three nickel atoms bridge between the two ligands.

Variations to $MeC^{Et}P_3{}^{Ph}$ containing either nitrogen ($N^{Et}P_3{}^{Ph}$) or phosphorus ($P^{Et}P_3{}^{Ph}$) apical moieties are more widely studied than carbon-centred $MeC^{Et}P_3{}^{Ph}$ and predominantly form tri- or tetradentate complexes (Fig. 14). These geometries have been reported for a wide range of late transition metals [71], including the stabilisation of rare geometries such as trigonal bipyramidal platinum (II) complexes [72]. Recently complexes of the $P^{Et}P_3{}^{Ph}$ ligand have been used in a wide range of catalytic reactions such as the dehydrogenation of formic acid [73, 74], urea reduction [75], CO_2 reduction [76, 77], alkyne reduction [78], nitroarene reduction [79], C–C coupling [80] and for the formation of gold clusters [81].

Branched triphosphine ligands with a methylene bridge between the apical moiety and phosphine groups (Fig. 15) have also generated much interest over the past five decades for both coordination chemistry and catalytic applications. The so-called 'triphos' ligand scaffold was introduced in 1962 with the first report of the eponymous carbon-centred triphos ligand ($CH_3C(CH_2PPh_2)_3$, $MeCP_3{}^{Ph}$) [82] and was subsequently studied extensively, predominantly by the pioneering work of Bianchini and co-workers [83]. There are also analogous ligands which feature non-carbon-centred apical moieties; however, these are much rarer. Reports featuring these heteroatom-centred ligands demonstrate that there remains a great deal of scope for investigation [84].

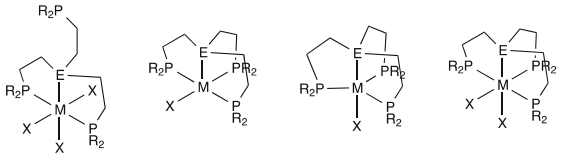

Fig. 14 Coordination modes of $E^{Et}P_3^{Ph}$ (E = N, P) and $N^{Pr}P_3^{Ph}$

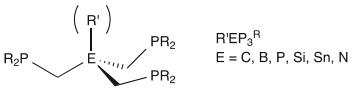

Fig. 15 General structure of the triphos ligand scaffold (E = apical atom, PR_2 = phosphine coordinating moiety, R′ = ancillary arm)

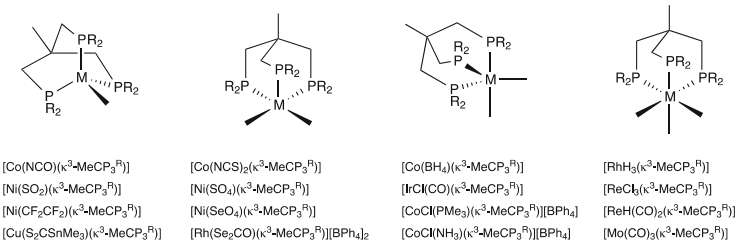

Fig. 16 Common coordination geometries adopted by $MeCP_3^{Ph}$ with selected crystallographically characterised examples [86, 88–98]

Complexes of $MeCP_3^{Ph}$ or the corresponding ligand with dimethylphosphine groups ($MeCP_3^{Me}$) with transition metals have been reported across the d-block [67]. Often the ligand is triligating in an imposed *fac* geometry; however in some cases, it can be biligating due to steric or electronic factors [12, 85]. In most cases, five- or six-coordinate species are observed, while four-coordinate complexes remain rare [12, 67] and higher coordination numbers rarer still (for instance, $[ReH_5(\kappa^3\text{-}MeCP_3^{Ph})]$, $[ReH_7(\kappa^2\text{-}MeCP_3^{Ph})]$, $[ReH_3(PPh_3)(\kappa^3\text{-}MeCP_3^{Ph})]$ and $[ReH_3(CO)(\kappa^3\text{-}MeCP_3^{Ph})]$) [86, 87]. The four most predominant complex geometries are shown in Fig. 16, with selected crystallographically characterised examples for each. Other examples of complexes from across the d-block with especially unusual bonding motifs are also highlighted.

Group 4 complexes have been reported with $MeCP_3^{Me}$ which react with $[MCl_2]\cdot(THF)_2$ (M = Ti, Zr, Hf) under reducing conditions (K/naphthalene) and an atmosphere of CO to afford the seven-coordinate 4:3 piano-stool complexes $[M(CO)_4(\kappa^3\text{-}MeCP_3^{Me})]$ [99]. The $MeCP_3^{Me}$ was found to be instrumental in stabilising the '$[Zr^0(CO)_4]$' fragment.

The stoichiometry of reagents and oxidation state of the metal can influence the denticity of the resultant complex, as demonstrated by a series of chromium complexes. Reaction of one equivalent of $MeCP_3^{Me}$ with $[CrCl_3]$ afforded $[CrCl_3(\kappa^3\text{-}MeCP_3^{Me})]$ (Scheme 1a), while reaction of two equivalents of $MeCP_3^{Me}$

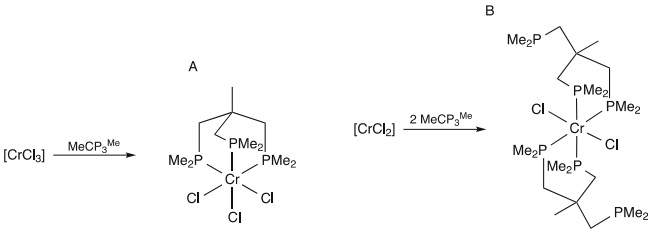

Scheme 1 Chromium complexes featuring $MeCP_3^{Me}$

with $[CrCl_2]$ afforded trans-$[CrCl_2(\kappa^2\text{-}MeCP_3^{Me})_2]$ (Scheme 1b) [89]. Molybdenum complexes of $MeCP_3^{Ph}$ are generally well-defined octahedral complexes such as $[Mo(CO)_3(\kappa^3\text{-}MeCP_3^{Ph})]$ [100–102] or $[MoCl_3(\kappa^3\text{-}MeCP_3^{Ph})]$ [103], from which subsequent reactivity was studied.

Rhenium complexes mentioned above form high-coordination number complexes with hydride ligands [86, 87]. The manganese complexes are generally octahedral with $MeCP_3^{Ph}$ triligating and either cationic $([Mn(CO)_3(\kappa^3\text{-}MeCP_3^{Ph})][X]$ where $X = BPh_4$, ClO_4, PF_6, OTf) [104, 105] or neutral $([MnR(CO)_2(\kappa^3\text{-}MeCP_3^{Ph})]$ where $R = H$, CH_3, $COCH_3$, CN, CNMe) [106–108].

Groups 8 and 9 are the most studied transition metals for coordination with $MeCP_3^{R}$, as well as their catalytic applications. Iron complexes are generally octahedral [12], whereas cobalt, rhodium and iridium are more geometrically versatile and can adopt tetrahedral, square-based pyramidal, trigonal bipyramidal or octahedral geometries [67]. There are many similar structures reported featuring either Group 8 or 9 metals, and these are the precursors used for further coordination studies and/or catalysis [12, 67]. Common ancillary ligands to the triphosphine include halides, carbonyls, hydrides (and borohydrides) and nitriles.

Iridium, similar to chromium, forms monometallic trichloride complexes of general formula $[IrCl_3(\kappa^3\text{-}MeCP_3^{R})]$ ($R = Me$, Ph) [93]; however, both monometallic and bimetallic structures have been reported for cobalt and rhodium [97, 109–111]. Cobalt especially showed versatility in its geometry depending on the oxidation state of the metal centre, with cobalt(I) forming tetrahedral $[CoCl(\kappa^3\text{-}MeCP_3^{Ph})]$ and cobalt(III) forming octahedral $[CoCl_3(\kappa^3\text{-}MeCP_3^{Me})]$, and depending on the reaction conditions, cobalt(II) was found to adopt either a monomeric or dimeric structure, $[CoCl_2(\kappa^3\text{-}MeCP_3^{Ph})]$ and $[Co(\mu\text{-}Cl)(\kappa^3\text{-}MeCP_3^{Ph})]_2^{2+}$, respectively (Fig. 17) [97, 109].

A common entry point to Group 8 and 9 carbonyl complexes is via dicarbonyl complexes of general formula $[M(CO)_2(\kappa^3\text{-}MeCP_3^{Ph})]^{n+}$ ($M = Fe$, Co, Rh, Ir) [112–114]. As these species are five-coordinate and typically in a low oxidation state, they readily undergo reaction with Lewis basic ligands such as tertiary phosphines or oxidative addition with appropriate reagents such as HCl, MeI, etc., to form coordinationally saturated complexes. The reaction of dicarbonyl species with hydride/proton donors is a convenient method to access metal–hydride complexes of general formula $[MH_x(CO)_y(\kappa^3\text{-}MeCP_3^{Ph})_2]^{n+}$ ($M = Fe$, Co, Rh, Ir) that can be synthesised (Fig. 18) [93, 115–118]. Additionally, $[Rh(CO)_2(\kappa^3\text{-}MeCP_3^{Ph})]^+$ can

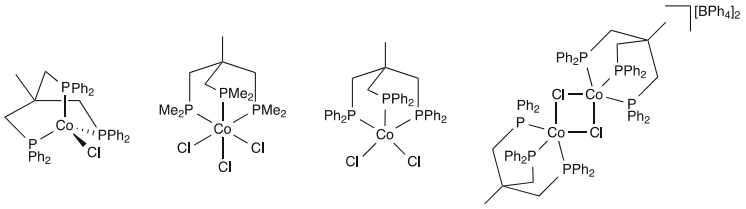

Fig. 17 Cobalt complexes featuring $MeCP_3^R$ (R = Me, Ph)

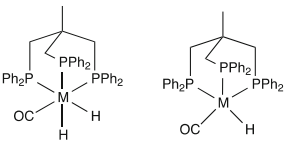

Fig. 18 Group 8 and 9 hydride complexes featuring $MeCP_3^{Ph}$

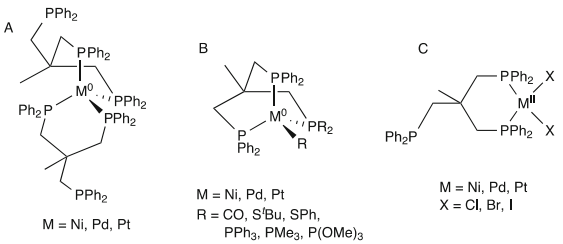

Fig. 19 Group 10 complexes featuring $MeCP_3^{Ph}$

undergo further reaction to afford the carbonyl-bridging dimer [Rh(μ-CO)(κ^3-$MeCP_3^{Ph}$)]$_2$ that includes an Rh–Rh bond [119].

Group 10 complexes with $MeCP_3^{Ph}$ typically adopt two different four-coordinate geometries, predominantly determined by the oxidation state of the metal as expected (Fig. 19). In the zero oxidation state, a tetrahedral geometry is adopted, with $MeCP_3^{Ph}$ in either a bi- or tridentate coordination mode, in the former case the remaining two coordination sites being occupied by a second κ^2-$MeCP_3^{Ph}$ ligand, while in the latter by a Lewis basic ligands (Fig. 19a and b, respectively). In the 2+ oxidation state, the d^8-metal centres adopt a square-planar geometry as expected, with a κ^2-$MeCP_3^{Ph}$ ligand and two halides (Fig. 19c).

Reactions of $MeCP_3^{Ph}$ with Cu(I) and Ag(I) tend to result in less well-defined complexes owing to the lability of the P–M coordinate bond with these metals. Thus, in addition to bidentate and tridentate complexes [120–123] that form, more unusual multimetallic coordination structures [124, 125] and coordination polymers [46, 126, 127] have been prepared. Reaction of $MeCP_3^{Ph}$ with Au(I) precursors can result in the formation of a range of different coordination modes and mono-, bi- or

trimetallic gold complexes [128, 129]. Interestingly trimetallic $MeCP_3^{Ph}$–Au_3 complexes have been used as building blocks to synthesise a range of heterometallic complexes [130, 131] and other larger coordination complexes [132, 133].

6 Catalytic Applications with Triphos Complexes

Triphos complexes have recently been used as catalysts for a range of conventionally difficult catalytic transformations. The area is relatively small in comparison to the use of bidentate phosphine complexes for catalysis but appears to growing for certain types of catalytic applications that require forcing conditions or where the active catalytic species benefits from of the *fac* coordination geometry of the ligand. The commercially available $MeCP_3^{Ph}$ ligand has been most widely used and imparts inherent stability via multidentate coordination of three phosphine arms that is thought to prevent, or at least slow, catalyst decomposition over the course of a reaction. Additionally, the necessary cis arrangement of other coordinated groups means these are primed to undergo further organometallic transformations. Traditionally difficult catalytic applications that triphos complexes have recently been applied to include:

- Hydrogenation of esters to alcohols [53, 134, 135]
- Hydrogenation of carboxylic acids to alcohols [136]
- Selective hydrogenation of amides to amines with preservation of the C–N bond [137, 138]
- Methylation of amines using CO_2 or formic acid as the C_1 source [139–141]
- Hydrogenation of levulinic acid to 2-MTHF [142, 143]

6.1 Hydrogenation of Esters and Carboxylic Acids to Alcohols

The hydrogenation of dimethyl oxalate (DMO) first to methyl glycolate (MG) and then to ethylene glycol (EG) is a commonly studied benchmark test for the hydrogenation of biogenic esters (Scheme 2a). The relative ease of conversion of DMO to MG is due to the activating nature of the second ester moiety in DMO; however, hydrogenation of MG to EG is substantially harder as the remaining ester moiety is no longer activated. Consequently, the conversion of MG to EG typically requires very harsh conditions (200 bar H_2, 180°C) [134]. When a catalytic system comprised of $[Ru(acac)_3]/MeCP_3^{Ph}$ was used, DMO conversion to EG was achieved in 95% yield under relatively mild conditions (80 bar H_2, 120°C) [53]. This catalyst system was also found to efficiently hydrogenate similarly difficult aromatic and aliphatic esters to their corresponding alcohols: dimethyl phthalate, benzyl benzoate, dimethyl maleate and methyl palmitate (Scheme 2b–e)

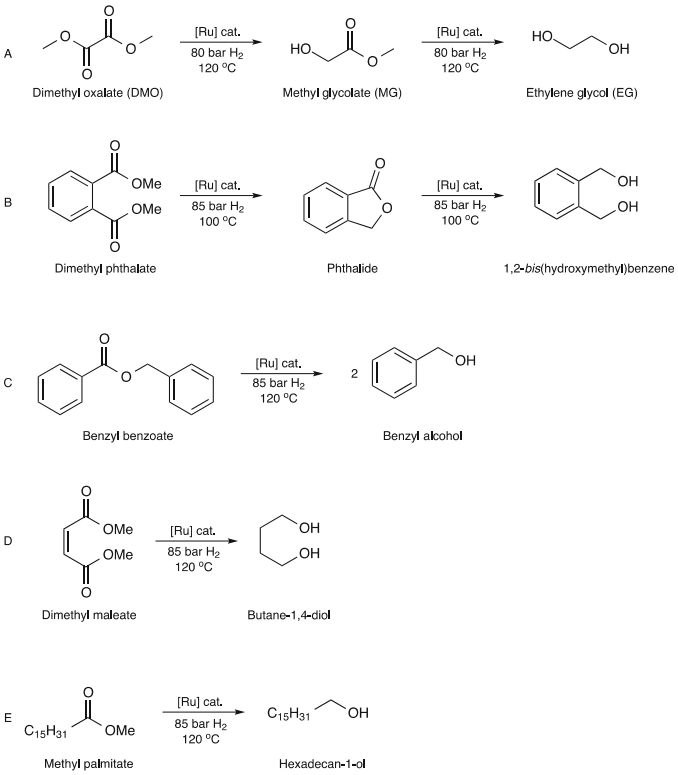

Scheme 2 Hydrogenation of aromatic and aliphatic esters to their corresponding alcohols using $[Ru(acac)_3]/MeCP_3^{Ph}$ as the pre-catalyst

[135]. Many ligand systems were studied for the conversion of DMO to EG; however, $MeCP_3^{Ph}$ was uniquely found to exhibit high activity over other mono-, bi-, tri- or tetradentate phosphine systems, as well as arsenic- and nitrogen-donor ligands [53]. The comparison of $MeCP_3^{Ph}$ to other tridentate phosphines, which can adopt either a facial or meridional coordination geometry, demonstrated that the imposed facial coordination of $MeCP_3^{Ph}$ was critical for high activity.

The $[Ru(acac)_3]/MeCP_3^{Ph}$ catalyst system was extended to a wider range of more challenging substrates to hydrogenate, including lactones and dicarboxylic acids, in both cases ultimately leading to diols [136]. The triphos system was found to be highly active under similarly relatively mild conditions (80 bar H_2, 120°C) compared to those typically currently utilised in industrial processes, which require heterogeneous catalysts normally based on copper–chromium systems, at high temperatures (200–300°C) and high pressures (200–300 bar H_2) [136].

A sulphur derivative of $MeCP_3$, $CH_3C(CH_2S^nBu)_3$ ($TriSulf^{Bu}$) has been used for the selective homogeneous ruthenium-catalysed hydrogenation of DMO to MG but was unable to catalyse further hydrogenation to EG [144]. It should be noted that the most active catalyst for the hydrogenation of nonactivated aromatic and

aliphatic esters under mild conditions is a ruthenium hydride complex reported by Milstein and co-workers featuring a PNN pincer ligand. This complex was able to hydrogenate a range of esters to their corresponding alcohols in high yields using only 5.3 bar H_2 pressures and 115–140°C [145].

6.2 Hydrogenation of Amides to Amines

The production of amines (particularly via amide hydrogenation) is of vital importance, especially within the pharmaceutical industry, and consequently has been identified by the American Chemical Society Green Chemistry Institute and members of Pharmaceutical Roundtable as one of the three most desirable reactions for development [146]. Traditionally these reactions are performed using $LiAlH_4$ or borane-reducing agents, which are pyrophoric, difficult to handle, require complicated work-up procedures and produce waste by-products. The use of hydrosilanes as reductants circumvents some of these problems, and these reagents can give good selectivity for amine formation but remain less atom efficient than using molecular hydrogen. Heterogeneous catalysts require harsh conditions and give very poor selectivity, in addition to often producing over-hydrogenated products, for instance, hydrogenating aromatic systems. It is desirable to develop a catalytic system which selectively hydrogenates amides to amines with preservation of the C–N bond [138].

The $[Ru(acac)_3]/MeCP_3^{Ph}$ catalytic system used to hydrogenate esters and carboxylic acids was also effective for the selective hydrogenation of amides to amines (Scheme 3) [137]. Although only relatively low pressures of hydrogen were required to realise the desired transformation (70 bar), high temperatures (>200°C) were also found to be critical [138]. Detailed evaluation of the interactions of preformed ruthenium hydride complexes $[RuH_2(CO)(\kappa^3\text{-}MeCP_3^{Ph})]$ and $[RuH(\kappa^2\text{-}CH_3CO_2)(\kappa^3\text{-}MeCP_3^{Ph})]$ with methanesulfonic acid (MSA) as a cocatalyst both in the presence and absence of substrate and H_2 revealed the presence of a range of complexes containing coordinated monodentate or chelating $CH_3SO_3^-$, usually without hydride ligands present (Fig. 20).

The complexes featuring coordinated $CH_3SO_3^-$ were found to be relatively stable considering the weakly bound nature of the $CH_3SO_3^-$ ligand, with several being structurally characterised by X-ray diffraction analysis [138]. Heating mixtures of the compounds shown in Fig. 20 in the presence of amide substrates, and under a pressure of 10 bar H_2, to 130°C resulted in no reaction according to NMR analysis. The stability of these ruthenium species is therefore likely to be the cause of the high-temperature requirement for catalysis (>200°C). At temperatures above 130°C, it was suggested that the mixture of compounds shown in Fig. 20 acts as a reservoir of the $[Ru(\kappa^3\text{-}MeCP_3^{Ph})]^{2+}$ fragment, which is the true active catalytic species [138].

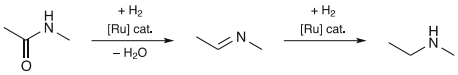

Scheme 3 Hydrogenation of amides to amines using $[Ru(acac)_3]/MeCP_3^{Ph}$ as the pre-catalyst with preservation of the C–N bond

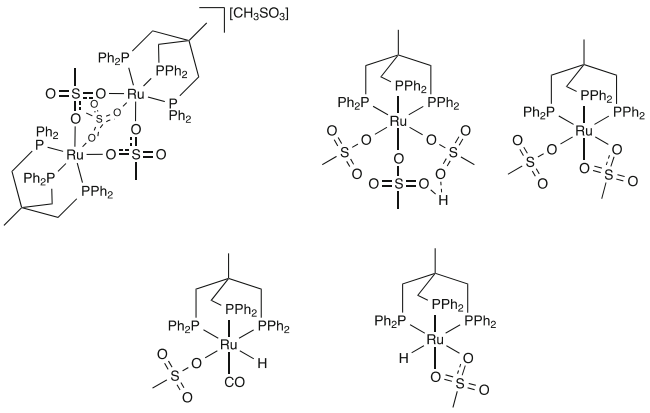

Fig. 20 Selected reaction products observed during reaction of $[RuH_2(CO)(\kappa^3\text{-}MeCP_3^{Ph})]$ or $[RuH(\kappa^2\text{-}CH_3CO_2)(\kappa^3\text{-}MeCP_3^{Ph})]$ with MSA

Table 2 Methylation of amines using alternative C_1 sources in conjunction with a reductant

C_1 Source	Reductant	Catalyst	Temperature (°C)	Additive
CO_2 (30 bar)	$PhSiH_3$	$[RuCl_2(DMSO)_4]/^nBuPAd_2$	100	–
CO_2 (1 bar)	$PhSiH_3$	$[ZnCl_2]$/NHC	100	–
HCOOH	$PhSiH_3$	$[Pt(CH_2=CHSiMe_2)_2O]$/dppp	RT	–
CO_2 (20 bar)	H_2 (60 bar)	$[Ru(acac)_3]/MeCP_3^{Ph}$	140	MSA
CO_2 (20 bar)	H_2 (60 bar)	$[Ru(tmm)(\kappa^3\text{-}MeCP_3^{Ph})]$	150	$HNTf_2$
HCOOH	HCOOH	$[Ru(methylallyl)_2(cod)]/MeCP_3^{Ph}$	150	$HNTf_2$

6.2.1 Methylation of Amines Using CO_2 or Formic Acid

$MeCP_3^{Ph}$ ruthenium complexes have shown high activity for the methylation of primary and secondary amines using alternative C_1 sources that avoid toxic methylating agents such as methyl iodide, dimethyl sulphate or diazomethane. These alternative C_1 sources feature carbon in higher oxidation states than direct methylating agents and consequently require the use of a reductant in tandem. Initial research detailed the use of CO_2 as the source of carbon in conjunction with $PhSiH_3$ as a reductant and either zinc [147] or ruthenium [148] salts to generate the catalytic species. Subsequent reports revealed that triphos–Ru complexes proved to be highly active using H_2 as the reductant. Table 2 gives an overview of the different

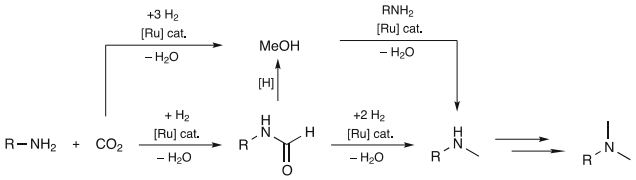

Scheme 4 Proposed reaction pathway for methylation of using carbon dioxide as C_1 source

carbon sources and reductants used in concert with Ru–$MeCP_3^{Ph}$ complexes (and others for comparison) as catalysts for the synthesis of methyl amines.

The use of CO_2 as the C_1 source also required high pressures of H_2 (60 bar) as the reductant, as well as other additives [140]. With careful tuning of the catalyst loadings and reaction times, selective monomethylation over dimethylation was achieved for over 15 examples of primary aromatic amines, while changing the additive from MSA to LiCl allowed selective dimethylation of aliphatic primary amines. A reaction mechanism was proposed (utilising a range of control experiments) which involves the initial formation of a formamide intermediate, which in turn is rapidly reduced to the corresponding methylated product (Scheme 4). An alternative mechanism involving direct methylation with methanol, which is generated in situ from the hydrogenation of CO_2 in the presence of ruthenium, was found to contribute to a lesser extent (Scheme 4) [140].

Formic acid has been innovatively used as both the carbon source and reductant [139]. An acidic additive was found to be crucial for obtaining methylated amines, only trace amounts of product were detected in the absence of either MSA or $HNTf_2$, with the later being found to be more effective. Formic acid can undergo disproportionation to methanol, CO_2 and H_2O, or dehydrogenation to CO_2 and H_2 in the presence of ruthenium catalysts, and consequently any of these species may be implicated in the mechanism for amine methylation. In fact, a similar mechanism as that reported for the CO_2/H_2 system was suggested, with the reaction proceeding via a formyl intermediate, and not via direct methylation with methanol. The formylation agents were proposed to be both formic acid and CO_2, while the subsequent reduction was achieved by both hydrogenation using H_2 and transfer hydrogenation using formic acid itself. [139] Using either CO_2/H_2 or formic acid as the methylation system for aromatic primary amines, the reaction was found to be highly sensitive to the electronic nature of the substituents on the aryl rings [139, 140].

The preformed ruthenium complex [Ru(tmm)(κ^3-$MeCP_3^{Ph}$)] (tmm = trimethylenemethane) is an effective catalyst for the methylation of secondary amines and dimethylation of primary amines using CO_2/H_2 [149]. Acidic additives such as $HNTf_2$, MSA or *para*-toluenesulfonic acid (*p*-TsOH) were once again found to be critical to achieve any significant reactivity, and a qualitative trend towards lower reactivity with increasing basicity of the substrate was established.

This approach was extended to include *N*-methylation of isolated imines as well as the direct coupling of amines with aldehydes and the subsequent reductive

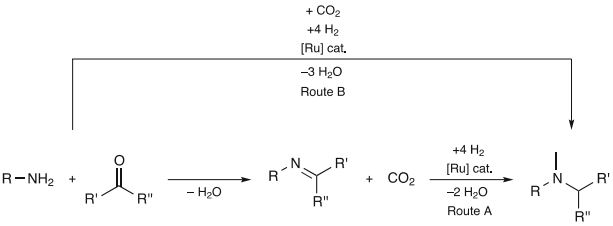

Scheme 5 Catalytic reductive methylation of imines with CO_2 and H_2 (Route A) and one-step synthesis of unsymmetrical tertiary *N*-methyl amines through a three-component coupling of primary amines, aldehydes ($R^3 = H$) and CO_2/H_2 (Route B)

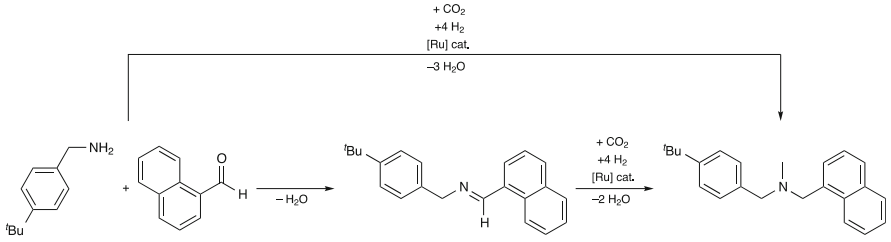

Scheme 6 Synthesis of antifungal agent butenafine using reductive methylation of imines with CO_2 and H_2

methylation of the in situ formed imines (Scheme 5) [150]. As a demonstration of the synthetic utility of this *N*-methylation strategy, the antifungal agent butenafine was synthesised starting from commercially available 1-naphthalene aldehyde and 4-*tert*-butylbenzyl amine in 88% yield if the intermediate imine was isolated or 60% yield in a direct three-component coupling reaction (Scheme 6) [150].

6.3 *Hydrogenation of CO_2*

The direct and efficient reduction of CO_2 using molecular hydrogen to useful chemicals such as formic acid or methanol is a highly desirable process. Currently, the majority of catalysts for the hydrogenation of CO_2 to methanol are heterogeneous, with few examples of molecularly defined species capable of achieving this transformation with significant turnover numbers (TONs) [151]. Ruthenium (II) pincer complexes were the first reported homogeneous catalysts that were able to hydrogenate carbonic acid derivatives and formates to methanol [152]. Due to the conversion of CO_2 to formates in the presence of ruthenium complexes being feasible, it should also be possible to convert CO_2 directly to methanol in the presence of molecularly well-defined ruthenium complexes. This approach was recently demonstrated, where the hydrogenation of carbon dioxide to methanol was accomplished in a cascade reaction with different homogeneous

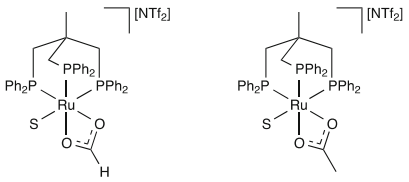

Fig. 21 Catalyst precursor for the hydrogenation of CO_2 to methanol ($[Ru(S)(\eta^2\text{-}O_2CCH_3)(\kappa^3\text{-}MeCP_3{}^{Ph})]NTf_2$) and the structure of the catalytically active intermediate ($[Ru(S)(\eta^2\text{-}O_2CH)(\kappa^3\text{-}MeCP_3{}^{Ph})]NTf_2$) (S = solvent)

catalysts via formic acid and methyl formate intermediates. The multicomponent catalytic system required a complicated mixture of three different catalysts, and partial incompatibility made a spatial separation of reaction steps essential, resulting in a maximum TON of 21 equivalents of methanol per ruthenium centre [153].

Ruthenium $MeCP_3{}^{Ph}$ catalytic species generated in situ from a mixture of [Ru(acac)$_3$] and $MeCP_3{}^{Ph}$ have proven to be promising catalysts for the hydrogenation of CO_2 to methanol giving TONs of 52. Ethanol was added as an alcohol component to tentatively stabilise any intermediates (assumed to be formates) as esters, and an acidic cocatalyst (MSA) was once again found to be essential for any reactivity [154]. Higher TONs (63) were observed for this reaction when the preformed complex $[Ru(tmm)(\kappa^3\text{-}MeCP_3{}^{Ph})]$ was used in conjunction with MSA. A subsequent in-depth mechanistic and computational study of this process revealed additional alcoholic components were not necessary, as the direct conversion of CO_2 to methanol via formate was feasible within the coordination sphere of the metal, thus requiring no intermediate stabilisation [151]. The role of the acidic additive was determined to be for the generation of a cationic ruthenium species, with the formate-bound complex $[Ru(S)(\eta^2\text{-}O_2CH)(\kappa^3\text{-}MeCP_3{}^{Ph})]NTf_2$ (S = solvent) being the sole spectroscopically observed phosphorus-containing species under catalytic conditions (Fig. 21). When pressurised with CO_2 (20 bar) and H_2 (60 bar), $[Ru(S)(\eta^2\text{-}O_2CCH_3)(\kappa^3\text{-}MeCP_3{}^{Ph})]NTf_2$ was able to catalytically turnover, producing methanol directly from CO_2 in the absence of both an alcohol component or acidic additive [151]. A mechanism based on these investigations was proposed and corroborated by DFT calculations to be energetically feasible (Scheme 7).

$[Ru(tmm)(\kappa^3\text{-}MeCP_3{}^{Ph})]$ has proven to be a versatile catalyst for the hydrogenation of carboxylic and carbonic acid derivatives, generally affording either alcohols or primary or secondary amines depending on the substrate, in the presence of $HNTf_2$ as the acidic additive [155]. The range of possible hydrogenations using $[Ru(tmm)(\kappa^3\text{-}MeCP_3{}^{Ph})]$ is summarised in Scheme 8, with carboxylic acids and esters, acid anhydrides, imides and primary amide substrates all being converted to alcohols in the absence of $HNTf_2$ (i.e. via a neutral catalytic cycle), while secondary amides and urea derivatives were converted to secondary amines and formamide, respectively. In the presence of $HNTf_2$ (via a cationic catalytic cycle), primary amides and urea derivatives retain their C–N bond and afford

Scheme 7 Basic catalytic cycle for the transformation of CO_2 to methanol at the Ru–triphos fragment. P_3Ru denotes the Ru^{II}–$MeCP_3^{Ph}$ fragment

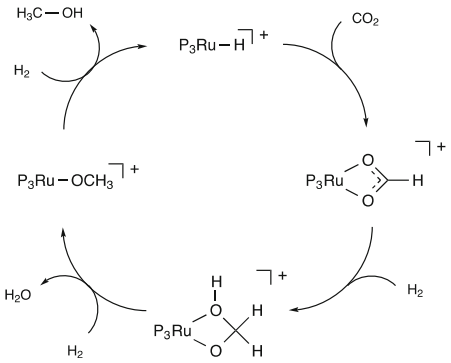

Scheme 8 Scope of selective hydrogenation of challenging substrates using [Ru(tmm)(κ^3-$MeCP_3^{Ph}$)] as catalyst precursor

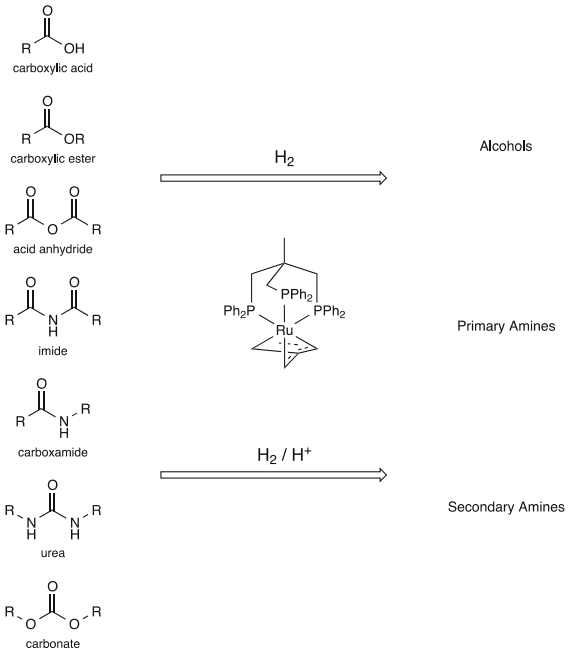

secondary and primary amines, respectively. Carbonate species show no reactivity in the absence of acidic additives but are hydrogenated to alcohols in the presence of 1.5 mol% $HNTf_2$ [155].

6.4 Hydrogenation of Levulinic Acid to 2-MTHF

Levulinic acid (LA) is now well recognised as viable platform chemical, derived from lignocellulose biomass, that can be up-converted into more valuable chemical

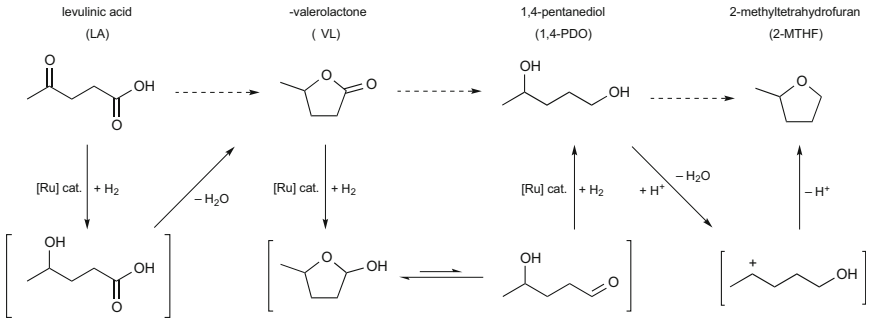

Scheme 9 Reaction sequence for the selective conversion of levulinic acid (LA) into γ-valerolactone (γVL), 1,4-pentanediol (1,4-PDO) and 2-methyltetrahydrofuran (2-MTHF)

commodities. In a series of hydrogenation/dehydration reactions, LA can be converted to 2-methyltetrahydrofuran (2-MTHF) (a useful solvent and potential biofuel) via γ-valerolactone (γVL) and 1,4-pentanediol (1,4-PDO) (Scheme 9). The hydrogenation of levulinic acid past γVL to either 1,4-PDO or 2-MTHF had previously only been achieved using heterogeneous catalysts; however recently a series of homogeneous catalysts based on Ru-phosphine complexes have also proven to be useful for this transformation under milder temperatures and pressures [142]. Of these complexes, Ru/$MeCP_3^{Ph}$ appears to be the most promising for this transformation [143]. Using a catalyst form in situ from $Ru(acac)_3$ and $MeCP_3^{Ph}$, the conversion of LA to 1,4-PDO was achieved in 95% in the absence of any acidic additives. The addition of acidic additives such as NH_4PF_6 or *para*-toluenesulfonic acid (*p*-TsOH) enabled the direct conversion of LA to 2-MTHF. A stronger acid component, a mixture of NH_4PF_6 in the acidic ionic liquid 1-butyl-2-(4-sulfobutyl) imidazolium-*p*-toluenesulfonate, resulted in higher conversions of LA to 2-MTHF (92%) after 18 h at 160°C, 100 bar H_2 [142]. The active catalyst was proposed to be the tridentate Ru(II) hydride complex $[(MeCP_3^{Ph})RuH]^+$; however, an active neutral species cannot be ruled out. A detailed mechanistic analysis revealed a common pathway for the reduction the carbonyl functionality in intermediate aldehydes, ketones, lactones and carboxylic acids [155].

7 N-Triphos Complexes and Catalysis

While the tridentate ligand featuring an *ethylene* bridge between the apical nitrogen and phosphine moieties is very well studied [12, 67], the methylene-bridged N-triphos analogue $N(CH_2PPh_2)_3$ (NP_3^{Ph}) is less well known [156]. Despite its structural similarity to the well-known triphos, N-triphos has not been widely used as a tridentate ligand. Synthesis of this ligand and other derivatives is relatively straightforward and is achieved via a phosphorus-based Mannich reaction of hydroxymethylphosphines with ammonia. Alternatively, the hydroxymethylphosphine reagents can

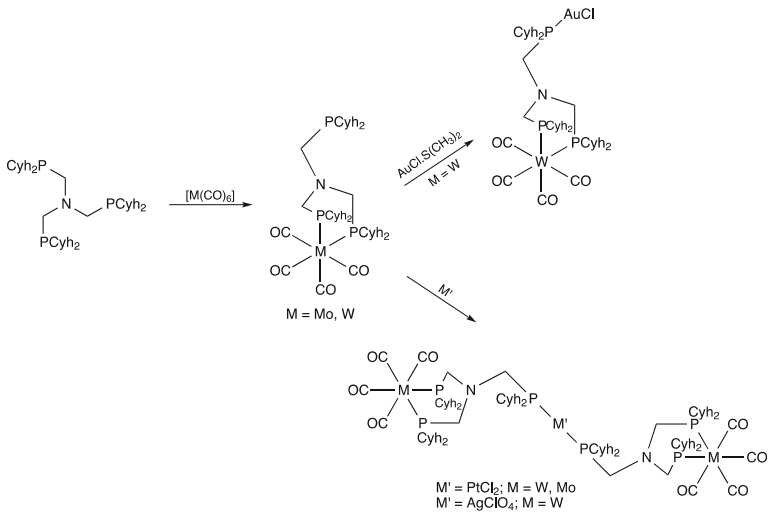

Scheme 10 Synthesis of tungsten–NP_3^{Cyh} complexes

be generated in situ from the corresponding air-stable phosphonium salts in the presence of base [157].

The coordination chemistry of N-triphos (NP_3^{Ph}) is similar to the parent triphos ligand and is known to form a series of facially capping complexes of the type [M(L)$_3$(κ^3-NP_3^R)] with Mo and W [156]. One of the key features of this N-triphos ligand system is the ease with which other phosphine derivatives can be prepared. For example, the bulky cyclohexyl (NP_3^{Cyh}) and tert-butyl (NP_3^{tBu}) derivatives of the N-triphos ligand are shown to significantly alter the coordination chemistry [157]. Coordination of NP_3^{Cyh} to molybdenum(0) and tungsten(0) carbonyls exclusively afforded bidentate, tetracarbonyl complexes with one arm of the tripodal ligand remaining uncoordinated (Scheme 10). The pendant arm was used to coordinate to different metals (gold, platinum and silver) affording hetero-multimetallic complexes (Scheme 10) [157].

Further derivatisation of the phosphine moieties was achieved through the use of chiral phospholane substituents: NP_3^{DMP} and NP_3^{DPP} (Fig. 22). Complexation of these ligands to the rhodium(I) precursor [Rh(cod)$_2$]BF$_4$ showed different coordination modes, with the less bulky NP_3^{DMP} coordinating through all three phosphine groups to afford [Rh(cod)(κ^3-NP_3^{DMP})], while the sterically cumbersome NP_3^{DPP} only through two: [Rh(cod)(κ^2-NP_3^{DPP})] (Scheme 11). DFT calculations confirmed this discrepancy to be steric in nature, as the theoretical tridentate complex [Rh(cod)(κ^3-NP_3^{DPP})] sits 65.7 kJ mol^{-1} higher in energy than its bidentate analogue, while the bidentate [Rh(cod)(κ^2-NP_3^{DMP})] sits 25.9 kJ mol^{-1} higher in energy than its isolated tridentate counterpart. [158] The pendant arm of [Rh(cod)(κ^2-NP_3^{DPP})] was coordinated to various gold salts, accessing hetero-bimetallic systems. Moreover, two trimetallic gold complexes of ligands NP_3^{DMP} and NP_3^{DPP} were synthesised, where each phosphine was coordinated to a separate AuCl unit

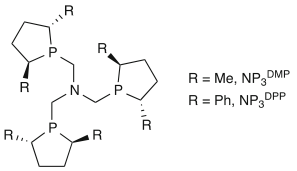

Fig. 22 Phospholane ligands NP_3^{DMP} and NP_3^{DPP}

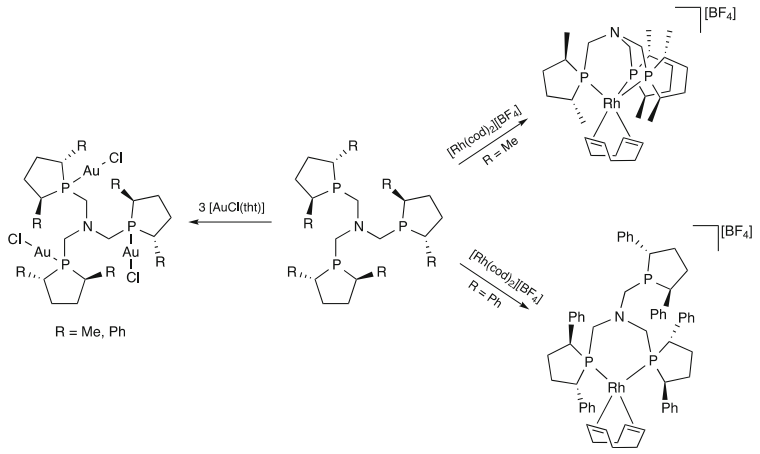

Scheme 11 Complexes of phospholane NP_3^{R} ligands

(Scheme 10) [159]. Both inter- and intramolecular aurophilic interactions were found in $[Au_3Cl_3(\mu^3{:}\kappa^1\text{-}NP_3^{DMP})]$ and $[Au_3Cl_3(\mu^3{:}\kappa^1\text{-}NP_3^{DPP})]$, respectively. The metallophilic interactions lead to a zigzag arrangement in the solid state of crystalline $[Au_3Cl_3(\mu^3{:}\kappa^1\text{-}NP_3^{DMP})]$ and intramolecular aggregation of $[Au_3Cl_3(\mu^3{:}\kappa^1\text{-}NP_3^{DPP})]$ in solution, even at low temperatures.

Similar to the reactivity observed on rhodium, the steric encumbrance of the triphosphine ligand affected the resultant geometry of ruthenium complexes. The reaction of less bulky NP_3^{iPr} or NP_3^{DMP} ligands with [Ru(methylallyl)$_2$(cod)] afforded $[Ru(tmm)(\kappa^3\text{-}NP_3^{R})]$ (R = ^{i}Pr, DMP), first by displacement of cod before further heating results in intramolecular deprotonation and formation of the tmm ligand (Scheme 12) [160]. On the other hand, the sterically larger NP_3^{DPP} afforded $[Ru(\kappa^3P{:}\kappa^2C\text{-}NP_3^{DPP})]$, in which dicyclometalation has occurred, displacing both cod and the in situ formed tmm ligand [161].

Ru–C bonds in cyclometalated complexes are readily cleaved, and thus the dicyclometalated ruthenium complex $[Ru(\kappa^3P{:}\kappa^2C\text{-}NP_3^{DPP})]$ was investigated for reactivity with both H_2 and Ph_2SiH_2 [161]. In the presence of H_2, the cyclometalated complex rapidly establishes an equilibrium between two species featuring both classical and nonclassical hydrides (Scheme 13). In the first instance, one Ru–C bond is cleaved and the vacant coordination site is filled with one hydride

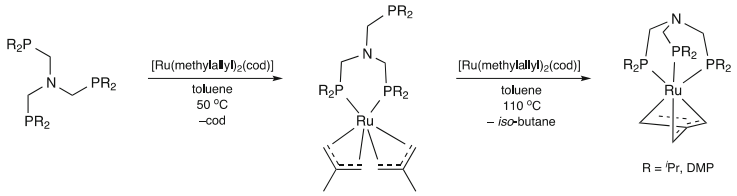

Scheme 12 Synthesis of [Ru(tmm)(κ^3-NP_3^R)] (R = ^{i}Pr, DMP)

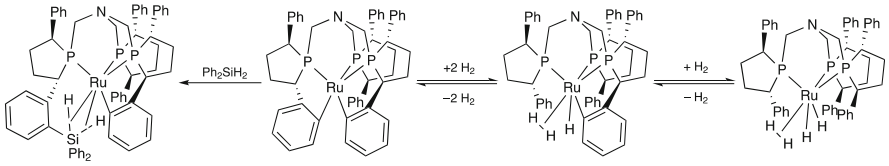

Scheme 13 Reactivity of [Ru(κ^3P:κ^2C-NP_3^{DPP})] with H_2 and Ph_2SiH_2

and one dihydrogen ligand. The second major species is formed after cleavage of both Ru–C bonds and their replacement with two hydrides and a single dihydrogen ligand. The equilibrium between the two compounds can be shifted by altering the H_2 pressure [161]. Interestingly, upon release of the H_2 pressure and after purging with argon, the starting complex, [Ru(κ^3P:κ^2C-NP_3^{DPP})], was obtained quantitatively, indicating complete reversibility of Ru–C bond cleavage.

Treatment of [Ru(κ^3P:κ^2C-NP_3^{DPP})] with Ph_2SiH_2 cleanly afforded the silyl dihydride complex [Ru(η^3-H_2SiPh_2)(κ^3P:κ^1C-NP_3^{DPP})] (Scheme 13), where the silane has inserted into the one Ru–C bond and coordinated to ruthenium in a rare η^3-H_2Si-binding mode. Complete oxidative addition of the silane had not occurred, suggesting that ruthenium complexes with EP_3^R-type ligands (E = PhB, N) can efficiently stabilise these transient species, but whether this is steric or electronic in nature is not certain [161].

Recently N-triphos ligands have been shown to be as active for the hydrogenation of levulinic acid as the carbon-centred analogues [162]. Using the preformed complex [$RuH_2(PPh_3)(NP_3^{Ph})$] as a pre-catalyst with $HNTf_2$ acting as the acidic component, conversion of LA to 2-MTHF was achieved in 87% selectivity, under relatively mild conditions compared to those using $MeCP_3^{Ph}$. Additionally, in the absence of any acidic component, almost quantitative conversion of LA to 1,4-PDO was observed under the same conditions, making this catalyst system highly versatile. A labile PPh_3 ancillary ligand was found to be critical for reactivity, as the relatively more robust [$RuH_2(CO)(NP_3^{Ph})$] is far less active [163].

8 Concluding Remarks

The coordination chemistry of multidentate phosphines continues to attract attention for synthesis of discrete monometallic and multimetallic complexes and clusters. The main driver for research in phosphine chemistry continues to be homogenous catalysis; however, other areas that exploit the photophysical properties of these complexes are also proving important. The coordination chemistry of these ligands is dictated by arrangement of their P atoms in either linear or branched arrangements, the length of bridging spacers and the appended R groups. We have emphasised the most commonly used multidentate phosphine ligands: linear etp, branched triphos and tetraphosphine $P^{Et}P_3$ that have recently been used to generate a range of complexes and catalytic active species. In particular, Ru–triphos and other derivatives of this ligand set that impose a strict facial coordination environment on Ru have been shown to be some of the most active homogeneous catalysts for the conversion of biomass-derived compounds and other challenging substrates such as esters and amides. The tetraphosphine $P^{Et}P_3$ has also proven to be an exceptionally good ligand for enforcing a strict coordination environment around Fe forming active homogenous catalysts for the dehydrogenation of formic acid and for other catalytic reactions. These three classes of multidentate phosphines will indeed continue to attract attention for their interesting coordination chemistries and as effective ligands for homogeneous catalysis.

References

1. van Leeuwen PWNM, Kamer PCJ, Reek JNH, Dierkes P (2000) Chem Rev 100:2741
2. Cotton FA, Hong B (1992) Polydentate phosphines: their syntheses, structural aspects, and selected applications. In: Lippard SJ (ed) Progress in inorganic chemistry, vol 40. Wiley, Hoboken
3. Tolman CA (1970) J Am Chem Soc 92:2956
4. Tolman CA, Seidel WC, Gosser LW (1974) J Am Chem Soc 96:53
5. Tolman CA (1977) Chem Rev 77:313
6. Müller TE, Mingos DMP (1995) Transition Met Chem 20(6):533
7. Tolman CA (1970) J Am Chem Soc 92:2953
8. Andersen NG, Keay BA (2001) Chem Rev 101:997
9. Allen DW, Taylor BF (1982) J Chem Soc Dalton Trans 51
10. Dyer PW, Fawcett J, Hanton MJ, Kemmitt RDW, Padda R, Singh N (2001) Dalton Trans 104
11. Tuxworth L, Baiget L, Phanopoulos A, Metters OJ, Batsanov AS, Fox MA, Howard JAK, Dyer PW (2012) Chem Commun 48:10413
12. Hierso JC, Amardeil R, Bentabet E, Broussier R, Gautheron B, Meunier P, Kalck P (2003) Coord Chem Rev 236:143
13. DuBois DL, Miedaner A, Haltiwanger RC (1991) J Am Chem Soc 113:8753
14. Chakraborty S, Blacque O, Fox T, Berke H (2014) Chem Eur J 20:12641
15. Arashiba K, Kinoshita E, Kuriyama S, Eizawa A, Nakajima K, Tanaka H, Yoshizawa K, Nishibayashi Y (2015) J Am Chem Soc 137:5666
16. Hanna BS, MacIntosh AD, Ahn S, Tyler BT, Palmore GTR, Williard PG, Bernskoetter WH (2014) Organometallics 33:3425

17. Balch AL, Catalano VJ (1992) Inorg Chem 31:2569
18. Fleischmann M, Duetsch L, Moussa ME, Schindler A, Balazs G, Lescop C, Scheer M (2015) Chem Commun 51:2893
19. Welsch S, Lescop C, Balazs G, Reau R, Scheer M (2011) Chem Eur J 17:9130
20. Takemura Y, Nakajima T, Tanase T (2009) Eur J Inorg Chem 2009:4820
21. Dau TM, Shakirova RJ, Domenech A, Jaenis J, Haukka M, Grachova EV, Pakkanen TA, Tunik SP, Koshevoy OI (2013) Eur J Inorg Chem 2013:4976
22. Bardaji M, Laguna A, Orera VM, Villacampa MD (1998) Inorg Chem 37:5125
23. Xiao H, Weng YX, Wong WT, Mak TCW, Che CM (1997) J Chem Soc Dalton Trans 221
24. Li D, Che CM, Peng SM, Liu ST, Zhou ZY (1993) J Chem Soc Dalton Trans 189
25. Lu W, Chan MCW, Cheung KK, Che CM (2001) Organometallics 20:2477
26. Shao P, Sun W (2007) Inorg Chem 46:8603
27. Kui SCF, Sham IHT, Cheung CCC, Ma HW, Yan B, Zhu N, Che CM, Fu WF (2007) Chem Eur J 13:417
28. Balch AL, Fossett LA, Olmstead MM (1987) Organometallics 6:1827
29. Balch AL, Linehan JC, Olmstead MM (1986) Inorg Chem 25:3937
30. Balch AL, Fossett LA, Linehan JC, Olmstead MM (1986) Organometallics 5:691
31. Balch AL, Fossett LA, Guimerans RR, Olmstead MM, Reedy PE, Wood FE (1986) Inorg Chem 25:1248
32. Balch AL, Linehan JC, Olmstead MM (1985) Inorg Chem 24:3975
33. Balch AL, Fossett LA, Guimerans RR, Olmstead MM (1985) Organometallics 4:781
34. Balch AL, Olmstead MM, Guimerans RR (1984) Inorg Chim Acta 84:L21
35. Balch AL, Guimerans RR, Olmstead MM (1984) J Organomet Chem 268:C38
36. Olmstead MM, Guimerans RR, Balch AL (1983) Inorg Chem 22:2473
37. Yamamoto Y, Kosaka Y, Tsutsumi Y, Sunada Y, Tatsumi K, Fumie T, Shigetoshi T (2004) Dalton Trans 2969
38. Yamamoto Y, Kosaka Y, Tsutsumi Y, Kaburagi Y, Kuge K, Sunada Y, Tatsumi Y (2004) Eur J Inorg Chem 2004:134
39. Kosaka Y, Shinozaki Y, Tsutsumi Y, Kaburagi Y, Yamamoto Y, Sunada Y, Tatsumi K (2003) J Organomet Chem 671:8
40. Zhang YL, Xu LJ, Zhang X, Wang JY, Li J, Chen ZN (2013) Inorg Chem 52:5167
41. Xu LJ, Wang JY, Zhang LY, Shi LX, Chen ZN (2013) Organometallics 32:5402
42. Xu LJ, Wang JY, Zhu XF, Zeng XC, Chen ZN (2015) Adv Funct Mater 25:3033
43. Krytchankou IS, Krupenya DV, Karttunen AJ, Tunik SP, Pakkanen TA, Chou PT, Koshevoy IO (2014) Dalton Trans 43:3383
44. Raoof F, Esmaeilbeig AR, Nabavizadeh SM, Hosseini FN, Kubicki M (2013) Organometallics 32:3850
45. Chen ZH, Zhang YL, Chen ZN (2012) Organometallics 31:256
46. Effendy C Pettinari, Pettinari R, Ricciutelli M, Skelton BW, White AH (2005) Inorg Chim Acta 358:4009
47. Ning Y, Sarjeant AA, Stern CL, Peterson TH, Nguyen SBT (2012) Inorg Chem 51:3051
48. Mukhopadhyay TK, Flores M, Feller RK, Scott BL, Taylor RD, Paz-Pasternak M, Henson NJ, Rein FN, Smythe NC, Trovitch RJ, Gordon JC (2014) Organometallics 33:7101
49. Mukhopadhyay TK, Feller RK, Rein FN, Henson NJ, Smythe NC, Trovitch RJ, Gordon JC (2012) Chem Commun 48:8670
50. Eckert NA, Dougherty WG, Yap GPA, Riordan CG (2007) J Am Chem Soc 129:9286
51. vom Stein T, Weigand T, Merkens C, Klankermayer J, Leitner W (2013) ChemCatChem 5:439
52. Suarez T, Fontal B (1988) J Mol Catal 45:335
53. van Engelen MC, Teunissen HT, de Vries JG, Elsevier CJ (2003) J Mol Catal A: Chem 206:185
54. Muller TE, Lercher JA, Van Nhu N (2003) AIChE J 49:214
55. Richmond E, Moran J (2015) J Org Chem 80:6922

56. Van Leeuwen PWNM, Roobeek CF (1985) J Mol Catal 31:345
57. Beck CM, Rathmill SE, Park YJ, Chen J, Crabtree RH, Liable-Sands LM, Rheingold AL (1999) Organometallics 18:5311
58. Schmitt DC, Lee J, Dechert-Schmitt AMR, Yamaguchi E, Krische MJ (2013) Chem Commun 49:6096
59. Zhao SB, Wang RY, Nguyen H, Becker JJ, Gagne MR (2012) Chem Commun 48:443
60. Shakirova JR, Grachova EV, Melnikov AS, Gurzhiy VV, Tunik SP, Haukka M, Pakkanen TA, Koshevoy IO (2013) Organometallics 32:4061
61. Shakirova JR, Grachova EV, Melekhova AA, Krupenya DV, Gurzhiy VV, Karttunen AJ, Koshevoy IO, Melnikov AS, Tunik SP (2012) Eur J Inorg Chem 2012:4048
62. Shakirova JR, Grachova EV, Gurzhiy VV, Koshevoy IO, Melnikov AS, Sizova OV, Tunik SP, Laguna A (2012) Dalton Trans 41:2941
63. Takahashi Y, Akita M, Moro-Oka Y (1997) Chem Commun 1557
64. Fornies J, Martinez F, Navarro R, Tomas M, Urriolabeitia EP (1994) J Chem Soc Dalton Trans 505
65. Mrutu A, William WN, Kemp RA (2012) Inorg Chem Commun 18:110
66. Fornies J, Navarro R, Urriolabeitia EP (1993) J Organomet Chem 452:241
67. Mayer HA, Kaska WC (1994) Chem Rev 94:1239
68. Cecconi F, Midollini S, Orlandini A, Sacconi L (1980) Inorg Chim Acta 42:59
69. Bianchini B, Ghilardi CA, Meli A, Midollini S, Orlandini A (1985) Inorg Chem 24:924
70. Broadwood-Strong GTL, Chaloner PA, Hitchcock PB (1993) Polyhedron 12:721
71. Mealli C, Ghilardi CA, Orlandini A (1992) Coord Chem Rev 120:361
72. Ghilardi CA, Midollini S, Moneti S, Orlandini A, Scapacci G, Traversi A (1990) J Chem Soc Dalton Trans 2293
73. Mellmann D, Barsch E, Bauer M, Grabow K, Boddien A, Kammer A, Sponholz P, Bentrup U, Jackstell R, Junge H, Laurenczy G, Ludwig R, Beller M (2014) Chem Eur J 20:13589
74. Boddien A, Mellmann D, Gaertner F, Jackstell R, Junge H, Dyson PJ, Laurenczy G, Ludwig R, Beller M (2011) Science 333:1733
75. Pouessel J, Jacquet O, Cantat T (2013) ChemCatChem 5:3552
76. Drake JL, Manna CM, Byers JA (2013) Organometallics 32:6891
77. Federsel C, Boddien A, Jackstell R, Jennerjahn R, Dyson PJ, Scopelliti R, Laurenczy G, Beller M (2010) Angew Chem Int Ed 49:9777
78. Wienhoefer G, Westerhaus FA, Jagadeesh RV, Junge K, Junge H, Beller M (2012) Chem Commun 48:4827
79. Wienhoefer G, Sorribes I, Boddien A, Westerhaus F, Junge K, Junge H, Llusar R, Beller M (2011) J Am Chem Soc 133:12875
80. Aizawa SI, Majumder A, Yokoyama Y, Tamai M, Maeda D, Kitamura A (2009) Organometallics 28:6067
81. Wan XK, Yuan SF, Lin ZW, Wang QM (2014) Angew Chem Int Ed 53:2923
82. Hewertson W, Watson HR (1962) J Chem Soc 1490
83. Bianchini C, Meli A, Peruzzini M, Vizza F, Zanobini F (1992) Coord Chem Rev 120:193
84. Phanopoulos A, Miller PW, Long NJ (2015) Coord Chem Rev 299:39
85. Chaplin AB, Dyson PJ (2011) J Organomet Chem 696:2485
86. Costello MT, Fanwick PE, Green MA, Walton RA (1992) Inorg Chem 31:2359
87. Bianchini C, Peruzzini M, Zanobini F (1993) J Organomet Chem 451:97
88. Ott J, Venanzi LM (1985) J Organomet Chem 291:89
89. Arif AM, Hefner JG, Jones RA, Whittlesey BR (1986) Inorg Chem 25:1080
90. Browning J, Penfold BR (1973) J Chem Soc Chem Commun 198
91. Dapporto P, Midollini S, Orlandini A, Sacconi L (1976) Inorg Chem 15:2768
92. Benelli C, Di Vaira M, Noccioli G, Sacconi L (1977) Inorg Chem 16:182
93. Janser P, Venanzi LM (1985) J Organomet Chem 296:229
94. Bianchini B, Masi D, Mealli C, Meli A, Sabat M, Vizza F (1988) Inorg Chem 27:3716
95. Klein HF, Montag J, Zucha U, Flörke U, Haupt HJ (1990) Inorg Chim Acta 177:35

96. Bianchini C, Marchi A, Marvelli L, Peruzzini M, Romerosa A, Rossi R, Vacca A (1995) Organometallics 14:3203
97. Heinze K, Huttner G, Zsolnai L, Schober P (1997) Inorg Chem 36:5457
98. Rupp R, Huttner G, Kircher P, Soltek R, Büchner M (2000) Eur J Inorg Chem 1745
99. Blackburn DW, Chi KM, Frerichs SR, Tinkham ML, Ellis JE (1988) Angew Chem Int Ed 27:437
100. Chatt J, Watson HR (1961) J Chem Soc 4980
101. Fox MA, Campbell KA, Kyba EP (1981) Inorg Chem 20:4163
102. Piana H, Schubert U (1991) J Organomet Chem 411:303
103. Walter O, Huttner G, Zsolnai L (1993) Z Naturforsch 48b:636
104. Ellermann J, Linder HA (1976) Z Naturforsch 31b:1350
105. Connolly J, Genge ARJ, Levason W, Orchard SD, Pope SJA, Reid G (1999) J Chem Soc Dalton Trans 2343
106. Kraihanzel CS, Maples PK (1976) J Organomet Chem 117:159
107. Ellermann J, Linder HA (1979) Z Naturforsch 34b:799
108. Cardoza LA, Angelici RJ (1999) Inorg Chem 38:1708
109. Suzuki T, Tsukuda T, Kiki M, Kaizaki S, Isobe K, Takagi HD, Kashiwabara K (2005) Inorg Chim Acta 358:2501
110. Bachechi F (1994) Acta Cryst C 50:1069
111. Suzuki T, Isobe K, Kashiwabara K, Fujita J, Kaizaki S (1996) J Chem Soc Dalton Trans 3779
112. Behrens H, Feilner HD, Lindner E (1971) Z Anorg Allg Chem 385:321
113. Ellermann J, Schindler JF (1975) Z Naturforsch 30b:914
114. Siegl WO, Lapporte SJ, Collman JP (1971) Inorg Chem 10:2158
115. Guilera G, McGrady GS, Steed JW, Burchell RPL, Sirsch P, Deeming AJ (2008) New J Chem 32:1573
116. Ellermann J, Schindler JF, Behrens H, Schlenker H (1976) J Organomet Chem 108:239
117. Johnston GG, Baird MC (1989) Organometallics 8:1894
118. Johnston GG, Hommeltoft SI, Barid MC (1989) Organometallics 8:1904
119. Allevi C, Golding M, Heaton BT (1987) J Organomet Chem 326:C19
120. Camalli M, Caruso F (1990) Inorg Chim Acta 169:189
121. Cain MF, Hughes RP, Glueck DS, Golen JA, Moore CE, Rheingold AL (2010) Inorg Chem 49:7650
122. Bruce MI, Zaitseva NN, Skelton BW, Somers N, White AH (2007) Inorg Chim Acta 360:681
123. Gambarotta S, Strologo S, Floriani C, Chiesi-Villa A, Guastini C (1984) Organometallics 3:1444
124. James SL, Mingos DMP, White AJP, Williams DJ (1998) Chem Commun 2323
125. Miller PW, Nieuwenhuyzen M, Xu X, James SL (2002) Chem Commun 2008
126. Wang XJ, Langetepe T, Fenske D, Kang BS (2002) Z Anorg Allg Chem 628:1158
127. Montes JA, Rodriguez S, Fernandez D, Garcia-Seijo MI, Gould RO, Garcia-Fernandez ME (2002) J Chem Soc Dalton Trans 1110
128. Fernandez EJ, Gimeno MC, Laguna A, Laguna M, Lopez-de-Luzuriaga JM, Olmos E (1996) J Organomet Chem 514:169
129. Sevillano P, Garcia ME, Habtemariam A, Parsons S, Sadler PJ (1999) Met Based Drugs 6:211
130. Ferrer M, Julia A, Rossell O, Seco M, Pellinghelli MA, Tiripicchio A (1997) Organometallics 16:3715
131. Hashimoto Y, Yoshinari N, Matsushita N, Konno T (2014) Eur J Inorg Chem 2014:3474
132. Rodriguez L, Lodeiro C, Lima JC, Crehuet R (2008) Inorg Chem 47:4952
133. Rodriguez L, Lima JC, Ferrer M, Rossell O, Engeser M (2012) Inorg Chim Acta 381:195
134. Teunissen HT, Elsevier CJ (1997) Chem Commun 667
135. Teunissen HT, Elsevier CJ (1998) Chem Commun 1367
136. Rosi L, Frediani M, Frediani P (2010) J Organomet Chem 695:1314
137. Núñez AA, Eastham GR, Cole-Hamilton DJ (2007) Chem Commun 3154

138. Coetzee J, Dodds DL, Klankermayer J, Brosinski S, Leitner W, Slawin AMZ, Cole-Hamilton DJ (2013) Chem Eur J 19:11039
139. Savourey S, Lefèvre G, Berthet JC, Cantat T (2014) Chem Commun 50:14033
140. Li Y, Sorribes I, Yan T, Junge K, Beller M (2013) Angew Chem Int Ed 52:12156
141. Sorribes I, Junge K, Beller M (2014) Chem Eur J 20:7878
142. Geilen FMA, Engendahl B, Harwardt A, Marquardt W, Klankermayer J, Leitner W (2010) Angew Chem Int Ed 49:5510
143. Geilen FMA, Engendahl B, Hölscher M, Klankermayer J, Leitner W (2011) J Am Chem Soc 133:14349
144. Boardman B, Hanton MJ, van Rensburg H, Tooze RP (2006) Chem Commun 2289
145. Zhang J, Leitus G, Ben-David Y, Milstein D (2006) Angew Chem Int Ed 45:1113
146. Constable DJD, Dunn PJ, Hayler JD, Humphrey GR, Leazer JL, Linderman RJ Jr, Lorenz K, Manley J, Pearlman BA, Wells A, Zaks A, Zhang TY (2007) Green Chem 9:411
147. Jacquet O, Frogneux X, Das Neves Gomes C, Cantat T (2013) Chem Sci 4:2127
148. Li Y, Fang X, Junge K, Beller M (2013) Angew Chem Int Ed 52:9568
149. Beydoun K, vom Stein T, Klankermayer J, Leitner W (2013) Angew Chem Int Ed 52:9554
150. Beydoun K, Ghattas G, Thenert K, Klankermayer J, Leitner W (2014) Angew Chem Int Ed 53:11010
151. Wesselbaum S, Moha V, Meuresch M, Brosinski S, Thenert KM, Kothe J, vom Stein T, Englert U, Hölscher M, Klankermayer J, Leitner W (2015) Chem Sci 6:693
152. Balaraman E, Gunanathan C, Zhang J, Shimon LJW, Milstein D (2011) Nat Chem 3:609
153. Huff CA, Sandford MS (2011) J Am Chem Soc 133:18122
154. Wesselbaum S, vom Stein T, Klankermayer J, Leitner W (2012) Angew Chem Int Ed 51:7499
155. vom Stein T, Meuresch M, Limper D, Schmitz M, Hölscher M, Coetzee J, Cole-Hamilton DJ, Klankermayer J, Leitner W (2014) J Am Chem Soc 136:13217
156. Märkl G, Jin GY (1981) Tetrahedron Lett 22:1105
157. Miller PW, White AJP (2010) J Organomet Chem 695:1138
158. JFillol JL, Kruckenberg A, Scherl P, Wadepohl H, Gade LH (2011) Chem Eur J 17:14047
159. Rodríguez LI, Roth T, Fillol JL, Wadepohl H, Gade LH (2012) Chem Eur J 18:3721
160. Scherl P, Kruckenberg A, Mader S, Wadepohl H, Gade LH (2012) Organometallics 31:7024
161. Scherl P, Wadepohl H, Gade LH (2013) Organometallics 32:4409
162. Phanopoulos A, White AJP, Long NJ, Miller PW (2015) ACS Catal 5:2500
163. Phanopoulos A, Brown NJ, White AJP, Long NJ, Miller PW (2014) Inorg Chem 53:3742

Struct Bond (2017) 171: 63–78
DOI: 10.1007/430_2015_175

Published online: 7 August 2015

Sigma Bonds as Ligand Donor Groups in Transition Metal Complexes

Robert H. Crabtree

Dedicated to Greg Kubas in recognition of his foundational contributions to the field

Abstract Covalent X–H bonds, particularly where X is H, C, B, and Si, can act as Lewis base ligands in forming metal complexes of general type $L_nM(H–X)$, where the M–H–X angle is strongly bent so that the coordination can best be considered as side-on. The binding is greatly enhanced by back donation from the metal into the X–H σ* orbital. This elongates and eventually breaks the X–H bond, leading to characteristic structural, physicochemical characteristics and alteration of the reactivity of the ligand. The requirement for back donation means that the appropriate L_nM fragment must usually have appreciable π donor character. Since the binding of the X–H bond to the metal center is relatively weak, and the binding of the deprotonated X^- group left behind is much stronger, the binding also facilitates proton loss from the X–H bond. This electron redistribution results in reactivity differences which may be exploited. The case of H_2 is treated in most detail in this review, because of its central place in the field.

Keywords Agostic complex · Dihydrogen complex · Sigma complex

Contents

R.H. Crabtree (✉)
Department of Chemistry, Yale University, 225 Prospect Street, New Haven, CT 06520-8107, USA
e-mail: robert.crabtree@yale.edu

Abbreviations

2e,3c	Two-electron three-center bonding
CD	Chatt–Dewar (bonding model)
Cy	Cyclohexyl
dppe	$Ph_2PCH_2CH_2PPh_2$
dppp	$Ph_2PCH_2CH_2CH_2PPh_2$
MCP	Metalacyclopropane (bonding model)
pz	Pyrazolyl
T_1	Spin–lattice relaxation time (in NMR spectroscopy)

1 Introduction

Werner introduced the coordination concept in which metal ions, in his case typically Co^{3+}, bind multiple weak bases such as NH_3 or Cl^- to give a coordination complex, such as $[Co(NH_3)_4Cl_2]Cl$. The extension of Lewis' two-electron covalent bond description to coordination complexes may be largely attributed to Sidgwick who proposed the dative covalent bond and expanded the inert gas rule to coordination complexes. In the 1950s, it became clear that ligand π bonding electrons, for example, of ethylene, could also form dative bonds if supplemented by π back donation effects. Extending this series from lone pair donors such as NH_3 through π bond donors such as C_2H_4 leads to σ bond donor ligands such as H_2 (Fig. 1). The study of the latter, most recently discovered ligand class of the three, has brought to light a wide variety of different X–Y σ complexes, where X can be a variety of groups and Y is typically H. Being so weakly basic, however, neither σ nor π electron donation alone is usually sufficient to produce a stable complex as illustrated by the fact that pure Lewis acidic metals such as Co(III) do not usually provide sufficient back bonding to form isolable complexes of this type. Only π

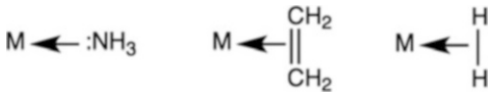

Fig. 1 Examples of the three general classes of ligand discussed here: a lone pair donor, a π bond donor, and a σ complex

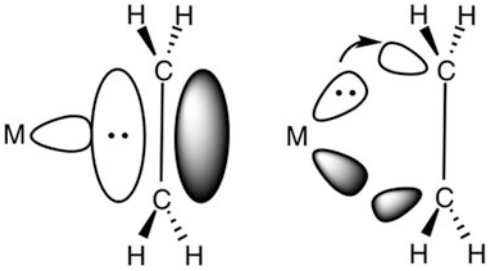

Fig. 2 Chatt–Dewar bonding model. Ligand π-to-metal d_σ donation (*left*) is accompanied by metal d_π-to-ligand π* back donation (*right*)

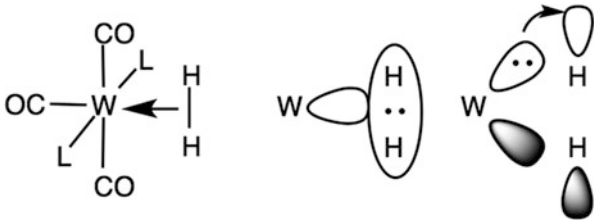

Fig. 3 The Kubas complex (L = PCy_3) and the proposed bonding scheme. Donation of the H_2 σ bonding pair into an empty d_σ orbital is accompanied by π back donation from a filled metal d_π orbital into the H_2 σ* orbital

basic metals such as Pt(II) or Ag(I) have filled d_π orbitals that are sufficiently basic to be able to back donate into the C=C π* orbital (Fig. 2) or H–H σ* orbital (Fig. 3) to a sufficient extent to permit formation of an isolable complex. The resulting Chatt–Dewar bonding model of Fig. 2 that combines ligand-to-metal σ donation with metal-to-ligand π back donation explains the observed pattern of stable π complex formation and can be extended to cover σ complexes as shown in Fig. 3 [1]. In this case the H_2 σ and σ* take on the donor and acceptor functions that are assigned to the C_2H_4 π and π* in the alkene case.

The most important and striking example of σ complexation emerged from Kubas' groundbreaking work on dihydrogen complexes. The H_2 ligand having no other electron pairs available than the H–H σ bonding pair means that no ambiguity is possible concerning the nature of the donor function of the ligand – it must be the H–H σ bonding electron pair, since no other electrons are present. Likewise, the only plausible acceptor orbital available to H_2 is the empty σ*, so that its role as the acceptor component of the back bond is equally clear. As a result, the Kubas complex, $[W(H_2)(CO)_3(PCy_3)_2]$ (Fig. 3), has become one of the most intensely studied complexes in the history of coordination chemistry [2]. Both C_2H_4 and H_2 bind in a side-on fashion so as to maximize favorable overlap for both σ and π components of the metal–ligand bond. The central place held by H_2 in the sigma complex field justifies our emphasis on this ligand in the present review.

Many readily available reviews, both early and recent, have appeared on different aspects of the field, so emphasis in this review is placed on fundamental points

as well as providing references for further study for the interested reader. Above all, Kubas' book, *Metal Dihydrogen and σ-Bond Complexes*, stands as the definitive account of relevant work up to 2000 and the point of departure for understanding the field [3]. Other notable reviews in the dihydrogen area include one by Kubas himself [4], a review by Heinekey and Oldham [5], a study of the reactivity of H_2 complexes by Jessop and Morris [6], a review of computational aspects [7], and one by the present author [8]. Beyond H_2, a number of reviews treat other classes of sigma complex, such as the study of alkane complexes by Hall and Perutz [9] and reviews of σ complexation in general [10, 11].

2 Historical Development

Although electron-deficient H-bridged structures were known from much earlier, as in B_2H_6 [12], the earliest case in which similar bridges were observed and such structures were found in transition metal complexes seems to be the 1960 report by Nöth and Hartwimmer [13] on $Cp_2Ti(H_2BH_2)$ in which a Ti–$(H)_2$–B bis-bridged structure was proposed on the basis of IR spectroscopy. Five years later, Kaesz, Dahl, and their coworkers were the first to identify B–H–M bridging crystallographically in $[Mn_3(CO)_{10}(H)(B_2H_6)]$, which has one Mn–H–Mn bridge and six B–H–Mn bridges [14]. The first example of a C–H bond bridging to a metal comes from a 1968 report by Trofimenko [15], who proposed that a C–H···M interaction is present in $[\{Et_2B(pz)_2\}Mo(CO)_2(\eta^3\text{-2-methylallyl})]$ based on the high-field signal from the bridging H in the ^{1}H NMR spectrum ($\delta = -2.4$ ppm) and evidence of a weakened C–H bond from the ν(C–H) bands at 2,664 and 2,704 cm^{-1} in the IR spectrum. Here, as in many other cases of σ complexes, the chelate effect must contribute to the stability of the X–H bond complex, but chelation is not always required. Binding of an alkane via a C–H–M bridge unassisted by any chelate effect was detected by Turner and coworkers from 1972 from the photogenerated unsaturated $M(CO)_5$ (M = Cr, Mo, W) fragment in a cryogenically cooled matrix [16–18]. Here, the low temperature lowered the entropic contribution to the free energy change for decomplexation. The long intervals between successive reports emphasize the slow development of the field at this time, perhaps because these structures were both rare and much harder to characterize than the classes of complexes typically investigated in this period. In addition, it was not clear that these complexes had any special importance or unusual reactivity.

The symbolic starting gun for a more rapid advance in the field was a 1983 review by Brookhart and Green, followed by other more extended ones on the same topic in 1988 and 2007 [19–21]. These authors gathered together numerous examples so as to draw attention to the generality and importance of C–H···M bridging. They also showed that if the C–H group were regarded as a 2e donor ligand, almost all of the known examples conformed to the conventional 18 valence electron count picture [1]. The term *agostic*, borrowed from ancient Greek, was also proposed by them for situations in which a C–H bond of a ligand interacts with the metal, but it is

now often extended to cover intramolecular σ complexation in general. The 1984 report by Kubas and coworkers [22] on the complex, $[W(H_2)(CO)_3(PCy_3)_2]$, brought the early period to a close by demonstrating that even H_2 could bind without any encouragement in the form of an electrostatic contribution to binding as in the case of borohydride complexes, or chelation, as in the case of the Trofimenko complex, or low temperature, as in the case of the matrix work. Kubas himself has covered the subsequent historical development of H_2 complexation in a very recent personal account [23].

3 Structure and Bonding

According to the bonding model of Fig. 3, the ligand-to-metal electron donation is expected to weaken but not break the H–H bond since the electron pair becomes located in an orbital that is bonding with respect to all three centers. In contrast, the back donation component does have the possibility of breaking the H–H bond by filling the H–H σ* orbital. Indeed, the Kubas complex itself is in equilibrium with the classical dihydride $[W(H)_2(CO)_3(PCy_3)_2]$ as a minority tautomer (Eq. 1).

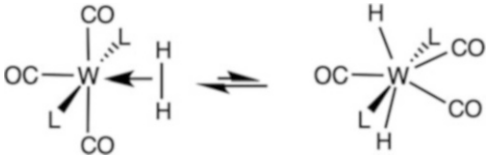

(1)

There is an interesting analogy between H_2 and C_2H_4 complexes in this context. $M(H_2)$ bonding corresponds to the Chatt–Dewar (CD) extreme model for $M(C_2H_4)$ bonding in which ligand-to-metal electron donation is dominant. A CD complex thus retains much of the original C=C double bond character as a result. In the metalacyclopropane (MCP) extreme of metal–alkene bonding, back donation becomes dominant. By filling the C=C π* orbital, this back donation breaks the C=C π bond but leaves the C–C σ bond unaffected. If a dihydrogen complex is formed, ligand-to-metal electron donation must dominate, and we have the analogue of a CD structure (Fig. 4, left). If back donation is dominant, we expect the H–H bond to be broken and we have the analogue of an MCP structure (Fig. 4, right).

Polyhydrides such as $[MH_4(PR_3)_3]$ (M = Fe, Ru, and Os) are relevant because they were originally assumed to be classical complexes with all-terminal metal–hydride bonds. The advent of H_2 complexes posed new questions in this area because a classical structure could no longer be safely assumed. Careful analysis of the $[MH_4(PR_3)_3]$ series by spectroscopy and in one case by neutron diffraction identified the Os complex as classical, having the structure that had always been assumed, but the Fe and Ru complexes as nonclassical, having the structure $[M'H_2(H_2)(PR_3)_3]$ (M′ = Fe, Ru). T_1 NMR data was particularly useful as a rapid

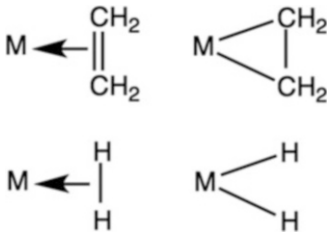

Fig. 4 The analogy between Chatt–Dewar alkene complexes and dihydrogen complexes (*left*) and metalacyclopropane alkene complexes and dihydride structures (*right*). In each case strong back donation breaks a bond within the ligand

way to help make the classical–nonclassical structural distinction, as is discussed in more detail below [24].

The typical H–H distance in a dihydrogen complex is 0.8–0.95 Å, but in rare cases much longer distances are found, typically 1–1.6 Å. These tend to appear where the back donation component of the M–L bonding is strong, and they have been termed stretched or elongated dihydrogen complexes or sometimes compressed dihydrides.

A general structural characteristic of σ complexation by X–H bonds to metals is the strongly bent X–H–M substructure that results. Of course, in most agostic cases, this can hardly be helped because of the constraints imposed on the X–H–M angle by chelation. Once again, the Kubas complex provided key evidence: although there are no constraints on the binding of the H_2 molecule, a side-on geometry is clearly preferred. This geometry implies that the metal is interacting with the electrons in the X–H bond and thus has to approach from the side, a geometry that also permits π back donation into the X–H σ* orbital.

Bond strengths are very variable depending on the situation, but, considering series of similar compounds, there is general trend toward weaker M–L bonds as we go from lone pair complexes to π complexes to σ complexes. For example, M–H bond strengths can easily lie in the range 50–70 kcal/mol, while M–(H_2) bond strengths are typically 15–25 kcal/mol [3]. These values also depend on the type of X–H bond considered. Alkane C–H bonds tend to bind more weakly and silane Si–H bonds more strongly than H_2, all else being equal. For example, in the well-studied $CpMn(CO)_2L$ series, where L is heptane, H_2 and Et_3SiH bind with solution ΔH values of 10, 14, and 24.4 kcal/mol, respectively [3].

Among possible X–H bonds that might form σ bond complexes, X is most commonly H, C, or Si, but apparently never N or O. The electronegativity difference between X and H must be a factor here. Electropositive elements are likely to form X–H bonds that are more basic and may even be polarized in the X^+–H^- direction.

Bridging systems of the type N–H···M do exist and might be thought of as σ complexes. In fact, closer examination suggests that these are in fact hydrogen bonds in which the proton acceptor component is the metal. As an indicator that this

is a more appropriate description, the N–H···M angle is close to linear, as required for hydrogen bonding, and not strongly bent, as is the case for σ complexation [25].

Back donation is not absolutely required for σ complexation, because in some cases, d^0 complexes can form σ complexes if the Lewis acidity of the metal fragment and the Lewis basicity of the ligand are sufficient. Cases have been discussed by Scherer, Eickerling, Roesky, and their coworkers [26].

4 Spectroscopy

Although both σ and π components of the M–H_2 bond are expected to reduce the H–H bond order, the σ component is expected to be less effective because the H–H bonding pair is delocalized over three centers, retaining much H–H bonding character in the bound state. The π component is much more effective – indeed in the extreme, the H–H bond can be completely broken in an oxidative addition (Eq. 1). An estimate of the H–H bond order reduction on complexation can be obtained from the ^{1}J(H,D) coupling constant in the proton NMR spectrum. This takes a value of 43 Hz for free H–D, but the upper limit of the range seen in complexes is 32 Hz. The bond order in such a case, where back donation is minimal, is thus ca. 75% of that in free H_2; the lower end of the usual ^{1}J(H,D) range is ca. 15 Hz; thus ca. 35% of the H–D bond remains in these cases, where back donation is evidently much more important [3].

It might be thought that the effect of binding of H_2 to a metal on the H–H distance would most directly be seen in the structural data. Hydrogen atoms are poorly located by X-ray methods, particularly in the presence of a heavy atom. For accurate localization of the H atoms, neutron diffraction would be the natural choice but few such studies are extant. In addition, the libration of the H_2 molecule in the bound state complicates the interpretation. Libration leads to a banana-shaped distribution of the H atoms, but the usual structure solution strategy models the hydrogens with ellipsoidal atom distributions. If no account is taken of libration, the result is that the apparent H–H bond distance appears shorter than the real value. Of course attempts have been made to apply a librational model, but even when this is considered, a tumbling motion of the H_2 molecule in the M–H–H plane may complicate the picture. In some cases, a fourfold potential is present at the H_2 binding site in which case hopping can occur between two equally occupied sites 90° apart, another factor that can complicate the interpretation [6].

As a result of the structural problems mentioned, the ^{1}H NMR spectral data seem best adapted to provide access to the degree of H–H bond order reduction in the bound state. In H_2 itself, the equivalence of the two nuclei prevents us seeing the H, H coupling, but in a strategy first introduced by Kubas, the H–D molecule provides the needed information. In the free state, the H–D molecule has a ^{1}J(H,D) coupling constant of 43 Hz, but on binding this value is strongly reduced. If we take the reduction of the ^{1}J(H,D) value in the bound state as a measure of the reduction in the H–D bond order, the usual range of 15–32 Hz found in typical H_2 complexes is

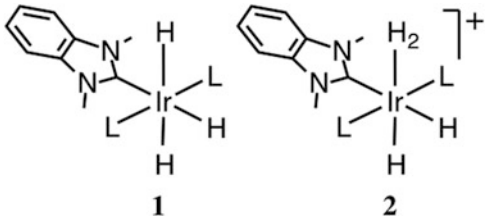

Fig. 5 Closely analogous classical (**1**) and nonclassical (**2**) hydrides with T_1 (min) values of 350 ms (**1**) and 30 ms (**2**) (L = PPh_3)

consistent with a bond order range that seems entirely reasonable: 0.35–0.75 versus 1.0 for free H–D. Morris [6] has proposed an empirical equation that reliably connects measured ^{1}J(H,D) values in Hz with predicted H–D bond distances in Å (Eq. 2):

$$d_{HH} = 1.42 - 0.0167\left\{^1\mathrm{J(H,D)}\right\} \tag{2}$$

A second approach via NMR involves measurement of the minimum T_1 at variable temperature for the M–H_2 signal. The proximity of the two H nuclei leads to exceptionally fast T_1 relaxation, a typical value being 30 ms for M–H_2 versus 300 ms or more for a terminal M–H proton. The requirement for variable temperature has to do with adjusting the tumbling rate for the molecule to maximize the T_1 relaxation, thus making the data comparable across different classes of H_2 complex. Applying standard equations to the T_1 data allows estimates to be made of the H–H bond distances, as discussed in detail in the literature [6].

An example of the utility of this method is shown by the closely analogous hydrides **1** and **2** shown in Fig. 5. The ^{1}J(H,D) criterion cannot be used because the system is very fluxional, having only one hydride peak at all accessible temperatures. The great difference in the T_1 (min) values for the two cases defines the situation clearly. The classical trihydride, **1**, has a T_1 (min) value of 350 ms, consistent with other similar classical hydrides. In contrast, the nonclassical dihydrogen complex, **2**, as a T_1 (min) value of 30 ms is a result of rapid relaxation of the H_2 protons. The dependence of the T_1 (min) on the inverse sixth power of the H–H distance is the key factor that makes the method so sensitive to the presence of a bound H_2 molecule. Computational data support the assignment and confirm the low barrier for fluxionality (5 kcal/mol) and the short H–H distance 0.82 Å, compared to 0.74 Å in free H_2 and >1.8 Å in classical hydrides [27]. It might be thought that the method could be vitiated if H_2 dissociates reversibly from a classical hydride. Such is not the case, however, because free H_2 has a long relaxation time as a result of the much more rapid molecular motion of the free molecule, so any exchange with free H_2 would lengthen the T_1.

Vibrational spectroscopy is not often satisfactory because the H–H stretch is only fully allowed in the Raman spectrum, but attempts to obtain Raman spectra from H_2 complexes have not generally been successful, probably because the laser beam results in photolytic decomposition. Infrared data have been obtained for many H_2 complexes even though the H–H stretch is forbidden in the IR, because

mixing with adjacent allowed vibrations, such as a *cis* CO in Kubas' complex, does give it some intensity. Of course, the vibrational coupling needed to obtain some intensity means that the position of the resulting band is not that of a "pure" H–H vibration. Nevertheless, the IR data is broadly in agreement with the NMR results, with the H–H band for Kubas' complex itself coming at 2,690 versus 4,161 cm^{-1} for free H_2 (Raman) [3].

Bakhmutov has obtained quadrupolar coupling constant (DQCC) parameters from solid-state ^2H NMR data of a number of D_2 complexes. Combined with density functional theory calculations, this work led to a criterion for using the relaxation data to distinguish rapidly spinning dihydrogen ligands from nonrotating ones. Not only free rotation but librations and 180° jumps in a twofold potential were also considered in the analysis ([28] and references cited).

Inelastic neutron scattering (INS) has also given a valuable insight into the rotational barrier for H_2 complexes. Features in the INS spectrum that are associated with rotational tunneling can give the rotational barrier height. For the *trans*-$[Ru(H_2)(H)(dppe)_2]^+$ cation, for example, the barrier proved to be ~1.4 kcal/mol; this shows how INS can make low barrier heights accessible, ones in a range of values not accessible by other means ([29] and references cited).

5 Reactivity of H_2 Complexes

Sigma complexes are important intermediates in two main reaction pathways. In the first, sigma complexation leads onto oxidative addition as in Eq. (1), a pathway that is commonly observed when back donation is predominant. Since this is a well-known reaction [3], we do not discuss it in detail here. In the second, binding of the H–H bond to the metal acidifies the system to such an extent that a proton is easily lost [30]. This reactivity pattern tends to be seen when the back donation is relatively less important than the direct ligand-to-metal σ bonding. The H_2 ligand is thus depleted of electron density, leading to its acidification. Breaking the H–H bond is compensated thermodynamically by tight binding to the metal of the H^- that is left behind as well as bond formation between the relevant base, Q, and the newly released proton to form a new Q–H bond. This acidification is very much greater than is the case for classical ligands such as NH_3 where the M–NH_3 and M–NH_2 bond strengths do not differ as much as in the case of, say, M(H–H) and M–H, where the M–(H_2) bond markedly weaker than the product M–H bond. The acidification can be modest, as in $[RuH_2(H_2)(PPh_3)_3]$ where the pK_a is 36 compared to ~50 for the free H_2 ligand. For cationic, electrophilic metals with weak back donation power, the acidification can be dramatic, for example, $[OsH_2(CO)(dppp)_2]^{2+}$ has a pK_a value of −5.7 [3]. This step may be involved in H_2 activation by Fe or Ni sites in hydrogenase enzymes [31].

One of the consequences of the acidification of H_2 on binding is the availability of new mechanistic pathways for catalysis. For example, classical mechanisms of homogeneous catalysis are not very effective for reduction of *N*-heterocycles.

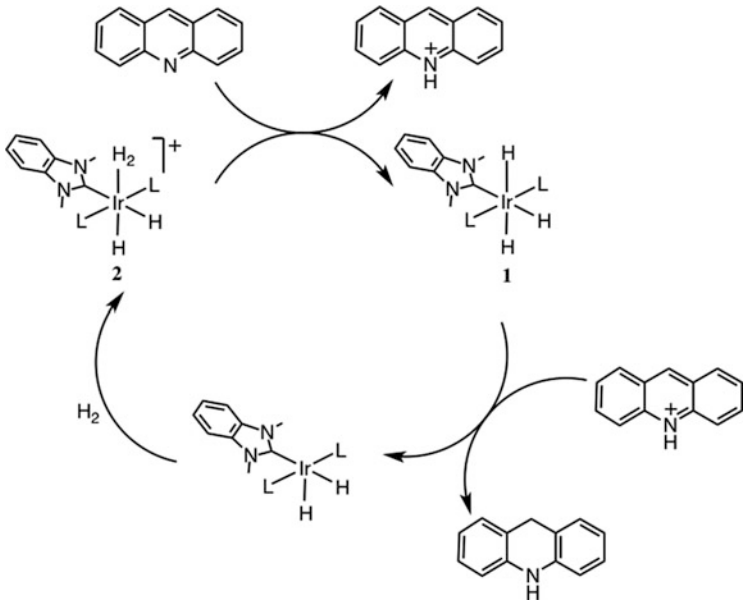

Fig. 6 A reactivity consequence of the acidification of H_2 on binding. The H_2 ligand of catalyst **2** protonates the acridine substrate, activating it for subsequent hydride transfer from trihydride **1**

Normally, this requires either high pressures or else high temperatures or even both together. In recent work, complex **2** of Fig. 6 has been shown to bring about the hydrogenation of *N*-heterocycles such as acridine by a novel outer sphere mechanism (Fig. 6) [27]. The dihydrogen complex first protonates the acridine nitrogen and in that way activates the heterocycle for the next step: rate-determining hydride transfer from the trihydride **1** to the acridinium ion to form the product shown. Notably, only the *N*-heterocyclic ring of the substrate is reduced. This pathway has also been implicated in the reverse reaction, dehydrogenation of the hydrogenated *N*-heterocycle [32], a pathway that may have value as an approach to hydrogen storage in liquid organic heterocycles [33].

6 Agostic Complexes and Their Reactivity

The term agostic as applied to metal complexes was originally restricted to intramolecular cases in which a C–H bond of a bound ligand forms a sigma complex. In the commonest case, a β-C–H bond of an alkyl complexes to the metal. The term is now sometimes applied to intramolecular cases as well, in which case it becomes synonymous with the term "C–H sigma complex."

As for dihydrogen complexes, the interest in agostic complexes goes beyond structure and bonding – they also show useful reactivity analogous to the two pathways discussed for H_2. When back donation is dominant, the C–H bond can be broken in an oxidative addition to form an C–M–H grouping (Eq. 3). On the other hand, if the Lewis acidity of the metal is dominant, the coordinated C–H bond is depleted of electron density and thus can now be broken in a different way, via proton abstraction by a suitable base, leaving the residual anionic carbon fragment directly bound to the metal (Eq. 4) and possibly also in C–H activation by the Shilov Pt(II) catalyst [34]. Sigma complexes are thus plausible waypoints on two related pathways of central importance in organometallic catalysis: concerted oxidative addition and heterolytic cleavage of X–H bonds.

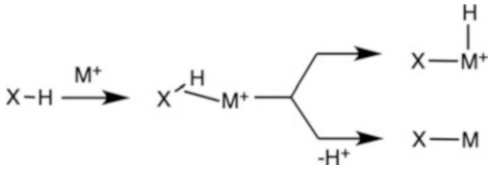

(3, 4)

Reactivity can also be affected by the propensity of a given system to form agostic structures. Beta elimination plausibly passes through an agostic structure on the way to the transition state; thus, whatever favors or disfavors an agostic structure should favor or disfavor beta elimination. Hartwig [35] has noted that in similar complexes, beta elimination of an NMe_2 group is much slower than of an analogous $CHMe_2$ group. This observation is consistent with the idea that the amido group has a lower tendency to become agostic because the N lone pair is an alternative donor to the metal that can outcompete the C–H bond, particularly because the effective electronegativity of the C of the agostic C–H bond in question is higher than in the isopropyl case, and so the amido C–H bond is less Lewis basic. Scherer et al. have verified the lower agostic tendency of the amido complex versus the ethyl case in $CpTiCl_2(XMe)$ ($X = CH_2$ or NMe) [26].

Beyond the more common β-agostic structures mentioned above, α-agostic structures are also possible. In this case, one α-C–H bond, for example, of a M–Me group, swings toward the metal and binds. These structures have special importance in metallocene polymerization catalysis, where the resulting distortion of the M–Me system is believed to facilitate alkene insertion, the key step in alkene polymerization [36, 37].

Not all apparent agostic complexes are authentic; however, where the H atom of our X–H bond is close to a metal center, σ complexation might well be suspected. Exceptions exist, however. One is the case of hydrogen bonding where a complex may contain a close M···H interaction in an M···H–N,O grouping. Instead of being bound side-on, however, as in the 2e,3c sigma complexes we have been discussing,

the OH or N–H unit is in this case bound end-on in an overall linear arrangement as expected for a four-electron, three-center hydrogen bond [25].

7 Borane and Boryl σ Complexes

Borane and borohydride complexes with M–H–B bridges have been reviewed by Ephritikhine [38] and by Smith [39]. Another example occurs in the series $[(H)_2Cl(PMe_3)_2M(\sigma\text{-H–BR})]$ (M = Fe, Ru, Os; R = OMe, NMe_2, Ph), where a boryl ligand becomes α agostic by interaction of a B–H bond with the metals. Computational work has given a detailed account of the bonding [40].

8 Silane σ Complexes

Silane complexation has been reviewed by Lin [41]. Silanes, as intrinsically stronger σ donors, are ligands that do not require chelation for stability. They also adopt a canted side-on structure in their unconstrained σ complexes, as in the example shown in Fig. 7. This canting of $R_3Si–H$ is no doubt a result of the greater size of the R_3Si unit versus the H atom. Silane σ complexes show a wide range of Si–H distances, presumably because the low-energy Si–H σ* orbital more readily accepts back donation than the higher-lying H–H σ* and the stretched variant structure is more common than for H_2. For example, compared to the ca. 1.5 Å bond length typical of free Si–H bonds, the bound form shows distances all the way from 1.6 to 2.5 Å, the latter being oxidative addition products with significant Si···H interactions. These interactions are often attributed to the facility with which Si becomes hypervalent [42].

A novel reactivity pathway is apparent for silane σ complexes having a weak back donation component to the bonding. In such a case, nucleophilic attack at Si can transfer the $\{SiR_3\}^+$ group to the nucleophile, leaving a hydride behind on the metal. Thus, a number of catalysts can mediate silane alcoholysis in alcohol solvents, where the alcohol is also the nucleophile [43].

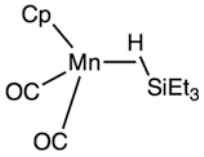

Fig. 7 A typical silane complex, showing the canted structure and the absence of chelation (Cp = C_5H_5)

9 C–C Agostic Complexes and Related Species

So far, we have considered only X–H bonds, never X–Y bonds (X,Y≠H), a point that requires a deeper look. The fact that H in X–H has no lone pairs or substituents other than X means that the back bonding into the X–H σ* is relatively unhindered because the side-on approach suffers from minimal steric opposition. In addition, there is no lone pair on H that could outcompete σ complexation. As soon as we move to an X–Y system, these favorable factors are typically eliminated, although the formation of X–Y σ complexes is not completely ruled out. In the most important case of C–C agostic species, a very recent comprehensive review is available [44]. Notably, Weller and coworkers have identified cases where an agostic C–C is present [45–47]. Not only is the C–C bond close to what would otherwise be a 16e metal (*d*Rh–C = 2.352(3), 2.369(3) Å), but the C–C bond itself is significantly elongated to 1.604(4) Å, and the agostic carbons show significant J coupling to Rh in the ^{13}C NMR spectrum (J(Rh,C) = 9 Hz). A number of Milstein's pincer ligands also show evidence of a weaker level of agostic C–C bonding [48, 49].

In another class of agostic complex, even though a ligand C–C bond is not only close to a metal but also oriented side-on, closer examination may indicate that the grouping is merely sterically enforced and does not represent a true attractive interaction. Such is the case for $[(C_5H_4MeEt)Ir(PPh_3)_2]BF_4$ (**3**), for example [50].

3

10 Conclusion and Outlook

In spite of its relatively recent discovery, sigma complexation has already been identified in thousands of cases. In some of these, this binding facilitates novel reactivity pathways of great importance. Alkene polymerization is perhaps the most important of these, but Shilov chemistry [34, 51] and heteroarene hydrogenation illustrate the wide variety of possibilities already identified. It is likely that further discoveries will include the finding that sigma complexation plays a key role in known reactions of as yet unknown mechanisms. In other cases, it should be possible to use these new structural types in a designed way to accomplish novel goals.

References

1. Crabtree RH (2013) The organometallic chemistry of the transition metals. Wiley-VCH, Hoboken
2. Kubas GJ (2007) Chem Rev 107:4152
3. Kubas GJ (2001) Metal dihydrogen and σ-bond complexes. Kluwer/Plenum, New York
4. Kubas GJ (1988) Acc Chem Res 21:120
5. Heinekey DM, Oldham WJ (1993) Chem Rev 93:913
6. Jessop PG, Morris RH (1992) Coord Chem Rev 121:155
7. Maseras F, Lledos A, Clot E, Eisenstein O (2000) Chem Rev 100:601
8. Crabtree RH (1990) Acc Chem Res 23:95
9. Hall C, Perutz RN (1996) Chem Rev 96:3125
10. Crabtree RH (1993) Angew Chem Int Ed 32:789
11. McGrady GS, Guilera G (2003) Chem Soc Rev 32:383
12. Bauer SH (1937) J Am Chem Soc 59:1096
13. Nöth R, Hartwimmer R (1960) Chem Ber 93:2238
14. Kaesz HD, Fellman W, Wilkes GR, Dahl LF (1965) J Am Chem Soc 87:2753
15. Trofimenko S (1968) J Am Chem Soc 90:4754
16. Graham MA, Turner JJ, Poliakoff M, Perutz RN (1972) J Organomet Chem 34:C34
17. Poliakoff M, Turner JJ (1974) Dalton Trans 1974:2276
18. Perutz RN, Turner JJ (1975) J Am Chem Soc 97:4791
19. Brookhart M, Green MLH (1983) J Organomet Chem 250:395
20. Brookhart M, Green MLH, Wang LL (1988) Prog Inorg Chem 36:1
21. Brookhart M, Green MLH, Parkin G (2007) Proc Natl Acad Sci U S A 2007:6908
22. Kubas GJ, Ryan RR, Swanson BI, Vergamini PJ, Wasserman HJ (1984) J Am Chem Soc 106:451
23. Kubas GJ (2014) J Organomet Chem 751:33
24. Crabtree RH, Hamilton DG (1986) J Am Chem Soc 108:3124
25. Yao W, Eisenstein O, Crabtree RH (1997) Inorg Chim Acta 254:105
26. Scherer W, Wolstenholme DJ, Herz V, Eickerling G, Brück A, Benndorf P, Roesky PW (2010) Angew Chem Int Ed 49:2242
27. Dobereiner GE, Nova A, Schley ND, Hazari N, Miller SJ, Eisenstein O, Crabtree RH (2011) J Am Chem Soc 133:7547
28. Bakhmutov VI (2004) Magn Reson Chem 42:66
29. Albinati A, Klooster WT, Koetzle TF, Fortin JB, Ricci JS, Eckert J, Fong TP, Lough AJ, Morris RH, Golombek AP (1997) Inorg Chim Acta 259:351
30. Esteruelas MA, Oro LA (1998) Chem Rev 98:577
31. Greco C, Zampella G, Bertini L, Bruschi M, Fantucci P, De Gioia L (2007) Inorg Chem 46:108
32. Manas MG, Sharninghausen LS, Lin EB, Crabtree RH (2015) J Organomet Chem doi:10.1016/j.jorganchem.2015.04.015
33. Crabtree RH (2008) Energy Environ Sci 1:134
34. Crabtree RH (2004) J Organomet Chem 689:4083
35. Hartwig JF (1996) J Am Chem Soc 118:7010
36. Grubbs RH, Coates GW (1996) Acc Chem Res 29:85
37. Piers WE, Bercaw JE (1990) J Am Chem Soc 112:9406
38. Ephritikhine M (1997) Chem Rev 97:2193
39. Smith MR (1999) Prog Inorg Chem 48:505
40. Pandey KK (2012) Dalton Trans 41:3278
41. Lin ZY (2002) Chem Soc Rev 31:239
42. Nikonov GI (2001) J Organomet Chem 635:24
43. Luo XL, Crabtree RH (1989) J Am Chem Soc 111:2527
44. Etienne M, Weller AS (2014) Chem Soc Rev 43:242

45. Brayshaw SK, Green JC, Kociok-Köhn G, Sceats EL, Weller AS (2006) Angew Chem Int Ed 45:452
46. Brayshaw SK, Sceats EL, Green JC, Weller AS (2007) Proc Natl Acad Sci U S A 104:6921
47. Chaplin AB, Weller AS (2013) J Organomet Chem 730:90
48. Vigalok A, Rybtchinski B, Shimon LJW, Ben-David Y, Milstein D (1999) Organometallics 18:895
49. van der Boom ME, Milstein D (2003) Chem Rev 103:1759
50. Maseras F, Crabtree RH (2004) Inorg Chim Acta 357:345
51. Goldshleger NF, Shteinman AA, Shilov AE, Eskova VV (1972) Zh Fiz Khim 46:1353

Struct Bond (2017) 171: 79–140
DOI: 10.1007/430_2015_206

Published online: 19 March 2016

The Covalent Bond Classification Method and Its Application to Compounds That Feature 3-Center 2-Electron Bonds

Malcolm L.H. Green and Gerard Parkin

Abstract This article provides a means to classify and represent compounds that feature 3-center 2-electron (3c–2e) interactions according to whether (1) the two electrons are provided by one or by two atoms; (2) the central bridging atom provides two, one, or zero electrons; and (3) the interaction is open or closed. Class I 3c–2e bonds are defined as those in which two atoms each contribute one electron to the 3-center orbital, while Class II 3c–2e bonds are defined as systems in which the pair of electrons are provided by a single atom. The use of appropriate structure-bonding representations enables the $[ML_lX_xZ_z]$ covalent bond classification of the element of interest to be evaluated. This approach is of considerable benefit in predicting metal–metal bond orders that are in accord with theory for dimetallic compounds that feature bridging hydride and carbonyl ligands.

Keywords Agostic interaction • Bridging alkyl • Bridging carbonyl • Bridging hydride • 3c–2e interaction • σ-Complex

Contents

M.L.H. Green (✉)
Inorganic Chemistry Laboratory, South Parks Road, Oxford OX1 3QR, UK
e-mail: malcolm.green@chem.ox.ac.uk

G. Parkin (✉)
Department of Chemistry, Columbia University, New York NY 10027, USA
e-mail: parkin@columbia.edu

1 Introduction

Following the classic 1916 paper by Lewis on "The Atom and the Molecule" [1–3], the ability to represent molecules by so-called Lewis structures [4], in which a 2-center 2-electron (2c–2e) bond is illustrated as a solid black line between two atoms, must be regarded as one of the most important developments in molecular chemistry over the past 100 years. Despite its importance and the elegance of its simplicity, however, the limitations of the 2c–2e bond as a bonding model are well known, such that many molecules, as exemplified by B_2H_6,[1] must be represented in terms of multicenter bonding. Although the nature of such compounds is best analyzed by the application of theoretical methods, this approach lacks the simplicity of allowing one to evaluate the chemical reasonableness of a molecule by employing simple electron counting procedures, such as the octet [2, 3, 8, 9][2] and 18-electron [8, 11, 12] rules. However, despite the fact that the bonding in such compounds may be highly delocalized, it can often be expressed in terms of a combination of 2-center 2-electron and 3-center 2-electron (3c–2e) interactions. Therefore, we describe herein ways to represent various classes of 3-center 2-electron (3c–2e) interactions such that they can be used in conjunction with the covalent bond classification (CBC) method for analyzing molecules [13–16].

2 The Covalent Bond Classification Method: A Synopsis

Although covalent molecules are often classified in terms of the oxidation states of the atoms of interest, it is evident that this approach has a number of shortcomings. For example, since the oxidation state corresponds to the charge on *an isolated atom, with no ligands attached*, the assigned values often either convey no useful chemical information or can result in misleading interpretations [13–17]. In contrast to the oxidation state approach, however, which focuses on the charge on an isolated atom, the covalent bond classification (CBC) method evaluates a molecule

[1] It is interesting to note that the bridged structure of B_2H_6 was first proposed in 1943, 27 years after Lewis' introduction of the 2c–2e bond and only 3 years prior to his death; see [5–7].

[2] Kossel also recognized the tendency for atoms to form ions with the adjacent noble gas configuration but did not extend this concept to the formation of molecules; see [10].

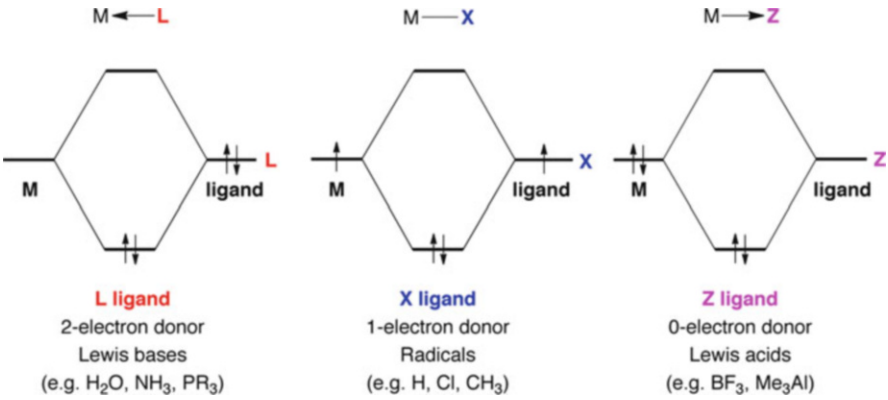

Fig. 1 The covalent bond classification (CBC) of L, X, and Z ligands. Note that the ligands are always classified in their neutral forms. The metal, ligand, and metal–ligand orbitals are arbitrarily placed at the same respective energies

by identifying the number and types of bonds that surround the element of interest (M). As such, by evaluating the *intact molecule*, the classification provides a more comprehensive description of the molecule than that which is provided by the oxidation state.

The basic premise of the CBC method is that many covalent molecules can be satisfactorily represented in terms of 2-center 2-electron bonding interactions in which the neutral monodentate ligands may contribute either two (L), one (X), or zero (Z) electrons to the bonding orbitals. The molecular orbital representations of these interactions are illustrated in Fig. 1, while representative examples of L-, X-, and Z-type ligands are listed in Table 1.[3] Thus, (1) L-type ligands (electron pair donors) are neutral molecules that have available lone pairs and are Lewis bases (e.g., H_2O, H_3N, and R_3P), (2) Z-type ligands (electron pair acceptors) are neutral molecules that exist as Lewis acids (e.g., BF_3) [25, 26], and (3) X-type ligands (one-electron donors) are neutral molecules that are radicals (e.g., $H^{\bullet}$, $Cl^{\bullet}$, and $H_3C^{\bullet}$).

Interactions involving X-type ligands correspond to M–X normal covalent bonds, whereas those involving L- and Z-type ligands correspond to dative covalent bonds [13, 27] and are represented with the use of arrows, as either M←L or M→Z. In addition to representing a dative bond with an arrow, it can also be represented as a line with formal charges,[4] i.e., $M^- - L^+$ and $M^+ - Z^-$ (Fig. 2); however, it must be emphasized that, despite these different appearances, they correspond to exactly the same electronic structure and are *not* resonance structures [28]. For example,

[3] For examples of textbooks that employ the classification of ligands as L, X, or Z type, see [18–24].

[4] The formal charge is the charge remaining on an atom when all ligands are removed homolytically. See [17].

Table 1 Classifications of some common ligands

Ligand	CBC description	Electron donor number
PR_3	L	2
H	X	1
R	X	1
BR_3	Z	0
AlR_3	Z	0
η^2-C_2H_4	L[a]	2
η^3-C_3H_5	LX	3
η^4-C_4H_6	L_2[a]	4
η^4-C_4H_4	LX_2	4
η^5-C_5H_5	L_2X	5
η^6-C_6H_6	L_3[a]	6
η^7-C_7H_7	L_2X_3	7
η^8-C_8H_8	L_3X_2	8
[κ^3-$Tp^{R,R'}$]	L_2X	5
[κ^1-OC(O)Me]	X	1
[κ^2-O_2CMe]	LX	3
CO	L[a]	2
NO	X[a] (bent)	1
	X_3 (linear)	3
O	Z	0
	X_2	2
	LX_2	4
N	X_3	3
OR	X (bent)	1
	LX (bent)	3
	L_2X (linear)	5
NR	X_2 (bent)	2
	LX_2 (linear)	4
NR_2	X (pyramidal)	1
	LX (planar)	3
CR_2	X_2 (Schrock alkylidene)	2
	L[a] (Fischer carbene)	2
CR	X_3	3

[a]These classifications pertain to the *primary* bonding interactions. However, some ligands (e.g., C_2H_4 and CO) have relatively low-energy empty orbitals such that backbonding may provide an important supplement to the bonding. In such cases, the ligand should be classified with additional Z functions to provide a more complete description of the bonding.

H_3NBH_3 can be represented by either of the two representations shown in Fig. 2, both of which depict an electron pair bond between N and B; however, since the electrons are in the same location, the two representations do not correspond to resonance structures.

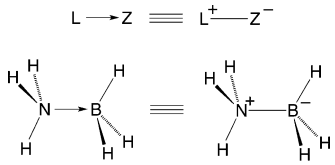

Fig. 2 Two alternative, but equivalent, representations for a dative bond, as illustrated for H_3NBH_3. Note that the representations are not resonance structures

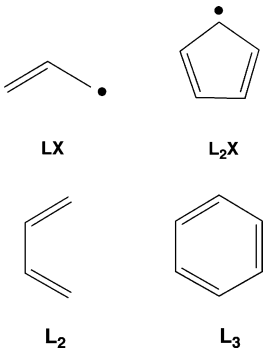

Fig. 3 $[L_lX_xZ_z]$ classifications of some common ligands as derived by summing the individual components that correspond to the valence bond representation

Multidentate and multiply bonded ligands that are attached by more than one covalent bond may be classified as $[L_lX_xZ_z]$, where l, x, and z are the respective number of L, X, and Z functionalities that are associated with the frontier orbitals of the ligand in the geometry that corresponds to its binding mode. Common examples of such ligands include allyl, cyclopentadienyl, and benzene, as illustrated in Fig. 3 and Table 1.

In many cases, the classification can be simply derived by summing the individual bonding components that are implied by their valence bond representations, but, in certain cases, consideration of the frontier orbitals is essential to obtaining the correct representation. As an illustration, the η^7-cycloheptatrienyl ligand is classified as L_2X_3 rather than L_3X because of the availability of Z functions (Fig. 4). Another illustration of a multifunctional ligand that features a Z function is provided by linear NO, which results in a classification of X_3 [29].

Structure-bonding representations for some of these cyclic ligands are provided in Fig. 5, which also includes the familiar forms that use a single line between the metal center and the ring centroid to indicate connectivity.

After the ligands attached to the element of interest have been identified according to the CBC method, the molecule itself is classified in the form $[ML_lX_xZ_z]^{Q\pm}$ by summing all the L, X, and Z functionalities, where $Q\pm$ is the charge on the molecule. Comparison of molecules that have different charges, however, require the $[ML_lX_xZ_z]^{Q\pm}$ assignment to be reduced to its "equivalent neutral class" by *formally* localizing the $Q\pm$ charge on the ligands, rather than on M. The equivalent neutral class is thus the classification that results if the

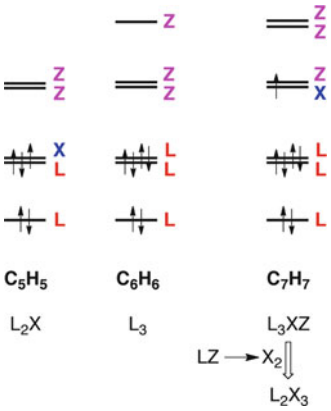

Fig. 4 Frontier orbitals for a variety of ligands indicating the L, X, and Z character of each orbital according to whether it is doubly occupied (L), singly occupied (X), or empty (Z). Note that the rule LZ → X_2 must be applied to cycloheptatrienyl because Z is degenerate with the half occupied X orbital

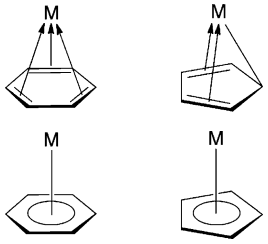

Fig. 5 Structure-bonding representations for benzene and cyclopentadienyl ligands (*top*) and representations that are commonly used for clarity to indicate connectivity (*bottom*)

Q ± charge were to be localized on the ligand rather than on the metal center. The reduction of $[ML_lX_xZ_z]^{Q\pm}$ to its equivalent neutral class is described in detail elsewhere [14–16] and is readily achieved by the application of some simple transformations, the most essential of which are:

(1) For cations, $L^+ \rightarrow X$ and, if no L ligand is present, $X^+ \rightarrow Z$
(2) For anions, $X^- \rightarrow L$ and, if no X ligand is present, $L^- \rightarrow LX$

If the derived classification after performing these transformations contains both an L and a Z function, the classification is reduced further by using the transformation LZ → X_2.

Illustrations of these procedures are provided by (1) $[Cp_2WH_3]^+$, which is classified as $[ML_4X_5]^+$, transforming to $[ML_3X_6]$ by application of the rule $L^+ \rightarrow X$, and (2) $[Cp_2ZrR_3]^-$, which is classified as $[ML_4X_5]^-$, transforming to $[ML_5X_4]$ by application of the rule $X^- \rightarrow L$ (Fig. 6).

Not only does the CBC method provide a simple classification of a covalent molecule, but the $ML_lX_xZ_z$ description also contains useful information pertaining to the nature of a molecule, such as the electron number (EN), valence number (VN), number of nonbonding electrons (v^n, i.e., d^n for transition metals), and ligand bond number (LBN), as summarized in Table 2.

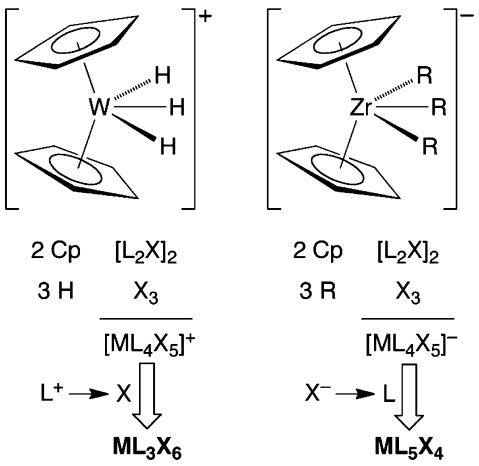

Fig. 6 $[ML_lX_xZ_z]$ classifications of some metallocene compounds

Table 2 Definitions pertaining to the CBC method and the equivalent neutral class

Symbol	Definition
L	Two-electron donor function
l	Number of L functions
X	One-electron donor function
x	Number of X functions
Z	Zero-electron donor function
z	Number of Z functions
m	Number of valence electrons on neutral M atom
VN	Valence number
	$VN = x + 2z$
LBN	Ligand bond number
	$LBN = l + x + z$
EN	Electron number (or electron count)
	$EN = m + 2l + x$
v^n	Number of electrons in "nonbonding" M orbitals[a]:
	$n = m - x - 2z = m - VN$

[a] v^n corresponds to d^n for transition metal compounds.

3 Classification of 3-Center 2-Electron Bonds and Their Representations

The representation of 2-center 2-electron bonds in terms of "lines" and "arrows" (according to whether the interactions are either normal or dative covalent bonds) and the classification of the ligands as either L, X, or Z type are of immense utility in evaluating the nature of a molecule. It is, therefore, appropriate to extend this approach for molecules in which the bonding cannot be described in terms of only 2-center 2-electron bonds but which requires the participation of 3-center 2-electron interactions.

By analogy to the fact that 2c–2e bonds can be classified according to the number of electrons that each partner contributes, i.e., [XX] (normal covalent) or [LZ] (dative covalent), 3c–2e interactions can likewise be classified according to the number of electrons that each center contributes, with the only possibilities being [X_2Z] (Class I) and [LZ_2] (Class II). Thus, a Class I interaction corresponds to a situation in which two atoms each contribute one electron to the bonding molecular orbital, whereas a Class II interaction corresponds to a situation in which a single atom contributes both electrons. These interactions can also be subclassified according to (1) the identity of the bridging atom, i.e., μ–L, μ–X, or μ–Z, and (2) whether the interaction is open (i.e., little overlap between one pair of orbitals) or closed (i.e., substantial overlap of all three orbitals) [30], as distinguished by the symbols μ^o- and μ^c-, respectively. Unless one is dealing with symmetric [AB_2] 3c–2e interactions where the identity of the bridge (A) is self-evident, more than one reasonable interpretation is possible for an asymmetric [ABC] arrangement. Therefore, for clarity, the identity of the bridging atom should always be specified when using the μ–Z, μ–X, and μ–L classification to describe the bonding within an asymmetric [ABC] arrangement. With respect to the issue of whether the interaction is open or closed, appropriate consideration needs to be given to ascertain whether there is an interaction between all pairs of atoms, recognizing that such differentiation may not be possible for borderline situations, in which case it is preferable to just use μ- rather than μ^o- or μ^c-.

A summary of the structure-bonding representations of the various 3c–2e interactions is presented in Fig. 7. For example, with respect to μ–Z interactions, the μ^c–Z closed form can be conveniently represented by drawing an arrow from the midpoint of the X–X bond to Z, which clearly illustrates how the X–X bonding pair of electrons serves as a "dative bond" to Z and thus contributes two electrons to its electron count (Fig. 8).[5] This class of bonding is illustrated well by dihydrogen compounds, in which coordination by H_2 to a metal center (Z) increases the electron count by two.

An open μ^o–Z interaction may be depicted by using a "dot-dashed-line" representation, i.e., "•----," in which each dot is intended to convey the electron that is provided by each X to the 3c–2e interaction, while the two dashed lines attached to each Z are intended to indicate that the electron number of Z has increased by two units. Conceptually, the open μ^o–Z interaction may be considered to emerge from the closed form by breaking the X–X bond in a homolytic manner, thereby localizing, in a formal sense, an unpaired electron on X (Fig. 9).

Note that the two dashed lines attached to Z do not modify the valence of Z since, by definition, Z does not contribute any electrons to the bond; as such, the two X atoms of an open μ^o–Z interaction may be viewed as serving as an L donor toward Z, in a similar way that the X–X bond serves as an L donor in a closed μ^c–Z interaction. With respect to the X groups, although not connected directly, the

[5] The notion of using an arrow to represent donation of electron density from a bond to another atom was first introduced by Walsh to describe the bonding in B_2H_6; see [31].

Class	Class I				Class II	
Full name	X–μ^c-Z–X	X–μ^o-Z–X	X–μ^c-X–Z	X–μ^o-X–Z	Z–μ^c-L–Z	Z–μ^o-L–Z
Short name	μ^c–Z	μ^o–Z	μ^c–X	μ^o–X	μ^c–L	μ^o–L
Open or closed	closed	open	closed	open	closed	open
Alternative orbital representations	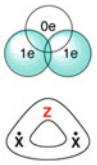	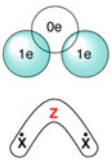	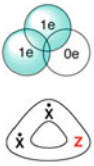	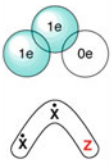	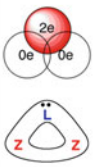	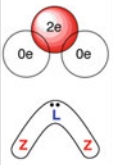
Representation in structure-bonding figure			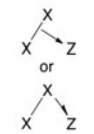	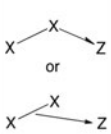		

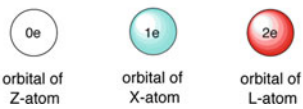

Fig. 7 Classification of 3-center 2-electron (3c–2e) interactions according to the nature of the specified bridging atom. Although the orbitals shown are depicted as s-orbitals, the classification also applies to p-, d-, and sp^n-hybrid orbitals. Note that the μ^c–X description is an alternative setting for μ^c–Z. Two structure-bonding representations are shown for μ^c–X and μ^o–X; of these, the upper ones are preferred but the lower ones are also acceptable. Class II [ZZL] interactions are not included in this table because (1) we are not aware of any Class II μ^o–Z interactions and (2) the closed Class II [ZZL] μ^c–Z interaction is formally equivalent to the closed Class II [ZLZ] μ^c–L

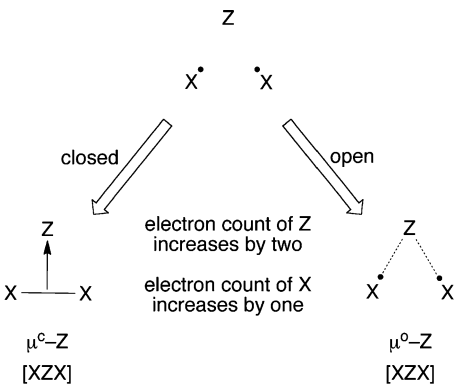

Fig. 8 Illustration of how three atoms, one with a Z function and two with X functions, may combine to form open and closed 3c–2e interactions in which Z is assigned as the bridge. In each case, the electron count of the Z atom increases by two, while that for the X atoms increases by one. The closed μ^c–Z form can be conveniently represented by drawing an arrow from the midpoint of the X–X bond to Z, while the open μ^o–Z interaction may be depicted by using a "dot-dashed-line" representation, i.e., "•----"

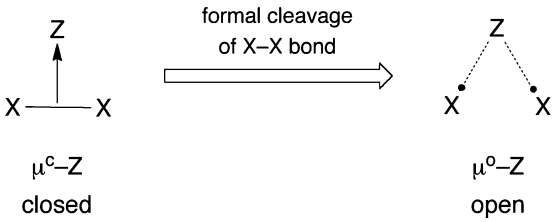

Fig. 9 Illustration of how the open μ^o–Z interaction is derived from the closed μ^c–Z interaction via a formal cleavage of the X–X bond

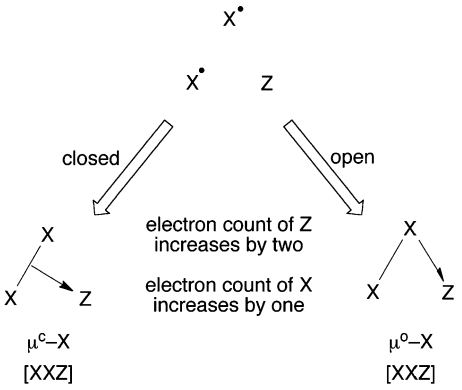

Fig. 10 Illustration of how three atoms, one with a Z function and two with X functions, may combine to form open and closed 3c–2e interactions in which X is assigned as the bridge. In each case, the electron count of the Z atom increases by two, while that for the X atoms increases by one. The closed μ^c–Z form can be conveniently represented by drawing an arrow from the midpoint of the X–X bond to Z, while the open μ^o–Z interaction may be depicted by using a "half-arrow" representation, i.e., "X–X→Z"

electron count of each X increases by one because the electrons are shared with its partner by virtue of the 3c–2e orbital. In essence, the empty orbital on Z provides a mechanism for the two electrons on X to couple even though there is no direct interaction between the atoms.

Similar to a closed μ^c–Z interaction, a closed μ^c–X interaction can also be represented with an arrow drawn from the midpoint of the X–X bond to Z (Fig. 10) because these two descriptions are formally equivalent and merely differ by the identity of the atom that is ascribed to being the bridge. For example, in the case of η^2-dihydrogen compounds, the symmetry of the situation (i.e., two equivalent X substituents) is such that the metal (i.e., Z) can be chosen as the bridge, whereas in, for example, η^2-silane compounds, [M–H–Si], the hydrogen atom (i.e., X) could be selected as the bridge on the basis that it has the two shortest bonds. Thus, as noted above, it is essential for one to specify the identity of the bridging atom when discussing a *closed* Class I system. Although the situation is less ambiguous, it is also prudent to assign the bridging atom in an open μ^o–X system in order to remove any uncertainty.

Since there is no interaction between the outer X and Z atoms in an open μ^o–X interaction, the bonding is more conveniently represented by using the X–X→Z "half-arrow" notation in which the "half arrow" is drawn from the central X atom to the outer Z atom (Figs. 7 and 10) [32]. Whereas a closed μ^c–X interaction typically requires an angle at the central X atom that is distinctly nonlinear, an open μ^o–X interaction is characterized by a large bond angle, as illustrated by the bridging hydride complex, $\{[(CO)_5Cr]_2(\mu\text{-}H)\}^-$ [30]. The purpose of using a half arrow (rather than a full arrow) from the atom is to emphasize that the arrow does not correspond to donation of a lone pair but rather donation of the X–X bond pair. In this regard, both the representation of a full arrow from the center of the X–X bond in a closed μ^c–X system [31] and a half arrow from the central X in a μ^o–X system convey the same information with respect to the impact on Z in terms of electron counting purposes, i.e., donation of a pair of electrons. In many cases, the precise nature (i.e., open versus closed) of the bonding of an asymmetric [XXZ] system may not be known, either experimentally or theoretically. However, since both bonding representations convey the same information with respect to electron counting purposes, the form that is used may be a matter of convenience and should not necessarily be used as a criterion to indicate whether an author considers that the interaction is open or closed, unless it is explicitly stated.

For both open and closed μ–L interactions, the bridging L atom contributes a pair of electrons to the 3-center orbital, while the outer Z atoms provide no electrons. Since all three atoms share the pair of electrons, the donor L atom may be regarded as contributing two electrons to the electron count of *both* outer Z atoms (Fig. 11). This type of interaction may be represented by a pair of half arrows that are drawn from the central atom (L) to each outer atom (Z); half arrows, rather than full

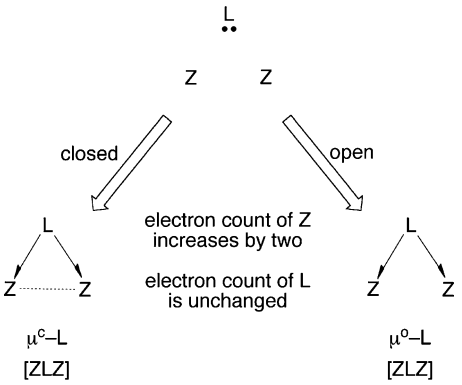

Fig. 11 Illustration of how three atoms, one with an L function and two with Z functions, may combine to form open and closed 3c–2e interactions in which L is assigned as the bridge. In each case, the electron counts of the Z atoms increase by two, while that for the L atom is unchanged. Both open and closed interactions are represented with a pair of half arrows that are drawn from L to Z to indicate that a *single* electron pair is being shared simultaneously with both Z atoms. A dashed line is shown between the two Z atoms of the closed form to indicate that these atoms are within bonding distance. Unlike a 2c–2e bond, however, none of the electron density between these atoms derives from the Z atoms but derives only from the L atom

arrows, are used to indicate that a *single* electron pair is being shared simultaneously with both Z atoms. A dashed line is shown between the two Z atoms of the closed form to indicate that these atoms are within bonding distance. However, it is possible that the close proximity of these atoms may not solely be a consequence of the 3c–2e interaction because closed-shell metallophilic interactions can also provide a means to bring two atoms into proximity [33–37].

Examples of metal-containing moieties that feature these types of interactions and the corresponding CBC designation with respect to the metal are summarized in Table 3.

Table 3 Summary of CBC designations for coordination of various ligands that feature 3c–2e interactions

Description	Example	CBC classification with respect to M
Class I: μ^c–Z	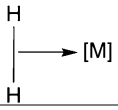	L
Class I: μ^o–Z		L
Class I: μ^o–Z	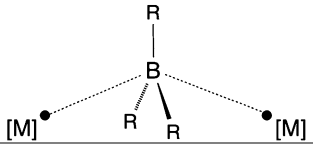	X
Class I: μ–X	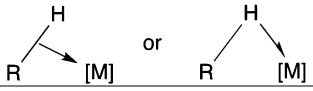	L
Class I: μ–X	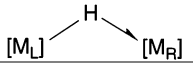	X, [M_L] L, [M_R]
Class I: μ–X	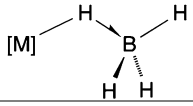	X
Class I: μ–X	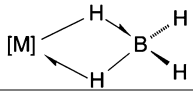	LX
Class I: μ–X	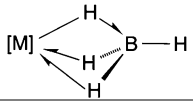	L_2X
Class II: μ–L	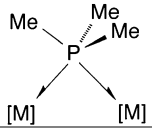	L
Class II: μ–L	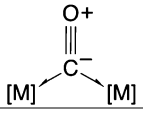	L

4 Examples of Compounds with 3c–2e Bonds

4.1 Class I: Closed μ^c–Z 3c–2e Bonds

4.1.1 Trinuclear [M_3] Interactions

The simplest example of a species that may be categorized as possessing a Class I closed μ^c–Z interaction is provided by $[H_3]^+$, as illustrated by the structure-bonding representation in Fig. 12. Although $[H_3]^+$ has not been isolated, the isolobal trinuclear gold compound, $[([IPr]Au)_3](OTf)$, which is supported by an N-heterocyclic carbene ligand (Fig. 13), has been structurally characterized by X-ray diffraction [38]. The trinuclear cation, $[([IPr]Au)_3]^+$, has approximate D_3 symmetry with Au–Au bond lengths in the range 2.644–2.663 Å and may be described by the structure-bonding representations shown in Fig. 13.[6] DFT

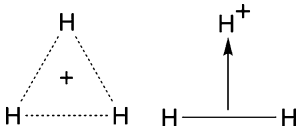

Fig. 12 Connectivity (*left*) and structure-bonding representation (*right*) of $[H_3]^+$

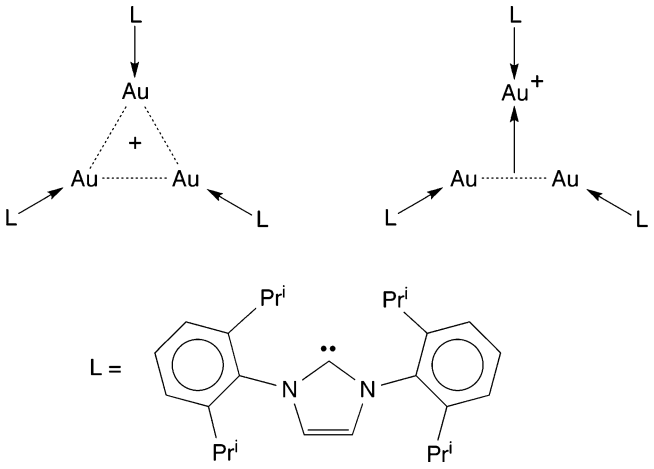

Fig. 13 Connectivity (*left*) and structure-bonding representation (*right*) of a trinuclear gold compound

[6] For other examples in which 3c–2e bonding is represented as donation of a M–M bonding pair of electrons to Au^+, see [39].

calculations indicate that the HOMO is an orbital that is primarily composed of gold σ-orbitals.

Closely related trinuclear compounds that possess a $[Au_2M]$ motif are also known, e.g., $\{(Ph_3PAu)_2[CpMo(CO)_2(PMe_3)]\}^+$, with an Au–Au bond length of 2.738 Å [40], and $\{(Ph_3PAu)_2[Cr(CO)_4(PPh_3)]\}$, with an Au–Au bond length of 2.694 Å.[7] As such, these compounds can be described by the structure-bonding representations illustrated in Fig. 14.

4.1.2 M(η²-H–H) Interactions

Classic examples of closed μ^c–Z interactions are provided by dihydrogen complexes, $[M](\eta^2\text{-}H_2)$ (Fig. 15) [43–50], which belong to a class of molecules referred to as σ-complexes [51–54].

The first example of a dihydrogen complex to be isolated and structurally characterized by X-ray diffraction is the tungsten complex, $W(PPr^i_3)_2(CO)_3(\eta^2\text{-}H_2)$, as illustrated in Fig. 16 [43–50, 55]. Shortly thereafter, a chromium counterpart, $Cr(CO)_5(\eta^2\text{-}H_2)$, was generated in liquid xenon solution, and the presence of the dihydrogen ligand was demonstrated by IR spectroscopy [56] and subsequently by NMR spectroscopy [57, 58]. A large variety of dihydrogen complexes has been subsequently identified, and a selection of examples is presented in Fig. 16 [43–50].

In each case, the dihydrogen ligand donates a pair of electrons to the metal center, thereby serving the role of an L-type ligand. However, although the bonding

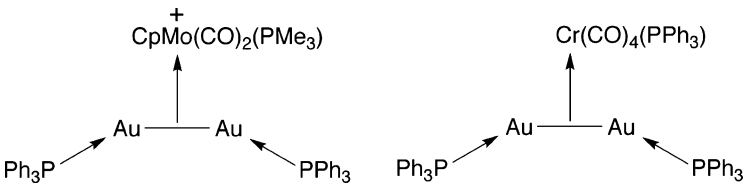

Fig. 14 Trinuclear $[Au_2M]$ compounds that feature μ^c–Z interactions

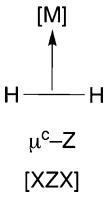

Fig. 15 An example of a 3c–2e interaction with a μ–Z bridge

[7] Another closely related species is the hydride derivative, $[([IPr]Au)_2H]^+$, in which a gold center is formally replaced by hydrogen and which possesses an Au–Au distance of 2.701 Å. See [41, 42].

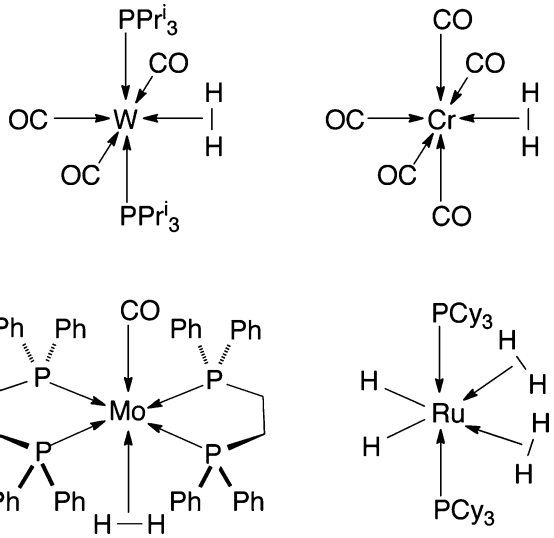

Fig. 16 Early examples of transition metal dihydrogen complexes

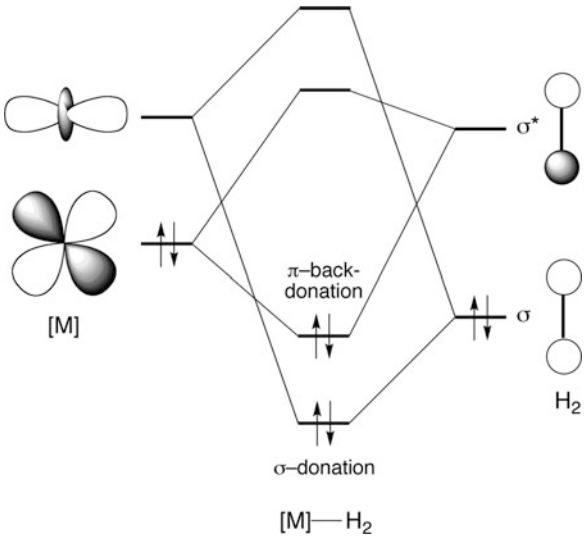

Fig. 17 Qualitative molecular orbital diagram for dihydrogen complexes

in dihydrogen complexes is normally represented with the metal center simply serving as a Lewis acid (Fig. 15), it must be emphasized that supplementary π-backbonding into the H–H σ* orbital provides a critical stabilizing interaction (Fig. 17). Extensive π-backbonding, however, results in cleavage of the H–H bond to form a dihydride tautomer. A continuum of structures, therefore, exists in which the H–H distance depends on the relative degrees of σ-donation and π-backbonding (Fig. 18) [45]; for simplicity, however, dihydrogen complexes are invariably represented without illustrating the backbonding interaction (cf. metal carbonyls).

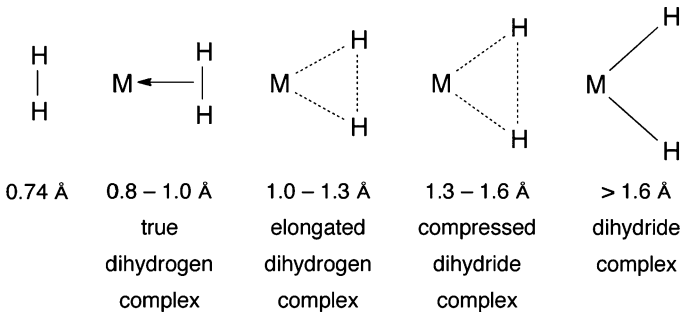

Fig. 18 Classification of M[H_2] tautomers as a function of H–H distance

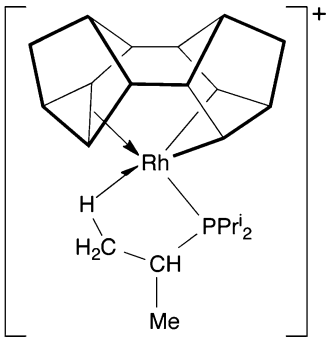

Fig. 19 An example of a compound which features coordination of a C–C bond to a metal center

4.1.3 M(η^2-C–C) Interactions

Another class of molecules that feature closed μ^c–Z interactions is provided by σ-complexes that are derived by coordination of C–C single bonds. Such complexes are, however, much less common than dihydrogen complexes, primarily due to the directionality associated with the sp^3 hybrid orbitals that compose the C–C bond [59]. Indeed, isolated examples of σ-complexes that feature coordination of C–C bonds are limited to intramolecular situations where the C–C bond is a component of a ligand [60], as exemplified by the rhodium and iridium complexes, $[M(PR_3)(BINOR–S)]^+$ (M = Rh, Ir; BINOR-S = 1,2,4,5,6,8-dimetheno-*S*-indacene), of which the rhodium derivative is illustrated in Fig. 19 [61–65]. As would be expected, the C–C bond involved in the σ-interaction [1.604(4) Å] is significantly longer than the corresponding value in free BINOR-S [1.497(6) Å], while the Rh–C bond lengths [2.352(3) and 2.369(3) Å] are longer than those associated with the Rh–C alkyl σ-bonds [2.032(3) and 2.042(3) Å] [61].

In concluding this section, it is pertinent to note that the coordination of olefins and alkynes to a metal center also involve a closed μ^c–Z interaction (Fig. 20). However, an important difference between the coordination of dihydrogen and olefins/alkynes

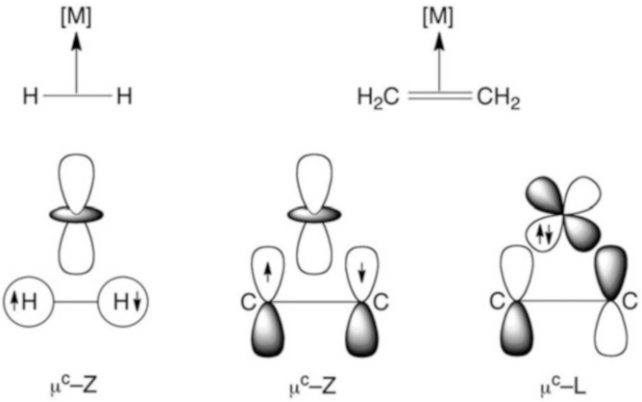

Fig. 20 Comparison of closed μ^c–Z interactions in dihydrogen and olefin adducts. Note that the olefin interaction is supplemented by a μ^c–L backbonding interaction from the metal

is that the accompanying π-backbonding interactions for the latter do not cleave the C–C bond since the carbon atoms are also attached by a σ-bond; in contrast, π-backbonding cleaves the bond in dihydrogen. The π-backbonding interaction for olefins is classified as a μ^c–L interaction (vide infra), and thus coordination of an olefin may be considered to be comprised of both μ^c–Z and μ^c–L interactions.

4.1.4 M(η^2-Si–Si) Interactions

More common than σ-complexes that feature coordination of C–C bonds are those that feature Si–Si bonds [66]. In this regard, it is interesting to note that the first example of a transition metal compound that is now recognized to involve coordination of Si–Si bonds to a transition metal [67, 68] was originally proposed to be a hexasilyl derivative (Fig. 21) [69].[8]

Another example of an intermolecular coordination of a Si–Si bond is provided by the copper complex, $\{[Ph_2P(C_6H_4)SiMe_2–SiMe_2(C_6H_4)PPh_2]Cu\}^+$, as illustrated in Fig. 22 [71]. Evidence for the interaction is provided by the observation that the Cu–Si distances [2.7196(14) and 2.7212(14) Å] are only 12% longer than the sum of the covalent radii.

An interesting example of an intermolecular disilane adduct is provided by the N-heterocyclic carbene platinum complex, [IPr]Pt(η^2-$Me_2PhSi–SiMe_2Ph$), as illustrated in Fig. 23, although it was originally formulated as a disilyl derivative, $[IPr]Pt(SiMe_2Ph)_2$ [72, 73]. However, key data to support the formulation as a disilane σ-complex are provided by a very acute Si–Pt–Si bond angle [80.9(1)°] and a Si–Si distance [2.980(5)°] that is much shorter than that in four-coordinate

[8] For a highlight of this article, see [70].

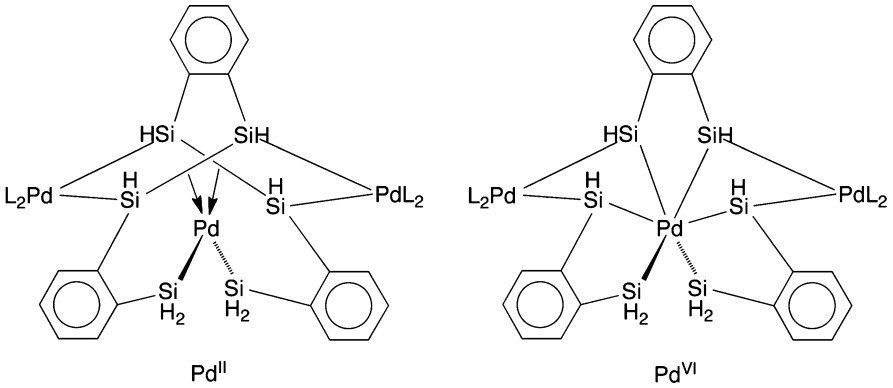

Fig. 21 A compound that was originally proposed to be a hexasilyl derivative (*right*) but was subsequently identified as a compound that features coordination of Si–Si bonds

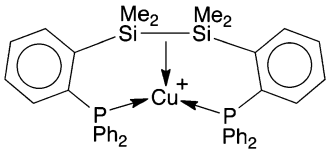

Fig. 22 An example of a copper compound which features coordination of a Si–Si bond to a metal center

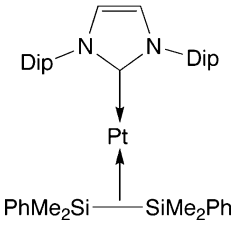

Fig. 23 A platinum compound that features coordination of a disilane molecule

$(Me_2PhP)_2Pt(SiMe_2Ph)_2$ [3.233(1) Å] [72], albeit much longer than typical Si–Si single bond lengths (2.3 Å).

4.1.5 Coordination of Lewis Acids to Multiple bonds

(a) Coordination of MOTf

Lewis acids such as AgOTf and $(CuOTf)_2$ react at the Ru = Si double bond of the ruthenium silylene compound, Cp*(IXy)Ru(H)[Si(H)Trip], to afford adducts that feature triangular [RuMSi] moieties (M = Ag, Cu), as illustrated

in Fig. 24 [74]. The bonding in these complexes can be considered to be comprised of a closed [XZX] interaction, in which Z is either AgOTf or CuOTf.

(b) Coordination of CO_2

While carbon dioxide binds to a single metal center via either unidentate η^1(C), unidentate η^1(O), or side-on bidentate η^2(C,O) coordination modes, it also serves as a bridging ligand with a multitude of bonding motifs (Fig. 25) [75–83]. With respect to the latter class of compounds, the carbon atom of the bridging CO_2 motif typically coordinates to only a single metal center, and the first example in which the carbon atom bonds to two metal centers, namely, $[(IPr)Ni]_2(\mu\text{-}CO)(\mu\text{-}\eta^2,\eta^2\text{-}CO_2)$, was reported in 2007 [83]. More recently, a $\mu\text{-}\eta^2,\eta^2\text{-}CO_2$ adduct has been spectroscopically identified as an intermediate in the reaction of the dinuclear *bis*(pentalene) titanium complex, $(\mu\text{-}\eta^5,\eta^5\text{-}Pn^R)_2Ti_2$ ($Pn^R = 1,4\text{-}\{Pr^i{}_3Si\}_2C_8H_4$), with one equivalent of CO_2 to afford the μ-oxo derivative, $(\mu\text{-}\eta^5,\eta^5\text{-}Pn^R)_2Ti_2(\mu\text{-}O)$, and extrude CO [84–86]. In particular, the $\mu\text{-}\kappa^1\text{-}CO_2$ adduct, $(\mu\text{-}\eta^5,\eta^5\text{-}Pn^R)_2Ti_2(\mu\text{-}CO_2)$, was identified by absorptions at 1,678 cm^{-1} and 1,236 cm^{-1} in the IR spectrum, attributable to the asymmetric and symmetric modes of the CO_2 ligand.

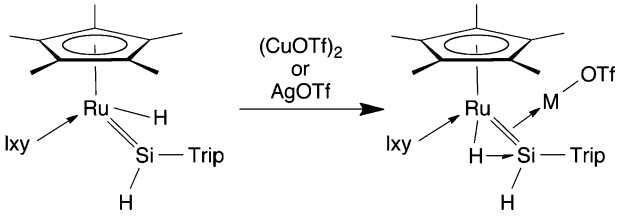

Fig. 24 Coordination of a Lewis acid (Ag^+ and Cu^+) to a Ru = Si double bond

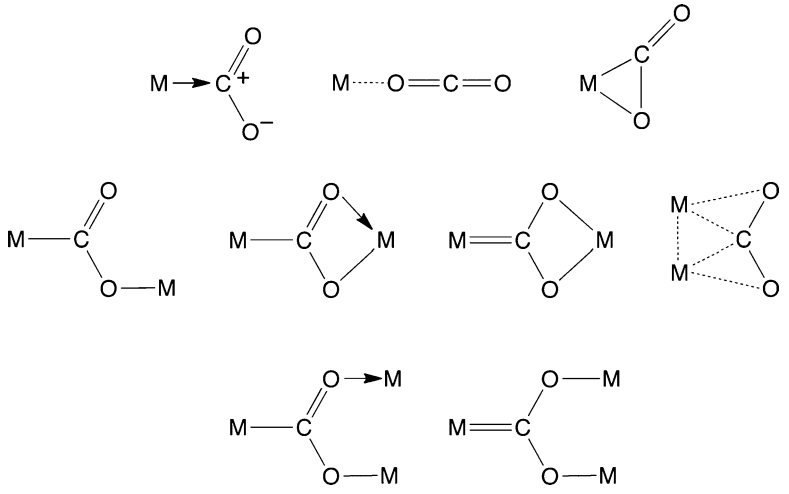

Fig. 25 Some coordination modes of CO_2

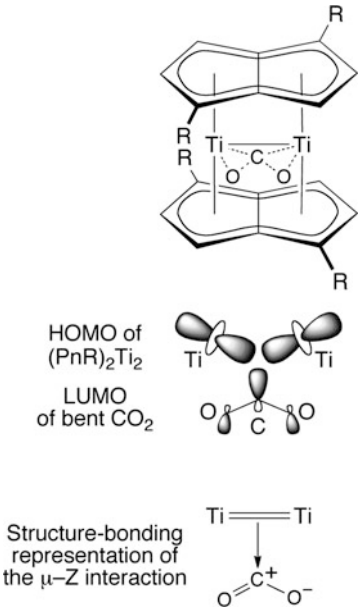

Fig. 26 A closed 3c–2e μ^c–Z interaction in $(\mu\text{-}\eta^5,\eta^5\text{-}Pn^R)_2Ti_2(\mu\text{-}CO_2)$

The bonding within $(\mu\text{-}\eta^5,\eta^5\text{-}Pn^R)_2Ti_2(\mu\text{-}CO_2)$ was addressed by computational studies on the unsubstituted derivative, $(\mu\text{-}\eta^5,\eta^5\text{-}Pn)_2Ti_2(\mu\text{-}CO_2)$, in which $Pr^i{}_3Si$ groups were replaced by H atoms. Significantly, the calculated vibrational frequencies (1,669 and 1,214 cm^{-1}) compare well with the experimental values. Analysis of the molecular orbitals indicates that the key bonding interaction involves donation of electron density from the HOMO of the $(\mu\text{-}\eta^5,\eta^5\text{-}Pn)_2Ti_2$ fragment (which is a Ti–Ti bonding orbital) to the LUMO of bent CO_2. Therefore, it is evident that the bonding within $[Ti_2C]$ is classified as a closed 3c–2e μ^c–Z interaction in which the CO_2 serves as the acceptor. This component of the bonding can be appropriately depicted with the structure-bonding representation shown in Fig. 26, in which one of the bonds of the Ti = Ti unit serves as a donor to carbon. In accord with this being the dominant interaction, the M–C distances in compounds that feature this motif are shorter than the M–O distances. The M–O distances are, nevertheless, within bonding values, and so it is possible that an additional weaker dative component between oxygen and the metal centers completes the bonding description.

4.2 Class I: Open μ^o–Z 3c–2e Bonds

By comparison to their closed counterparts, compounds that feature open μ^o–Z interactions are not common. However, such interactions are present in a variety of systems and most notably in boron derivatives. A simple representation of a motif that is encountered in boron chemistry is illustrated in Fig. 27, which shows how a

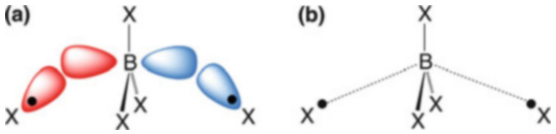

Fig. 27 An open μ^o–Z interaction involving boron. (**a**) Overlap of the boron p-orbital with the σ-symmetry orbitals of two X atoms results in a 3c–2e interaction that results in the electron count of boron increasing by two (but not its valence), while the electron count of each X increases by one. (**b**) Structure-bonding representation of the interaction

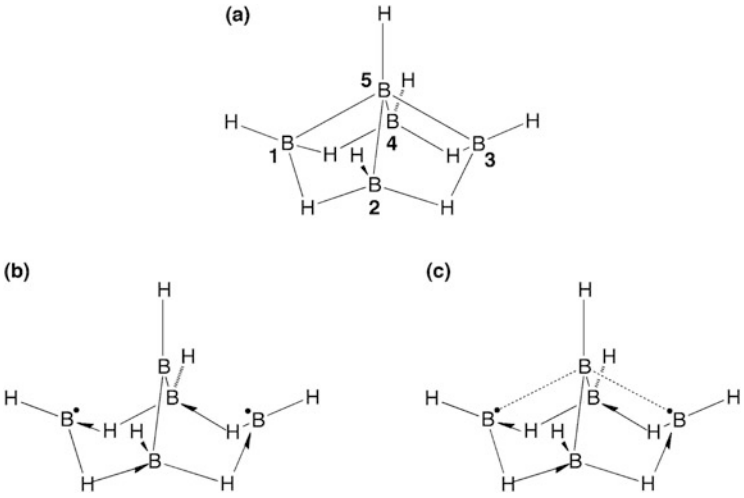

Fig. 28 (**a**) Structure of B_5H_9 showing connectivity. (**b**) Structure-bonding representation of B_5H_9 in the absence of an open μ^o–Z interaction, which indicates that B_5 has a sextet configuration, while B_1 and B_3 have septet configurations. (**c**) Structure-bonding representation of B_5H_9 showing that each boron has an octet MLX_3 configuration in the presence of an open μ^o–Z interaction

three-coordinate trivalent boron center with a sextet configuration interacts with two X-type ligands. Specifically, an overlap of the boron p-orbital with appropriate σ-symmetry orbitals on X provides a means for the boron to achieve an octet configuration, while each X atom increases the electron count by one.

4.2.1 B_5H_9, Pentaborane(9)

A good illustration of a μ^o–Z interaction is provided by pentaborane(9), B_5H_9, which possesses molecular C_{4v} symmetry with the connectivity illustrated in Fig. 28a [87–89].[9] A structure-bonding representation which incorporates an open μ^o–Z interaction and features octet configurations for each boron atom is presented

[9] For a discussion of the bonding in B_5H_9, see [90–92].

in Fig. 28c. It should be noted that Fig. 28c represents only one resonance structure. Specifically, all four equatorial boron atoms (B_1–B_4) are equivalent by virtue of a C_4 axis, and thus an equivalent resonance structure in which there is a μ^o–Z interaction involving B_2, B_4, and B_5 also exists. For comparison, the structure-bonding representation for the form without the μ^o–Z interaction is illustrated in Fig. 28b. This structure features an axial boron (B_5) that possesses a sextet configuration and two equatorial boron atoms (B_1 and B_3) that have septet configurations; the remaining two equatorial boron atoms (B_2 and B_4) possess octet configurations. Thus, comparison of these two structure-bonding representations (Fig. 28a and b) makes it evident how the presence of the μ^o–Z interaction allows the axial boron (B_5) and the two of the equatorial boron atoms (B_1 and B_3) to achieve an octet configuration.

4.2.2 (B_4H_8)[M], Metallatetraborane Complexes

The axial [BH] moiety of B_5H_9 may be formally replaced by metal centers to give (B_4H_8)[M] derivatives. Two illustrative examples are provided by the iron and cobalt compounds, $(B_4H_8)Fe(CO)_3$ [93] and $(B_4H_8)CoCp$ [94–96], which, by analogy with B_5H_9, can be illustrated by the structure-bonding representations in Fig. 29. As with B_5H_9, it is worth noting that equivalent resonance structures can also be drawn with bonds between the other two boron atoms and the metal centers. Consideration of the structure-bonding representations indicates that the iron compound belongs to the 18-electron class of ML_4X_2, while the cobalt compound belongs to the 18-electron class of ML_3X_3. Both of these descriptions correspond to well-known CBC designations for the respective metals.[10]

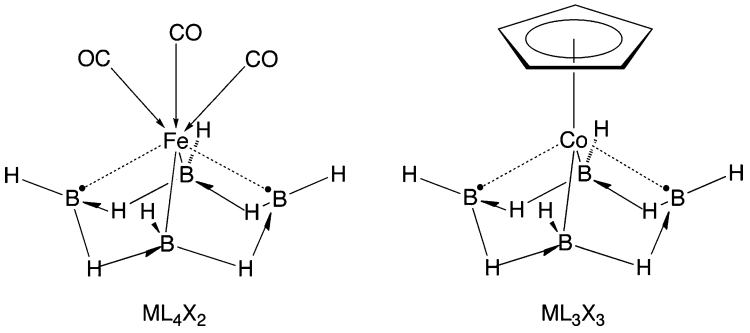

Fig. 29 Structure-bonding representations of $(B_4H_8)Fe(CO)_3$ and $(B_4H_8)CoCp$ illustrating that the open μ^o–Z interaction allows the metal centers to achieve 18-electron configurations

[10] It is pertinent to note that, in contrast to B_5H_9, the iron and cobalt compounds have additional valence electrons such that they could support additional 2c–2e bonds. For such a situation, the iron and cobalt compounds would be, respectively, categorized as ML_3X_4 and ML_2X_5, which are much less common than ML_4X_2 and ML_3X_3 for these elements.

4.3 Class I: μ–X 3c–2e Bonds

Compounds with Class I interactions that feature a μ–X bridge are very common, as illustrated by (1) hydrocarbon and silane σ-complexes, (2) bridging hydride complexes, and (3) agostic complexes.[11] In many of these complexes, however, there may be insufficient experimental or theoretical evidence to distinguish whether the interaction is best described as closed or open. Therefore, compounds corresponding to both classes of interactions are included in this section, with it being recognized that the choice of representation, i.e., a full arrow from the center of the X–X or a half arrow from the central X, is not necessarily being used to distinguish between closed and open situations.

4.3.1 Hydrocarbon and Silane σ-Complexes

Transition metal hydrocarbon [54, 98–100] and silane [101–111] adducts correspond to a class of σ-complexes [51–54] in which C–H and Si–H bonds interact with a metal center (Fig. 30).[12] Such molecules are closely related to η^2-dihydrogen complexes but are classified as possessing μ–X rather than μ–Z interactions because they lack the symmetry that is present in η^2-dihydrogen complexes. Thus, the hydrogen atom of hydrocarbon and silane adducts is more appropriately designated as the bridge on the basis that it exhibits the two shortest bond distances. Two representations to describe these interactions are provided in Fig. 30, recognizing that they can be used equivalently to determine the electron count and CBC designation of a metal center.

By comparison to η^2-dihydrogen complexes, hydrocarbon σ-complexes are particularly unstable, with there being no crystal structures of adducts that persist in solution. Interactions between alkanes and a metal center have, nevertheless, been observed in the solid state by X-ray diffraction, although their

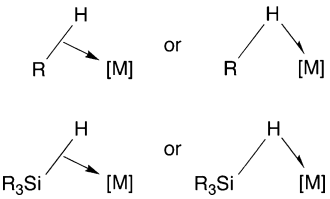

Fig. 30 Two representations of hydrocarbon (*top*) and silane (*bottom*) σ-complexes. Both representations are intended to convey the same information with respect to electron counting

[11] It should be emphasized that not all M–H–Y interactions must be described as 3c–2e bonds because some are better represented as 3c–4e "hydrogen bond" interactions. See, e.g., [97].

[12] Compounds that feature coordination of Ge–H and Sn–H bonds have also been investigated; see, e.g., [112].

integrity upon dissolution is unknown [113–116]. An illustration of a structurally characterized alkane adduct is provided by the norbornane species $[Rh(PBu^i_2(CH_2)_2PBu^i_2)(C_7H_{12})]^+$, which features two σ-C–H interactions (Fig. 31) and which is generated in the solid state by hydrogenation of a norbornadiene precursor, $[Rh(PBu^i_2(CH_2)_2PBu^i_2)(C_7H_8)]^+$ [115, 116].

Despite the paucity of structural data, alkane adducts have, nevertheless, been spectroscopically identified in matrices or solutions at low temperature [51–54, 117–128], and evidence for their existence as intermediates in reductive-elimination and oxidative-addition reactions has been provided by deuterium labeling and kinetic isotope effects [129–134].

In contrast to the absence of stable alkane σ-complexes, a variety of silane σ-complexes have been structurally characterized by X-ray diffraction [101–104, 110, 111, 135–138], as illustrated in Fig. 32. Analysis of the structures of these compounds indicates that the M···Si interactions are highly variable. For example, $(Cp^{Me})Mn(CO)_2(\eta^2\text{-}HSiHPh_2)$ is characterized by a Mn–Si distance of 2.391(12) Å [111], while $[(POCOP)Ir(\eta^1\text{–}HSiEt_3)]^+$ (POCOP = 2,6-$[OPBut_2]_2C_6H_3$) is characterized by a long Ir···Si distance of 3.346(1) Å [136]. Corresponding to the large range of M···Si distances, the angles at hydrogen are also highly variable, with $(Cp^{Me})Mn(CO)_2(\eta^2\text{-}HSiHPh_2)$ having an acute bond angle [89.7(7)°], while that for $[(POCOP)Ir(\eta^1\text{–}HSiEt_3)]^+$ is close to linear [157(1)°]. On the basis of these metrical data, it is evident that $(Cp^{Me})Mn(CO)_2(\eta^2\text{-}HSiHPh_2)$ is best described as possessing a closed μ^c–X interaction, while $[(POCOP)Ir(\eta^1\text{–}HSiEt_3)]^+$ possesses an open μ^o–X interaction. Although not structurally characterized, silane adducts of the type

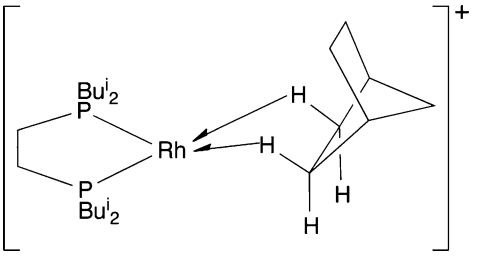

Fig. 31 A structurally characterized alkane adduct

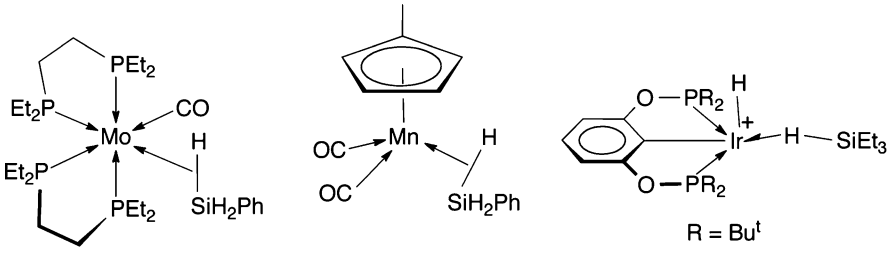

Fig. 32 Examples of structurally characterized silane σ-complexes

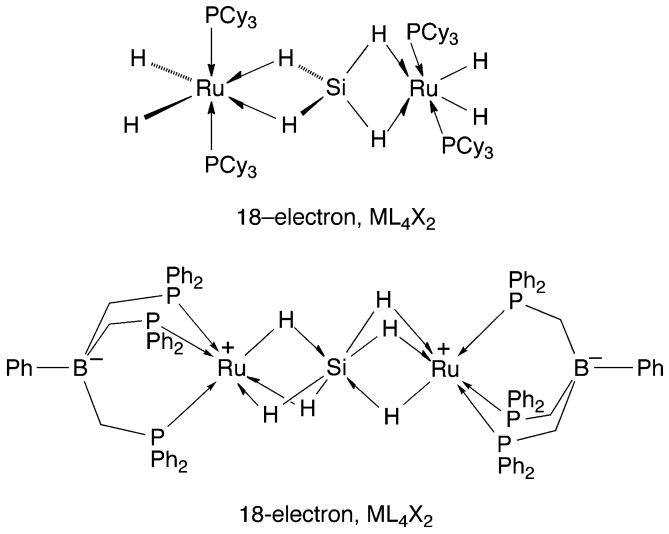

Fig. 33 Bridging silane compounds, including one that features a six-coordinate hypervalent silicon center

$M(CO)_5(\sigma\text{-}HSiR_3)$ (M = Cr, Mo, W) have also been investigated by using spectroscopic and photoacoustic calorimetric methods [139–142].

The observation that silane σ-complexes are much more common than alkane σ-complexes has been proposed to be a consequence of the Si–H bond being more polar and polarizable than a C–H bond; as such, a Si–H bond is both a better σ-donor and π-acceptor than a C–H bond [51–54, 101–111]. In addition, silanes can (1) participate in so-called interligand hypervalent interactions (IHI) [103] and secondary interactions between silicon and hydrogen atoms (SISHA) [106, 143] and (2) interact with more than one metal center, as illustrated by $[(PCy_3)_2RuH_2]_2(\mu\text{-}SiH_4)$ [144, 145] and $\{[PhBCH_2CH_2PPh_2]Ru\}_2(\mu\text{-}SiH_6)$ [146],[13] which are presented in Fig. 33.

4.3.2 Borane, Alane, and Gallane σ-Complexes

Lewis base adducts of boranes, alanes, and gallanes (LEH_3; E = B, Al, Ga) are isoelectronic with methane and silanes, and so the interaction of the E–H bonds in these molecules with metal centers can likewise be represented by the use of either the full-arrow or half-arrow notations (Fig. 34).

Examples of borane compounds that feature such interactions are provided by the chromium, molybdenum, and tungsten complexes, $(CO)_5M(\kappa^1\text{-}H_3BL)$

[13] Note that the hypervalent representation of the silicon of $\{[PhBCH_2CH_2PPh_2]Ru\}_2(\mu\text{-}SiH_6)$ is drawn for convenience.

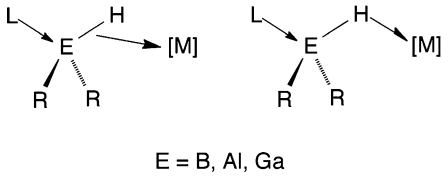

Fig. 34 Structure-bonding representations for coordination of E–H σ-bonds of Lewis base adducts of boranes, alanes, and germanes to a metal center

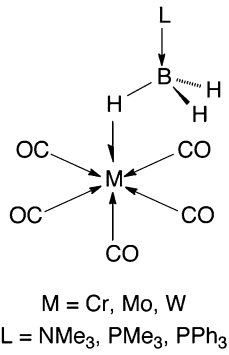

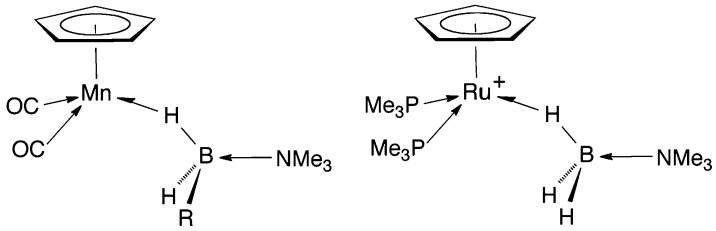

Fig. 35 B–H σ-complexes of Lewis base adducts of boranes

(L = NMe_3, PMe_3, PPh_3), which represent early examples of this class of compounds (Fig. 35) [147–149].

A variety of other adducts of four-coordinate neutral boranes have also been synthesized [150–152], including compounds in which the borane coordinates via two of the hydrogen atoms, e.g., $[Rh(PBu^i_3)_2H_2(\kappa^2\text{–}H_3BNMe_3)]^+$ [153] and $[Nacnac^{Ar_2}]Cu(\kappa^2\text{–}H_3BL)$ (L = Me_3N, lutidine) [154], as illustrated in Fig. 36.

σ-Complexes of Lewis base adducts of alanes [155, 156] and gallanes [157, 158] have also been reported, as illustrated in Figs. 37 and 38.

The B–H bond of electronically unsaturated three-coordinate boranes, R_2BH, can also interact with a metal center. However, an important distinction with respect to the coordination of the B–H bond of tetrahedral LBH_3 is that the boron of R_2BH has an additional empty orbital that enhances the backbonding interaction

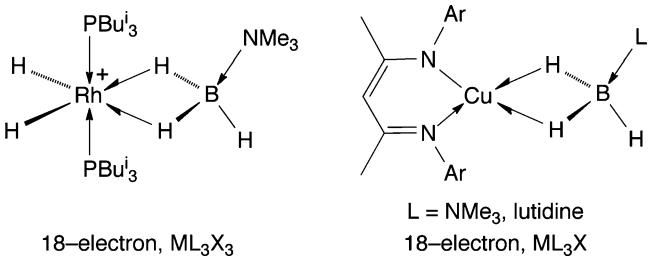

Fig. 36 B–H σ-complexes of Lewis base adducts of boranes involving bidentate coordination

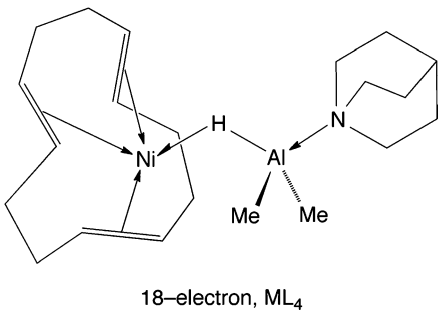

Fig. 37 Al–H σ-complex of an allane Lewis base adduct

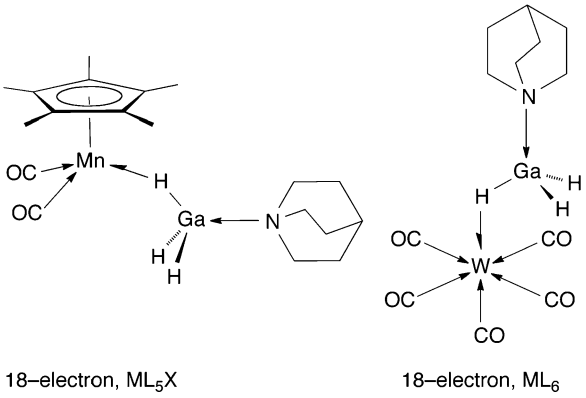

Fig. 38 Ga–H σ-complexes of Lewis base adducts of gallanes

[105, 159, 160]. The coordination of R_2BH can, therefore, be described in terms of two interactions, namely, (1) a 3c–2e interaction that involves donation from the B–H bond to the metal (i.e., L) and (2) a 2c–2e backdonation interaction from the metal to boron (i.e., Z), as illustrated in Fig. 39 (left).

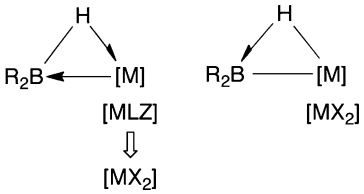

Fig. 39 Two alternative, but equivalent, structure-bonding representations for coordination of R_2BH to a metal center. In addition to a 3c–2e B–H–M interaction, there is also a 2c–2e M–B interaction. The metal center in both representations is classified as $[MX_2]$ because LZ is equivalent to X_2

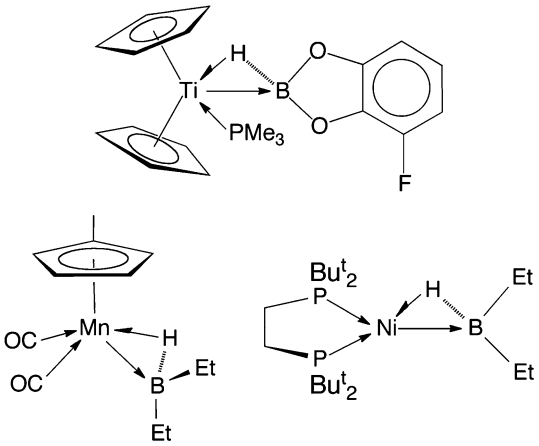

Fig. 40 Examples of B–H σ-complexes that feature coordination of electronically unsaturated boranes

Alternatively, since an LZ combination is equivalent to X_2 [13], the molecule can also be viewed as a boryl hydride derivative in which the M–H bond donates its electron density to an electronically deficient boron center (Fig. 39, right). In this regard, the description is similar to that of an agostic alkyl, although in this case the M–H bond relieves the electron deficiency of boron, rather than a C–H bond relieving the electron deficiency of a metal center. It must be emphasized that, despite their different appearances, the two structure-bonding representations in Fig. 39 represent the same electronic structure for the molecule. For example, in both cases, the boron atom is classified as $[BLX_3]$ according to the covalent bond classification [13]. Examples of complexes that feature coordination of electronically unsaturated R_2BH molecules to a metal center are illustrated in Fig. 40 [161–163].

4.3.3 Bridging Hydride Complexes

Compounds that feature [MHM'] moieties are referred to as bridging hydride complexes, and, as such, the hydrogen atom is classified as the bridging ligand.

A large variety of bridging hydride compounds are known [30, 164–166], and the angle at hydrogen may be very obtuse. For example, the average Cr–H–Cr bond angle of $[(Ph_3P)_2N]\{[(CO)_5Cr]_2(\mu\text{-}H)\}$ is 155.8° [167]. As such, the half-arrow representation to describe the bonding is particularly appropriate (Fig. 41). In addition to [MHM'] bridges involving transition metals, variants in which one of the metals is a main group element are also known. For example, $[Nacnac^{Ar_2}]Cu(\eta^2\text{-toluene})$ reacts with aluminum and zinc hydride compounds to afford $[Nacnac^{Ar_2}]Cu(\sigma\text{-}HML_n)$ (e.g., $ML_n = [Nacnac^{Ar'_2}]Zn$, $[Nacnac^{Ar''_2}]AlH$) [168]. However, the formation of $[Nacnac^{Ar_2}]Cu(\sigma\text{-}HML_n)$ is reversible, such that these complexes have been described as weak copper(I) σ-complexes [168].

Compounds that feature double, triple, and quadruple hydride bridges are also known (Figs. 42 and 43) [164] and can likewise be represented by the half-arrow representation.

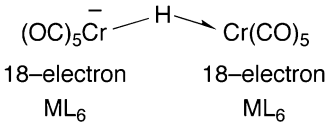

Fig. 41 An example of a bridging hydride complex with a large M–H–M bond angle

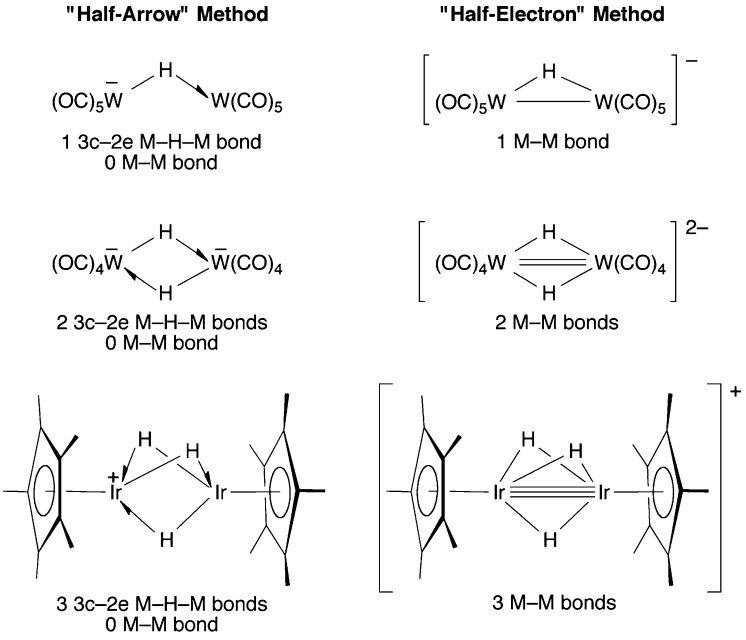

Fig. 42 Different descriptions of the metal–metal bond orders in some dinuclear complexes with bridging hydride ligands according to the electron counting method. The "half-arrow" method (*left*) predicts M–M bond orders that are in accord with theory, in contrast to the "half-electron" method (*right*)

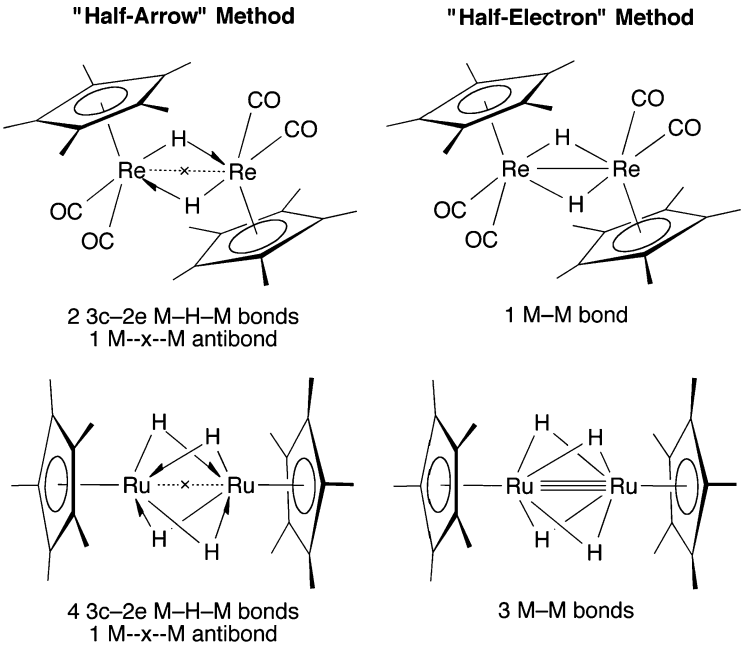

Fig. 43 Bridging hydride compounds that feature M–×–M antibonding interactions

An important feature of employing the half-arrow representation is that it provides means to predict direct metal–metal bond orders that are in accord with theoretical calculations; in contrast, the electron counting formalism that apportions half of the valence electron of hydrogen to each metal center (i.e., the "half-electron" method) results in direct metal–metal (M–M) bond orders that are greater than the values predicted theoretically [164]. For example, the half-arrow representation for $\{[(CO)_5Cr]_2(\mu\text{-}H)\}^-$ predicts that there is no direct metal–metal bond because each metal center can achieve an 18-electron configuration in its absence (Fig. 41). This prediction is in accord with experimental and theoretical studies which also indicate that there is no direct metal–metal bond path in $\{[(CO)_5Cr]_2(\mu\text{-}H)\}^-$ [169–171]. In contrast, the half-electron method predicts a Cr–Cr single bond for this compound, which is not in agreement with the experimental and theoretical studies.

The half-arrow method can also be used to predict direct M–M bond orders for compounds that feature double, triple, and quadruple hydride bridges, as illustrated in Figs. 42 and 43. In each case, the M–M bond order obtained by the half-arrow method correlates with theory [164]. Furthermore, the half-arrow method is also capable of predicting the existence of M–M antibonding interactions.

For example, neglecting any potential Re–Re interaction in $[Cp^*Re(CO)_2]_2(\mu\text{-}H)_2$, application of the "half-arrow" method predicts a 19-electron configuration for each rhenium center. Since the compound is diamagnetic, a direct Re–Re interaction is

implied, thereby resulting in a 20-electron configuration at each metal. This electron count indicates that a M–M antibonding orbital is occupied, such that the direct interaction may be described as a M–×–M antibond [172]. The overall bonding situation is, therefore, best represented as comprising two 3c–2e Re–H–Re bonds and a Re–×–Re antibond. In contrast, the half-electron method predicts a Re–Re single bond.

Similar issues in derived M–M bond orders are observed for a variety of other compounds, such as $[Cp^*Ru]_2(\mu\text{-}H)_4$ [173, 174]. Thus, $[Cp^*Ru]_2(\mu\text{-}H)_4$ was originally proposed to have a Ru≡Ru triple bond (Fig. 43, right) on the basis of the half-electron method [173], but subsequent calculations led to the conclusions that "... the Ru atoms do not have enough atomic orbitals to form so many bonds as suggested by the 18-electron rule" and that the direct Ru–Ru interaction is repulsive [173]. The results of the calculations are, nevertheless, consistent with the Ru–×–Ru antibond that is predicted by employing the half-arrow electron counting procedure.

4.3.4 Borohydride Complexes

The borohydride ligand exhibits a variety of coordination modes in which hydrogen serves as a bridge between boron and a metal [175–177]. For example, the borohydride ligand may coordinate to a single metal center by either one (κ^1), two (κ^2), or three (κ^3) hydrogen atoms [175–177], as illustrated in Fig. 44.[14]

The bonding in these complexes can also be represented with the half-arrow notation, but, in contrast to the coordination of Lewis base adducts, $[LBH_3]$, coordination of borohydride requires that one of the half arrows is drawn from hydrogen to boron in order for the latter to achieve an octet configuration (Fig. 44).[15]

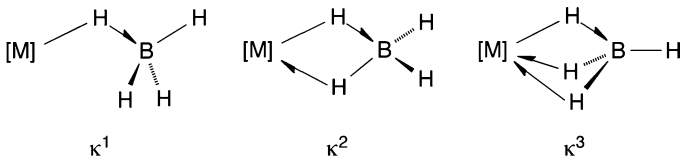

Fig. 44 Structure-bonding representations for $M[BH_4]$ tautomers

[14] Although the hapto "η^x" notation [178] is often used to describe the coordination mode of borohydride ligands [175–177], such notation is strictly inappropriate because η^x refers to the number of *contiguous* atoms that are attached to a specific element [179]. If the atoms are not contiguous, as in borohydride, the kappa "κ^x" notation [180] should be used instead.

[15] Note that alternative structure-bonding representations involving donation of electron density from a B–H bond of anionic $[BH_4]^-$ to cationic M^+ can also be drawn. Such representations, however, are equivalent to those shown in Fig. 44, which do not portray formal charges.

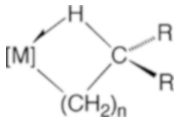

Fig. 45 Structure-bonding representation of an agostic interaction

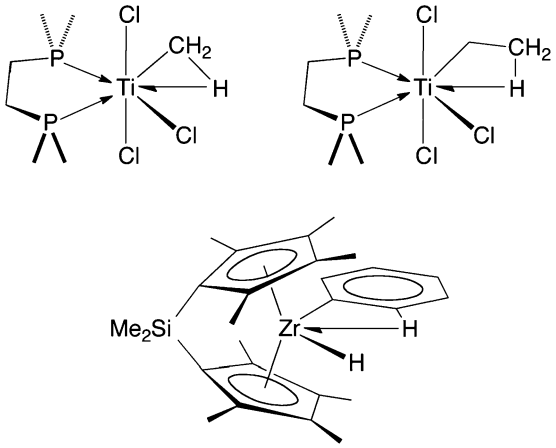

Fig. 46 Early examples of compounds that feature ∝- and β-agostic interactions (*top*) and an example of an agostic phenyl ligand (*bottom*)

4.3.5 Agostic Alkyl and Aryl Complexes

Agostic compounds, i.e., those which feature 3c–2e M–H–C interactions (Fig. 45), are now recognized to be an important feature of organometallic chemistry [181–183]. Particularly notable examples of compounds that possess agostic interactions are provided by the titanium alkyl compounds, (dmpe)$TiMeCl_3$ and (dmpe)$TiEtCl_3$, in which the titanium centers interact, respectively, with the ∝- and β-C–H bonds (Fig. 46) [184–186]. Agostic interactions are also observed in aryl compounds, as illustrated in Fig. 46 [187]. In each case, an agostic ligand is considered to be an LX three-electron donor.[16]

4.3.6 Bridging Alkyl Complexes

Bridging alkyl groups adopt a variety of coordination modes, some of which may feature agostic interactions [13, 192–195], although the energetic preferences may

[16] This view of the bonding in agostic compounds is necessarily simplistic. For more detailed discussions, see [188–191].

be small [196]. As an illustration of the types of coordination modes, the methyl group can be classified as (1) symmetric pyramidal, (2) symmetric trigonal planar, (3) monohapto agostic, (4) dihapto agostic, and (5) trihapto agostic (Fig. 47) [13, 193–195].

Of the coordination modes that do not feature agostic interactions, the bridging methyl group can either coordinate in a manner in which the methyl group is (1) planar, with a M–C–M angle of approximately 180°, or (2) pyramidal with a M–C–M angle that is significantly less than 180°. Representative examples of compounds that feature trigonal planar methyl groups are provided by $[Cp_2Zr(\eta^2\text{-}OCMe_2)]_2(\mu\text{-}AlMe_2)(\mu\text{-}Me)$ [197] and $(Cp^{Me})_3U(\mu\text{-}Me)U(Cp^{Me})_3$ [198], while examples with pyramidal groups are provided by $Me_2Al(\mu\text{-}Me)_2AlMe_2$ [199] and $ArMn(\mu\text{-}Me)_2MnAr$ [200]. Structure-bonding representations for these two coordination modes are illustrated in Fig. 48, which indicates that the bridging methyl ligand behaves like a μ–LX donor, regardless of whether it is symmetric pyramidal or symmetric trigonal planar.

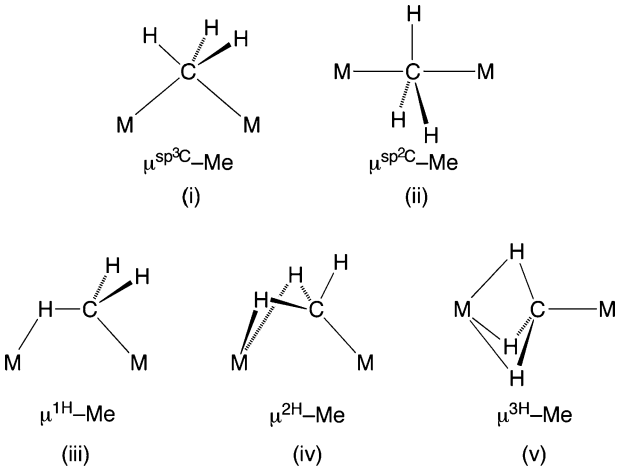

Fig. 47 Coordination modes of bridging methyl ligands (the lines between atoms are only to indicate connectivity and are not intended to be structure-bonding representations)

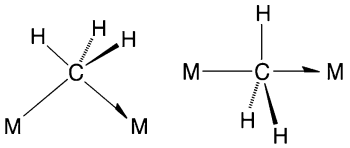

Fig. 48 Half-arrow structure-bonding representations for symmetrically bridging methyl groups

4.4 *Class II μ–L 3c–2e Bonds*

Compounds that possess Class II interactions with μ–L bridges, in which a single atom provides both electrons for the 3-center interaction, are much less common than those with Class I interactions in which two of the atoms each provide one electron. As with Class I compounds, there may be insufficient experimental or theoretical data to identify whether the interaction is best described as closed or open. Therefore, for expediency, the compounds described herein are represented with the open form, but it must be emphasized that this representation is not being used to infer that the interaction is not closed.

4.4.1 Bridging PR_3, AsR_3, and SbR_3 Complexes

While PR_3, AsR_3, and SbR_3 ligands almost exclusively coordinate in a terminal manner, examples in which these ligands bridge two metals are also known, as illustrated by the rhodium compounds shown in Fig. 49 [201, 202].[17] The migration of PR_3 ligands between two metal centers has also been postulated to occur via intermediates that possess μ-PR_3 ligands [212]. In addition, μ-phosphole derivatives of Pd [213–215], Pt [213, 216], Cu [213, 217, 218], and Ag [219] have also been synthesized (Fig. 50).

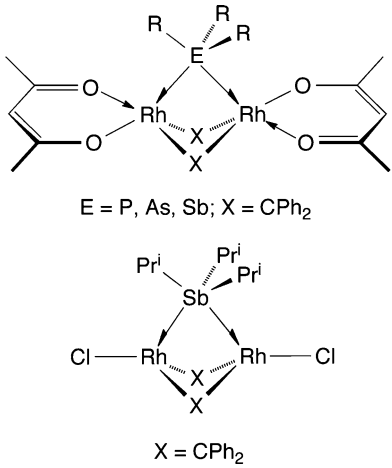

Fig. 49 Examples of compounds that feature bridging PR_3, SbR_3, and AsR_3 ligands

[17] Compounds with triply bridging PF_3 ligands are also known; see, e.g., [203–205]; for an early speculation of a complex with a bridging PR_3 ligand, see [206]; for compounds with asymmetrically bridging PR_3 ligands, see [207–210]; for calculations on hypothetical bridging PF_3 complexes, see [211].

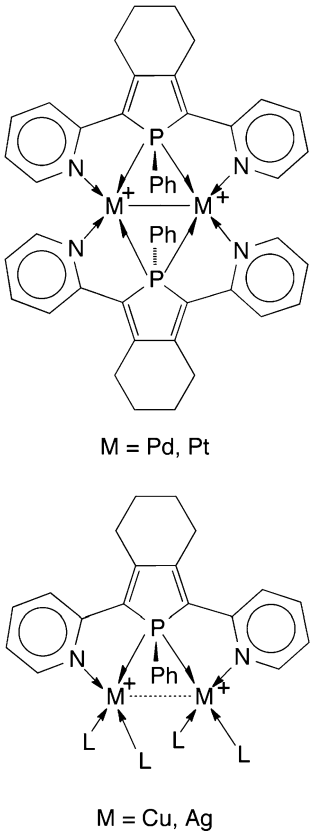

Fig. 50 Examples of compounds that feature bridging phosphole ligands (the dotted lines indicate metallophilic interactions)

4.4.2 Bridging MeCN Ligands

The nitrogen atom of acetonitrile has also been shown to bind in a similar manner and bridge two metals in a variety of compounds [220–227], as illustrated by the dinuclear copper compound, $[(dpen)Cu_2(\mu\text{-}NCMe)]^{2+}$ (Fig. 51) [221]. The bonding in this complex involves overlap of the nitrogen lone pair with an empty in-phase combination of sp^n hybrids on each copper (Fig. 52). Density functional theory calculations indicate that there is no formal bond between the two copper centers of $[(dpen)Cu_2(\mu\text{-}NCMe)]^{2+}$ because all pairs of Cu–Cu bonding and antibonding orbitals are filled [221], while the quantum theory of atoms in molecules predicts a bond critical point that has characteristics which are consistent with a cuprophilic closed-shell interaction, rather than that of a formal single bond. Consistent with this description, the structure-bonding representation of this molecule (Fig. 51) indicates that each copper belongs to the 18-electron class ML_3X, such that a direct Cu–Cu bond would not be expected.

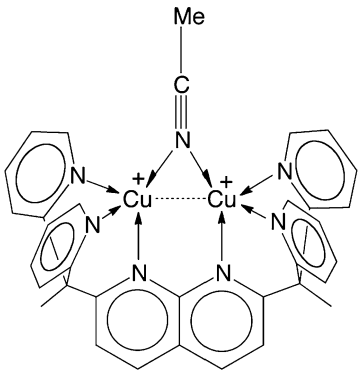

Fig. 51 An example of a compound that features a bridging MeCN ligand, [(dpen) Cu_2(μ-NCMe)]$^{2+}$ (the dotted line indicates a cuprophilic interaction)

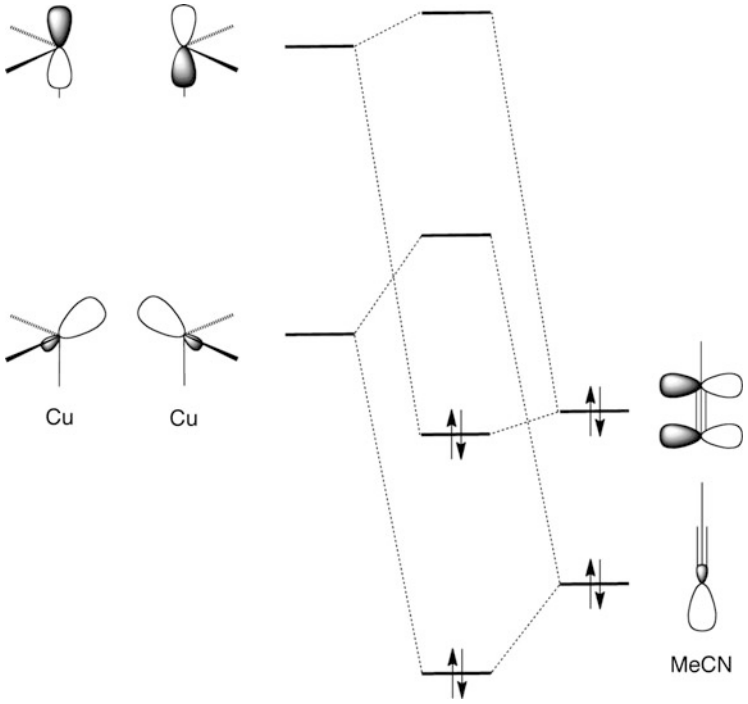

Fig. 52 Qualitative molecular orbital diagram for a bridging acetonitrile compound adapted from [221]; the primary interaction involves donation of the nitrogen lone pair into the empty in-phase combination of sp^n-hybrid orbitals on copper

4.4.3 Symmetrically Bridging Carbonyl Ligands

Symmetrically bridging carbonyl ligands are ubiquitous in transition metal chemistry,[18] with the first example being provided by $Fe_2(CO)_9$ [238–240]. Interestingly, $Fe_2(CO)_9$ was not originally proposed to have the now commonly recognized structure in which the carbonyl ligands bridge via only the carbon atom. Rather, the structure proposed was one with the formulation $(CO)_4Fe \leftarrow CO \rightarrow Fe(CO)_4$, in which a single carbonyl bridged in a linear asymmetric manner [241]. Also of interest, while there was originally caution in attributing the Fe–Fe distance of 2.46 Å [240] to the presence of a chemical bond [240],[19] Sidgwick and Powell [243] shortly thereafter represented the compound with an Fe–Fe bond that has subsequently appeared in many articles and textbooks [244–256]. The ready acceptance of the presence of an Fe–Fe bond is undoubtedly a consequence of the notion that the "ketonic" [257] description of the bridging carbonyl ligand requires $Fe_2(CO)_9$ to possess an Fe–Fe bond in order for each iron center to achieve an 18-electron configuration. Emphasizing the perceived significance of this Fe–Fe interaction, Braterman stated that "This bond is real, not formal" [258].

In view of the widespread acceptance of the notion that $Fe_2(CO)_9$ possesses an Fe–Fe bond, it was of most importance that Hoffmann et al. reported in the 1970s that the Fe···Fe interaction in this compound is actually *antibonding* and *repulsive* [259, 260]. This view, which is counter to decades of representations that feature a Fe–Fe bond, has subsequently been supported by a large variety of calculations [171, 261–271]. For example, Ponec and Gatti state: "In our opinion, for any interaction to be classified as [a] 'chemical bond', it must be possible to associate it with an electron pair, but as it is clearly evident from the DAFH analysis, there is no electron pair that could be associated with the Fe···Fe bond [271].[20]

Despite the above preponderance of evidence, however, the molecular structure of $Fe_2(CO)_9$ continues to appear in textbooks [244–256], with an Fe–Fe bond.[21] Furthermore, other dinuclear bridging carbonyl compounds for which calculations and experiments indicate the absence of such interactions have also been

[18] In addition to bridging in a symmetric manner, carbonyl ligands are also known to adopt bent semibridging and linear semibridging coordination modes; the bonding in these complexes is highly varied and is not part of the scope of the present article; for key references, see [228–237].

[19] A subsequent higher-quality structure revealed an Fe–Fe distance of 2.523(1) Å; see [242].

[20] Although some theoretical articles have suggested the possibility of a weak direct Fe–Fe attractive interaction in $Fe_2(CO)_9$, the interpretation has been questioned [271].

[21] We are aware of only two textbooks that discuss the absence of a direct Fe–Fe bond in $Fe_2(CO)_9$. Of these, one does not include a drawing of the molecule [272], while the other draws the molecule both without an Fe–Fe bond and also with a dotted Fe···Fe bond [273]; however, there is no discussion as to how the latter description should be employed with respect to electron counting purposes. Also of note, $[CpM(CO)(\mu\text{-}CO)]_2$ has been represented on the cover of a textbook, without including a M–M bond, but the bonding was not discussed [274].

represented with M–M bonds, as illustrated by the bridged form[22] of $Co_2(CO)_8$ [265, 275, 277][23] and $[CpFe(CO)(\mu\text{-}CO)]_2$ [278–286].[24]

The origin of the widespread misrepresentation of such molecules is due to the fact that symmetrically bridging carbonyl ligands are normally considered to be $\mu\text{-}X_2$ "ketonic" in character. However, as discussed below, a symmetrically bridging carbonyl ligand can also be described as a μ–L donor [13], and this difference allows metal centers to achieve 18-electron configurations without the necessity of forming a M–M bond [13, 288].

Representation of 3c–2e Bonds in Symmetrically Bridging M(μ-CO)M Carbonyl Systems

The bonding of a symmetrically bridging carbonyl ligand can be described in terms of two 3-center molecular orbitals derived from the interactions of the 5σ HOMO [289–291] and a 2π* orbital of CO with appropriate metal d-orbitals [171, 258, 260–271, 292]. For example, an in-phase combination of metal d-orbitals is of appropriate symmetry to interact with the 5σ HOMO of CO (i.e., σ-donation), while the out-of-phase metal combination is of appropriate symmetry to interact with one of the 2π* C–O antibonding orbitals (i.e., π-backbonding), as illustrated in Fig. 53.

If both the σ-bonding and π-backbonding orbitals are occupied, the overall interaction can be represented in terms of two 2c–2e bonds, as in ketones (Fig. 54a). However, if only the σ-bonding orbital is occupied and there is no π-backbonding, then it is not possible to describe the bonding in terms of two 2c–2e bonds, and it can only be represented as a 3c–2e interaction (Fig. 54b).

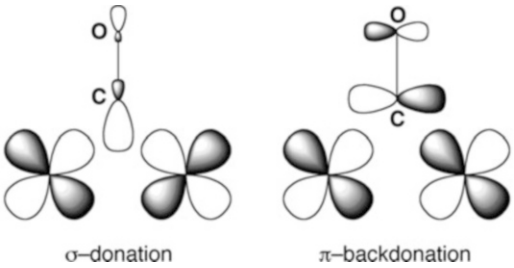

Fig. 53 The two bonding molecular orbitals derived from interaction of the 5σ HOMO and one of the 2π* C–O antibonding orbitals with the in-phase and out-of-phase combination of metal d-orbitals

[22] $Co_2(CO)_8$ exists as an equilibrium between bridged, $(CO)_3Co(\mu\text{-}CO)_2Co(CO)_3$, and non-bridged isomers, $(CO)_4Co\text{–}Co(CO)_4$, of which the former is the major isomer.

[23] Experimental charge-density studies are also in accord with the absence of a direct Co–Co bond in the bridged form of $Co_2(CO)_8$; see [276].

[24] For other articles that describe the absence of M–M bonds in other carbonyl bridged compounds, for a similar reason, see [287].

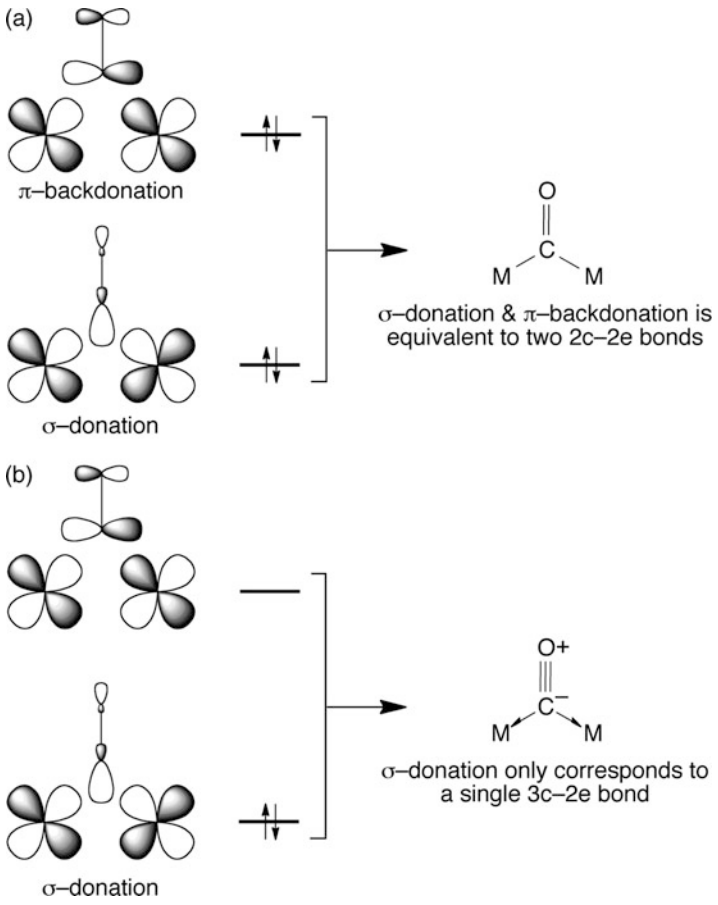

Fig. 54 MOs for a M(μ-CO)M interaction (**a**) occupied by four electrons, giving two 2c–2e bonds, and (**b**) occupied by two electrons, giving a 3c–2e bond because the orbital corresponding to π-backdonation is empty. For (**a**), the CO is classified as a μ–X_2 donor and contributes one electron to each metal, whereas for (**b**), the CO is classified as a μ–L donor and contributes a pair of electrons to both metals

The consequence of this modified bonding description is that the carbonyl ligand is a μ–L donor, such that the pair of electrons contributes to the electron count of *both* metals (Fig. 54b). Since a "ketonic" CO contributes one electron to each metal (Fig. 54a), it is evident that the two types of carbonyl ligand result in different electron counts for the metal centers and hence different M–M bond orders. As will be discussed in more detail below, recognizing that a carbonyl ligand can serve as a μ–L donor provides a simple means to reconcile the theoretically computed M–M bond orders with those predicted on the basis of electron counting.

Analysis of the Bridging Interactions in $Fe_2(CO)_9$

The bonding within $Fe_2(CO)_9$ has received considerable attention, and a simple molecular orbital description that focuses on the bridging interactions (Fig. 54) in D_{3h} symmetry is provided in Fig. 55 [259, 260]. Thus, each $[Fe(CO)_3]$ fragment has three orbitals and two electrons available for bonding, while each bridging carbonyl ligand contributes a 5σ orbital, the $2\pi_z^*$ orbital that lies parallel to Fe–Fe axis (*z*),[25] and a pair of electrons. The component of the molecular orbital diagram that pertains to the $Fe(\mu\text{-}CO)_3Fe$ moiety thus contains ten electrons, with six being contributed by the three CO ligands and four being contributed by the two $[Fe(CO)_3]$ fragments (Fig. 55).

The most important aspect of this molecular orbital diagram is that there are three occupied bonding orbitals (a_1' and *e*') that correspond to donation by the three 5σ orbitals (Fig. 55), but only two occupied bonding orbitals (*e*") that correspond to backbonding into the $2\pi_z^*$ orbitals (Fig. 55). Since each $\mu\text{–}X_2$ "ketonic" description of a carbonyl ligand requires occupation of both the σ- and π-type orbitals, it is evident that the bonding within $Fe_2(CO)_9$ cannot be described as possessing three "ketonic" bridging carbonyl ligands. The bonding within $Fe_2(CO)_9$ is thus more appropriately described as a resonance hybrid in which each structure possesses two $\mu\text{–}X_2$ "ketonic" carbonyl ligands and one μ–L carbonyl ligand (Fig. 56). This resonance description of the bridge bonding is in accord with other theoretical studies. For example, Ponec et al. state that ". . . 4 out of the 5 bonding electron pairs are involved in localized 2c–2e bonding of two bridging ligands, while the remaining ligand is bonded via a delocalized electron pair with the character of [a] 3c–2e bond" [271].

If the three bridging carbonyl ligands in $Fe_2(CO)_9$ are described by one μ–L and two $\mu\text{–}X_2$ interactions, each iron center may achieve an electron count of 18 without the necessity of forming an Fe–Fe bond, as illustrated by the structure-bonding representation in Fig. 57.

Electron counting viewing carbonyl ligands as $\mu\text{–}X_2$ "ketonic" moieties is often invoked for assigning M–M bond orders, with the outcome that it often results in bond orders that are not in accord with theory. In contrast, consideration of the possibility that a carbonyl ligand can serve as a μ–L ligand results in M–M bond orders that are in better accord with theory. For example, structure-bonding representations of the bridged form of $Co_2(CO)_8$ and $[CpFe(CO)(\mu\text{-}CO)]_2$[26] [294], which depict the absence of M–M bonds that are in accord with theory [265, 275, 278–286], are illustrated in Fig. 58.

Thus, whereas a symmetrically bridging carbonyl is commonly represented as a $\mu\text{–}X_2$ "ketonic" ligand, it is evident that its alternative description as a μ–L donor can provide a more accurate representation of the bonding, which thereby allows the prediction of M–M bonds that are in better accord with theory.

[25] The $2\pi^*$ orbitals of CO which are perpendicular to the Fe–Fe axis are neglected from the analysis on the basis that there is little overlap with the metal d-orbitals.

[26] For discussion pertaining to bonding in $[CpFe(CO)(\mu\text{-}CO)]_2$, see [293].

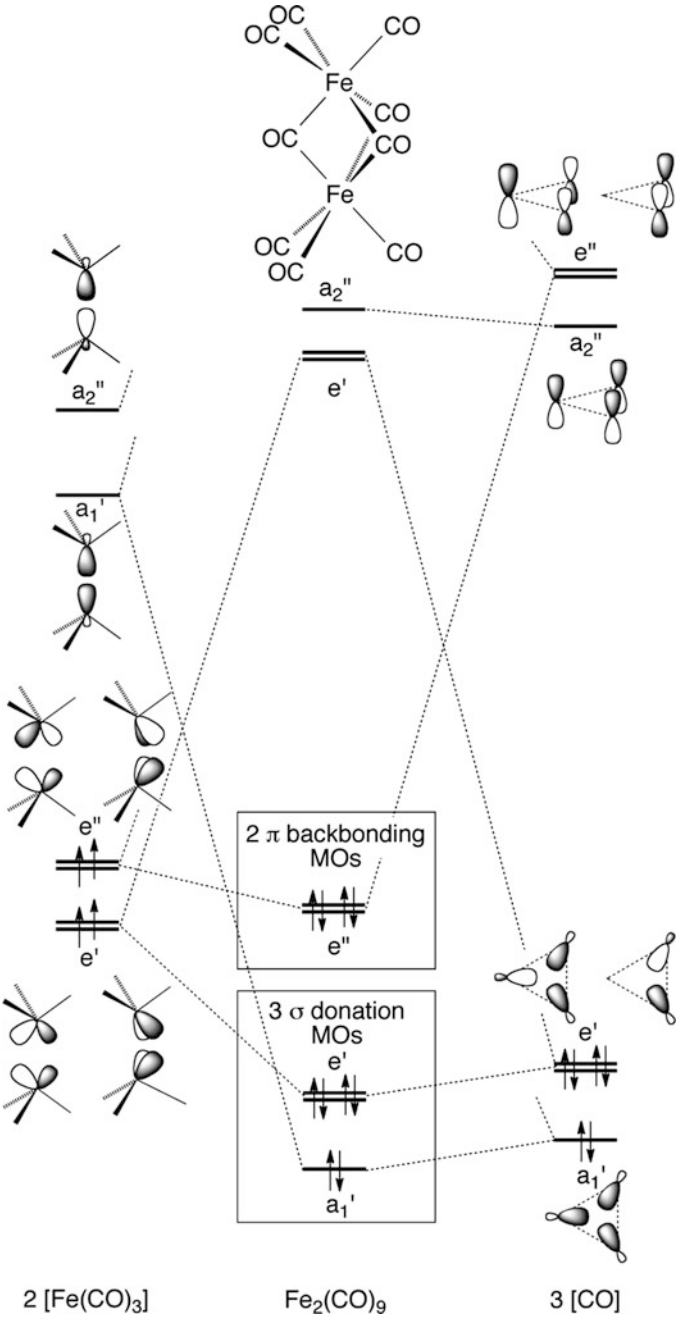

Fig. 55 Qualitative molecular orbital diagram showing the interaction of fragment orbitals involved in bridge bonding in $Fe_2(CO)_9$ with D_{3h} symmetry (the z axis is coincident with the Fe···Fe vector). For clarity, orbitals associated with bonding to the terminal carbonyl ligands are not illustrated, while only the carbon $2p_z$ orbital is used to represent the $2\pi^*$ orbital of CO (adapted from [13])

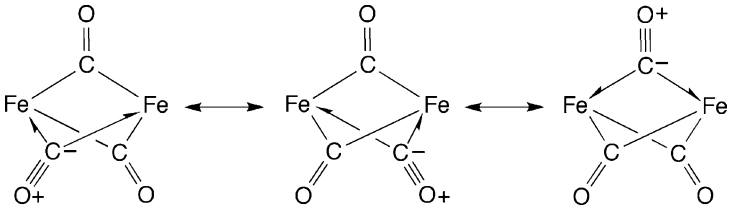

Fig. 56 Three resonance structures that correspond to the bonding illustrated in the molecular orbital diagram of Fig. 55. Each structure corresponds to three donor and two backbonding interactions

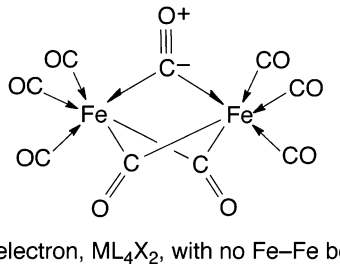

Fig. 57 Structure-bonding representation of $Fe_2(CO)_9$ illustrating that each iron can achieve an 18-electron configuration without an Fe–Fe bond

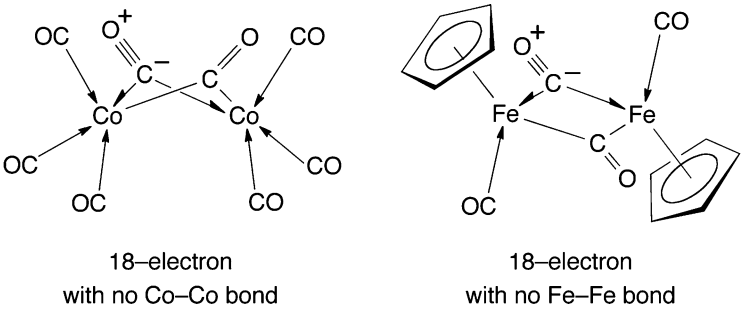

Fig. 58 Structure-bonding representations of $Co_2(CO)_8$ and $[CpFe(CO)(\mu\text{-}CO)]_2$ which depict that each metal can achieve an 18-electron configuration without the presence of a M–M bond (Cp is an L_2X donor)

4.4.4 Bridging BR Ligands

Compounds that feature μ-BR ligands are known, as exemplified by $[CpMn(CO)_2]_2(\mu\text{-}BBu^t)$ [295, 296]. Assuming that the bonding between Mn and B were to be described in terms of two 2c–2e bonds, each Mn center would be classified as 17 electron, such that a Mn–Mn bond would be invoked to rationalize the diamagnetic nature of the compound (Fig. 59, left). However, calculations indicate that there is no direct Mn–Mn bond, which is also in accord with

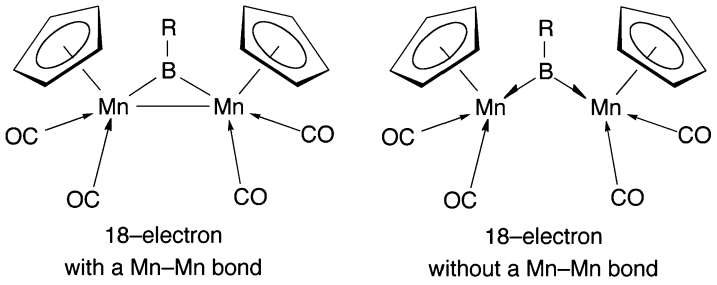

Fig. 59 Structure-bonding representations of $[CpMn(CO)_2]_2(\mu\text{-BR})$ that feature two 2c–2e Mn–B bonds (*left*) and one 3c–2e Mn–B–Mn bond (*right*). The former requires a direct Mn–Mn bond to achieve an 18-electron configuration, whereas the latter does not require a Mn–Mn bond and is in accord with both experiment and theory

experimental studies [295, 296]. The experimental and computational studies may, however, be reconciled by viewing the RB: ligand as a μ–L donor (Fig. 59, right). In this way, the manganese centers can achieve an 18-electron configuration without having to form a Mn–Mn bond.

4.4.5 Coordination of a d^2 Metal Center to a Pair of Lewis Acid Centers

The *bis*(catecholborane)titanocene compound, $Cp_2Ti(\eta^2\text{-HBcat})_2$ (Fig. 60) [161, 297], is an example of a compound in which a metal serves as the L donor in a Class II 3c–2e bond, thereby allowing the close approach of two boron atoms. Specifically, the two boron atoms are separated by 2.11 Å, a distance that is too short for a nonbonding interaction but too long for a conventional B–B bond [299].[27] A direct interaction between the boron atoms in this molecule would be otherwise unexpected because the boron atoms in HBcat are trivalent and unable to form an additional normal covalent 2c–2e bond. Viewing the interaction between titanium and HBcat as involving coordination of the B–H bond, a bonding interaction between the two boron centers may, nevertheless, be achieved via a 3c–2e interaction in which the d^2 titanium center provides the pair of electrons. The structure-bonding representation for this description is provided in Fig. 60 (left), in which the two half arrows, which correspond to donation of a single d^2 pair of electrons from the titanium to the boron atoms, describe the 3c–2e interaction. This description of the bonding is supported by calculations, with the key orbital being shown in the partial molecular orbital diagram of Fig. 61 [159, 300].

In view of the fact that the titanium uses a pair of electrons to enable a B···B interaction, the titanium adopts a d^0, rather than a d^2, configuration (Fig. 61). This situation is very similar to coordination of a single Lewis acid ligand to a metal

[27] For example, the B...B distance of 2.11 Å is ca. 0.4 Å longer than the value in catBBcat derivatives; see [298].

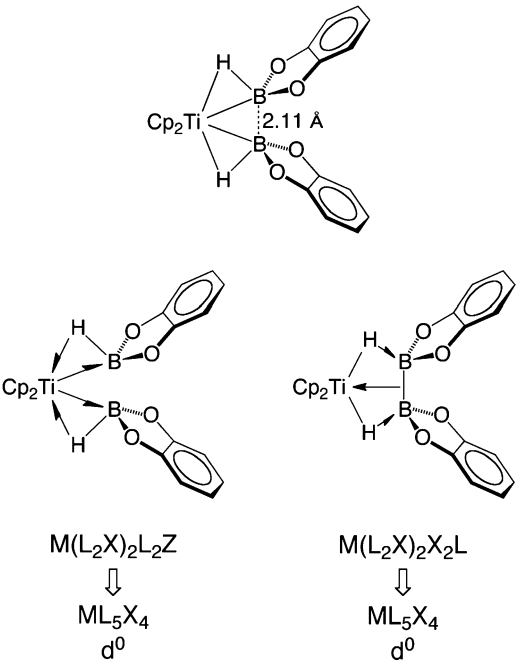

Fig. 60 Structural representation (*top*), in which lines are used merely to indicate connectivity, and structure-bonding representations (*bottom*) for $Cp_2Ti(\eta^2\text{-HBcat})_2$. The structure on the *bottom left* views the compound as an adduct between $[Cp_2Ti]$ and two HBcat moieties, whereas the structure on the *bottom right* views the compound as an adduct between Cp_2TiH_2 and catBBcat

center, in which a d^n metal center becomes d^{n-2} [28, 301–303]. As such, the titanium center of $Cp_2Ti(\eta^2\text{-HBcat})_2$ is classified as tetravalent d^0 18-electron ML_5X_4 (Fig. 60), rather than as a Ti(II) derivative [161, 297]. Correspondingly, the boron is classified as MLX_3 with an octet configuration.

While the view of $Cp_2Ti(\eta^2\text{-HBcat})_2$ as an adduct between $[Cp_2Ti]$ and two molecules of HBcat (Fig. 60, bottom left) is useful because the compound is obtained via a reaction with HBcat, other bonding descriptions are also possible. In particular, $Cp_2Ti(\eta^2\text{-HBcat})_2$ can be regarded as an adduct between Cp_2TiH_2 and the diborane, catBBcat (Fig. 60, bottom right). Such a description is of use because it emphasizes the B–B bonding interaction. Regardless of which bonding description one prefers to adopt, however, the CBC descriptions of the molecule (ML_5X_4) are the same. In contrast, formalisms based on oxidation state concepts result in different descriptions, namely, Ti(II) and Ti(IV) [161, 297].

4.5 Polyfunctional Bridging Ligands

4.5.1 Bridging Benzene, Cyclopentadienyl, and Borole Ligands

In addition to the examples described above in which a bridging ligand coordinates via a single atom, there are many examples in which a ligand coordinates in a multifunctional manner to two metals. While these compounds are not explicitly

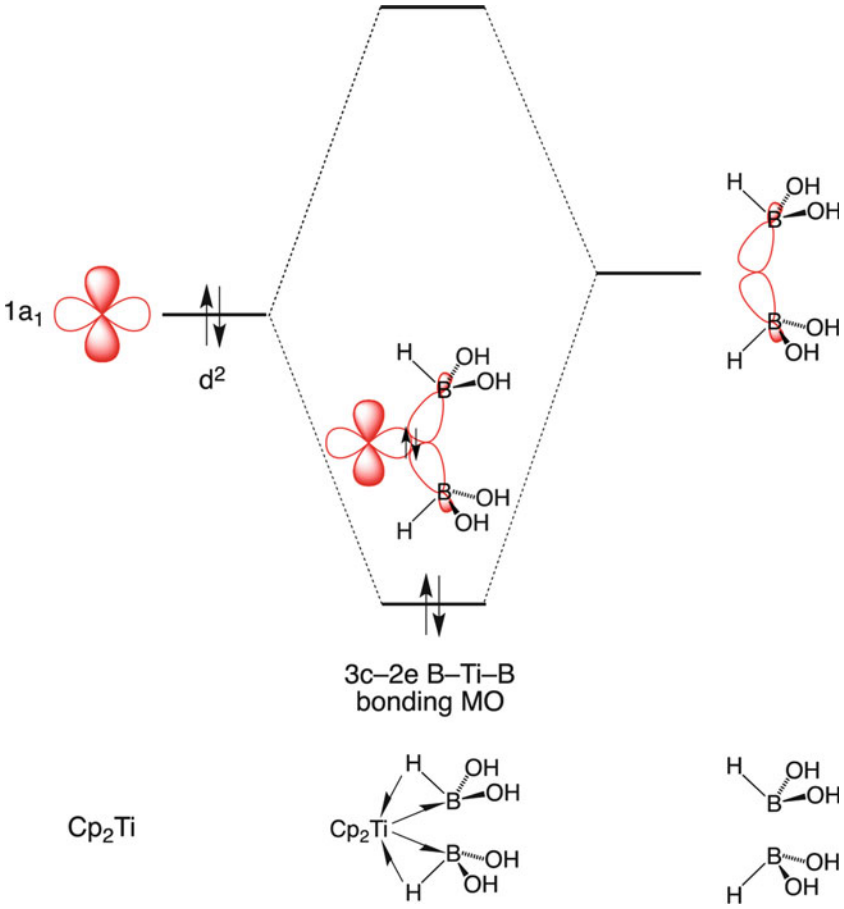

Fig. 61 3c–2e interaction for $Cp_2Ti[\eta^2\text{-}HB(OH)_2]_2$. Note that while the configuration of the titanium in the $[Cp_2Ti]$ moiety is d^2, it becomes d^0 upon coordination of the two borane ligands and formation of the 3c–2e bond

classified as possessing 3-center 2-electron interactions, the representations used above can also be used for such compounds. For example, ligands such as benzene, cyclopentadienyl, and borole may coordinate to two metals in a symmetric manner via their opposite faces. Such compounds are often called "inverse sandwiches," as illustrated by the examples in Figs. 62 [304–307],[28] 63 [308–310], and 64 [311, 312]; structure-bonding representations for these interactions are provided in Fig. 65, which show that (1) a bridging benzene ligand serves as an L_3 donor to each metal, (2) a bridging cyclopentadienyl ligand serves as an L_2X ligand to one

[28] The structure-bonding representation for the zirconium compound is one in which only one of the oxygen lone pairs of each aryloxide ligand participates in π-donation; additional π-donation would result in an 18-electron ML_6X_2 classification.

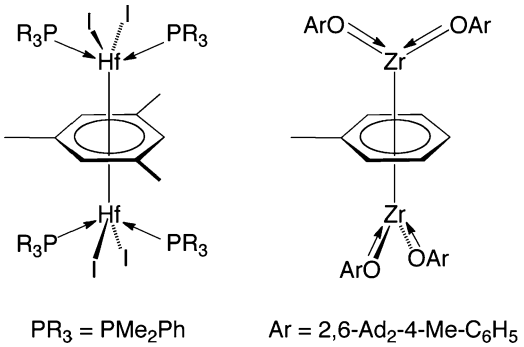

Fig. 62 Examples of compounds that feature bridging arene ligands

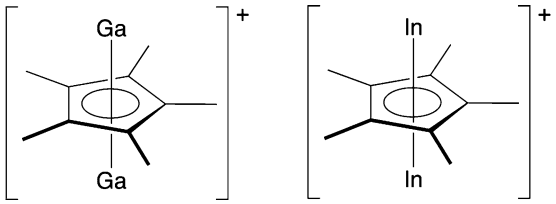

Fig. 63 Examples of compounds that feature bridging cyclopentadienyl ligands

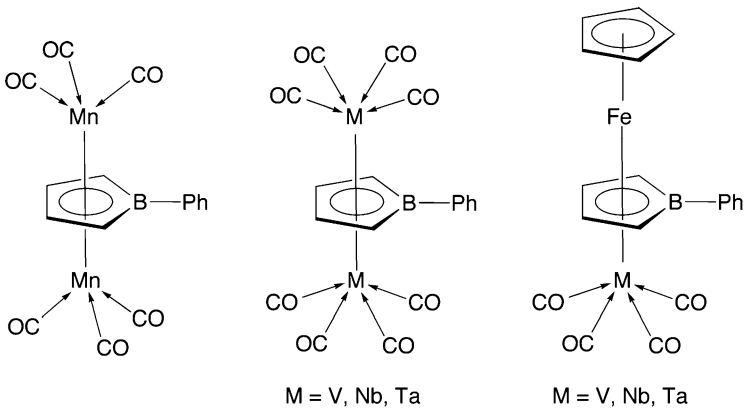

Fig. 64 Examples of compounds that feature bridging borole ligands

metal (M') and as an L_3 ligand to the other (M), and (3) a bridging borole ligand serves as an L_2X ligand to each metal.

Furthermore, these motifs may be elaborated into multi-decker structures. For example, triple-decker arene complexes are common [313, 314], of which a classic example is provided by the mesitylene complex (η^6-MesH)Cr(μ-η^6,η^6-MesH)Cr(η^6-MesH) [315, 316] (Fig. 66, left). Since bridging arene ligands serve as L_3 donors to each

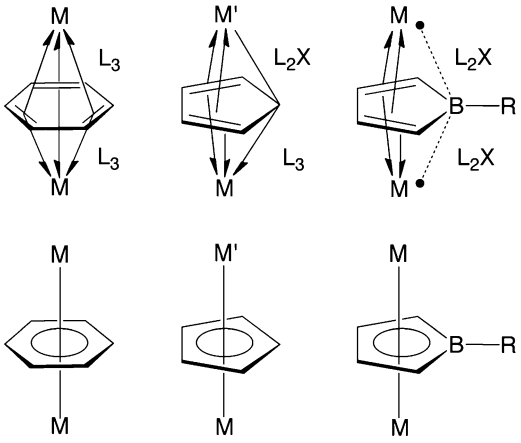

Fig. 65 Structure-bonding representations (*top*) for bridging benzene, cyclopentadienyl, and borole ligands, together with the simplified versions that are used to indicate connectivity (*bottom*)

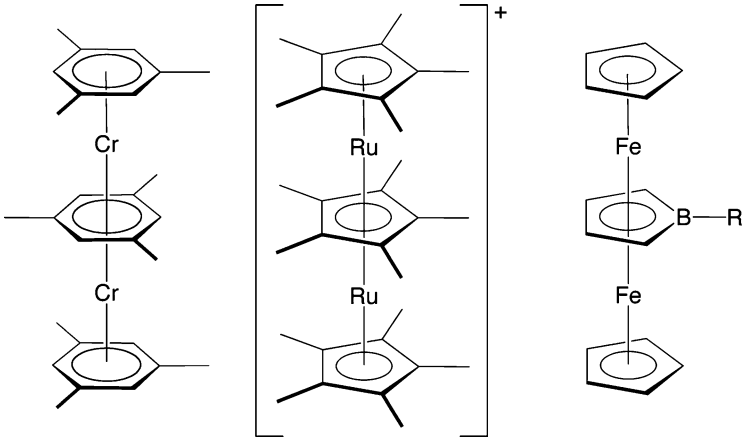

Fig. 66 Triple-decker compounds that feature bridging benzene, cyclopentadienyl, and borole ligands

metal center [313], both chromium centers of (η^6-MesH)Cr(μ-η^6,η^6-MesH)Cr(η^6-MesH) possess 18-electron configurations. Triple-decker compounds with bridging cyclopentadienyl compounds are also well known for both transition metals [313, 317, 318] and main group metals [319, 320], as illustrated by $[Cp^*_3Ru_2]^+$ (Fig. 66, center) [318]. Likewise, borole ligands also form triple-decker compounds, as illustrated by $[CpFe]_2(C_4H_4BR)$ (Fig. 66, right) [321].

4.5.2 Dinuclear Pentalene Complexes

In contrast to benzene, cyclopentadienyl, and borole, organic ligands that possess more than one ring system typically coordinate to two metals via different rings rather than the same ring. An interesting example of a ligand that behaves in this manner is provided by pentalene (C_8H_6), which is an 8π-electron bicyclic antiaromatic molecule (Fig. 67) that is unstable with respect to dimerization but may be stabilized by either formation of the dianion or by coordination to a metal center [322–324]. A wide variety of metal complexes that contain pentalene or its derivatives are known [325, 326], with a particularly interesting class of molecules being those in which the pentalene ligand coordinates to two metal centers. The metal centers in such compounds may reside on either the same face of the pentalene ligand (syn) or on opposite faces (anti), as illustrated in Fig. 68.

Pentalene can be represented by a variety of resonance structures (Fig. 67) and conventional electron counting procedures simply apportion four electrons of a neutral bridging pentalene ligand to each metal center [327, 328]. For such a scenario, the pentalene ligand behaves as an L_2 donor to each metal (Fig. 69, left).

However, the pentalene ligand can also be considered to coordinate in such a manner that the double bond associated with the ring junction of the *bis*(allyl) class of resonance structures (Fig. 67, bottom) can serve as an L donor to *both* metals. In this scenario, the pentalene ligand acts as a five-electron L_2X donor to each metal center (Fig. 69, right). These two different coordination modes clearly result in different electron counts at the metal centers. However, calculations indicate that the pentalene ligand is most appropriately described as coordinating in an L_2X manner to each metal center.

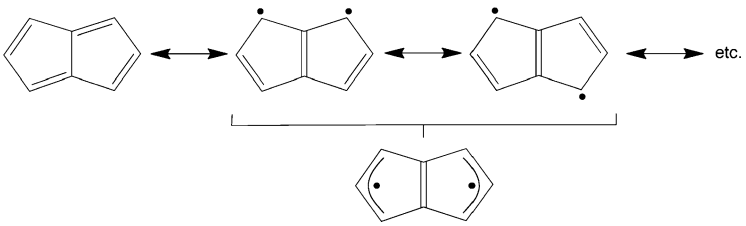

Fig. 67 Some of many resonance structures of pentalene

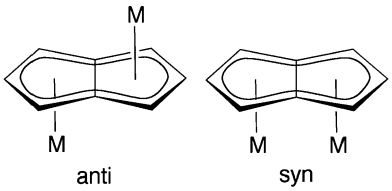

Fig. 68 Anti- and *syn*-coordination of two metals to a pentalene ligand, indicating only connectivity

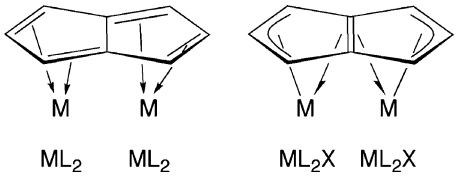

Fig. 69 Conventional electron counting assigns a pentalene ligand as a four-electron donor to each metal (*left*). However, a pentalene ligand behaves as a five-electron L_2X donor (*right*) to each metal if the double bond of the ring junction is considered to serve as a μ–L donor (the allyl portion is an LX donor)

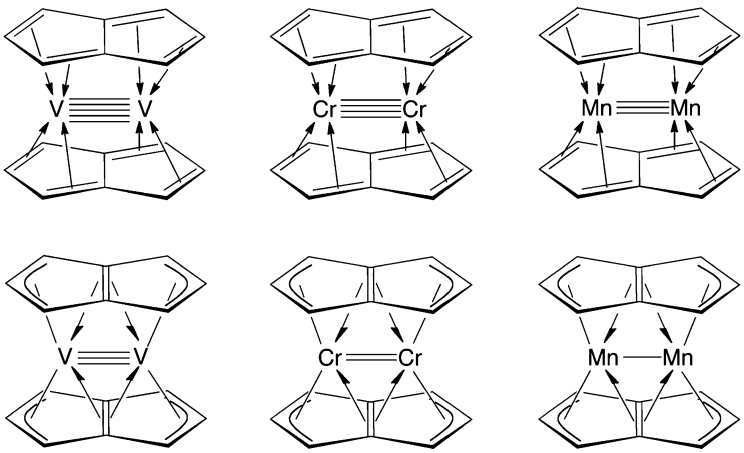

Fig. 70 M–M bond orders for some dinuclear *bis*(pentalene) derivatives (substituents are not shown for clarity) predicted by assuming that the bridging pentalene is either (i) a four-electron L_2 donor to each metal (*top*) or (ii) a five-electron L_2X donor to each metal (*bottom*). The M–M bond orders predicted by the latter method are in accord with theory, whereas those predicted by the former approach are in disagreement

For example, assuming that the pentalene ligand coordinates as an L_2 donor to each metal center, metal–metal bond orders of 5 for V, 4 for Cr, and 3 for Mn would be predicted for the dinuclear *bis*(pentalene) derivatives, $(\mu\text{-}\eta^5,\eta^5\text{-}Pn^R)_2M_2$, on the basis of the 18-electron rule (Fig. 70, top). Density functional theory calculations, however, predict lower values for the metal–metal bond orders (Fig. 70, bottom) [327–329]. As an illustration, $(\mu\text{-}\eta^5,\eta^5\text{-}Pn^{1,4-(SiPr^i_3)_2})_2Cr_2$ is calculated to have a formal Cr = Cr double bond rather than a quadruple bond [328]. The bond orders predicted by density functional theory calculations are, nevertheless, in accord with the values predicted by assuming that the pentalene acts as an L_2X donor to each metal center. Furthermore, a Ti=Ti double bond is predicted for a dinuclear *bis*(pentalene) derivative of titanium, thereby allowing each titanium to achieve a 16-electron configuration [86, 87]. Calculations on a rhodium derivative indicate a Rh–×–Rh antibonding interaction, which is also in accord with the pentalene ligand serving as a five-electron donor to each metal [330].

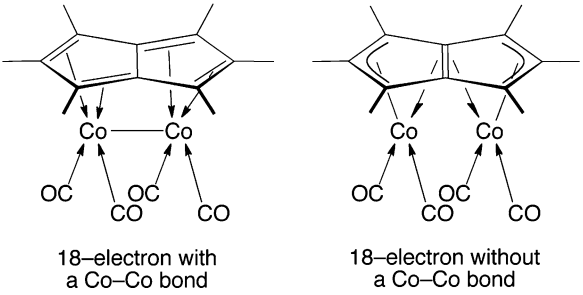

Fig. 71 (μ-η^5,η^5-Pn*)[Co(CO)$_2$]$_2$ is predicted to have a Co–Co single bond if the bridging pentalene is a four-electron L_2 donor to each metal (*left*) and no Co–Co bond if it is a five-electron L_2X donor to each metal (*right*). The latter is in accord with both experiment and theory

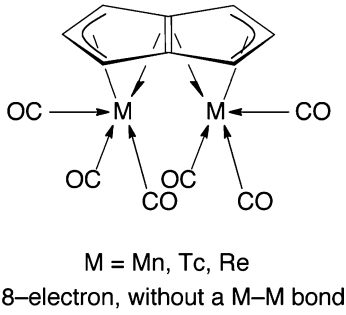

Fig. 72 Structure-bonding representation of *syn*-(μ-η^5,η^5-Pn)[M(CO)$_3$]$_2$ (M = Mn, Tc, Re) indicating that a M–M bond is not required to achieve an 18-electron configuration

In addition to dinuclear *bis*(pentalene) compounds, dinuclear mono(pentalene) compounds are also known and the metal–metal bond orders in such compounds can also be predicted by considering the pentalene ligand to serve as a five-electron L_2X donor to each metal center. As an illustration, the cobalt centers of *syn*-(μ-η^5,η^5-Pn*)[Co(CO)$_2$]$_2$ (Pn* = C_8Me_6) achieve the 18-electron ML_4X classification without the need to form a Co–Co bond (Fig. 71), which is also in accord with theory [331, 332].

Likewise, the rhenium counterpart *syn*-(μ-η^5,η^5-Pn)[Re(CO)$_3$]$_2$ has a long Re···Re distance (3.23 Å) that is indicative of no direct interaction, which is consistent with the ML_5X classification that is predicted by considering the pentalene ligand serving as a five-electron L_2X donor (Fig. 72) [333]. This description of the bonding in *syn*-(μ-η^5,η^5-Pn)[Re(CO)$_3$]$_2$ is also in accord with calculations on *syn*-(μ-η^5,η^5-Pn)[M(CO)$_3$]$_2$ (M = Mn, Tc, Re), which indicate that there is no direct M–M bond in these complexes [334].[29]

[29] For other calculations on this system which propose a Mn–Mn bond, see [335].

DFT calculations also indicate the absence of an Fe–Fe bond in the iron compound *syn*-(μ-η^5,η^5-Pn*)[Fe(CO)$_2$]$_2$(μ-CO) [331], which is of note because the less substituted derivative, *syn*-(μ-η^5,η^5-Pn)[Fe(CO)$_2$]$_2$(μ-CO), has been described as possessing a formal Fe–Fe single bond on the basis that the pentalene ligand donates four π-electrons to each iron (Fig. 73, top) [336, 337]. However, the absence of an Fe–Fe bond is predicted by adopting the view that the pentalene ligand is an L_2X donor to each iron center (Fig. 73, bottom).

The ruthenium compound *syn*-(μ-η^5,η^5-Pn)[Ru(CO)$_2$(GeMe$_3$)]$_2$ has also been represented with a metal–metal bond (Fig. 74, top) [338, 339], but subsequent calculations indicate that there is no significant interaction between the metal centers [340]. As such, the calculations are in agreement with the structure-bonding representation that invokes the pentalene ligand as an L_2X donor to each ruthenium (Fig. 74, bottom).

Two metal centers may also coordinate via opposite faces of the pentalene ligand in an anti-manner. The bonding in complexes with this arrangement can likewise be viewed in terms of the double bond of the ring junction acting as a μ–L donor, such that each ring is a five-electron L_2X donor to each metal. In this manner, the iron and manganese complexes, anti-(μ-η^5,η^5-Pn)[FeCp*$_2$] [341, 342] and anti-(μ-η^5,η^5-Pn)[Mn(CO)$_3$]$_2$, are predicted to have 18-electron configurations (Fig. 75) rather than the 17-electron configurations that would otherwise be predicted if the pentalene ligands were simply considered to be four-electron donors to each metal.

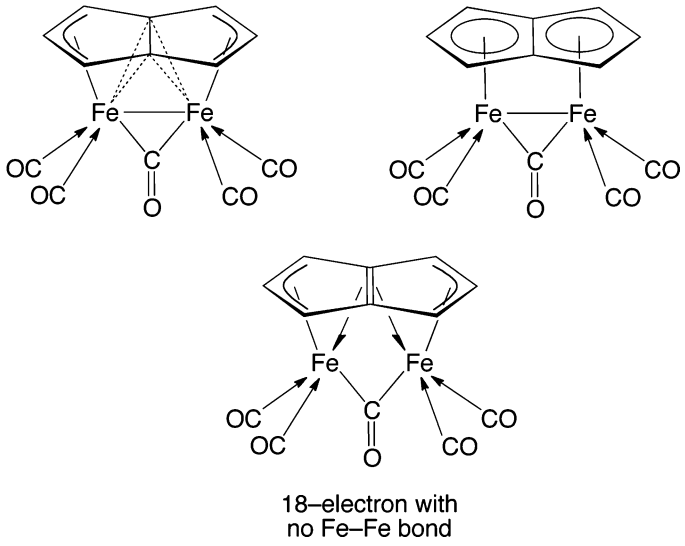

Fig. 73 Literature representations [336, 337] of *syn*-(μ-η^5,η^5-Pn)[Fe(CO)$_2$]$_2$(μ-CO) that portray an Fe–Fe bond (*top*) and an alternative structure-bonding representation that requires no Fe–Fe bond to achieve an 18-electron configuration (*bottom*). The latter description is in accord with theoretical calculations on *syn*-(μ-η^5,η^5-Pn*)[Fe(CO)$_2$]$_2$(μ-CO). Pentalene substituents for the latter are not included for clarity

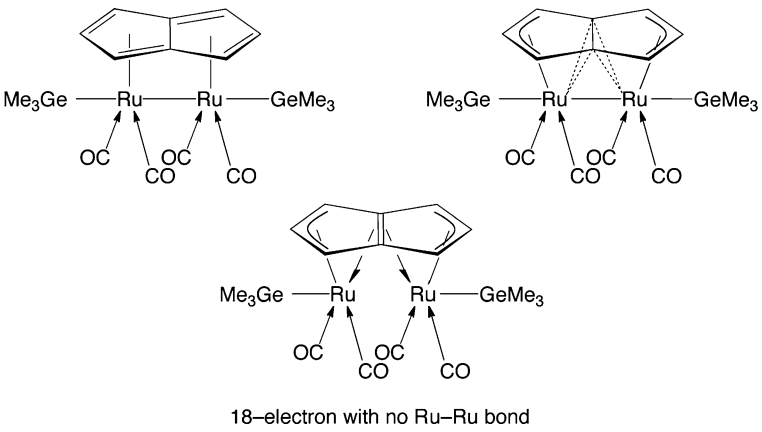

Fig. 74 Literature representations of *syn*-(μ-η^5,η^5-Pn)[Ru(CO)$_2$(GeMe$_3$)]$_2$ which include a Ru–Ru bond (*top*) and a structure-bonding representation that requires no Ru–Ru bond to achieve an 18–electron configuration (*bottom*). The latter description is in accord with theoretical calculations

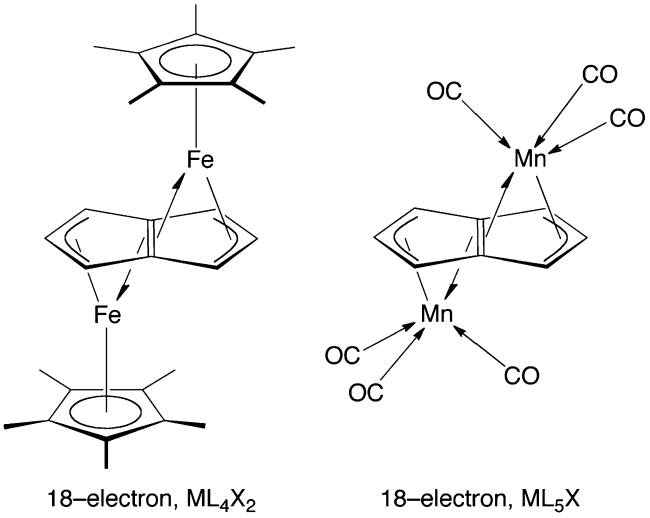

Fig. 75 Structure-bonding representations of anti-(μ-η^5,η^5-Pn)[FeCp*$_2$] (*left*) and anti-(μ-η^5,η^5-Pn)[Mn(CO)$_3$]$_2$ (*right*), which illustrate how each metal achieves an 18-electron configuration if the pentalene serves as an L$_2$X ligand to each metal

The metal centers in these compounds are, therefore, formally analogous to those in the well-known cyclopentadienyl compounds, CpMn(CO)$_3$ and Cp$_2$Fe, which thereby reiterates the validity of classifying the pentalene ligand as an L$_2$X donor to each metal.

5 Summary

While it is possible to represent the bonding in most compounds in terms of 2c–2e bonds, there are many compounds for which this bonding description is inappropriate, such that the bonding must be represented in terms of multicenter interactions. This article provides a method for classifying 3c–2e interactions according to the number of electrons that each partner contributes, in much the same way that 2c–2e bonds can be classified as (1) a normal covalent bond if each atom contributes one electron each and (2) a dative covalent bond if one atom contributes both electrons. Thus, a Class I 3c–2e interaction corresponds to a situation in which two atoms each contribute one electron to the bonding molecular orbital (i.e., $[X_2Z]$), while a Class II interaction corresponds to a situation in which a single atom contributes both electrons (i.e., $[LZ_2]$). Further subclassification takes into account (1) the identity of the bridging atom, i.e., μ–L, μ–X, or μ–Z, and (2) whether the interaction is open (μ^o) or closed (μ^c). Of these, the open μ^o–Z interaction had not previously been recognized.

The article also describes structure-bonding representations for these interactions, which thereby provide a means to count electrons on a metal center and determine its $[ML_lX_xZ_z]$ covalent bond classification. This approach is of particular benefit when the nature of a M–M bonding interaction is to be evaluated in the presence of a bridging ligand. For example, it provides a means to explain the absence of an Fe–Fe bond in $Fe_2(CO)_9$ and predicts M–M bond orders in bridging hydride compounds that are in accord with theory.

Acknowledgments G. P. thanks the US Department of Energy Office of Basic Energy Sciences (DE-FG02-93ER14339) for support. This report was prepared as an account of work sponsored by an agency of the US government. Neither the US government nor any agency thereof, nor any of their employees, makes any warranty, express or implied, or assumes any legal liability or responsibility for the accuracy, completeness, or usefulness of any information, apparatus, product, or process disclosed or represents that its use would not infringe privately owned rights. Reference herein to any specific commercial product, process, or service by trade name, trademark, manufacturer, or otherwise does not necessarily constitute or imply its endorsement, recommendation, or favoring by the US government or any agency thereof. The views and opinions of authors expressed herein do not necessarily state or reflect those of the US government or any agency thereof.

References

1. Lewis GN (1916) J Am Chem Soc 38:762–785
2. Lewis GN (1923) Valence and the structure of atoms and molecules. The Chemical Catalog, New York
3. Lewis GN (1933) J Chem Phys 1:17–28
4. Gillespie RJ, Robinson EA (2007) J Comput Chem 28:87–97
5. Longuet-Higgins HC, Bell RP (1943) J Chem Soc, 250–255
6. Bell RP, Longuet-Higgins HC (1945) Proc R Soc London, Ser A 183:357–374

7. Laszlo P (2000) Angew Chem Int Ed Engl 39:2071–2072
8. Langmuir I (1921) Science 54:59–67
9. Langmuir I (1919) Proc Natl Acad Sci U S A 5:252–259
10. Kossel W (1916) Ann Phys 49:229–362
11. Mingos DMP (2004) J Organomet Chem 689:4420–4436
12. Jensen WB (2005) J Chem Educ 82:28
13. Green JC, Green MLH, Parkin G (2012) Chem Commun 48:11481–11503
14. Green MLH (1995) J Organomet Chem 500:127–148
15. Parkin G (2006) Chapter 1. In: Crabtree RH, Mingos DMP (eds) Comprehensive organometallic chemistry III, vol 1. Elsevier, Oxford
16. Green MLH, Parkin G (2014) J Chem Educ 91:807–816
17. Parkin G (2006) J Chem Educ 83:791–799
18. Jean Y (2005) Molecular orbitals of transition metal complexes. Oxford University Press, London
19. Astruc D (2007) Organometallic chemistry and catalysis. Springer, New York
20. Spessard GO, Miessler GL (1996) Organometallic Chemistry. Prentice-Hall, Englewood Cliffs
21. Miessler GL, Fischer PJ, Tarr DA (2014) Inorganic chemistry, 5th edn. Prentice-Hall, Englewood Cliffs
22. Crabtree RH (2009) The organometallic chemistry of the transition metals, 5th edn. Wiley-Interscience, Hoboken
23. Hartwig J (2010) Organotransition metal chemistry: from bonding to catalysis. University Science Books, Sausalito
24. Seddon EA, Seddon KR (1984) Chapter 2. In: The chemistry of ruthenium. Elsevier, New York
25. Amgoune A, Bourissou D (2011) Chem Commun 47:859–871
26. Braunschweig H, Dewhurst RD (2011) Dalton Trans 40:549–558
27. Haaland A (1989) Angew Chem Int Ed Engl 28:992–1007
28. Parkin G (2006) Organometallics 25:4744–4747
29. Landry, VK, Pang, K, Quan, SM, Parkin, G (2007) Dalton Trans 820–824
30. Bau R, Teller RG, Kirtley SW, Koetzle TF (1979) Acc Chem Res 12:176–183
31. Walsh, AD (1947) J Chem Soc 89–92
32. Berry M, Cooper NJ, Green MLH, Simpson SJ (1980) J Chem Soc Dalton Trans 29–41
33. Jansen M (1987) Angew Chem Int Ed Engl 26:1098–1110
34. Pyykkö P (1997) Chem Rev 97:597–636
35. Sculfort S, Braunstein P (2011) Chem Soc Rev 40:2741–2760
36. Carvajal MA, Alvarez S, Novoa JJ (2004) Chem Eur J 10:2117–2132
37. Schmidbaur H, Schier A (2015) Angew Chem Int Ed 54:746–784
38. Robilotto TJ, Bacsa J, Gray TG, Sadighi JP (2012) Angew Chem Int Ed 51:12077–12080
39. Hall KP, Mingos DMP (1984) Prog Inorg Chem 32:237–325
40. Galassi R, Poli R, Quadrelli EA, Fettinger JC (1997) Inorg Chem 36:3001–3007
41. Esterhuysen MW, Raubenheimer HG (2003) Acta Crystallogr C59:m286–m288
42. Tsui EY, Müller P, Sadighi JP (2008) Angew Chem Int Ed Engl 47:8937–8940
43. Kubas GJ (2001) Metal dihydrogen and σ-bond complexes: structure, theory, and reactivity. Kluwer Academic/Plenum, New York
44. Kubas GJ (2001) J Organomet Chem 635:37–68
45. Kubas GJ (2007) Proc Natl Acad Sci U S A 104:6901–6907
46. Kubas GJ (2007) Chem Rev 107:4152–4205
47. Kubas GJ (2009) J Organomet Chem 694:2648–2653
48. Gordon JC, Kubas GJ (2010) Organometallics 29:4682–4701
49. Kubas GJ (2014) J Organomet Chem 751:33–49
50. Dutta S (2011) C R Chim 14:1029–1053
51. Crabtree RH (1993) Angew Chem Int Ed Engl 32:789–805

52. Perutz RN, Sabo-Etienne S (2007) Angew Chem Int Ed 46:2578–2592
53. McGrady GS, Guilera G (2003) Chem Soc Rev 32:383–392
54. Crabtree RH, Hamilton DG (1988) Adv Organomet Chem 28:299–338
55. Kubas GJ, Ryan RR, Swanson BI, Vergamini PJ, Wasserman HJ (1984) J Am Chem Soc 106:451–452
56. Upmacis RK, Gadd GE, Poliakoff M, Simpson MB, Turner JJ, Whyman R, Simpson AF (1985) J Chem Soc Chem Commun 27–30
57. Matthews SL, Heinekey DM (2006) J Am Chem Soc 128:2615–2620
58. Matthews SL, Pons V, Heinekey DM (2005) J Am Chem Soc 127:850–851
59. Rybtchinski B, Milstein D (1999) Angew Chem Int Ed 38:870–883
60. Etienne M, Weller AS (2014) Chem Soc Rev 43:242–259
61. Brayshaw SK, Green JC, Kociok-Kohn G, Sceats EL, Weller AS (2006) Angew Chem Int Ed 45:452–456
62. Brayshaw SK, Sceats EL, Green JC, Weller AS (2007) Proc Natl Acad Sci U S A 104:6921–6926
63. Chaplin AB, Weller AS (2013) J Organomet Chem 730:90–94
64. Chaplin AB, Green JC, Weller AS (2011) J Am Chem Soc 133:13162–13168
65. Sparkes HA, Kramer T, Brayshaw SK, Green JC, Weller AS, Howard JAK (2011) Dalton Trans 40:10708–10718
66. Nikonov GI (2003) Angew Chem Int Ed 42:1335–1337
67. Sherer EC, Kinsinger CR, Kormos BL, Thompson JD, Cramer CJ (2002) Angew Chem Int Ed 41:1953–1956
68. Aullon G, Lledos A, Alvarez S (2002) Angew Chem Int Ed 41:1956–1959
69. Chen WZ, Shimada S, Tanaka M (2002) Science 295:308–310
70. Crabtree RH (2002) Science 295:288–289
71. Gualco P, Amgoune A, Miqueu K, Ladeira S, Bourissou D (2011) J Am Chem Soc 133:4257–4259
72. Berthon-Gelloz G, de Bruin B, Tinant B, Marko IE (2009) Angew Chem Int Ed 48:3161–3164
73. Takagi N, Sakaki S (2012) J Am Chem Soc 134:11749–11759
74. Liu HJ, Raynaud C, Eisenstein O, Tilley TD (2014) J Am Chem Soc 136:11473–11482
75. Gibson DH (1996) Chem Rev 96:2063–2095
76. Leitner W (1996) Coord Chem Rev 153:257–284
77. Yin X, Moss JR (1999) Coord Chem Rev 181:27–59
78. English NJ, El-Hendawy MM, Mooney DA, MacElroy JMD (2014) Coord Chem Rev 269:85–95
79. Aresta M, Dibenedetto A (2007) Dalton Trans 2975–2992
80. Castro-Rodriguez, I, Meyer, K (2006) Chem Commun 1353–1368
81. Castro-Rodriguez I, Nakai H, Zakharov LN, Rheingold AL, Meyer K (2004) Science 305:1757–1759
82. Castro-Rodriguez I, Meyer K (2005) J Am Chem Soc 127:11242–11243
83. Lee CH, Laitar DS, Mueller P, Sadighi JP (2007) J Am Chem Soc 129:13802–13803
84. Kilpatrick AFR, Green JC, Cloke FGN (2015) Organometallics 34:4816–4829
85. Kilpatrick AFR, Green JC, Cloke FGN (2015) Organometallics 34:4830–4843
86. Kilpatrick AFR, Green JC, Cloke FGN, Tsoureas N (2013) Chem Commun 49:9434–9436
87. Greatrex R, Greenwood NN, Rankin DWH, Robertson HE (1987) Polyhedron 6:1849–1858
88. Hedberg K, Jones ME, Schomaker V (1952) Proc Natl Acad Sci U S A 38:679–686
89. Dulmage WJ, Lipscomb WN (1952) Acta Cryst 5:260–264
90. Lipscomb WN (1972) Pure Appl Chem 29:493–511
91. Lipscomb WN (1973) Acc Chem Res 6:257–262
92. Weinhold F, Landis CR (2005) Valency and bonding: a natural bond orbital donor-acceptor perspective. Cambridge University Press, New York, pp 327–332

93. Greenwood NN, Savory CG, Grimes RN, Sneddon LG, Davison A, Wreford SS (1974) J Chem Soc Chem Commun 718–718
94. Weiss R, Bowser JR, Grimes RN (1978) Inorg Chem 17:1522–1527
95. Venable TL, Sinn E, Grimes RN (1984) J Chem Soc Dalton Trans 2275–2279
96. Miller VR, Weiss R, Grimes RN (1977) J Am Chem Soc 99:5646–5651
97. Brammer L (2003) Dalton Trans 3145–3157
98. Hall C, Perutz RN (1996) Chem Rev 96:3125–3146
99. Crabtree RH (1995) Chem Rev 95:987–1007
100. Young RD (2014) Chem Eur J 20:12704–12718
101. Corey JY (2011) Chem Rev 111:863–1071
102. Corey JY, Braddock-Wilking J (1999) Chem Rev 99:175–292
103. Lin Z (2002) Chem Soc Rev 31:239–245
104. Nikonov GI (2005) Adv Organomet Chem 53:217–309
105. Alcaraz G, Sabo-Etienne S (2008) Coord Chem Rev 252:2395–2409
106. Schubert U (1990) Adv Organomet Chem 30:151–187
107. Lachaize S, Sabo-Etienne S (2006) Eur J Inorg Chem 2115–2127
108. Scherer W, Meixner P, Barquera-Lozada JE, Hauf C, Obenhuber A, Brück A, Wolstenholme DJ, Ruhland K, Leusser D, Stalke D (2013) Angew Chem Int Ed 52:6092–6096
109. Hauf C, Barquera-Lozada JE, Meixner P, Eickerling G, Altmannshofer S, Stalke D, Zell T, Schmidt D, Radius U, Scherer WZ (2013) Anorg Allg Chem 639:1996–2004
110. Scherer W, Eickerling G, Tafipolsky M, McGrady GS, Sirsch P, Chatterton, NP (2006) Chem Commun 2986–2988
111. McGrady GS, Sirsch P, Chatterton NP, Ostermann A, Gatti C, Altmannshofer S, Herz V, Eickerling G, Scherer W (2009) Inorg Chem 48:1588–1598
112. Handzlik J, Szymanska-Buzar T (2014) J Organomet Chem 769:136–143
113. Evans DR, Drovetskaya T, Bau R, Reed CA, Boyd PDW (1997) J Am Chem Soc 119:3633–3634
114. Castro-Rodriguez I, Nakai H, Gantzel P, Zakharov LN, Rheingold AL, Meyer K (2003) J Am Chem Soc 125:15734–15735
115. Pike SD, Thompson AL, Algarra AG, Apperley DC, Macgregor SA, Weller AS (2012) Science 337:1648–1651
116. Pike SD, Chadwick FM, Rees NH, Scott MP, Weller AS, Kramer T, Macgregor SA (2015) J Am Chem Soc 137:820–833
117. Perutz RN, Turner JJ (1975) J Am Chem Soc 97:4791–4800
118. Geftakis S, Ball GE (1998) J Am Chem Soc 120:9953–9954
119. Lawes DJ, Darwish TA, Clark T, Harper JB, Ball GE (2006) Angew Chem Int Ed 45:4486–4490
120. Lawes DJ, Geftakis S, Ball GE (2005) J Am Chem Soc 127:4134–4135
121. Ball GE, Brookes CM, Cowan AJ, Darwish TA, George MW, Kawanami HK, Portius P, Rourke JP (2007) Proc Natl Acad Sci U S A 104:6927–6932
122. Bernskoetter WH, Schauer CK, Goldberg KI, Brookhart M (2009) Science 326:553–556
123. Young RD, Hill AF, Hillier W, Ball GE (2011) J Am Chem Soc 133:13806–13809
124. Young RD, Lawes DJ, Hill AF, Ball GE (2012) J Am Chem Soc 134:8294–8297
125. Cowan AJ, George MW (2008) Coord Chem Rev 252:2504–2511
126. Calladine JA, Duckett SB, George MW, Matthews SL, Perutz RN, Torres O, Khuong QV (2011) J Am Chem Soc 133:2303–2310
127. Calladine JA, Vuong KQ, Sun XZ, George MW (2009) Pure Appl Chem 81:1667–1675
128. McNamara BK, Yeston JS, Bergman RG, Moore CB (1999) J Am Chem Soc 121:6437–6443
129. Jones WD (2003) Acc Chem Res 36:140–146
130. Bullock RM, Bende BR (2002) Isotope methods in homogeneous catalysis. In: Horváth IT (ed) Encyclopedia of catalysis. Wiley, New York
131. Parkin G (2009) Acc Chem Res 42:315–325
132. Parkin G (2007) J Label Compd Radiopharm 50:1088–1114

133. Janak KE (2006) In: Crabtree RH, Mingos DMP (eds) Comprehensive organometallic chemistry III, vol 1. Elsevier, Oxford
134. Gómez-Gallego M, Sierra MA (2011) Chem Rev 111:4857–4963
135. Luo XL, Kubas GJ, Bryan JC, Burns CJ, Unkefer CJ (1994) J Am Chem Soc 116:10312–10313
136. Yang J, White PS, Schauer CK, Brookhart M (2008) Angew Chem Int Ed 47:4141–4143
137. Zuzek AA, Neary MC, Parkin G (2014) J Am Chem Soc 136:17934–17937
138. Zuzek AA, Parkin G (2014) J Am Chem Soc 136:8177–8180
139. Matthews SL, Pons V, Heinekey DM (2006) Inorg Chem 45:6453–6459
140. Zhang SL, Dobson GR, Brown TL (1991) J Am Chem Soc 113:6908–6916
141. Kotz KT, Yang H, Snee PT, Payne CK, Harris CB (2000) J Organomet Chem 596:183–192
142. Burkey TJ (1990) J Am Chem Soc 112:8329–8333
143. Atheaux I, Delpech F, Donnadieu B, Sabo-Etienne S, Chaudret B, Hussein K, Barthelat JC, Braun T, Duckett SB, Perutz RN (2002) Organometallics 21:5347–5357
144. Atheaux I, Donnadieu B, Rodriguez V, Sabo-Etienne S, Chaudret B, Hussein K, Barthelat JC (2000) J Am Chem Soc 122:5664–5665
145. Ben Said R, Hussein K, Barthelat JC, Atheaux I, Sabo-Etienne S, Grellier M, Donnadieu B, Chaudret B (2003) Dalton Trans 4139–4146
146. Lipke MC, Tilley TD (2012) Angew Chem Int Ed Engl 51:11115–11121
147. Shimoi M, Nagai S, Ichikawa M, Kawano Y, Katoh K, Uruichi M, Ogino H (1999) J Am Chem Soc 121:11704–11712
148. Shimoi M, Katoh K, Uruichi M, Nagai S, Ogino H (1994) Syntheses and structures of transition metal complexes of lewis base adducts of borane and borylene. In: Kabalka GW (ed) Current topics in the chemistry of boron. The Royal Society of Chemistry, London, pp 293–296
149. Ariafard A, Amini MM, Azadmehr A (2005) J Organomet Chem 690:1147–1156
150. Alcaraz G, Sabo-Etienne S (2010) Angew Chem Int Ed 49:7170–7179
151. Piers WE (2000) Angew Chem Int Ed 39:1923–1925
152. Bera B, Jagirdar BR (2011) Inorg Chim Acta 372:200–205
153. Douglas TM, Chaplin AB, Weller AS (2008) J Am Chem Soc 130:14432–14433
154. Nako AE, White AJP, Crimmin MR (2015) Dalton Trans 44:12530–12534
155. Pörschke KR, Kleimann W, Tsay YH, Krüger C, Wilke G (1990) Chem Ber 123:1267–1273
156. Arndt P, Spannenberg A, Baumann W, Burlakov VV, Rosenthal U, Becke S, Weiss T (2004) Organometallics 23:4792–4795
157. Muraoka T, Ueno K (2010) Coord Chem Rev 254:1348–1355
158. Ueno K, Yamaguchi T, Uchiyama K, Ogino H (2002) Organometallics 21:2347–2349
159. Lin Z (2008) Struct Bond 130:123–148
160. Pandey KK (2009) Coord Chem Rev 253:37–55
161. Hartwig JF, Muhoro CN, He X, Eisenstein O, Bosque R, Maseras F (1996) J Am Chem Soc 118:10936–10937
162. Schlecht S, Hartwig JF (2000) J Am Chem Soc 122:9435–9443
163. Crestani MG, Muñoz-Hernández M, Arévalo A, Acosta-Ramírez A, García JJ (2005) J Am Chem Soc 127:18066–18073
164. Parkin G (2010) Struct Bond 136:113–146
165. Bortz M, Bau R, Schneider JJ, Mason SA (2001) J Clust Sci 12:285–291
166. Albinati A, Venanzi LM (2000) Coord Chem Rev 200:687–715
167. Petersen JL, Brown RK, Williams JM, McMullan RK (1979) Inorg Chem 18:3493–3498
168. Nako AE, Tan QW, White AJP, Crimmin MR (2014) Organometallics 33:2685–2688
169. Macchi P, Donghi D, Sironi A (2005) J Am Chem Soc 127:16494–16504
170. Matito E, Solà M (2009) Coord Chem Rev 253:647–665
171. Farrugia LJ, Macchi P (2012) Struct Bond 146:127–158
172. Casey CP, Sakaba H, Hazin PN, Powell DR (1991) J Am Chem Soc 113:8165–8166

173. Suzuki H, Omori H, Lee DH, Yoshida Y, Moro-oka Y (1988) Organometallics 7:2243–2245
174. Koga N, Morokuma K (1993) J Mol Struct 300:181–189
175. Marks TJ, Kolb JR (1977) Chem Rev 77:263–293
176. Xu Z, Lin Z (1996) Coord Chem Rev 156:139–162
177. Besora M, Lledós A (2008) Struct Bond 130:149–202
178. Cotton FA (1968) J Am Chem Soc 90:6230–6232
179. International Union of Pure and Applied Chemistry (2005) Nomenclature for inorganic chemistry, IR-10.2.5.1. RSC, London, p 216
180. Sloan TE, Busch DH (1978) Inorg Chem 17:2043–2047
181. Brookhart M, Green MLH, Parkin G (2007) Proc Natl Acad Sci U S A 104:6908–6914
182. Brookhart M, Green MLH, Wong LL (1988) Prog Inorganic Chem 36:1–124
183. Brookhart M, Green MLH (1983) J Organomet Chem 250:395–408
184. Dawoodi Z, Green MLH, Mtetwa VSB, Prout K (1982) J Chem Soc Chem Commun 802–803
185. Dawoodi, Z, Green MLH, Mtetwa VSB, Prout K, Schultz AJ, Williams JM, Koetzle TF (1986) J Chem Soc Dalton Trans 1629–1637
186. Dawoodi Z, Green MLH, Mtetwa VSB, Prout K (1982) J Chem Soc Chem Commun 1410–1411
187. Lee H, Desrosiers PJ, Guzei I, Rheingold AL, Parkin G (1998) J Am Chem Soc 120:3255–3256
188. Scherer W, McGrady GS (2004) Angew Chem Int Ed 43:1782–1806
189. Clot, E, Eisenstein, O (2004) Struct Bond 113, 1–36
190. Saβmannshausen J (2012) Dalton Trans 41:1919–1923
191. Scherer W, Herz V, Hauf C (2012) Struct Bond 146:159–208
192. Holton J, Lappert MF, Pearce R, Yarrow PIW (1983) Chem Rev 83:135–201
193. Baik MH, Friesner RA, Parkin G (2004) Polyhedron 23:2879–2900
194. Shin, JH, Parkin, G (1998) J Chem Soc Chem Commun 1273–1274
195. Braunstein P, Boag NM (2001) Angew Chem Int Ed 40:2427–2433
196. Bursten BE, Cayton RH (1986) Organometallics 5:1051–1053
197. Waymouth RW, Potter KS, Schaefer WP, Grubbs RH (1990) Organometallics 9:2843–2846
198. Stults SD, Andersen RA, Zalkin A (1989) J Am Chem Soc 111:4507–4508
199. Huffman JC, Streib WE (1971) Chem Commun 911–912
200. Ni C, Power PP (2009) Organometallics 28:6541–6545
201. Werner H (2004) Angew Chem Int Ed 43:938–954
202. Pechmann T, Brandt CD, Werner H (2004) Dalton Trans 959–966
203. Balch AL, Davis BJ, Olmstead MM (1993) Inorg Chem 32:3937–3942
204. Balch AL, Davis BJ, Olmstead MM (1990) J Am Chem Soc 112:8592–8593
205. Schinzel S, Muller R, Riedel S, Werner H, Kaupp M (2011) Chem Eur J 17:7228–7235
206. Bender R, Braunstein P, Dedieu A, Dusausoy Y (1989) Angew Chem Int Ed Engl 28:923–925
207. Murahashi T, Otani T, Okuno T, Kurosawa H (2009) Angew Chem Int Ed 39:537–540
208. Leoni P, Pasquali M, Sommovigo M, Laschi F, Zanello P, Albinati A, Lianza F, Pregosin PS, Ruegger H (1993) Organometallics 12:1702–1713
209. Budzelaar PHM, Vanleeuwen P, Roobeek CF, Orpen AG (1992) Organometallics 11:23–25
210. Albinati A, Lianza F, Pasquali M, Sommovigo M, Leoni P, Pregosin PS, Ruegger H (1991) Inorg Chem 30:4690–4692
211. Yang HQ, Li QS, Xie Y, King RB, Schaefer HF (2010) J Phys Chem A 114:8896–8901
212. Sun H, Gu J, Zhang Z, Lin H, Ding F, Wang Q (2007) Angew Chem Int Ed 46:7498–7500
213. Lescop C (2006) Actual Chim 30–33
214. Sauthier M, Le Guennic B, Deborde V, Toupet L, Halet JF, Reau R (2001) Angew Chem Int Ed 40:228–231
215. Leca F, Sauthier M, Deborde V, Toupet L, Réau R (2003) Chem Eur J 9:3785–3795
216. Leca F, Lescop C, Rodriguez-Sanz E, Costuas K, Halet JF, Réau R (2005) Angew Chem Int Ed 44:4362–4365

217. Nohra B, Rodriguez-Sanz E, Lescop C, Réau R (2008) Chem Eur J 14:3391–3403
218. Rodriguez-Sanz E, Lescop C, Réau R (2010) C R Chim 13:980–984
219. Welsch S, Nohra B, Peresypkina EV, Lescop C, Scheer M, Réau R (2009) Chem Eur J 15:4685–4703
220. Evans WJ, Greci MA, Ziller JW (1998) Chem Commun 2367–2368
221. Davenport TC, Tilley TD (2011) Angew Chem Int Ed 50:12205–12208
222. Lorber C, Choukroun R, Vendier L (2008) Organometallics 27:5017–5024
223. Beckwith JD, Tschinkl M, Picot A, Tsunoda M, Bachman R, Gabbai FP (2001) Organometallics 20:3169–3174
224. Lin P, Clegg W, Harrington, RW, Henderson, RA (2005) Dalton Trans 2349–2351
225. Al-Mandhary MRA, Fitchett CM, Steel PJ (2006) Aust J Chem 59:307–314
226. Hu Z, Gorun SM (2001) Inorg Chem 40:667–671
227. Li XL, Meng XG, Xu SP (2009) Chin J Struct Chem 28:1619–1624
228. Crabtree RH, Lavin M (1986) Inorg Chem 25:805–812
229. Colton R, McCormick MJ (1980) Coord Chem Rev 31:1–52
230. Horwitz CP, Shriver DF (1984) Adv Organomet Chem 23:219–305
231. Cotton FA (1976) Prog Inorg Chem 21:1–28
232. Morris-Sherwood BJ, Powell CB, Hall MB (1984) J Am Chem Soc 106:5079–5083
233. Sargent AL, Hall MB (1989) J Am Chem Soc 111:1563–1569
234. Sargent AL, Hall MB (1990) Polyhedron 9:1799–1808
235. Simpson CQ, Hall MB (1992) J Am Chem Soc 114:1641–1645
236. Miller TF, Strout DL, Hall MB (1998) Organometallics 17:4164–4168
237. Sironi A (1995) Inorg Chem 34:1342–1349
238. Dewar J, Jones HO (1905) Proc R Soc Lond 76:558–577
239. Brill R (1927) Z Krist 65:89–93
240. Powell, HM, Ewens, RVG (1939) J Chem Soc 286–292
241. Sidgwick NV, Bailey RW (1934) Proc R Soc Lond A 144:521–537
242. Cotton FA, Troup JM (1974) J Chem Soc Dalton Trans 800–802
243. Sidgwick NV, Powell HM (1940) Proc R Soc Lond 176:153–180
244. Astruc D (2007) Organometallic chemistry and catalysis. Springer, New York, p 157
245. Wulfsburg G (2000) Inorganic chemistry. University Science, California, p 557
246. Cotton FA, Wilkinson G, Murillo CA, Bochmann M (1999) Advanced inorganic chemistry, 6th edn. Wiley Inter-Science, New York, p 809
247. Cotton FA, Wilkinson G (1988) Advanced inorganic chemistry, 5th edn. Wiley Inter-Science, New York, p 1025
248. Miessler GL, Tarr DA (1998) Inorganic chemistry, 2nd edn. Prentice-Hall, Englewood Cliffs, p 440
249. Miessler GL, Tarr DA (1990) Inorganic chemistry, 1st edn. Prentice-Hall, Englewood Cliffs, p 430
250. Spessard GO, Miessler GL (1996) Organometallic chemistry. Prentice-Hall, Englewood Cliffs, p 68
251. Elschenbroich C, Salzer A (1989) Organometallics, 1st edn. VCH, Weinheim, p 224
252. Elschenbroich C, Salzer A (1992) Organometallics, 2nd edn. VCH, Weinheim, p 224
253. Greenwood NN, Earnshaw A (1986) Chemistry of the elements. Pergamon Press, New York, p 1283
254. King RB (1969) Transition-metal organometallic chemistry: an introduction. Academic Press, New York, p 118
255. Huheey JE, Keiter WA, Keiter RL (1993) Inorganic chemistry: principles of structure and reactivity, 4th edn. Harper Collins College, New York, p 636
256. Housecroft CE (1996) Metal-metal bonded carbonyl dimers and clusters. Oxford University Press, Oxford, p 9
257. Wardlaw W (1948) Endeavour 26:66–69
258. Braterman PS (1972) Struct Bond 10:57–86

259. Lauher JW, Elian M, Summerville RH, Hoffmann R (1976) J Am Chem Soc 98:3219–3224
260. Summerville RH, Hoffmann R (1979) J Am Chem Soc 101:3821–3831
261. Macchi P, Sironi A (2003) Coord Chem Rev 238:383–412
262. Heijser W, Baerends EJ, Ros P (1980) Faraday Symp Chem Disc 14:211–234
263. Bauschlicher CW (1986) J Chem Phys 84:872–875
264. Rosa A, Baerends EJ (1991) New J Chem 15:815–829
265. Ponec R, Lendvay G, Chaves J (2008) J Comput Chem 29:1387–1398
266. Bo C, Sarasa JP, Poblet JM (1993) J Phys Chem 97:6362–6366
267. Mealli C, Proserpio DM (1990) J Organomet Chem 386:203–208
268. Reinhold J, Hunstock E, Mealli C (1994) New J Chem 18:465–471
269. Reinhold J, Kluge O, Mealli C (2007) Inorg Chem 46:7142–7147
270. Reinhold J, Barthel A, Mealli C (2003) Coord Chem Rev 238:333–346
271. Ponec R, Gatti C (2009) Inorg Chem 48:11024–11031
272. Cotton FA, Murillo CA, Walton RA (2005) Multiple bonds between metal atoms, 3rd edn. Springer, New York, 3 pp
273. Elschenbroich C (2006) Organometallics, 3rd edn. Wiley-VCH, Weinheim, pp 359–361
274. Cotton FA, Wilkinson G, Gauss PL (1995) Basic inorganic chemistry, 3rd edn. Wiley, New York
275. Low AA, Kunze KL, Macdougall PJ, Hall MB (1991) Inorg Chem 30:1079–1086
276. Leung PC, Coppens P (1983) Acta Crystallogr B 39:535–542
277. Foroutan-Nejad C, Shahbazian S, Marek R (2014) Chem Eur J 20:10140–10152
278. Bénard M (1978) J Am Chem Soc 100:7740–7742
279. Bénard M (1979) Inorg Chem 18:2782–2785
280. Mitschler A, Rees B, Lehmann MS (1978) J Am Chem Soc 100:3390–3397
281. Jemmis ED, Pinhas AR, Hoffmann R (1980) J Am Chem Soc 102:2576–2585
282. Granozzi G (1988) J Mol Struct 173:313–328
283. Bursten BE, Cayton RH (1986) J Am Chem Soc 108:8241–8249
284. Bursten BE, Cayton RH, Gatter MG (1988) Organometallics 7:1342–1348
285. Andreocci MV, Bossa M, Cauletti C, Paolesse R, Ortaggi G, Vondrak T, Piancastelli MN, Casarin M, Dal CM, Granozzi G (1989) J Organomet Chem 366:343–55
286. Böhm MC (1982) Z Naturforsch 37A:241–247
287. Kostic NM, Fenske RF (1983) Inorg Chem 22:666–671
288. Ponec R (2015) Comput Theor Chem 1053:195–213
289. Radius U, Bickelhaupt FM, Ehlers AW, Goldberg N, Hoffmann R (1998) Inorg Chem 37:1080–1090
290. Bickelhaupt FM, Nagle JK, Klemm WL (2008) J Phys Chem A 112:2437–2446
291. Frenking G, Loschen C, Krapp A, Fau S, Strauss SH (2007) J Comput Chem 28:117–126
292. Macchi P, Garlaschelli L, Martinengo S, Sironi A (1999) J Am Chem Soc 121:10428–10429
293. Bitterwolf TE (2000) Coord Chem Rev 206:419–450
294. Labinger JA (2015) Inorg Chim Acta 424:14–19
295. Gotz K, Kaupp M, Braunschweig H, Stalke D (2009) Chem Eur J 15:623–632
296. Flierler U, Burzler M, Leusser D, Henn J, Ott H, Braunschweig H, Stalke D (2008) Angew Chem Int Ed 47:4321–4325
297. Muhoro CN, He X, Hartwig JF (1999) J Am Chem Soc 121:5033–5046
298. Nguyen P, Dai CY, Taylor NJ, Power WP, Marder TB, Pickett NL, Norman NC (1995) Inorg Chem 34:4290–4291
299. Nguyen P, Lesley G, Taylor NJ, Marder TB, Pickett NL, Clegg W, Elsegood MRJ, Norman NC (1994) Inorg Chem 33:4623–4624
300. Lam WH, Lin Z (2000) Organometallics 19:2625–2628
301. Landry VK, Melnick JG, Buccella D, Pang K, Ulichny JC, Parkin G (2006) Inorg Chem 45:2588–2597
302. Figueroa JS, Melnick JG, Parkin G (2006) Inorg Chem 45:7056–7058
303. Pang K, Parkin G (2006) Chem Commun, 5015–5017
304. Watanabe T, Ishida Y, Matsuo T, Kawaguchi H (2010) Dalton Trans 39:484–491

305. Cotton FA, Kibala PA, Wojtczak WA (1991) J Am Chem Soc 113:1462–1463
306. Krieck S, Gorls H, Yu L, Reiher M, Westerhausen M (2009) J Am Chem Soc 131:2977–2985
307. Evans WJ, Kozimor SA, Ziller JW, Kaltsoyannis N (2004) J Am Chem Soc 126:14533–14547
308. Jones JN, Macdonald CLB, Gorden JD, Cowley AH (2003) J Organomet Chem 666:3–5
309. Buchin B, Gemel C, Cadenbach T, Schmid R, Fischer RA (2006) Angew Chem Int Ed 45:1074–1076
310. Fernandez I, Cerpa E, Merino G, Frenking G (2008) Organometallics 27:1106–1111
311. Herberich GE, Hessner B, Boveleth W, Luthe H, Saive R, Zelenka L (1983) Angew Chem Int Ed Engl 22:996–996
312. Herberich GE, Hausmann I, Klaff N (1989) Angew Chem Int Ed Engl 28:319–320
313. Beck V, O'Hare D (2004) J Organomet Chem 689:3920–3938
314. Wadepohl H (1992) Angew Chem Int Ed Engl 31:247–262
315. Lamanna WM (1986) J Am Chem Soc 108:2096–2097
316. Lamanna WM, Gleason WB, Britton D (1987) Organometallics 6:1583–1584
317. Salzer A, Werner H (1972) Angew Chem Int Ed 11:930–932
318. Kudinov AR, Rybinskaya MI, Struchkov YT, Yanovskii AI, Petrovskii PV (1987) J Organomet Chem 336:187–197
319. Cowley AH, Macdonald CLB, Silverman JS, Gorden JD, Voigt A (2001) Chem Commun 175–176
320. Cowley AH (2004) Chem Commun 2369–2375
321. Loginov DA, Muratov DV, Kudinov AR (2008) Russ Chem Bull 57:1–7
322. Katz TJ, Rosenberg M (1962) J Am Chem Soc 84:865–866
323. Katz TJ, Rosenberg M (1963) J Am Chem Soc 85:2030–2031
324. Katz TJ, O'Hara RK, Rosenberg M (1964) J Am Chem Soc 86:249–252
325. Summerscales OT, Cloke FGN (2006) Coord Chem Rev 250:1122–1140
326. Cloke FGN (2001) Pure Appl Chem 73:233–238
327. Cloke FGN, Green JC, Jardine CN, Kuchta MC (1999) Organometallics 18:1087–1090
328. Balazs G, Cloke FGN, Gagliardi L, Green JC, Harrison A, Hitchcock PB, Shahi ARM, Summerscales OT (2008) Organometallics 27:2013–2020
329. Ashley AE, Cooper RT, Wildgoose GG, Green JC, O'Hare D (2008) J Am Chem Soc 130:15662–15677
330. Summerscales OT, Rivers CJ, Taylor MJ, Hitchcock PB, Green JC, Cloke FGN (2012) Organometallics 31:8613–8617
331. Ashley AE, Balazs G, Cowley AR, Green JC, O'Hare D (2007) Organometallics 26:5517–5521
332. Chen X, Du Q, Jin R, Wang HY, Wang L, Feng H, Xie YM, King RB (2014) Inorg Chim Acta 415:111–119
333. Jones SC, Hascall T, Barlow S, O'Hare D (2002) J Am Chem Soc 124:11610–11611.
334. Muñoz-Castro A, Carey DML, Arratia-Pérez R (2009) Polyhedron 28:1561–1567
335. Li HD, Feng H, Sun WG, Fan QC, Xie YM, King RB, Schaefer HF (2012) Mol Phys 110:1637–1650
336. Li H, Feng H, Sun W, Xie Y, King RB, Schaefer HF III (2011) Eur J Inorg Chem 2746–2755
337. Li H, Feng H, Sun W, Fan Q, Xie Y, King RB (2012) J Organomet Chem 700:4–12
338. Howard JAK, Woodward P (1978) J Chem Soc Dalton Trans 412–416
339. Brookes A, Gordon F, Howard J, Knox SAR, Woodward P (1973) J Chem Soc Chem Commun, 587–589
340. Bendjaballah S, Kahlal S, Costuas K, Bevillon E, Saillard JY (2006) Chem Eur J 12:2048–2065
341. Bunel EE, Valle L, Jones NL, Carroll PJ, Barra C, Gonzalez M, Munoz N, Visconti G, Aizman A, Manriquez JM (1988) J Am Chem Soc 110:6596–6598
342. Manriquez JM, Ward MD, Reiff WM, Calabrese JC, Jones NL, Carroll PJ, Bunel EE, Miller JS (1995) J Am Chem Soc 117:6182–6193

Struct Bond (2017) 171: 141–202
DOI: 10.1007/430_2015_201

Published online: 10 July 2016

Coordination of Lewis Acids to Transition Metals: Z-Type Ligands

Ghenwa Bouhadir and Didier Bourissou

Abstract This chapter provides a comprehensive review of M→Z complexes, that is to say complexes featuring Lewis acids coordinated as σ-acceptor ligands. The preparation, structure and bonding, as well as the characteristic features of M→Z complexes are discussed. Only Lewis acids derived from the p-block elements are considered, with a focus on two-center M→Z interactions supported by donor sidearms. The chapter is organized according to (1) the nature of the Lewis acid moiety (based on group 13, 14, 15 or 16 elements), (2) the way the M→Z interaction is formed (by B–H activation of pro-ligands or direct coordination of preformed ambiphilic ligands) and (3) the type of complexes (M→Z interactions supported by 3, 2 or 1 donor sidearms, unsupported M→Z interactions).

Keywords Ambiphilic ligands • Boranes • Lewis acids • M→Lewis acid interactions • M→Z interactions • Polyfunctional ligands • σ-acceptor ligands

Contents

G. Bouhadir and D. Bourissou (✉)
Université de Toulouse, UPS, Laboratoire Hétérochimie Fondamentale Appliquée, 118 route de Narbonne, 31062 Toulouse, France

CNRS, LHFA UMR 5069, 31062 Toulouse, France
e-mail: dbouriss@chimie.ups-tlse.fr

1 Introduction

Bonding is at the heart of chemistry. Analysis of the structure and bonding of chemicals is mandatory to understand and rationalize their chemical and physical behavior. In this respect, the pioneering work of Lewis and Kossel on chemical bonding a century ago is absolutely remarkable. Their landmark contributions provided the very basement of the description of covalent bonds. Lewis dot structures are very well suited for carbon compounds. They are also applicable and insightful for main-group derivatives and transition metal (TM) complexes, although more complicate bonding situations are frequently involved in these compounds (hypervalence).

As far as TM complexes are concerned, Werner first introduced the concept of coordination compounds, with a central metal surrounded by ligands. Sidgwick then proposed to explain their bonding via dative covalent bonds between electron-donor ligands and Lewis acidic metals. The model was progressively refined, and the possible involvement of ligand-to-metal donation as well as metal-to-ligand back-donation, such as in CO and olefin complexes, was recognized by Pauling, Dewar, Chatt, and Duncanson. In addition, the presence of partially filled electron shells confers Lewis base character to transition metals [1–3], and thus it is also conceivable that transition metals interact with Lewis acidic ligands.

Accordingly, ligands for transition metals are commonly classified as L, X, or Z type, according to the number of electrons they engage into the metal/ligand interaction (in the covalent model of bonding) [4, 5]. This simple formalism is very common and quite universal. It applies to two-center two-electron metal/ligand interactions (Fig. 1) as well as more complex situations involving

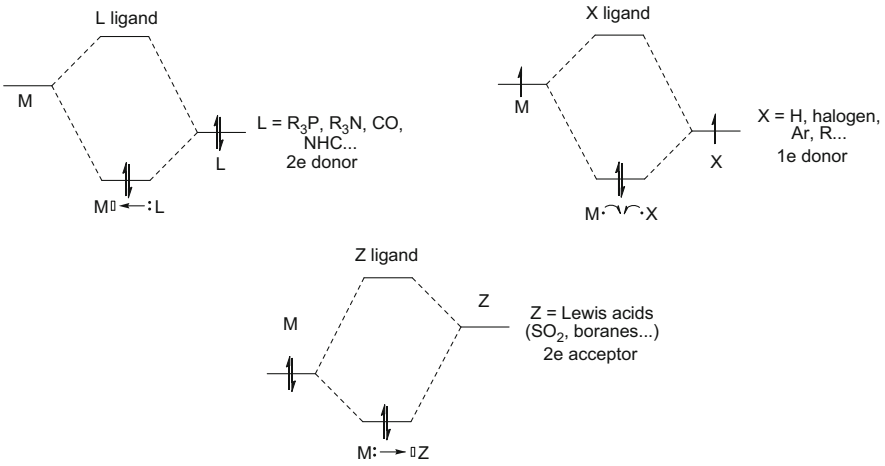

Fig. 1 Schematic representation of the bonding situations associated with L-, X-, and Z-type ligands, various types of two-center metal-ligand interactions

polyatomic ligands, which can be viewed as combinations of L-, X-, and Z-type moieties. Transition metals tend to complete their valence shell (18-electron rule). Their Lewis character prevails and not surprisingly, most ligands are L- or X-type σ-donors. Comparatively, the coordination of Lewis acids (LA) as σ-acceptors (Z-type ligands), which is associated with a transfer of electron density from the metal to the ligand, is rare. A few M→Z complexes were reported in the 1970s with simple Lewis acids such as $AlPh_3$ [6] or SO_2 [7] (a rare example of an ambivalent ligand which can behave as an L- as well as Z-type ligand; see Sect. 5). But the concept remained confidential for about two decades, until Hill reported the first unambiguous characterization of a transition metal→borane complex [8]. Over the last 15 years, the field attracted considerable interest from research groups all over the world. The scope of M→Z complexes rapidly expanded, in particular thanks to the use of polyfunctional ligands combining a Lewis acid moiety (preformed or generated upon coordination to the metal fragment) and donor sidearms that support the formation of M→Z interactions (chelate assistance) [9–17].[1] Accordingly, the concept of σ-acceptor ligands has become quite general. Nowadays, it is no longer considered as a chemical curiosity but rather as an original type of ligands, besides common L- and X-type ligands.

This chapter seeks to provide a comprehensive and updated review of M→Z complexes. The way they are prepared, their structure and bonding, as well as their characteristic features are discussed. Only Lewis acids derived from the p-block elements are considered (s- and d-block acidic metals are not included), with a focus on two-center M→Z interactions supported by donor sidearms [18, 19].[2]

[1] For reviews on M→Z interactions, TM→borane complexes, and ambiphilic ligands, see [9–17].

[2] M→Z interactions can be part of multicenter metal/ligand interactions as in the case of B–H bonds or BC_n moieties; see [18] and [19].

Polymetallic species involving bridging ligands are not included. For unsupported M→Z interactions with simple Lewis acids, the readers are invited to refer to our 2011 feature article [12]. Only selected examples and key aspects will be recalled and new such species will be presented here. The chapter does not follow chronological order but is organized according to (1) the nature of the Lewis acid moiety (based on group 13, 14, 15, or 16 elements), (2) the way the M→Z interaction is formed (by B–H activation of pro-ligands or direct coordination of preformed ambiphilic ligands), and (3) the type of complexes (M→Z interactions supported by 3, 2, or 1 donor sidearms, unsupported M→Z interactions).

2 Coordination of Group 13 Elements as Lewis Acids

2.1 Unsupported M→E_{13} Interactions

Trivalent compounds of the group 13 elements (E_{13} = B, Al, Ga, In) are the prototypes of Lewis acids and thus of σ-acceptor, Z-type ligands. As mentioned above, the $AlPh_3$ complex **1a** (Fig. 2) was among the very first TM→LA adduct to be unambiguously characterized in 1979 [6]. The structure and characteristic features of such unsupported M→E_{13} interactions have been thoroughly discussed in recent reviews [12, 20]. A few representative examples among ~ 40 structurally authenticated complexes are recalled in Fig. 2. The metal fragments are of four different types: anionic cyclopentadienyl carbonyl complexes (M = Fe, Mo),

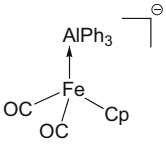

1a

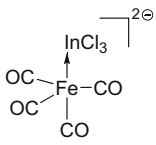

1b

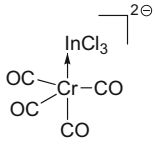

1c

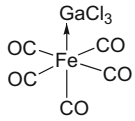

1d

	1a	1b	1c	1d
ME_{13} (Å)	2.510	2.517	2.608	2.574
r	0.99	0.92	0.93	1.01
$\Sigma E_{13}\alpha$ (°)	320	299	292	324

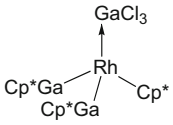

1e

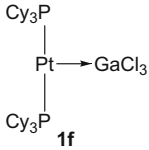

1f

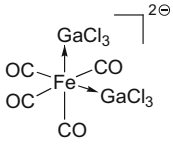

2

	1e	1f	2
ME_{13} (Å)	2.416	2.402	2.409
r	0.91	0.93	0.95
$\Sigma E_{13}\alpha$ (°)	307	307	302

Fig. 2 Selected examples of complexes with unsupported M→E_{13} interactions and associated characteristic features

anionic and neutral carbonyl complexes (M = Cr, Mo, W, Fe, Co), neutral cyclopentadienyl or arene complexes with Ga(I)Cp* or phosphine ligands (M = Rh and Ru), and neutral zerovalent and dicoordinate complexes (M = Pd, Pt). Except **1a**, all complexes involve trihalides of the heavier group 13 elements $E_{13}X_3$ (E_{13} = Al, Ga, In and X = Cl, Br, I). Complex **2** is remarkable in that it features two Lewis acids ($GaCl_3$) at a single metal center.

The presence of strong M→E_{13} interactions is apparent from the short M···E_{13} distances [for which the ratio $r = d(ME_{13})/\Sigma(r_{cov})$ gives a normalized value] and from the pyramidal environment around E_{13} (as quantified by the sum of $XE_{13}X$ bond angles). These characteristic features do not vary a lot from one complex to the other ($r \sim 0.95$, sum of bond angles ~ 305°). Compared with chelate systems deriving from polyfunctional ligands, unsupported M→Z interactions are free of geometric constraints, and their bond strengths can a priori be easily determined by simple dissociation. But in turn, the unsupported character inherently limits the scope of M→Z interactions since there is no way to control the way the Lewis acid coordinates to the metal fragment. Besides the metal itself, the Lewis acid can interact with other Lewis basic sites such as co-ligands or remote groups [9–11, 16, 17].

The recent studies in this area have concentrated on [L_2M→$E_{13}X_3$] complexes related to **1f**. The nature of the heavier group 13 element, of the group 10 metal, and of the co-ligand has been varied broadly (E_{13} = Al, Ga; X = Cl, Br, I; M = Pt, Pd; L = PCy_3, P*i*Pr_3, I*t*Bu, SIMes; homo- and heteroleptic complexes), and their respective influence has been determined [21–25]. A comprehensive computational study has also been performed [26].

Factors controlling the strength of unsupported M→E_{13} interactions have been identified, and Lewis acids have been used to gauge the Lewis basicity of zerovalent iron complexes in which CO has been replaced for phosphine, isonitrile, *N*-heterocyclic carbene, or borylene ligands [27]. The exchange of Lewis acids at metals has also emerged as a new route to unsupported M→Z complexes. A nice illustration by Braunschweig is given in Scheme 1. The Rh→$AlCl_3$ complex **1g** could not be prepared by direct coordination of $AlCl_3$ to Rh, but it was readily obtained by $AlCl_3$ transfer from [Pt(PCy_3)$_2$] to the more Lewis basic [(Cp)Rh(PMe_3)$_2$] fragment [28].

Reports discussing the coordination of boranes to transition metals have appeared since 1963 [29–33]. But to date, no complex with unsupported M→BR_3 interaction has been unambiguously characterized, and some of the claimed such compounds have been refuted later on [34, 35]. Boranes are apparently worse σ-acceptor ligands than their heavier analogs, and smaller bond dissociation energies were generally computed for the coordination of B vs Al, Ga, or In [26, 36]. In fact, when reacted with zerovalent dicoordinate Pt complexes such as [Pt(PCy_3)$_2$],

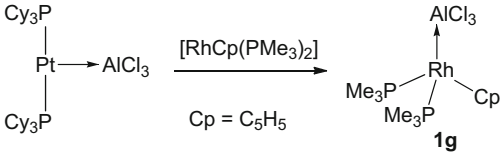

Scheme 1 Lewis acid exchange between unsupported Pt→Al and Rh→Al complexes

boron halides tend to form Pt(II) boryl complexes **3** rather than simple Pt→B adducts (Fig. 3) [36–41]. Oxidative additions of B–X bonds to Pt(0) are favored thermodynamically and readily proceed even with fluoro-boranes [36, 39, 41]. There reactions probably starts by Pt→B coordination, and the $(Cy_3P)_2Pt{\rightarrow}BF_2(Ar^F)$ complex [$Ar^F = 3,5\text{-}(CF_3)_2C_6H_3$] has been presumably characterized by low temperature NMR [36].

As mentioned above, thanks to the use of polyfunctional (pre)ligands, M→B interactions supported by donor sidearms have been authenticated. A first route to M→B interaction relies on the reaction of poly(azolyl) hydrido borates with metal fragments. Here, the Lewis acid is generated in the coordination sphere of the transition metal via B–H activation. Pioneered in 1999 by Hill with Ru and methimazolyl sidearms (2-mercapto imidazolyl) [8], this approach was then broadly developed, varying the metal, the nature, and number of the heterocycles used as donor buttresses. These studies are detailed hereafter.

2.2 *M→B Interactions in Cage Complexes Deriving from Tris(methimazolyl) Hydrido Borates*

As mentioned above, Hill reported in 1999 the first metallaboratrane **5a** upon reaction of the tris(methimazolyl) hydrido borate **4** with Ru(II) precursors (R = Ph, vinyl, H) (Scheme 2) [8, 42]. The presence of strong Ru→B interaction was apparent from the low field ^{11}B NMR resonance signal ($\delta = 17$ ppm, in the typical

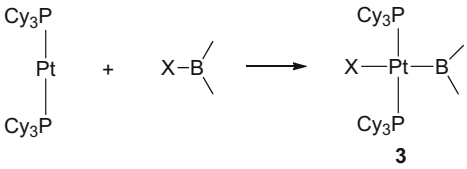

Fig. 3 Oxidative addition of B–X bond to Pt(0)

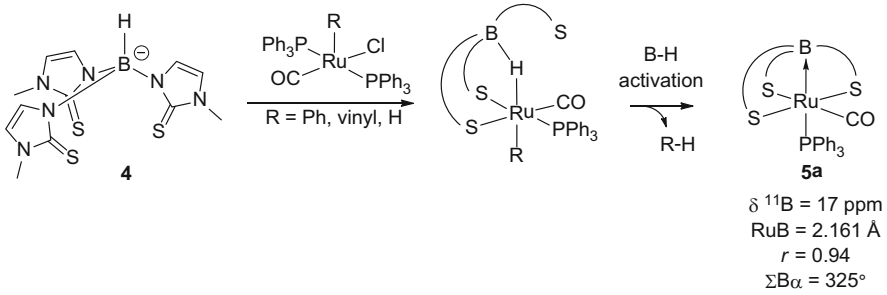

Scheme 2 Formation of the ruthenaboratrane **5a** from the tris(methimazolyl) hydrido borate **4**

range for tetracoordinate boron centers), the short Ru···B distance (2.161 Å, $r = d(RuB)/\Sigma(r_{cov}) = 0.94$), and the pyramidal environment around B (as quantified by the sum of NBN bond angles = 328°). The reaction proceeds via a B–H–Ru-bridged species (which has been unambiguously characterized by ^{1}H NMR and X-ray diffraction study for R=H) [42] (upon reaction of a bis(methimazolyl) dihydrido borate with $[RuCl_2(CHPh)(PCy_3)_2]$, Owen characterized an intermediate stage in the transfer of H between boron and ruthenium; see [43]). Activation of the B–H bond and release of R–H occur with formal reduction of the Ru center and coordination of the third methimazolyl group, giving ultimately the zerovalent ruthenaboratrane **5a**.

A few related ruthenaboratranes **5b–e** were then prepared (Fig. 4) [44]. The PPh_3 ligand in *trans* to boron in **5a** was readily exchanged for another CO co-ligand (complex **5b**) or an isonitrile (complexes **5c**,**d**), highlighting strong *trans* influence of the σ-acceptor B ligand. The thiocarbonyl complex **5e** was also prepared by reacting **4** with [Ru(vinyl)Cl(CS)(PPh_3)]. According to X-ray diffraction data, the Ru→B interaction remains quasi-invariant in this series of complexes. The geometric constraints associated with the cage structure probably alleviate the electronic properties of the different co-ligands.

The nature of the metal was varied as well, first remaining in group 8. Hill prepared the osmaboratrane **6** following the same route than for Ru (Scheme 3) [45]. Using a slightly different strategy and *t*Bu-substituted 2-mercapto imidazolyl sidearms, Parkin synthetized the bis(carbonyl) ferraboratrane **7** [46]. The structures of **6** and **7** are very similar to those of **5a** and **5b**. The metal is in pseudo-octahedral geometry, the Os/Fe···B distances are short ($r = 0.95$ and 0.98, respectively), and the boron is strongly pyramidalized (ΣB_α 323° and 327°, respectively). Note that the *trans* influence of boron is apparent from the dissymmetric coordination of the two carbonyl co-ligands in **7** [$Fe(CO)_{trans}/Fe(CO)_{cis} = 1.801/1.717$ Å].

The ability of boron to coordinate group 9 metals was also studied. In 2005, Hill applied the same methodology than for Ru and Os complexes and reacted **4** with the Rh(III) precursor $[Rh(Ph)Cl_2(PPh_3)_2]$ [47]. B–H activation and benzene elimination afforded complex **8a**, the first metallaboratrane with a metal in positive oxidation state (Fig. 5). Despite steric shielding, the PPh_3 co-ligand sits in the equatorial plane of **8a** so that the position *trans* to boron is occupied by the less π-accepting chloride co-ligand. Various cationic rhodaboratranes **8b–d** were then prepared by reacting

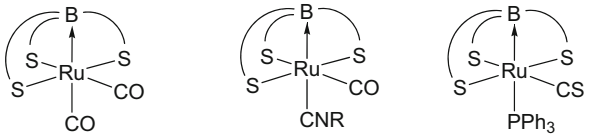

5c: R = *t*Bu **5d**: R = Mes

RuB (Å)	2.176	2.146	2.154
r	0.95	0.93	0.94
ΣBα (°)	326	325	325

Fig. 4 Structure and key features of the ruthenaboratranes **5b–e**

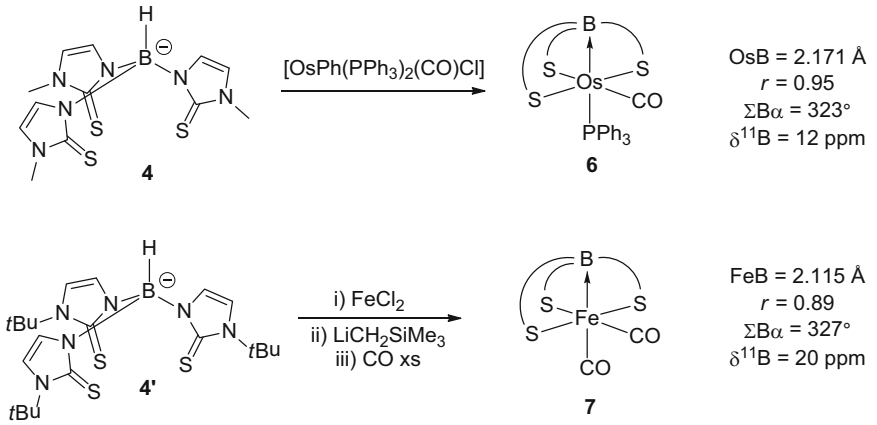

Scheme 3 Syntheses and key analytical data of the osma- and ferraboratranes **6** and **7**

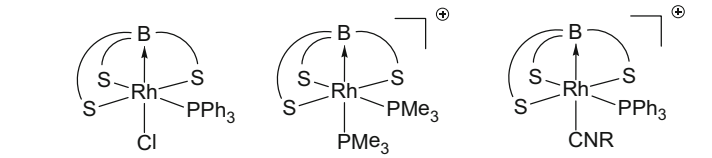

	8a	**8b**	**8c**: R = *t*Bu	**8d**: R = Xyl
RhB (Å)	2.127	2.149	2.155	2.146
r	0.94	0.95	0.95	0.95
ΣBα (°)	328	328	330	330
δ^{11}B (ppm)	2	9	9	9

Fig. 5 Structure and key features of the rhodaboratranes **8a–d**

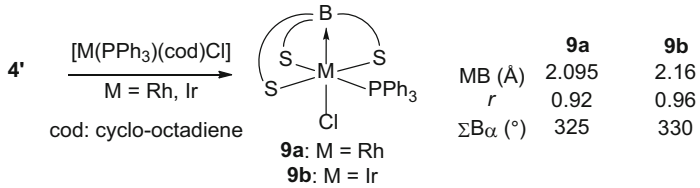

	9a	**9b**
MB (Å)	2.095	2.16
r	0.92	0.96
ΣBα (°)	325	330

Scheme 4 Syntheses and key analytical data of the rhoda- and irida-boratranes **9a** and **9b**

8a with Lewis bases (isonitriles, PMe_3) [48] (a bimetallic rhodaboratrane was also prepared by prolonged reaction of $[Rh(cod)Cl]_2$ with an excess of **4**; see [49]). The presence of strong Rh→B interaction in **8a–d** was inferred from the ^{11}B NMR chemical shift (δ 2–9 ppm), the short Rh···B distance, and the sum of NBN bond angles ($r \sim 0.95$, $\Sigma B_\alpha \sim 329°$). Here also, very little variations are noticed from one complex to the other.

Simultaneously, Parkin reported the rhoda- and irida-boratranes **9a** and **9b** with *t*Bu-substituted 2-mercapto imidazolyl sidearms (Scheme 4) [50]. In this case, the

corresponding hydrido borate was reacted with [M(cod)Cl(PPh_3)] precursors. The structures of **9a** and **9b** are very similar to each other and quasi-superposable to those of **8a**–**d**.

In 2010, Connelly applied his redox methodology (see the next session dedicated to M→B interactions supported by two methimazolyl arms) to prepare the cationic rhodaboratrane **11** (Scheme 5) [51]. The B–H agostic Rh(I) complex **10** was reacted with 2 equiv. of ferrocenium in the presence of iPr$_2$NH. Two-electron oxidation of the B–H–Rh bridge, deprotonation, and CO dissociation afforded **11**. The crystallographic study revealed a square-pyramidal cage complex, with no ligand in *trans* position to boron, but strong Rh→B interaction (Rh···B 2.077 Å, $r = 0.92$, $\Sigma B_\alpha = 333°$).

The cationic cobalt(I) complex **12** reported by Rabinovitch in 2004 completes the series of group 9 metallaboratranes (Fig. 6) [52]. It was obtained as a decomposition product of the corresponding tris(azolyl) hydrido borate Co(II) species. X-ray diffraction analysis revealed a cage structure of trigonal-bipyramidal geometry. The presence of strong Co→B interaction is indicated by the short Co···B distance (2.132 Å, $r = 0.91$) and the strong pyramidalization of boron ($\Sigma B_\alpha = 328.4°$).

Metallaboratranes were also reported with zero, mono, and divalent group 10 metals. The first such complexes were prepared in 2004 by Hill using a different route than that initially developed [53]. Reaction of the hydrido borate **4** with [$PtCl_2(PPh_3)_2$] proceeds by chloride and PPh_3 displacement, followed by insertion of Pt into the B–H bond (transfer of hydride from B to Pt, non-oxidative addition), to give the Pt(II) cage complex **13a** (Scheme 6). Dehydrochlorination with DBU

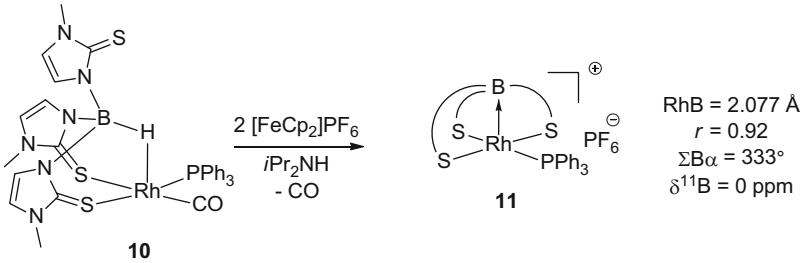

Scheme 5 Synthesis and key analytical data of the square-pyramidal rhodaboratrane **11**

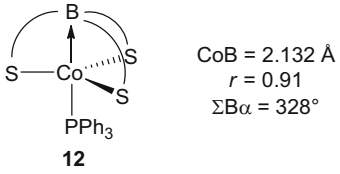

Fig. 6 Structure and key analytical data of the cobaltaboratrane **12**

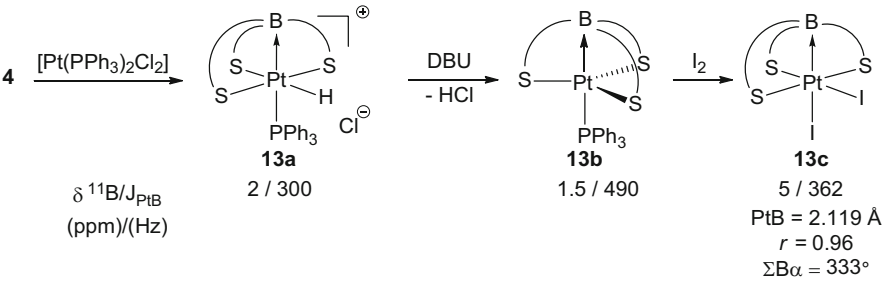

Scheme 6 Synthesis and key analytical data of the di- and zerovalent platinaboratranes **13a**,**b** and **13c**

then affords the corresponding Pt(0) complex **13b**. The two platinaboratranes have been characterized by multinuclear NMR spectroscopy. The presence of Pt→B interaction and the pseudo-octahedral/trigonal-bipyramidal geometry of **13a**,**b** were unequivocally established. But in the absence of X-ray diffraction and DFT data, the strength of the boron coordination is hardly comparable between Pt(II) and Pt (0). Dihalogens X_2 (X = Cl, Br, I) and iodomethane were shown to oxidatively add to the Pt center of **13b** with retention of the Pt→B interaction [54] (divalent platinaboratranes with different phosphines ($PoTol_3$, PMe_3, PEt_3) in *trans* to B were also characterized by NMR, and reversible B–H activation at Pt was evidenced; see [55]). The ensuing diiodo Pt(II) complex **13c** was characterized crystallographically (Pt···B 2.119 Å, $r = 0.96$, ΣB_α 333°). Significantly different Pt–I bond distances were observed for the iodine atoms in *trans*/*cis* position to boron (2.879/2.650 Å).

In parallel, Parkin reported a zerovalent palladium boratrane [56]. Complex **14** was prepared by reacting the *t*Bu-substituted tris(azolyl) hydrido borate with Pd $(OAc)_2$ and then PMe_3 (Fig. 7).[3] According to X-ray diffraction analysis, it adopts trigonal pyramidal geometry and features strong Pd→B interaction (Pd···B 2.050 Å, $r = 0.92$, ΣB_α 321°). Molecular orbital analysis indicates the presence of a three-center four-electron interaction along the P→Pd→B axis, with major contribution of boron in the second MO which is bonding between Pd and B and antibonding between P and Pd.

The first nickelaboratrane **15a** was described in 2006 by Tatsumi (Scheme 7) [57]. It is a rare example of paramagnetic metallaboratrane, a nickel(I) species obtained from $NiCl_2$ and the tris(azolyl) hydrido borate **4′** (Scheme 7). Two years later, Parkin explored the reactivity of **15a** and prepared three related species **15b–d** by substitution of Cl for OAc, SCN, and N_3 [58]. All complexes adopt trigonal pyramidal structures and display very similar features (little variations of the Ni···B distance, $r \sim 1.00$, and sum of bond angles $\Sigma B_\alpha \sim 331°$).

[3] A *S*-bridged dinuclear Pd complex is formed before addition of PMe_3.

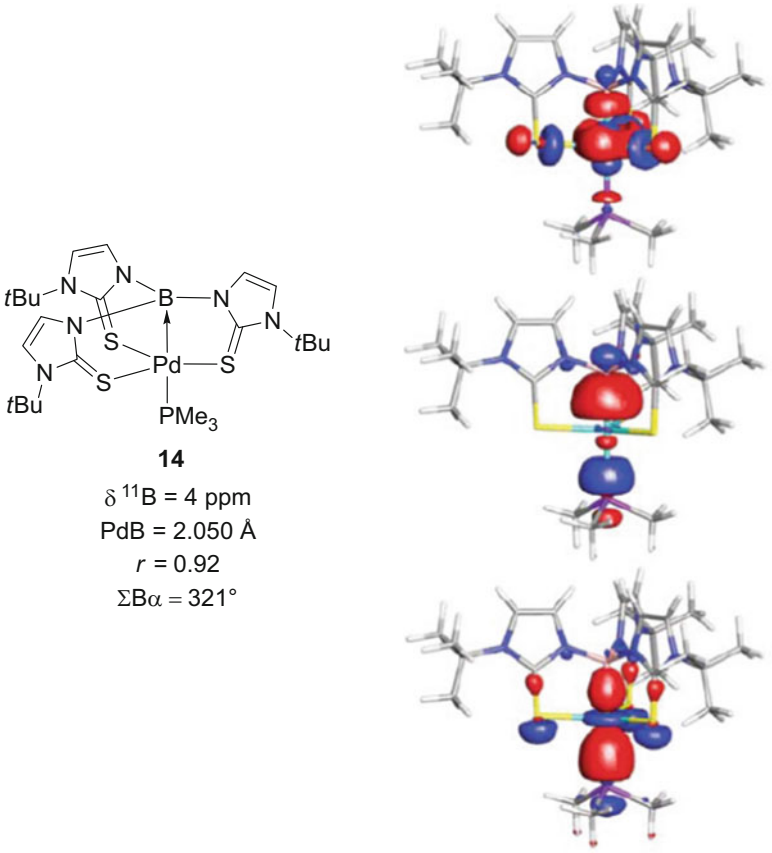

14

$\delta\,^{11}B = 4$ ppm

PdB = 2.050 Å

$r = 0.92$

$\Sigma B\alpha = 321°$

Fig. 7 Structure and key analytical data of the zerovalent palladaboratrane **14** (*left*), molecular orbitals associated with the three-center four-electron P→Pd→B interaction (*right*)

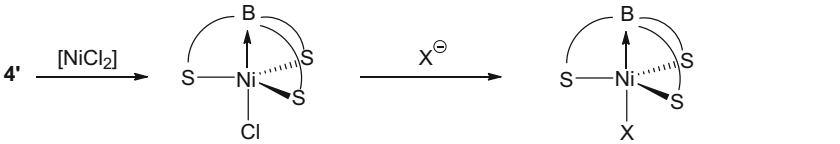

	15a	**15b**: X = OAc	**15c**: X = SCN	**15d**: X = N_3
NiB (Å)	2.111	2.112	2.079	2.092
r	1.01	1.01	0.99	1.00
$\Sigma B\alpha$ (°)	330	330	331	331

Scheme 7 Synthesis and key analytical data of the monovalent nickelaboratranes **15a–d**

2.3 Related Complexes with M→B Interactions Supported by Two Methimazolyl Arms

As shown above, tris(azolyl) hydrido borates tend to form metallaboratranes. The cage structure clearly favors and enforces M→B interactions, but the presence of three donor arms is not a prerequisite for the coordination of boron, as substantiated simultaneously by Hill and Parkin. Reaction of **4** and its *t*Bu- and Ph-substituted analogs with Vaska's complex [IrCl(CO)(PPh_3)$_2$] afforded complexes **16a**, **16b**, and **16c** (Fig. 8) [57–60]. The three complexes adopt very similar structures. The iridium center is in pseudo-octahedral geometry with the phosphine *trans* to B. Two of the azolyl arms are coordinated to Ir (in *cis*), and one remains pendant. Despite the absence of cage constraints, the Ir···B distance is short (2.18–2.19 Å, $r \sim 0.97$), and the boron is strongly pyramidalized ($\Sigma B_\alpha \sim 321°$), indicating that the Ir→B interaction is of same magnitude than in the iridaboratrane **9b**. Starting from a bis (methimazolyl) dihydrido borate, Hill also prepared complex **17**, and X-ray diffraction analysis revealed here also the presence of strong Ir→B interaction.

The results obtained with 2-mercapto imidazolyl sidearms have stimulated the study of other heterocycles as donor buttresses. As discussed below, the B–H activation approach of M→B interactions has been progressively extended to various moieties, namely, 5-mercapto 1,2,4-triazolyl, 2-mercapto pyridyl, 2-mercapto pyridazinyl, 2-mercapto benzothiazolyl, and 7-aza indoyl.

2.4 Complexes with M→B Interactions Supported by 5-Mercapto 1,2,4-Triazolyl Sidearms

Connelly used 5-mercapto 1,2,4-triazolyl sidearms and developed a new route to metallaboratranes based on the redox activation of the corresponding hydrido

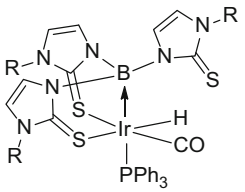

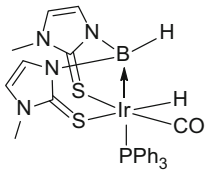

	16a	**16b**	**16c**	**17**
R	Me	*t*Bu	Ph	
$\delta\,^{11}$B (ppm)	3	/	/	- 4.5
IrB (Å)	2.193	2.179	2.186	2.210
r	0.97	0.97	0.97	0.98
ΣBα (°)	322	321	320	330

Fig. 8 Structure and key analytical data of the iridium complexes **16** and **17**, Ir→B interactions supported by two azolyl sidearms

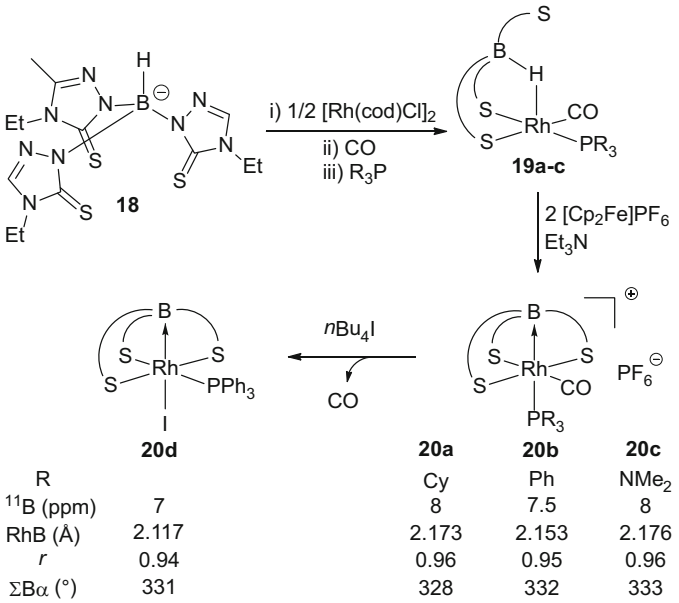

Scheme 8 Redox activation of the tris(5-mercapto 1,2,4-triazolyl) hydrido borate **18**, key analytical data of the ensuing rhodaboratranes **20a–d**

borate (Scheme 8) [61, 62]. It involves agostic B–H–Rh species as key intermediates,[4] which are then oxidized by 2 electrons (using Cp_2Fe^+,PF_6^-) in the presence of a base (triethylamine). Accordingly, the cationic rhodaboratranes **20a–c** were prepared with PPh_3, PCy_3, or $P(NMe_2)_3$ as co-ligand. In addition, the neutral complex **20d** was synthetized by substitution of CO for iodide. The presence of strong Rh→B interactions in **20a–d** was established crystallographically. The Rh···B distance is about the same in complexes **20a–c** (~2.16 Å, $r \sim 0.96$, marginal influence of the phosphine in *trans* to B) and slightly shorter in the neutral complex **20d** (2.12 Å, $r = 0.94$).

2.5 *Related Complexes with M→B Interactions Supported by 2-Mercapto Pyridyl Sidearms*

Metallaboratranes featuring 2-mercapto pyridyl sidearms were investigated by Owen. Zerovalent ruthenium complexes **23a** and **23b** [63] were prepared following Hill's route (Scheme 9), and their structures were compared with that of the original

[4] The 5-mercapto-1,2,4-triazolyl sidearm may coordinate through the N atom in β position to B, but only *S*-coordination was observed.

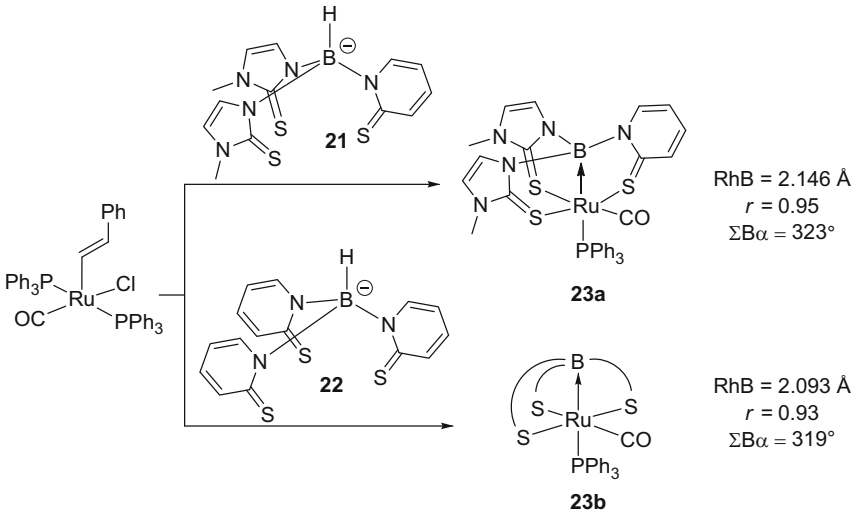

Scheme 9 Synthesis and key analytical data of the ruthenaboratranes **23a**,**b**, Ru→B interactions supported by 2-mercapto pyridyl sidearms

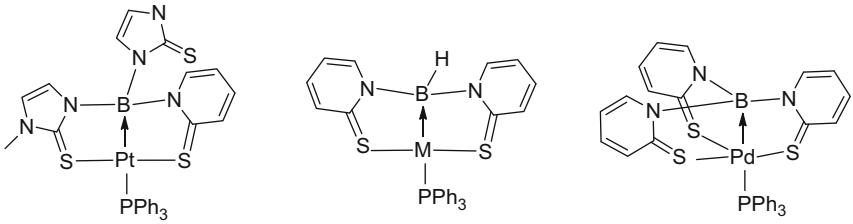

	24a	**24b**: M = Pt	**24c**: M = Pd	**24d**
δ ^{11}B (ppm)	11	15	12.5	17.5
MB (Å)	2.129	2.101	2.092	2.065
r	0.97	0.95	0.94	0.93
ΣBα (°)	328	326	326	324

Fig. 9 Structure and key analytical data of the Pt and Pd complexes **24a–d** featuring 2-mercapto pyridyl sidearms

Ru→B complex **5a**. Accordingly, the Rh···B distance slightly shortens (*r* goes from 0.94 in **5a** to 0.93 in **23b**), and the pyramidalization of B increases (ΣB_α from 325° in **5a** to 319° in **23b**) upon introduction of one or three 2-mercapto pyridyl arms.

A series of zerovalent Pt and Pd complexes **24a–d** with one or two 2-mercapto pyridyl arms were reported too (Fig. 9) [64, 65]. Complexes **24a–c** adopt distorted square-planar geometries (the PPh_3 co-ligand sits *trans* to B), while **24d** (a decomposition product of **24c**) is trigonal-bipyramidal. Note also that a methimazolyl remains pendant in **24a**. Despite the absence of cage structure, complexes **24b**,**c** display very short Pt/Pd···B distances ($r \sim 0.94$).

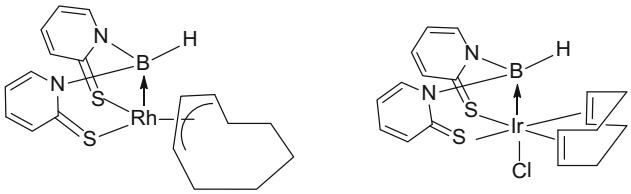

	25a	**25b**
δ ^{11}B (ppm)	4	8
MB (Å)	2.054	2.198
r	0.91	0.97
ΣBα (°)	320	320

Fig. 10 Structure and key analytical data of the Rh and Ir complexes **25a**,**b** featuring 2-mercapto pyridyl sidearms

Owen also used 2-mercapto pyridyl sidearms to prepare unlocked Rh and Ir complexes [66]. Complexes **25a**,**b** adopt square-pyramidal and pseudo-octahedral geometries, respectively (Fig. 10), but both display strong M→B interaction ($r \sim$ 0.94). Note that the H atoms at B were shown by X-ray diffraction to point away from Rh/Ir, ruling out the possibility of η^2(B–H) coordination instead of M→B interaction.

2.6 Complexes with M→B Interactions Supported by 2-Mercapto Pyridazinyl Sidearms

Mösch-Zanetti introduced another type of N,S-sidearm based on the 2-mercapto pyridazinyl moiety (substituted by *t*Bu or Me groups) [67, 68]. The monovalent Co, Ni, and Cu boratranes **27a**–**d** (Fig. 11) were prepared by reacting the corresponding hydrido borates **26** with MCl_2 salts. All complexes, except **27d**, are paramagnetic (for the Co species **27d**, the triplet state is favored by about 15 kcal/mol). They adopt trigonal-bipyramidal structures, and the M···B distances are similar than those of the corresponding tris(methimazolyl) complexes. The presence of three-center four-electron Cl–M→B interactions was substantiated by MO analysis. As depicted in Fig. 11, the second MO are M/B bonding and M/Cl antibonding.

2.7 Complexes with M→B Interactions Supported by 2-Mercapto Benzothiazolyl Sidearms

The monovalent Rh complexes **28a**,**b** featuring 2-mercapto benzothiazolyl sidearms were recently characterized by Ghosch [69–71]. The corresponding ligand is closely related to Hill's methimazolyl systems (benzannelated variante), but it was

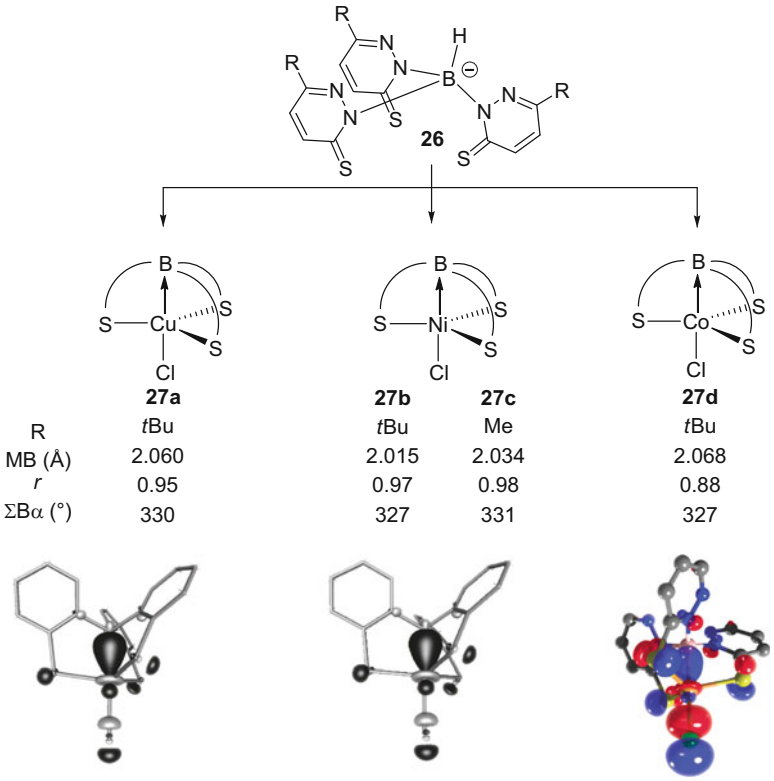

Fig. 11 Structure and key analytical data of the monovalent Co, Ni, and Cu complexes **27a–d** featuring 2-mercapto pyridazinyl sidearms, second MO of the three-center four-electron Cl–M→B interactions

generated by a very different route (Scheme 10). Reaction of **28a** with [W(CO)$_5$(thf)] afforded the bimetallic species **28b**. Both complexes feature strong Rh→B interaction, as apparent from ^{11}B NMR ($\delta = 10$ ppm), X-ray diffraction ($r \sim 0.98$), and DFT analysis (the corresponding NBO is depicted in Scheme 10).

2.8 *Complexes with M→B Interactions Supported by 7-Aza Indoyl Sidearms*

In all the structural modulations discussed above, S-donor sidearms were retained. But N-based buttresses can also be used, as exemplified by Owen with 7-aza indoyl moieties. Reaction of the corresponding hydrido borate **29** with [IrCl(cod)]$_2$ first gave a B–H–Ir-bridged species **30** (Scheme 11) [72, 73]. Under CO atmosphere, H migrates from B to Rh and cod inserts into the Ir–H bond to give the square-pyramidal complex **31a**. π-Accepting ligands (such as isonitriles or

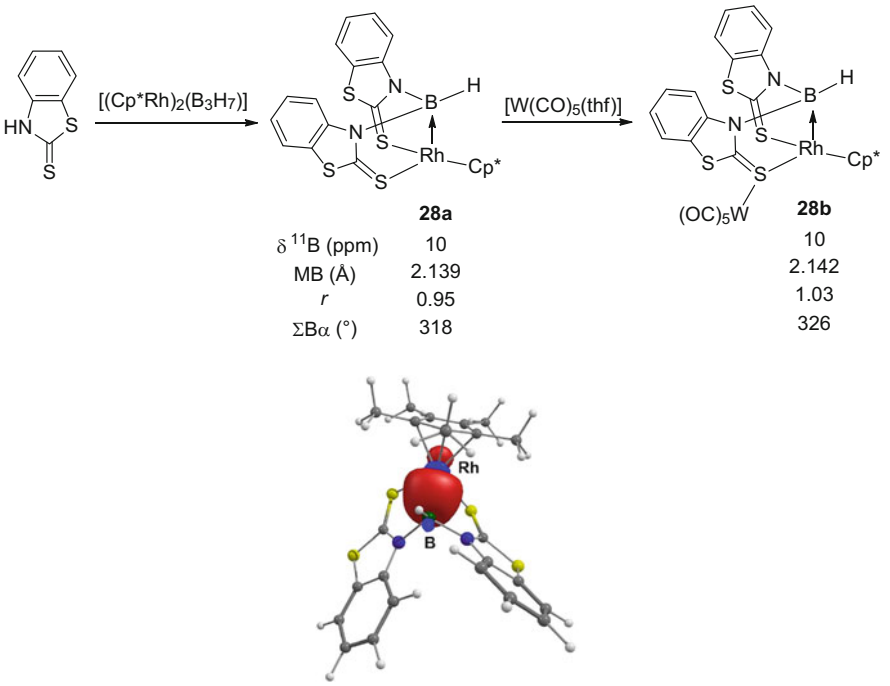

Scheme 10 Synthesis and key analytical data of complexes **28a**,**b**, Rh→B interactions supported by 2-mercapto benzothiazolyl sidearms, corresponding NBO

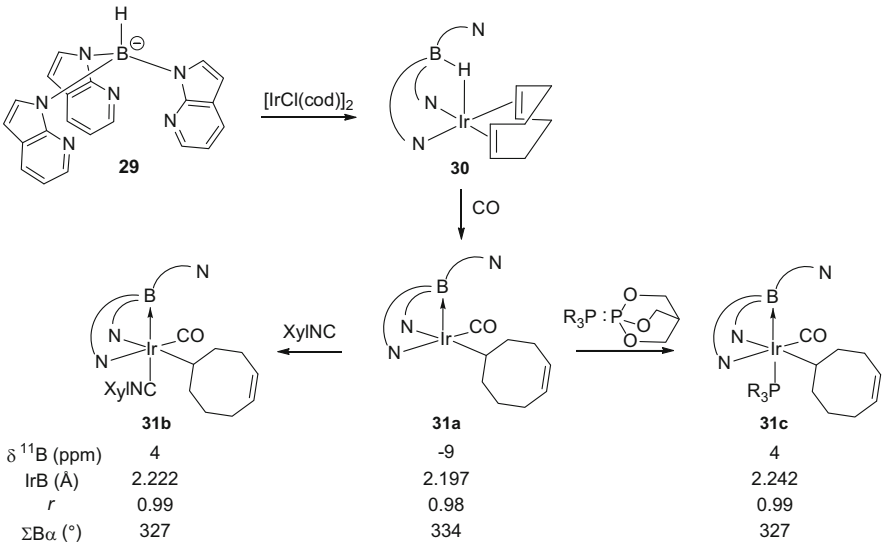

Scheme 11 Synthesis and key analytical data of complexes **31a**–**c**, Ir→B interactions supported by 7-aza indoyl sidearms

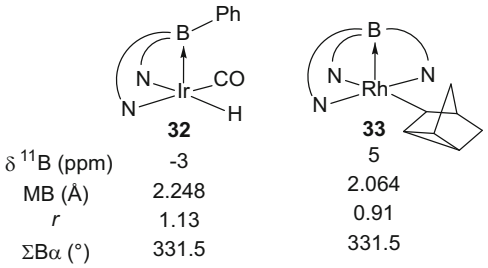

Fig. 12 Structure and key analytical data of complexes **32** and **33**, Ir/Rh→B interactions supported by 7-aza indoyl sidearms

phosphites) readily coordinate *trans* to B to give the pseudo-octahedral complexes **31b**,**c**. X-ray diffraction data are indicative of strong Ir→B interactions ($r \sim 0.99$, $\Sigma B_{\alpha} \sim 330°$), despite the fact that a 7-aza indoyl group remains pendant. And again, only small variations were observed between **31a–c**, despite the absence of cage constraints.

A few variations have been studied. Replacement of the pendant 7-aza indoyl moiety for a phenyl group led to complex **32**, analogous to **31a** (Fig. 12) [73]. Furthermore, the original rhodaboratrane **33** was obtained by reacting the tris(7-aza indoyl) hydrido borate with $[RhCl(nbd)]_2$ [74]. The latter reaction involves B–H–Rh bridging coordination, followed by H migration from B to the norbornadiene moiety, resulting in the formation of the cage complex **33** with a nortricycyl moiety. Complexes **32** and **33** adopt square-pyramidal geometries and feature strong Ir/Rh→B interactions.

2.9 Complexes with M→E_{13} Interactions Supported by Tetradentate Ambiphilic Ligands

In parallel with Hill's approach of metallaboratranes based on B–H activation of tris(methimazolyl) hydroborates, we envisioned to use preformed ambiphilic ligands featuring a central group 13 element (boron or one of its heavier congeneer) and three phosphine buttresses. In 2008, we introduced the triphosphine borane **34** and studied its coordination to group 10 and 11 metals [75, 76]. A complete series of metallaboratranes was prepared (Scheme 12), and the influence of the metal on M→B interactions was assessed. All the group 10 and 11 complexes adopt C_3 symmetry with the three phosphines coordinated in an equatorial plane and strong M→B interaction along the apical axis. An array of descriptors were considered to characterize and analyze the M→B interactions, including the ^{11}B NMR chemical shift, the M···B distance (and the *r* value we introduced to take into account and normalize the size of the atoms involved in the TM→LA interaction), the sum of bond angles around B, and the NBO delocalization energy associated with donor–

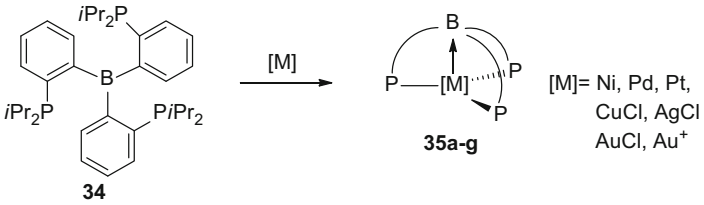

Scheme 12 Group 10 and 11 metallaboratranes deriving from the triphosphine borane **34**

Table 1 Selected data for the metallaboratranes **35a–g**

	35a	**35b**	**35c**	**35d**	**35e**	**35f**	**35g**
[M]	Ni	Pd	Pt	CuCl	AgCl	AuCl	Au^+
r	1.04	1.01	1.00	1.16	1.11	1.05	1.11
ΔE_{NBO} (kcal/mol)	61	65	145	8	14	47	26

acceptor M→B interactions. Selected data are included in Table 1. Tetradentate coordination of the triphosphine borane entails some rigidity, but the cage structure retains some flexibility. Indeed, the M→B distance and its strength vary significantly from one complex to another (*r* varies from 1.00 to 1.16, ΔE_{NBO} varies from 8 to 145 kcal/mol). The following trends have been delineated: M→B interactions are stronger for group 10 than group 11 metals and strengthen going down the groups, in line with the Lewis basicity of the metals [23]. The strongest interactions were found with Pt and Au ($r = 1.00$ and 1.05), which are more Lewis basic than their lighter congeners (relativistic effects raise 5d orbitals in energy). Cationization of gold by chloride abstraction reduces its electron density and weakens, but does not suppress, the Au→B interaction ($r = 1.11$). Analysis of the MO provides a clear picture of the bonding situation. Two-center two-electron M→B interactions are clearly apparent for metallaboratranes **35a–c** and **35g** (see Fig. 13, left for the corresponding MO of the platinaboratrane), while the neutral group 11 complexes **35d–f** feature three-center four-electron Cl–M→B interactions (see Fig. 13, right for the MO of the gold complex).

The influence of the Lewis acid center was then investigated and boron was replaced for heavier group 13 elements (Al, Ga, In). The triphosphine-aluminum ligand **36** was coordinated to AuCl and CuCl [77]. Aluminum abstracts the chloride from gold/copper (Al has a much stronger affinity for Cl^- than B), and zwitterionic cage complexes are obtained (Scheme 13). The metal center is in trigonal-planar geometry and the chlorine atom at Al sits *trans* to the metal (Al is in trigonal-bipyramidal environment). The Au···Al distance is relatively long (3.026 Å), but the *r* value (1.18) remains in the same range than those of weak M→B interactions (Cu, Ag, and Au^+ metallaboratranes), suggesting the presence of weak $Au^+ \rightarrow AlCl^-$ interaction. DFT calculations supported this view. NBO analysis revealed the presence of weak Au→Al donor–acceptor interaction ($\Delta E_{NBO} = 17$ kcal/mol). The transfer of chloride from Au to Al reduces the Lewis basicity of Au and the Lewis acidity of Al, but a weak Au→Al interaction pertains. The cage structure

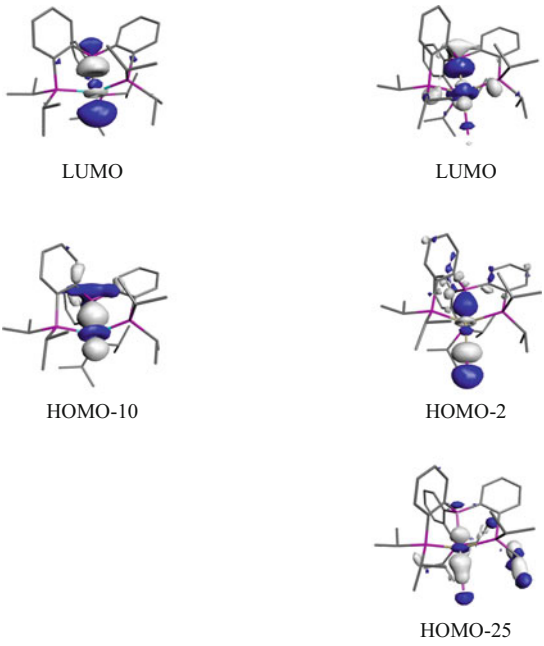

Fig. 13 MO accounting for the two-electron two-center Pt→B interaction in **35c** (*left*) and three-center four-electron Cl–Au→B interaction in **35f** (*right*)

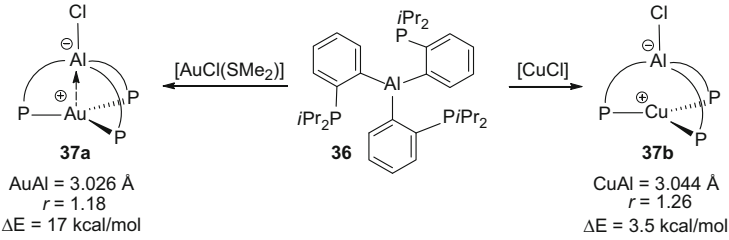

Scheme 13 Gold and copper cage complexes **37a**,**b** deriving from the triphosphine-aluminum ligand **36**

probably plays an important role here, by maintaining Au and Al in close proximity. The Lewis acidity of the chloroaluminate moiety involves the ability of Al to form hypervalent compounds and to accept electron density via σ* orbitals. All heavier elements possess this property and can thus a priori behave as σ-acceptor ligands (related systems based on the heavier group 14–16 elements are discussed in the following sections). The cage structure imposes about the same Cu···Al distance in **37b**, but given the smaller size and lower Lewis basicity of Cu compared with Au, this results in a significantly higher value of r (1.26) and only very weak $Cu^{+}\rightarrow AlCl^{-}$ interaction ($\Delta E_{NBO} = 3.5$ kcal/mol).

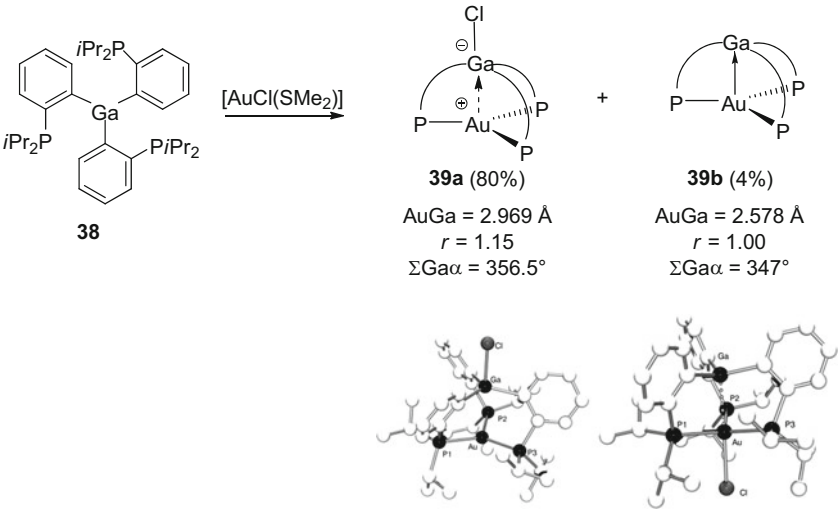

Scheme 14 Zwitterionic and neutral gold cage complexes **39a**,**b** deriving from the triphosphine-gallium ligand **38**, weak $Au^{+}\rightarrow GaCl^{-}$ and strong Au→Ga interactions

Coordination of the related triphosphine-gallium ligand to AuCl was also studied (Scheme 14) [78]. The zwitterionic complex **39a** was isolated in 80% yield. According to crystallographic and DFT studies, the bonding situation is very similar to that found in the corresponding Al complex **37a**. Ga abstracts chloride from Au but a weak $Au^{+}\rightarrow GaCl^{-}$ pertains ($r = 1.15$, $\Delta E_{NBO} = 8$ kcal/mol). Careful analysis of the reaction medium revealed the presence of the neutral form **39b** in low quantity (4%). This complex could be isolated (by extraction with pentane) and fully characterized. The Au→Ga interaction ($r = 1.0$, $\Sigma Ga_{\alpha} = 347°$, $\Delta E_{NBO} = 25$ kcal/mol) is much stronger than that of the zwitterionic complex and actually similar in magnitude to the Au→B interaction in complex **35f**. It is remarkable that the two coordination isomers are separable. The transfer of Cl between Au and Ga is probably prevented by the coordination of the three phosphines and the cage structure (as discussed later on, in the case of diphosphine gallium Au complexes, the zwitterionic and neutral forms interconvert relatively easily and are thus not separable).

To complete the study on heavier group 13 elements, the triphosphine indium ligand **40** was prepared [79]. Coordination to AuCl led to the zwitterionic complex **41a**, with transfer of Cl from Au to In (Scheme 15). The Au···In distance is relatively short ($r = 1.07$), and the presence of $Au^{+}\rightarrow InCl^{-}$ interaction was again apparent computationally ($\Delta E_{NBO} = 7.5$ kcal/mol). The corresponding neutral ClAu→In form is not observed experimentally (according to DFT calculations, it is about 7.6 kcal/mol higher in energy). Coordination of **40** to Pd(0) resulted in the cage complex **41b** with strong Pd→In interaction ($r = 0.93$, $\Delta E_{NBO} = 93$ kcal/mol). The environment around the Lewis acid is only marginally pyramidalized in this case ($\Sigma In_{\alpha} = 347°$), due to the larger size of indium and the constraints associated with the cage structure.

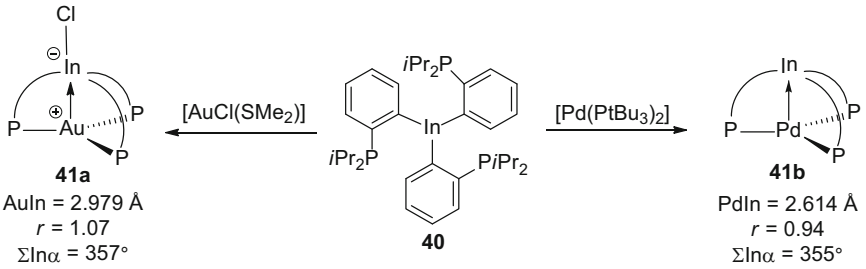

Scheme 15 Gold and palladium cage complexes **41a**,**b** deriving from the triphosphine indium ligand **40**, weak $Au^{+}\rightarrow InCl^{-}$ and strong Pd→In interactions

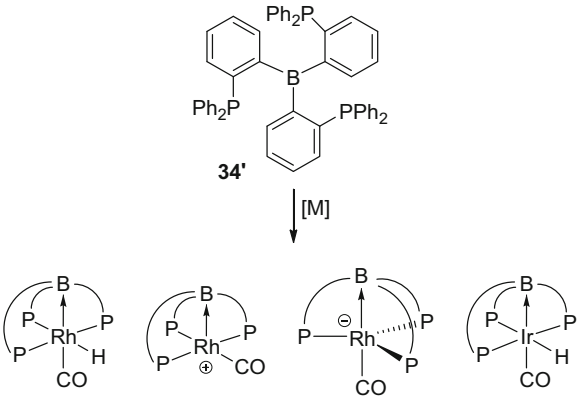

	42a	**42b**	**42c**	**42d**
M-B (Å)	2.370	2.287		2.326
r	1.05	1.01		1.03
ΣBα (°)	332.5	342		332.5

Fig. 14 Structure of the Rh and Ir metallaboratranes **42a**,**d** deriving from the triphosphine borane **34′**

The formation of metallaboratranes from triphosphine boranes was extended to group 9 and 8 metals. Kameo and Nakazawa studied the coordination of the Ph-substituted ligand **34′** (Fig. 14) and first reported a series of rhodium carbonyl complexes [80]: the neutral hydride species **42a**, the cationic derivative **42b** (obtained by protonolysis of **42a**), and the anionic compound **42c** (obtained by deprotonation of **42a**). They all feature Rh→B interaction, as apparent from ^{11}B NMR spectroscopy, X-ray diffraction analyses (for **42a**,**b**), and DFT calculations. The Rh···B distance is short ($r = 1.05$ for **42a** and 1.01 for **42b**), and the boron center is strongly pyramidalized ($\Sigma B_{\alpha} = 332°$ for **42a** and 342° for **42b**). Compared with the corresponding B-free complexes, the v(CO) stretching frequency is shifted to higher frequency by 76–98 cm^{-1}, indicating that the Rh→B interaction

withdraws a significant amount of electron density from Rh (and thus Rh→CO backdonation weakens). The constraints associated with the cage structure and the different geometries adopted by complexes **42a–c** (octahedral, square-pyramidal, and trigonal-bipyramidal, respectively) make comparisons quite hazardous, but overall the Rh→B interaction is weaker in the cationic complex **42b** (with no σ-donor ligand in *trans* to B) and practically identical in strength in the neutral and anionic complexes **42a** and **42c**. The Ir hydride complex **42d** related to **42a** was prepared soon after [81]. The Ir···B distance ($r = 1.03$) and B pyramidalization ($\Sigma B_\alpha = 331°$) indicate a slight increase of the M→B interaction, in line with the higher Lewis basicity of Ir over Rh.

Interestingly, the Rh and Ir metallaboratranes undergo reversible CO/phosphine ligand exchange (Scheme 16) [80, 81]. The reaction proceeds at room temperature for **42a** but requires heating at 80°C for **42d** and **42c**. Kinetic studies support a dissociative mechanism, and the M→B interaction plays a key role, by labilizing the ligand in *trans* position to B (such ligand exchange does not occur with related B-free complexes). X-ray diffraction studies suggest slight strengthening of the M→B interaction upon replacement of CO for PR_3, but steric factors also come to play here and tend to alleviate the stronger donor character of PR_3 vs CO.

In the frame of the reduction of dinitrogen into ammonia, Peters extensively studied iron complexes of the triphosphine borane **34** [82–86] (the term "elasticity" relates here to the ease of deformation of the ligand to adapt the metal fragment it coordinates to, as defined in [87]). An impressive variety of complexes was progressively prepared and characterized (Table 2). They all adopt a metallaboratrane structure and trigonal-bipyramidal geometry (except the cationic complex **44d**, which is trigonal pyramidal). The triphosphine borane ligand shows unique capacity to form stable Fe complexes in different oxidation and spin states. The strong coordination of the three phosphines in the equatorial plane, combined with the weak Fe→B axial interaction, provides stability and rigidity but also some elasticity [87]. It is remarkable that the Fe···B distance spans a broad range, from 2.222 Å in the neutral Fe(η^1-N_2) complex **44f** to 2.785 Å in the β-disilyl hydrazido complex **44h** (corresponding to r values from 1.03 to 1.29).

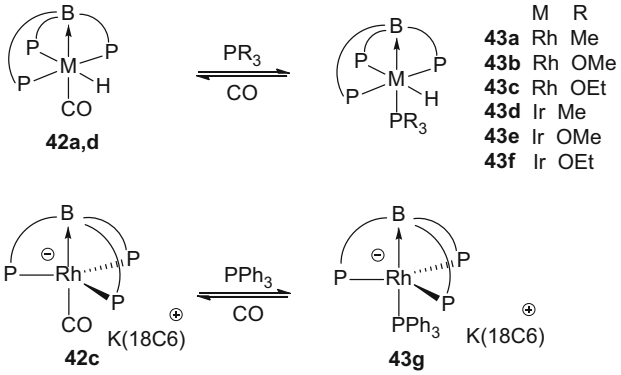

Scheme 16 CO/PR_3 exchange at Ir/Rh, *trans* effect of the σ-acceptor borane ligand

Table 2 Key features of the triphosphine borane Fe complexes **44a–j**, as determined crystallographically or calculated by DFT (*S* for spin state)

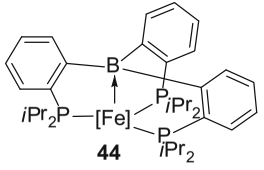

44

	44a	**44b**	**44c**	**44d**	**44e**	**44f**[a]	**44g**	**44h**[a]	**44i**	**44j**[a]
[Fe]										
FeB (Å)	2.459	2.229	2.523	2.217	2.280	2.222	2.311	2.785	2.435	2.770
r	1.04	0.94	1.07	0.94	0.97	0.94	0.97	1.29	1.13	1.28
ΣB_{α} (°)	342	339	341	347	341		330			
S	3/2	3/2	3/2	3/2	3/2	1	1/2	0	1/2	1/2

[a]DFT calculations

Their unique ability to accommodate low-valent N_2 as well as high-valent imido complexes makes triphosphine borane iron complexes ideal candidates for the activation/functionalization of N_2 [88]. Using excess of $HBAr^F{}_4$ (as proton source) and KC_8 (as reductant), N_2 could be converted into NH_3 in the presence of the anionic η^1-N_2 complex **44f** as catalyst [89]. About seven molecules of NH_3 were produced by Fe equivalent, and more than 44% of the protons were delivered to N_2 to produce NH_3.

Peters also investigated the coordination of the triphosphine borane **34** to cobalt. Co(I) and Co(0) species were reported (Fig. 15) [90, 91]. Most noticeable is the facile and reversible substitution of η^1-N_2 for η^2-H_2 at cobalt. Both complexes **45b** and **45c** were fully characterized and the energetic data for N_2 and H_2 binding were determined. Complex **45c** was the first σ-H_2 complex of Co to be structurally characterized and a rare example of a paramagnetic σ-H_2 complex ($S = ½$). Note that a neutron diffraction study has been carried out to resolve the side-on coordination of H_2 to cobalt. The dynamics of complex **45c** has been analyzed by EPR/ENDOR studies, and H_2 was found to undergo proton exchange in frozen solution at 2 K through rotation around the Co–H_2 axis [91]. Furthermore, the feasibility of N_2 to NH_3 conversion at Co (2.4 equiv. of NH_3 produced per Co center) was demonstrated [92].

Another original paramagnetic metallaboratrane complex was reported by Peters [93]. Coordination of the triphosphine borane **34** to CuBr in the presence of an excess of Na(Hg) led to the neutral complex **46a** (Fig. 16). According to EPR data, the unpaired electron is located in a σ-CuB orbital. This picture was confirmed by DFT calculations. The spin density is mainly located on B (57%, essential in the 2p orbital) and Cu (13%, essential in the 4p orbital). Complex **46a** was also characterized by X-ray diffraction analysis. It features short Cu···B distance (2.289 Å, $r = 1.06$) and the boron center is pyramidalized (ΣB_α 347°). The related cationic and anionic copper metallaboratranes **46b** and **46c** were prepared for comparison. In line with the low electron density at copper, the Cu→B interaction was found to be very weak in **46b** (2.495 Å, r 1.15, ΣB_α 355°, δ ^{11}B 67 ppm, ΔE_{NBO} 3.5 kcal/mol), even weaker than in the previously reported neutral CuCl complex **35d**. In contrast, the anionic complex **46c** features very strong Cu→B interaction (2.198 Å, r 1.02, ΣB_α 339°, δ ^{11}B 7 ppm), even stronger than in **46a**. Complex **46a** stands as a

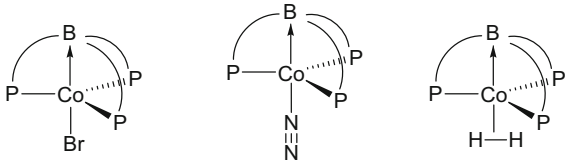

	45a	**45b**	**45c**
CoB (Å)	2.463	2.319	2.280
r	1.05	0.99	0.97
ΣBα (°)	342	339	336

Fig. 15 Structure of the Co metallaboratranes **45** deriving from the triphosphine borane **34**

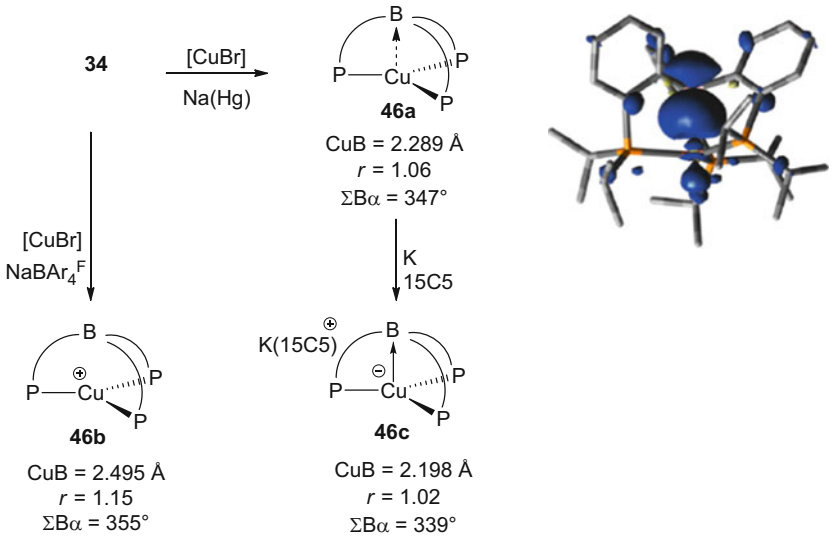

Fig. 16 Cationic, neutral, and anionic Cu metallaboratranes **46a–c** deriving from the triphosphine borane **34** (*left*), spin density of the neutral Cu complex **46a**, as calculated by DFT (*right*)

unique example of one-electron M–B bond, and altogether complexes **46a**, **46b**, and **46c** provide a unique series of cationic, neutral, and anionic metallaboratranes with formally zero-, one-, and two-electron M–B bonds. The ability of the triphosphine borane to accommodate different electronic environments, despite the cage structure, is once again remarkable.

Recently, Lu introduced another type of tetradentate ambiphilic ligand [94–96]. It is built on a tris(amino)amine core on which pendant phosphine arms are introduced. Introduction of a group 13 element, Al in the case of **47**, in the N_4 pocket results in a trigonal pyramidal aluminatrane, and coordination of the three phosphines then affords double-decker complexes with a central M···Al←N axis (Scheme 17). Zerovalent complexes were prepared first [94]. Whatever the metal fragment, Ni, Co(η^1-N_2), or Fe(μ-N_2), they all feature strong M→Al interactions, and the Al center is in trigonal-bipyramidal environment. The *r* value slightly increases from 1.00 (Ni) to 1.06 (Co) and 1.11 (Fe). It is interesting to note that the iron complex **48c** exhibits a one-electron reversible reduction wave very close in electrochemical potential to that of the related triphosphine borane Fe species reported by Peters (−2.08 and −2.19 V vs Cp_2Fe^+/Cp_2Fe, respectively), suggesting that B and Al have about the same influence on Fe. In the context of N_2 reduction/functionalization, the anionic and paramagnetic Co and Fe η^1-N_2 complexes **49b**,**c** were then prepared, and the N_β center of Yb was bis-silylated [95]. The Al center and Fe→Al interaction respond to the environment and electron density at iron: the Fe···Al distance is substantially shortened in the anionic Fe(−I) complex **49c** (2.574 Å, $r = 1.02$), while the neutral imido Fe(II) complex **50** displays a much looser contact (2.8237 Å, $r = 1.12$).

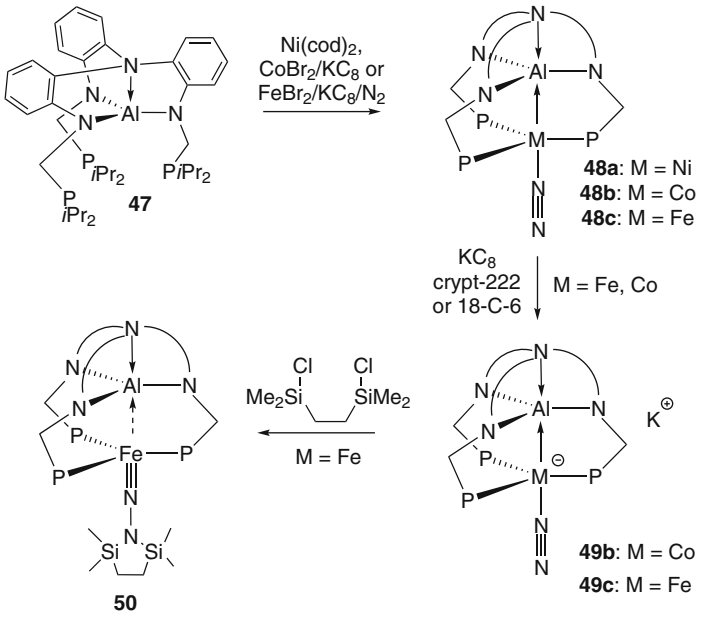

	48a	48b	48c	49b	49c	50
MAl (Å)	2.450	2.620	2.809	2.507	2.574	2.824
r	1.00	1.06	1.11	1.02	1.02	1.12
ΣNAlNα°	354.5	351.5	352	345	344	352

Scheme 17 Neutral and anionic Ni, Co, and Fe complexes **48–50** deriving from the double-decker triphosphine-aluminum ligand **47**

The influence of the group 13 element was then explored [96]. Al was replaced for Ga or In, and a series of Ni(0) complexes were characterized (Fig. 17). The "naked" species, without co-ligand at Ni, show a progressive shortening of the Ni···E_{13} distance (*r* from 1.00 to 0.92) with a slight increase of the pyramidalization around E_{13} (the sum of bond angles goes from 351° to 345°). The strengthening of the Ni→E_{13} interaction from Al to In was proposed to result from better orbital overlap (soft Ni(0) Lewis base, more polarizable E_{13} element) and better fit to the double-decker structure (Ni and E_{13} try to stay in the P_3 and N_3 coordination planes, respectively). Interestingly, the indium complex readily fixes N_2 to form an end-on species, while H_2 gives side-on adducts with both the gallium and indium derivatives. Compounds **51d**,**e** are rare examples of σ-H_2 Ni complexes. The Ni→E_{13} interaction plays a major here, withdrawing electron density from Ni and strengthening donation from H_2. Dihydrogen is weakly bonded in the Ga complex **51d** (which readily converts back to the naked species **51a**), while the related In complex **51e** is stable under vacuum (donation of σ-H_2 to Ni is enforced by the

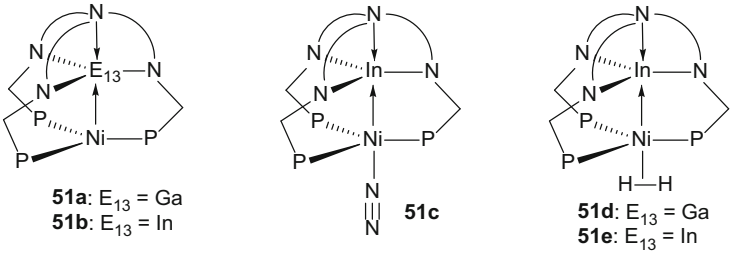

51a: E_{13} = Ga
51b: E_{13} = In

51c

51d: E_{13} = Ga
51e: E_{13} = In

	51a	51b	51c	51e
ME_{13} (Å)	2.379	2.457	2.526	2.487
r	0.97	0.92	0.95	0.94
$\Sigma NE_{13}N\alpha$ (°)	349.5	345	341	343

Fig. 17 Ni complexes **51a–e** deriving from double-decker triphosphine-gallium and indium ligands

stronger Ni→In interaction). Besides their structural interest, the two systems were successfully applied to catalyze the hydrogenation of olefins under mild conditions (5 mol%, RT, 1 atm).

2.10 Complexes with M→E_{13} Interactions Supported by Tridentate Ambiphilic Ligands

Diphosphine boranes are emblematic and archetypal ambiphilic ligands in many respects. We started our studies on σ-acceptor ligands with diphosphine boranes in the mid-2000s. The presence of two phosphine buttresses supports the establishment of TM→LA interactions (B but also Ga, and even weaker Lewis acids such as heavier group 14–16 elements; see below), but does not enforce them in cage structures, as in the case of tetradentate systems with three pendant donor sidearms. In our seminal 2006 and 2008 papers [97, 98], we reported a series of Rh (I) complexes (Fig. 18): the chloro-bridged dimer **53a**, the mononuclear DMAP complex **53b**, and the chloro-carbonyl complex **53c** (obtained as a mixture of diastereomers due to the relative position of the Ph group at B and Cl/CO at Rh). The first spectroscopic evidence for the presence of Rh→B interaction comes from ^{11}B NMR, with a resonance signal in the typical range of tetracoordinate boron center ($\delta \sim 19$–26 ppm for complexes **53a–c**). X-ray diffraction studies were systematically carried out to assess the bonding situation. The Rh center adopts square-pyramidal geometry in all complexes, with the two phosphines in *cis* (**53a** and **53b**) or *trans* (**53c**) geometry and the boron center at the apical position. The geometry

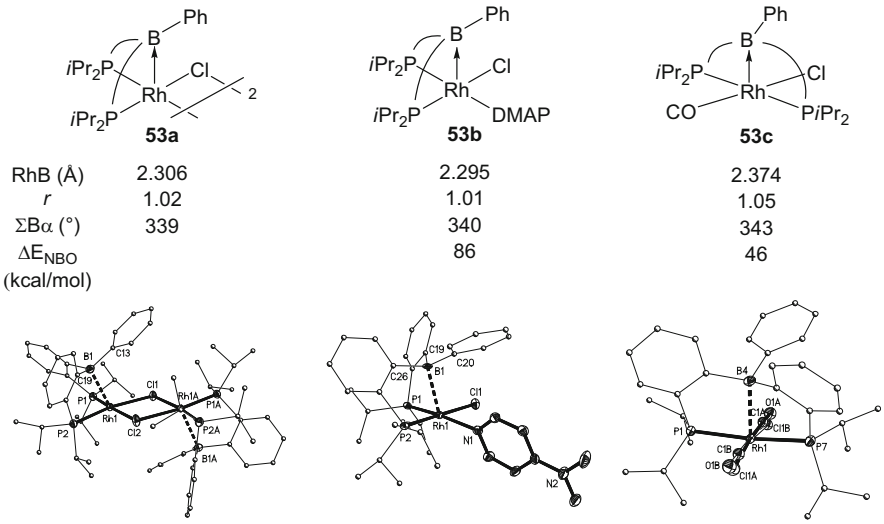

Fig. 18 Structure of the diphosphine borane Rh(I) complexes **53a–c**

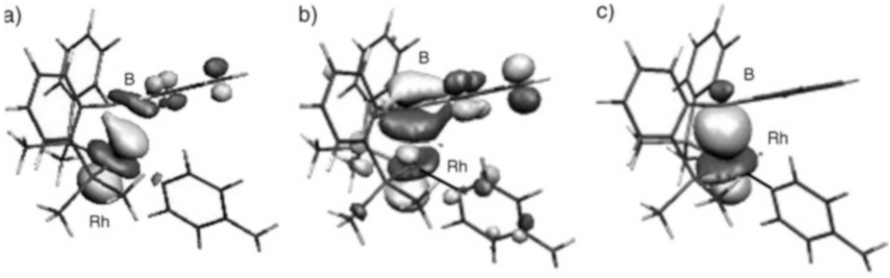

Fig. 19 Plots of the HOMO (**a**), LUMO (**b**), and NLMO (**c**) associated with the Rh→B interaction in complex **53b**

around boron is strongly pyramidalized ($\Sigma B_\alpha = 339–343°$), and the Rh···B distance is short [2.29–2.37 Å, $r \sim 1.03$], slightly shorter in **53a** and **53b** ($r = 1.02$) than in **53c** ($r = 1.05$), due to the π-accepting properties of CO (which reduces the electron density at Rh). Infrared spectroscopy showed that the coordination of B exerts a strong withdrawing effect on Rh, the ν(CO) band of complex **53c** (2,002 cm^{-1}) being shifted to higher frequency by as much as 35 cm^{-1} compared to that of the corresponding B-free complex [RhCl(CO)(iPr$_2$PPh)$_2$] **102**. Experimentally, a good indication for the strength of the Rh→B interaction is given by the reaction of **53a** with DMAP and CO leading to **53b** and **53c**. The transformations do not hit the B center, whose Lewis acid character is actually masked by coordination to Rh.

The nature of the Rh→B interaction was thoroughly analyzed by DFT calculations [97, 98]. The frontier molecular orbitals and NLMO accounting for the Rh→B interaction in complex **53b** are depicted in Fig. 19. Two-center two-electron

bonding interaction between Rh and B is apparent from the HOMO and LUMO, which correspond to bonding and antibonding interactions of the occupied d_z2 (Rh) and vacant 2p(B) orbitals. This explains why the boron center approaches Rh perpendicularly to its "first" coordination plane, so as to optimize orbital overlap. The corresponding NLMO is centered on rhodium (79%) with significant participation of boron (17%). Strong donor–acceptor Rh→B interaction is also identified by NBO ($\Delta E_{NBO} = 86$ kcal/mol). The same bonding picture is found for the carbonyl complex **53c**, albeit with a noticeably weakened Rh→B interaction ($\Delta E_{NBO} = 46$ kcal/mol).

Another series of Rh complexes was reported in 2011 by Britovsek starting from the diphosphine borane **52′** with Ph instead of *i*Pr groups at P (Fig. 20) [99]. In this case, the chloro-carbonyl complex was obtained as a mixture of *cis* (65%) and *trans* isomers (35%, again two forms with the Ph at B in *cis* position to CO or Cl at Rh). Cationic bis-carbonyl and bis-acetonitrile complexes **54b** and **54c** were also prepared and structurally characterized. Despite their cationic character and the reduced electron density at Rh, they feature noticeable Rh→B interactions, as substantiated by X-ray diffraction analyses. In line with the stronger π-accepting properties of CO vs CH_3CN, the Rh···B distance is longer and the B pyramidalization is smaller in **54b** than in **54c**. The bis-carbonyl complex was treated with esters (methyl acetate and trifluoromethyl acetate) with the aim to promote B-assisted oxidative cleavage of the C–O bond, but no reaction occurred. Even in this case, the Rh→B bonds are too strong.

As an extension of their work on triphosphine borane Rh and Ir hydride complexes, Kameo and Nakazawa studied related diphosphine borane species [100]. Here, very different coordination modes were observed with the two metals (Fig. 21). The Ir complex **55** adopts square-pyramidal geometry and features strong Ir→B interaction, while the Rh complex **56** is in trigonal pyramidal geometry and displays Rh–H→B interaction. Note also that the two phosphines are disposed *trans*

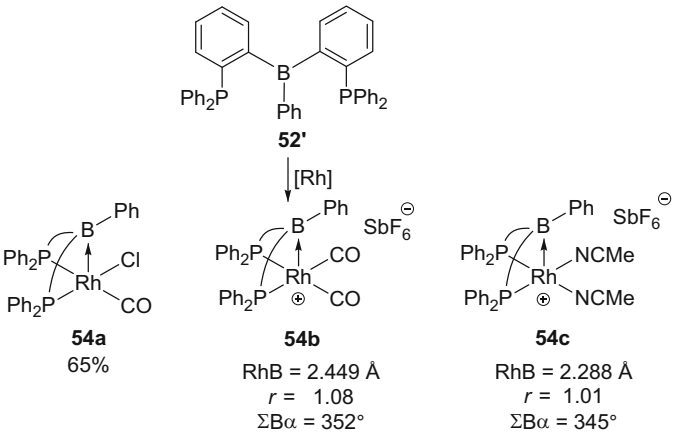

Fig. 20 Neutral and cationic diphosphine borane Rh(I) complexes **54a–c**

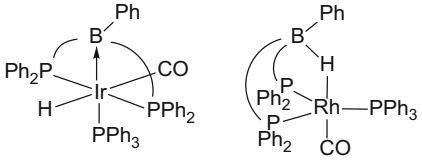

	55	**56**
δ ^{11}B (ppm)	22	11.5
δ ^{1}H (ppm)	- 9	- 12
MB (Å)	2.445	/
r	1.09	/
ΣBα (°)	332.5	341

Fig. 21 Ir and Rh diphosphine borane hydride complexes **55** and **56**, M→B vs M–H→B coordination

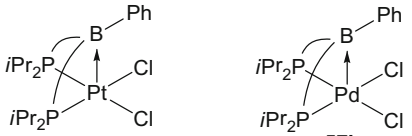

	57a	**57b**
MB (Å)	2.429	2.650
r	1.10	1.19
ΣBα (°)	347	355
ΔE_{NBO} (kcal/mol)	50	14

Fig. 22 Diphosphine borane Pt(II) and Pd(II) complexes

to each other in **55**. The Ir···B distance in complex **55** is slightly longer than that observed in the related triphosphine borane cage complex **42d**: 2.444 vs 2.326 Å ($r = 1.09$ vs 1.03). The transfer of electron density from Ir to B is apparent by IR from the shift of the v(CO) stretching frequency (by 40 cm^{-1} compared to the B-free complex [IrH(CO)(PPh_3)$_3$]) but again with slightly weaker magnitude than for the cage complex ($\Delta v = 52$ cm^{-1}). Computational studies were performed on both the Ir and Rh complexes to shed light into their bonding situations and understand the difference between the two systems. Energy minima were located in both cases for the M→B and M–H→B forms. In line with experimental observations and the higher Lewis basicity of Ir over Rh, the M→B form is favored energetically for Ir (by 2.4 kcal/mol), while Rh prefers to engage into M–H→B bonding ($\Delta E = 8.0$ kcal/mol).

In order to assess the influence of the metal on the magnitude of the M→B interaction among d^8 complexes, we prepared diphosphine borane Pd(II) and Pt(II) complexes **57a** and **57b** related to the Rh(I) species **53** (Fig. 22) [98]. Both complexes adopt square-pyramidal geometry, with *cis* coordination of the two P and the B center in the axial position. Thorough analysis of the experimental and theoretical data indicated progressive weakening of the M→B interaction in the

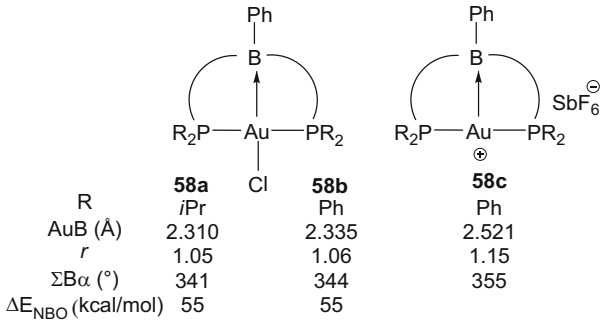

Fig. 23 Diphosphine borane gold(I) complexes **58a–c**

Rh/Pt/Pd series. This is apparent from ^{11}B NMR (δ shifts from 20 ppm in **53b** to 47 ppm in **57**), X-ray diffraction study (the r value and sum of bond angles ΣB_α increases from 1.01/340° in **53b** to 1.19/355° in **57b**), and NBO (the NBO delocalization energy ΔE_{NBO} associated with the donor–acceptor M→B interaction decreases from 86 kcal/mol in **53b** to 14 kcal/mol in **57b**). These variations are consistent with the higher Lewis basicity of Rh(I) vs Pt(II) and Pd(II), and it is important to note that despite the chelation by two phosphines, the M→B interaction retains important flexibility and adapts its magnitude to the metal in front.

Our understanding of TM→LA interactions significantly progressed upon coordination of diphosphine borane ligands to gold (Fig. 23) and thorough analysis of complexes **58a**,**b** [101]. Both species adopt square-planar geometry with *trans* coordination of the two phosphines and strong Au→B interaction (it is slightly stronger with *i*Pr vs Ph substituents at P). The ^{11}B NMR chemical shift (δ ~ 23 ppm), Au···B distance (~2.32 Å, $r = 1.05$), boron pyramidalization ($\Sigma B_\alpha \sim 342°$), and NBO delocalization energy (ΔE_{NBO} ~ 55 kcal/mol) are very similar to those observed in the related triphosphine borane complex **35f**, indicating that the third donor buttresses and cage structure do not reinforce the Au→B interaction. To shed light on the electronic structure of **58a**,**b**, ^{197}Au Mössbauer measurements were carried out. The resulting isomer shift (IS) and quadrupole splitting (QS) clearly position **58a**,**b** as gold(I) rather than gold(III) species, meaning that the transfer of electron density from Au to B is not large enough to consider that gold is oxidized into gold(III) (see the conclusion for a discussion of the bonding situation). In turn, the square-planar geometry of **58a**,**b** is unprecedented for gold(I) (known tetracoordinate gold(I) complexes have tetrahedral geometry). This observation pointed out the influence σ-acceptor ligands may have on geometry of TM complexes. Inagaki recently prepared cationic diphosphine borane gold complexes and reported interesting catalytic results in enyne cyclizations [102]. Of note, the tricoordinate complex **58c** was characterized by X-ray diffraction study (Fig. 24, right). As in the case of triphosphine borane complexes, the Au→B interaction weakens but does not vanish upon cationization (the Au→B distance increases and the boron is less pyramidalized).

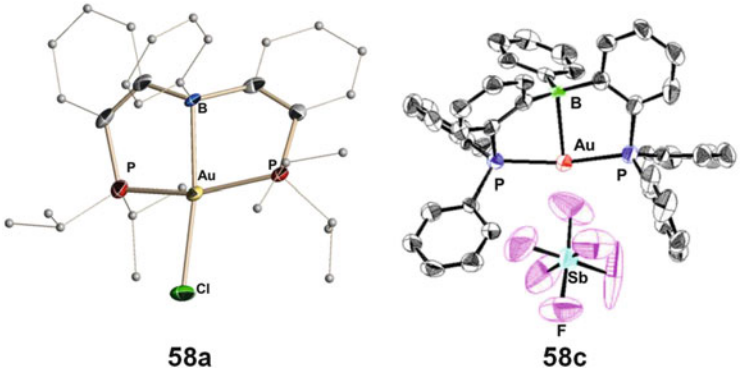

Fig. 24 Structure of the diphosphine borane Au(I) complexes **58a** and **58c**

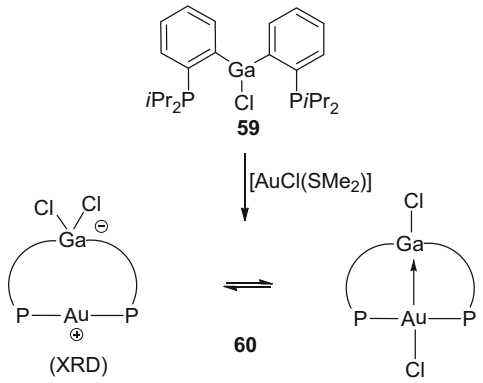

Scheme 18 Coordination of a diphosphine-gallane to gold, Au→Ga interaction vs zwitterionic complex (Au to Ga chloride transfer)

The propensity of diphosphine boranes to engage into TM→B interactions has stimulated the investigation of related ambiphilic ligands with heavier group 13 elements, in particular Al and Ga. So far, these studies were focused on gold complexes, given the peculiar square-planar structure of **58a**,**b**. Aluminum does not form a neutral Au→Al complex analogous to **58a**,**b** but abstracts the chloride from gold and gives a zwitterionic complex [103]. The behavior of gallium is in between those of Al and B [78]. Both the zwitterionic $Au^{+}/GaCl_2^{-}$ and neutral ClAu→GaCl forms are observed in solution (Scheme 18), and they actually slowly interconvert at the NMR timescale (in contrast with the related triphosphine gallane complexes which are separable). Only the zwitterionic structure of **60** could be characterized by X-ray diffraction study, but the presence of strong Au→Ga interaction in the neutral form was supported computationally (Au→Ga distance 2.59 Å, gallium pyramidalization ΣGa_{α} 345°, NBO delocalization energy 33 kcal/mol).

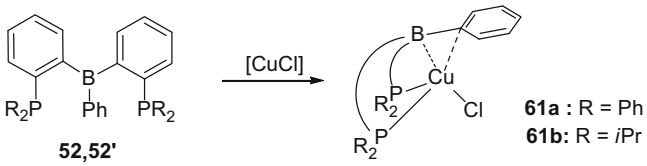

Fig. 25 Diphosphine borane copper complexes **61a**,**b**, η^2-BC_{ipso} coordination

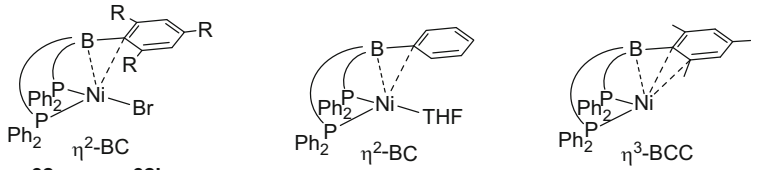

	62a	**62b**	**62c**	**62d**
R	H	Me		
MB (Å)	2.255	2.227	2.124	2.154
r	1.04	1.03	0.98	1.0
ΣBα (°)	355	354	352	358

Fig. 26 Diphosphine borane Ni(I/0) complexes **62a–d**, multicenter BC_n coordination

The nature of the coinage metal has also been varied to assess its influence within d^{10} complexes. Diphosphine borane copper complexes **61a**,**b** were readily prepared (Fig. 25) [104]. Here, the borane moiety does not simply behave as a σ-acceptor ligand but engages into η^2-BC_{ipso} coordination[5] (weak Cu→B interaction is supported by arene coordination), which precludes comparison between Cu and Au. This situation contrasts with the homologous series of Cu,Ag,Au complexes obtained from the triphosphine borane (the cage structure imposes geometric constraints but favors M→B interaction over other coordination modes) [76].

Upon coordination of diphosphine boranes to Ni, Peters observed multicenter B (arene) coordination too [105, 106]. Representative examples are depicted in Fig. 26. The privileged coordination mode, η^2-BC_{ipso} or η^3-$BC_{ipso}C_{ortho}$, depends on the oxidation state of Ni (I vs 0), on the co-ligand at Ni (THF, η^1-N_2 or μ-N_2, η^2-H_2, none), and on the substituents at B (Ph or Mes) and P (Ph or *i*Pr). Short Ni···B distances ($r \sim 1$) but low pyramidalizations around B ($\Sigma B_\alpha = 354-358°$) are observed in all cases. It is important to note that the strong B(arene) interactions do not prevent the Ni(0) species to react, and they actually readily activate dihydrogen and silanes via unusual TM/Lewis acid cooperation [107].

A related diphosphine borane Pd(0) complex **63** was recently reported by Tauchert (Fig. 27, left) [108]. Despite the coordination of a pyridine co-ligand, the central BPh moiety coordinates in an η^2-BC_{ipso} fashion. The geometry at Pd is in

[5] For a review on BC_n multicenter coordination to TM, see [19].

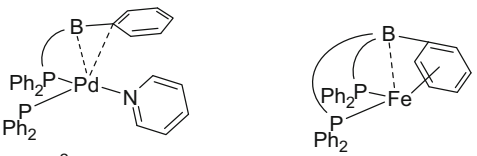

	η^2-BC	η^7-BPh
	63	**64**
MB (Å)	2.193	2.267
r	0.98	1.05
ΣBα (°)	346	359

Fig. 27 Diphosphine borane Pd(0) and Fe(0) complexes **63** and **64**, multicenter BC_n coordination

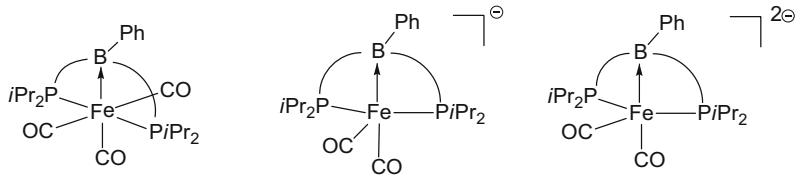

	65a	**65b**	**65c**
FeB (Å)	2.308	2.419	2.419
ΣBα (°)	342	330	330

Fig. 28 Diphosphine borane Fe carbonyl complexes **65**

between tetrahedral and square-planar, the Pd···B distance is short [2.194(3) Å, $r = 0.98$], and the boron center is significantly pyramidalized (ΣB_α 346°).

Diphosphine borane Fe and Co complexes also tend to involve BC_n coordination [109, 110]. Most remarkable is the η^7-BPh coordination observed in the Fe(0) species **64** (Fig. 27, right), despite the huge distortion it requires with a deviation of B from the $C_{ipso}C_{para}$ axis by more than 50°. In the frame of reductive coupling of CO, Peters also investigated diphosphine borane Fe carbonyl complexes. Here discrete Fe→B interactions were generally observed (Fig. 28) [111]. The neutral $Fe(CO)_3$ species **65a** adopts octahedral geometry with the two phosphines in *trans* position and a relatively long Fe···B distance (2.5263(6) Å, $r = 1.17$), as to compare with the related tris(methimazolyl) dicarbonyl complex **7**. The mono- and di-anionic dicarbonyl complexes **65b** and **65c** were prepared by K/15-C-5 reduction. The geometry of **65c** is trigonal-bipyramidal (PFeP = 120.6°), whereas that of **65b** is in between trigonal-bipyramidal and octahedral (PFeP = 143°). They both feature stronger Fe→B interaction ($r \sim 1.12$) than **65a**, in line with the reduction of Fe. But this phenomenon apparently levels out upon addition of the second electron, the extra electron density being largely absorbed by backbonding to CO (and P).

Recently, Emslie extended the variety of tridentate ambiphilic ligands to diphosphine featuring pendant B and Al center [112, 113]. A 1,1′-diphosphine-ferrocene core was used to provide some flexibility to the system, but the rigid *o*-

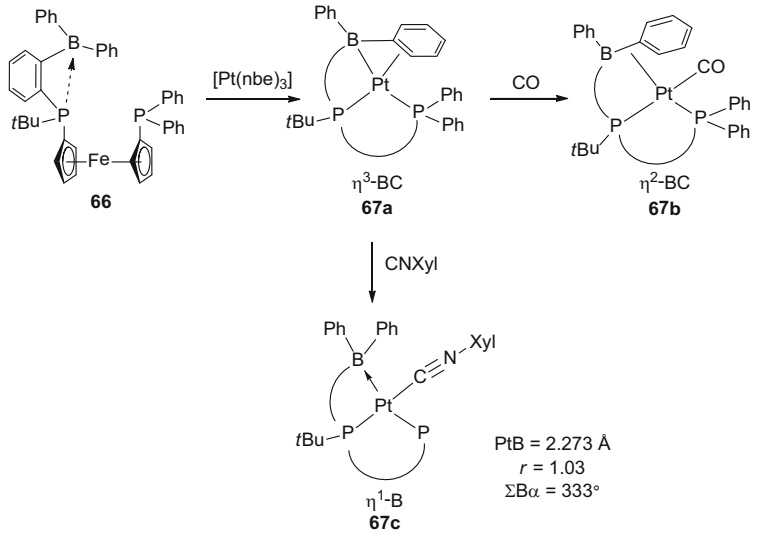

Scheme 19 Pt complexes of the diphosphine borane ligand **66**, coordination of a pendant BPh_2 moiety

phenylene linker was kept for the lateral Lewis acid moiety, to favor its interaction with metals. A series of Pt(0) were first prepared with the diphosphine borane **66** (Scheme 19) [112]. In the absence of co-ligand at Pt, η^3-BCC coordination is observed, while the carbonyl complex displays η^2-BC coordination. Introduction of a strong σ-donor isocyanide co-ligand at Pt shifts the coordination of the borane moiety to η^1. Complex **67c** adopts a distorted square-planar geometry with the two P atoms in *cis* arrangement. The Pt···B distance is short [2.27 Å, $r = 1.03$], the environment around boron is strongly pyramidalized ($\Sigma B_\alpha = 333°$), and the borane exerts strong *trans* effect, as apparent from the elongation of the opposite Pt−P bond [2.381 vs 2.268 Å].

Coordination of the related Al-appended diphosphine **68** to Pt was then investigated, and a series of Pt(0) and Pt(II) complexes **69a–f** featuring Pt→Al interactions were isolated (Fig. 29) [113]. Mononuclear Pt(0) complexes featuring $H_2C{=}CH_2$, PhCCPh, and CO ligands were structurally characterized. They adopt distorted trigonal pyramidal geometries, with the co-ligand sitting approximately in the PPtP plane and the Al center at the apical position. Upon heating, the corresponding nbe complex evolves into the dinuclear complex **69e**. The diphosphine moiety acts as a bridging ligand (thanks to the flexibility of the ferrocene core), and the Pt centers adopt T-shape geometry, with the two phosphines coordinated in *trans* fashion. The Pt(II) dihydride complex **69f** was also prepared by activation of H_2. It adopts square-pyramidal geometry. The two phosphines are in *trans* arrangement, and the Al center occupies the apical site and weakly interacts with one hydride at Pt. The Pt···Al distance remains about the same in all complexes (~2.55 Å), the longest being observed in the carbonyl

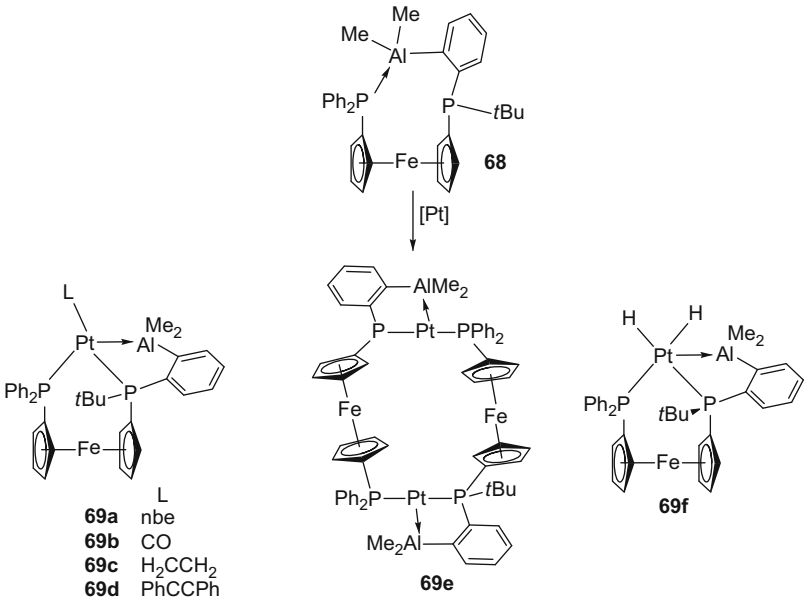

Fig. 29 Pt complexes **69a–f** deriving from the Al-appended diphosphine **68**, Pt(0) and Pt(II)→Al interactions

complex (2.624 Å) and the shortest in the dinuclear T-shape complex (2.482 Å). The Al center is strongly pyramidalized in all complexes ($\Sigma Al_\alpha \sim 336°$). The high Lewis acidity of Al favors relatively strong Pt→LA interactions, compared with the related B system. The $AlMe_2$ group also prevents multicenter $E_{13}C_n$ coordination, as observed with BPh_2.

2.11 *Complexes with M→E_{13} Interactions Supported by Bidentate Ambiphilic Ligands*

In few instances, bidentate ambiphilic ligands have been shown to engage into TM→LA interactions. Here, only one donor buttress assists the coordination of the Lewis acid, resulting in weak and/or cleavable interactions. The first such complexes were obtained by our group in 2006 upon coordination of *o*-phenylene-bridged phosphine boranes to AuCl (Scheme 20) [114]. The presence of weak Au→B interactions was supported by analytical and computational data. Most noticeable is the influence of the Lewis acidity of the boron center, stronger Au→B interaction being observed with the BFlu (for 9-borafluorene) vs BCy_2 derivative. This is apparent by ^{11}B NMR spectroscopy: upon coordination to Au, the resonance signal shifts to high-field by 10 ppm for BFlu but remains essentially

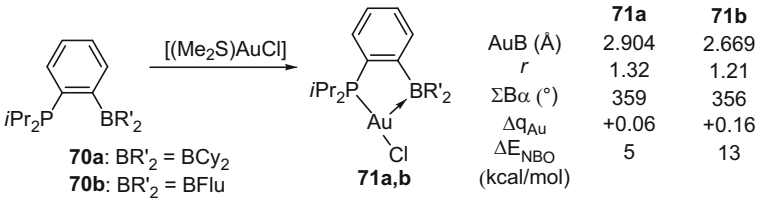

Scheme 20 Synthesis of phosphine borane Au complexes **71a**,**b**

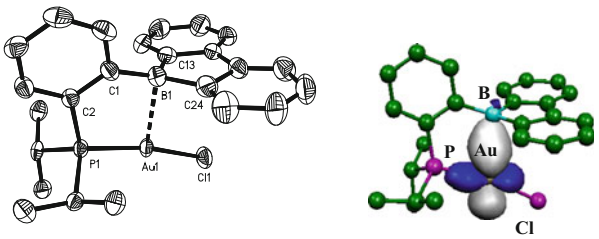

Fig. 30 Molecular structure of complex **71b** (*left*) and NLMO accounting for the Au→B interaction (*right*)

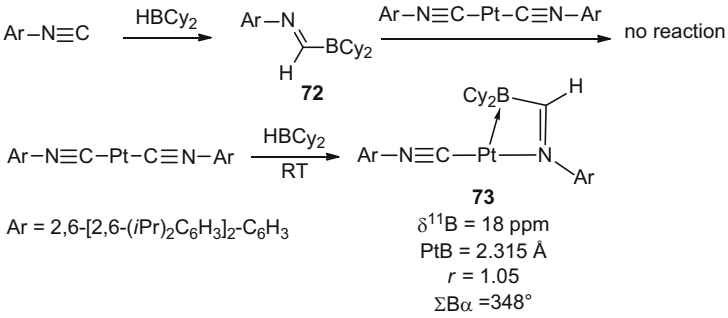

Scheme 21 Synthesis of the boryl imine ligand **72** and of the corresponding Pt complex **73**

the same for BCy_2. According to X-ray diffraction data, the boron atom comes closer to gold (the Au···B distance equals 2.903 Å in **71a** and 2.668 Å in **71b**, corresponding to *r* values of 1.32 and 1.21, respectively). Donor–acceptor interactions between an occupied Au-centered orbital and a vacant B-centered orbital are found in both cases by NBO, with delocalization energies ΔE_{NBO} increasing from 5 kcal/mol in **71a** to 13 kcal/mol for **71b** (Fig. 30). A transfer of electron density from Au to the borane fragment is also apparent from the computed atomic charges. Typically, a depletion of 0.06/0.16 e^- at gold is observed upon coordination of BCy_2/BFlu.

Figueroa reported in 2014 an original Pt complex **73** featuring an imine-borane ligand (Scheme 21) [115], providing another example of M→LA interaction

supported by a single buttress. The free N,B ligand **72** can be easily prepared by 1,1-hydroboration of the isocyanide Ar–NC, but it does not react with the [Pt(CNAr)$_2$] precursor [2,6-(2,6-(*i*Pr)$_2$C$_6$H$_3$)$_2$-C$_6$H$_3$]. To obtain complex **73**, the imine-borane ligand was prepared in the coordination sphere of Pt, by reacting [Pt(CNAr)$_2$] with Cy$_2$BH. No intermediate was detected by NMR during the course of the reaction, suggesting that the 1,1-hydroboration of CNAr and migration of Pt from C to N occur simultaneously.

Spectroscopic and crystallographic data indicate the presence of a strong Pt→B interaction. The ^{11}B NMR resonance signal is substantially shifted upfield (from 74 ppm in the free ligand to 18 ppm in complex **73**). The Pt···B distance is short (2.315 Å), corresponding to an *r* value of 1.05, and the boron environment is strongly pyramidalized ($\Sigma B_\alpha = 348°$). Computational data also support the presence of strong Pt→B interaction. A NLMO mainly centered on Pt (81%) and B (19%) with bonding character was found by NBO calculations (Fig. 31, right). The structure of complex **73** is remarkable and substantiates the ability of geminal ambiphilic ligands to engage into TM→LA interactions, despite the strain associated with the formation of four-membered rings, as apparent from the very acute NPtB bite angle (66°).

A similar bonding situation was recently met in gold complexes of a geminal P, Al ligand **74** [116]. Due to the high affinity of aluminum for chlorine, bridging M–Cl→Al interactions or chloride abstraction giving zwitterionic complexes were systematically observed upon coordination of **74** to Rh, Pd, or Au chlorides [117]. But with organogold(I) precursors, a series of T-shape complexes featuring Au→Al interactions were obtained (Scheme 22). Complexes **75a**,**b** were prepared from methyl and *p*-tolyl phosphine gold(I) precursors (note that the formation of Au→Al interaction probably acts as a driving force and favors the phosphine displacement at gold). They were spectroscopically characterized but could not be separated from the released P(*o*-Tol)$_3$. Complexes **75c**,**d** were readily obtained using [Au(CCPh)]$_n$ or [(tht)Au(C$_6$F$_5$)]. X-ray diffraction studies showed the presence of relatively strong Au→Al interactions, with Au···Al distances of 2.897 Å for **75c** ($r = 1.13$) and 2.758 Å for **75d** ($r = 1.07$) (Fig. 32). The Au→Al interaction is substantially enforced when the C$_6$F$_5$ group is replaced for the more electron-rich and less sterically demanding CCPh moiety. Here also, the coordination of the Lewis acid moiety induces significant ring strain, as apparent from the bending of

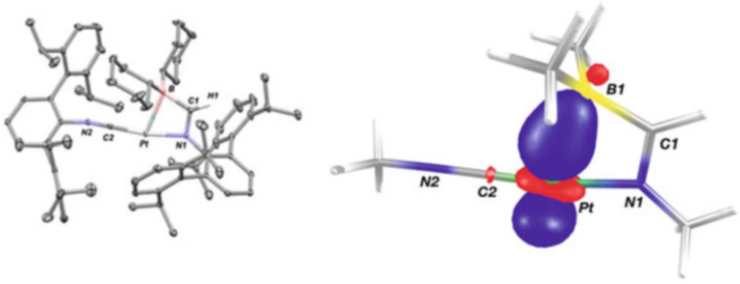

Fig. 31 Molecular structure of complex **73** (*left*) and NLMO accounting for the Pt→B interaction (*right*)

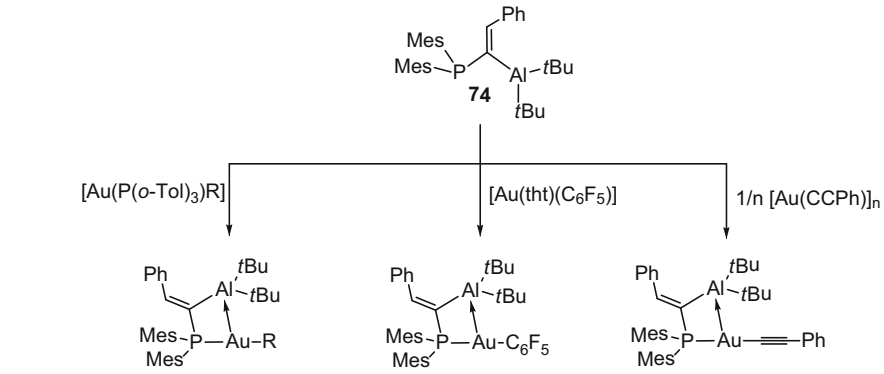

	75a*	75b*	75c	75d
R	Me	*p*-Tol		
AuAl (Å)	2.745	2.774	2.897	2.758
r	1.07	1.08	1.13	1.07
ΣAlα (°)	355	355	358	356
PAuAl (°)	73	72	73	72
ΔE_{NBO} (kcal/mol)	24	25	21	30

* by DFT calculations

Scheme 22 Au→Al interactions arising from the coordination of the geminal P,Al ligand **74** to organo gold(I) fragments

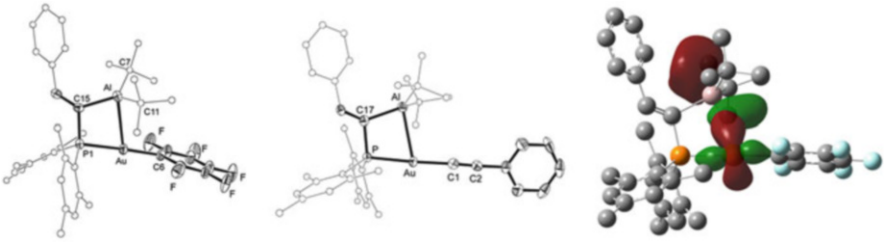

Fig. 32 Molecular structure of complexes **75c** (*left*) and **75d** (*middle*); superposition of the donor (Au-centered) and acceptor (Al-centered) NBO orbitals accounting for the Au→Al interaction in **75c** (*right*)

the P–C–Al framework, from 119° in the free ligand to 104–106° in **75c**,**d**! The presence of relatively strong Au→Al interactions has been confirmed by NBO calculations (Fig. 32) (ΔE_{NBO} delocalization energies range from 21 to 30 kcal/mol, depending on the R group at gold). It is interesting to note that the T-shape Au→Al structures observed experimentally are 6–9 kcal/mol more stable than the corresponding structures without Au→Al interactions. This confirms the ability and the propensity of geminal ambiphilic ligands such as **74** to engage into TM→LA interactions, despite the strain associated with the formation of four-membered rings. Note also that TM/Al compounds are rare and complexes **75** actually stand as the first derivatives combining Au and Al(III).

3 Coordination of (Heavier) Group 14 Elements as Lewis Acids

3.1 Complexes with M→E_{14} Interactions Supported by Phosphine Sidearms

Although formally electronically saturated, $E_{14}R_4$ compounds of the heavier group 14 elements are known to possess Lewis acid properties. They readily violate the octet rule and form penta- and hexacoordinate compounds upon association with organic Lewis bases (N, O, S, etc.). As for group 13 elements, it is conceivable that the electron-rich transition metals behave as Lewis bases and engage into TM→$E_{14}R_4$ interactions (E_{14} = Si, Ge, Sn). This would be accompanied by a change in geometry of the group 14 element from tetrahedral to trigonal-bipyramidal, and the associated orbital interaction would involve an occupied d orbital at the metal and a vacant low-lying σ* orbital (or combination of σ* orbitals) centered on the group 14 element (Fig. 33).

The possible existence of such metal→$E_{14}R_4$ interaction was discussed early on by Grobe in nickel and palladium complexes **76** and **77** deriving from triphosphine silane ligands (Fig. 34) [118–120]. The cage structure maintains the Si atom relative close to the metal center, but the associated M···Si distances remain quite long

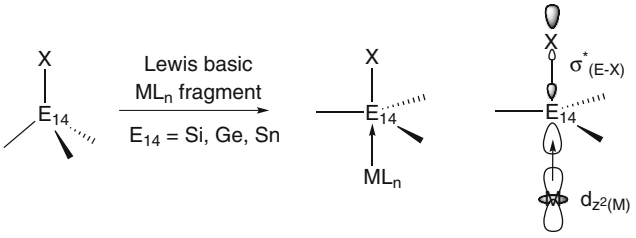

Fig. 33 Coordination of heavier group 14 elements as Lewis acids and associated orbital interaction

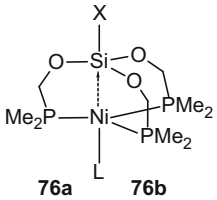

	76a	**76b**
X	Cl	Me
L	PPh_3	CO
NiSi (Å)	3.94	3.95
r	1.68	1.68

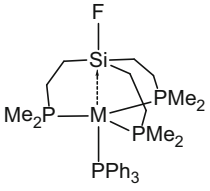

	77a	**77b**
M	Ni	Pd
MSi (Å)	3.92	3.87
r	1.66	1.55

Fig. 34 Cage complexes of triphosphine silane ligands structurally characterized by Grobe

($r > 1.55$), and the geometry around Si stays tetrahedral, indicating very weak, if any, M→Si interactions.

3.2 *Complexes with M→E_{14} Interactions Supported by Four Methimazolyl Sidearms*

Following our studies on the coordination of group 13 elements supported by phosphine buttresses, we explored related Si and Sn systems [121, 122]. Doing so, we also intended to assess to which extent the Lewis acidity of the Z-type ligand can be decreased while retaining significant interaction with the metal center. Gold complexes of diphosphine silane and stannane ligands were prepared, and their structures were extensively analyzed both experimentally and theoretically (Scheme 23) [121, 122]. X-ray diffraction studies of **79a** and **79b** provided the first unambiguous evidence for the coordination of silanes and stannanes as σ-acceptor ligands. The respective Au···Si,Sn distances are short ($r = 1.25$ and 1.05, respectively), and the group 14 elements tend to adopt trigonal-bipyramidal geometries with the gold and fluorine atoms in apical positions. NBO analyses confirmed the presence of Au→Si,Sn interactions, associated with delocalization energies of 8 and 23 kcal/mol, respectively. AIM calculations have also been performed in this case, and bond critical points with electron densities ρ(r) of 2.1 and 3.6×10^{-2} e bohr^{-3} were found between Au and Si,Sn. All data indicate that tin

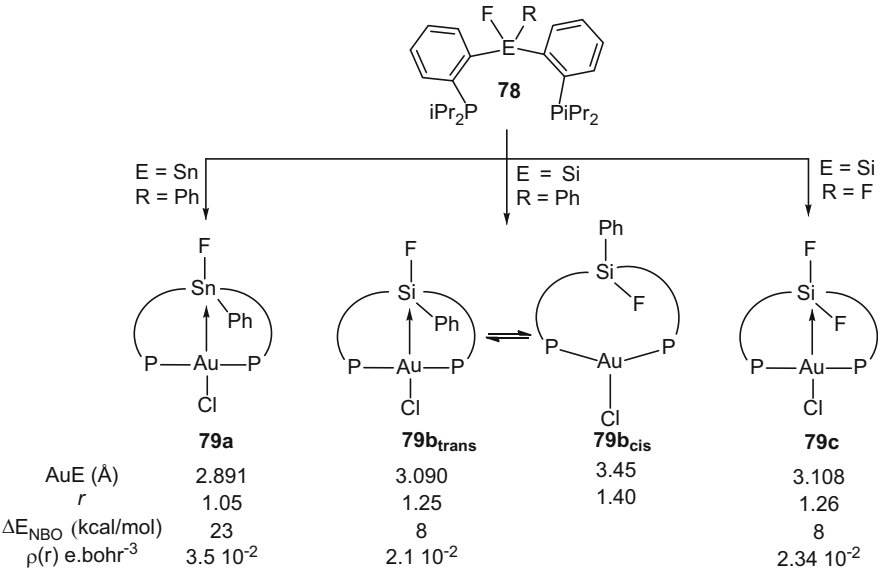

Scheme 23 Au→Si,Sn interactions arising from the coordination of diphosphine silane and stannane ligands

binds more strongly to gold than silicon, in line with the higher Lewis acidity of Sn vs Si compounds.

The nature and the position of the substituents at Si,Sn play an important role and deserve comments. The presence of an electronegative atom such as F (or Cl) at Si, Sn is essential to make the group 14 element Lewis acidic enough (the corresponding $\sigma^*E_{14}F$ orbitals are low in energy and therefore better acceptor). In complexes **79a** and **79b**, the F atom is positioned on an apical site, *trans* to gold, so as to optimize the orbital overlap of the $\sigma^*E_{14}F$ orbitals with the occupied d (Au) orbital. The influence of the position of the F atom is nicely illustrated by the different bonding situations of the two isomeric forms of complex **79b** (the two forms have been characterized by NMR; they slowly exchange at the NMR timescale). Only the one featuring the F *trans* to Au displays significant Au→Si interaction, as clearly apparent from ^{29}Si NMR ($\delta = -21$ vs -4 ppm), geometry optimization ($r = 1.25$ vs 1.40), and NBO analyses.

The approach was then extended to cage complexes. A complete series of triphosphine silane, germane, and stannanes complexes (Fig. 35) were prepared with the group 11 metals (Cu, Ag, and Au) [123]. Structural analyses were systematically performed and DFT calculations were carried out on all compounds. Accordingly, the strength of the central M→E_{14} interaction was found to increase going down in the periodic table (Si < Ge < Sn and Cu < Ag < Au). The stronger interaction is met in the gold stannane complex ($r = 1.08$, $\Delta E_{NBO} = 32$ kcal/mol). At the opposite, complex **80c** displays very weak, if any, Cu→Si interaction

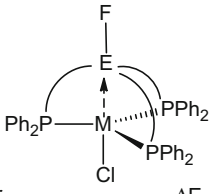

	E		M
80	Si	**a**	Cu
81	Ge	**b**	Ag
82	Sn	**c**	Cu

	r_{ME}			ΔE_{NBO} (kcal/mol)		
	Cu	Ag	Au	Cu	Ag	Au
E = Si	1.43	1.36	1.30	0.1	2	8.5
E =Ge	1.34	1.28	1.23	2	37	16
E = Sn	1.17	1.13	1.08	37	7	32

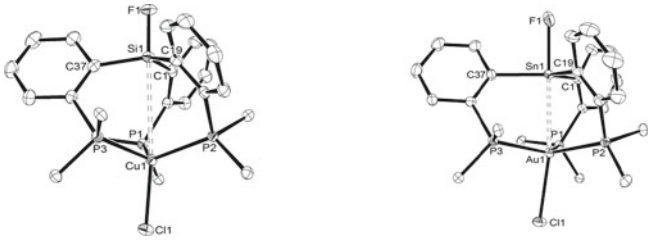

Fig. 35 Cu,Ag,Au→Si,Ge,Sn interactions within triphosphine cage complexes; molecular structures of **80c** and **82a**

($r = 1.43$, $\Delta E_{NBO} < 1$ kcal/mol). Note that in all these complexes, the group 14 element is again substituted by a fluorine atom (which sits *trans* to the metal in the cage complex, by constitution). The energy level of the $\sigma^*E_{14}F$ orbital in the frozen geometry of the complex actually nicely correlates with the strength of the M→E_{14} interaction and the degree of tetrahedral to trigonal-bipyramidal distortion of the group 14 element.

Changing the substituents at P usually does not influence a lot the coordination of ambiphilic ligands, but in the case of the triphosphine silane featuring Ph groups (instead of isopropyl), we observed spontaneous dissociation of the AuCl bond and obtained the trigonal pyramidal cage complex **84** (Scheme 24) [124]. Though cationic, the gold center is engaged in significant Au→Si interaction, as substantiated by NMR, XRD, and computational data (δ ^{29}Si = −28 ppm, $r = 1.20$, $\Delta E_{NBO} = 15$ kcal/mol).

In parallel with our work on M→E_{14} interactions supported by phosphine buttresses, Wagler extended Hill's approach and prepared metallasilatranes as well as metallastannatranes using methimazolyl donor groups (Fig. 36) [125, 126]. (M(I)–Sn(III) and M(0)→Sn(IV) formalisms have also been proposed to describe the bonding situation of pincer-type Pd complexes featuring hexacoordinate tin centers; see [127]). A complete series of lantern-like complexes

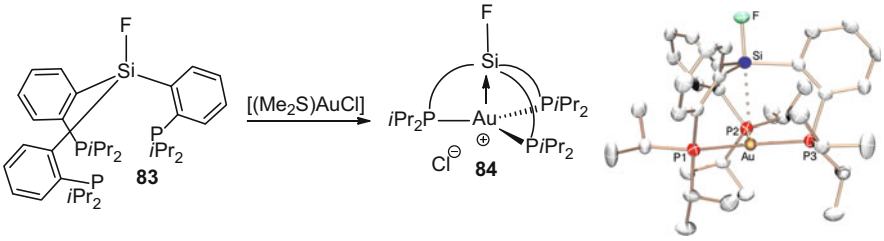

Scheme 24 Coordination of the triphosphine silane **83** to gold, Au→Si interaction in a cationic cage complex

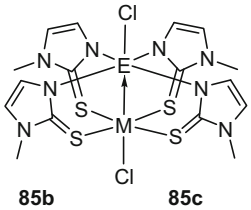

	85a	**85b**	**85c**	**85d**
M	Pd	Ni	Pd	Pt
E	Sn	Si	Si	Si
ME (Å)	2.605	2.598	2.527 to 2.569	2.447 to 2.469
r	0.94	1.10	1.01 to 1.03	0.80 to 0.89
$^{\delta}$ ^{29}Si NMR (ppm)		-188	-180.0 to -183.4	-213.2 to -218.5

Fig. 36 Ni,Pd,Pt→Si,Sn interactions housed by four methimazolyl groups

was reported with group 10 metals (Ni, Pd, and Pt). Structure analyses combine X-ray diffraction, DFT calculations (including NBO), and solid-state ^{29}Si NMR [128, 129].[6] Here, the M→E_{14} interaction is housed in a four-blade paddle wheel structure and does not vary much in strength, whatever the donating group 10 metal and accepting group 14 element ($r = 0.94$–1.00). Two halogen atoms, typically chlorine, occupy the apical positions and the group 14 element sits in an octahedral environment.

3.3 *Unsupported M→E_{14} Interactions*

In the last few years, unsupported M→E_{14} interactions have also been evoked occasionally (Fig. 37). Kawashima reported an anionic iron complex **86** of a spiro-germane [130]. According to SQUID measurements and NBO calculations, compound **86** was best described as a Ge(IV)/Fe(0) complex with a σ(Ge–Fe) bond polarized toward iron (68%).

As reported by Hahn and Grimme, the benzannulated *N*-heterocyclic plumbylene (NHPb) also displays unusual coordination properties upon interaction with M(PPh_3)$_3$ fragments (M = Pd, Pt) (Fig. 37) [131]. The NHPb plane deviates from the Pb–Pd,Pt axis by about $\theta \sim 125°$, suggesting that the coordination arises from M→p(Pb) interaction rather than n(Pb)→M interaction. A series of $E_{14}X_2$ Pt complexes **88a–f** (E_{14} = Ge, Sn, Pd and X = Cl, Br) have then been prepared by Braunschweig and Coll (Fig. 38) [132–134]. According to crystallographic studies, the E_{14} element is in highly pyramidalized environment (sum of bond angles ~ 301–310°), and the E_{14}–Pt axis strongly deviates from the $E_{14}X_2$ plane (by θ 110–116°).

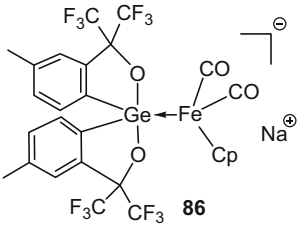

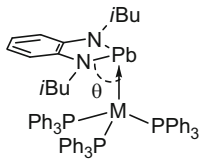

	87a	**87b**
M	Pd	Pt
MP (Å)	2.821	2.856
r	0.99	1.01
ΣPα (°)	310	308
θ (°)	125	124

Fig. 37 Unsupported M→E_{14} interactions in spiro-germane and *N*-heterocyclic plumbylene complexes

[6] The role of relativistic effects and spin-orbit coupling in M→Si interactions has been pointed out and analyzed thoroughly; see [128] and [129].

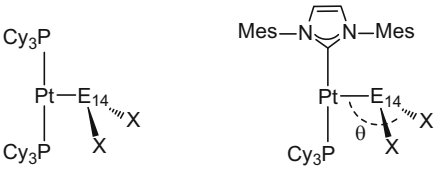

	88a	88b	88c	88d	88e	88f
E_{14}	Ge	Sn	Sn	Pb	Ge	Sn
X	Cl	Cl	Br	Cl	Cl	Cl
ME_{14} (Å)	2.397	2.599	2.605	2.730	2.410	2.595
r	0.94	0.94	0.95	0.97	0.94	0.94
$\Sigma E_{14}\alpha$ (°)	309	304	310	304	307	300
θ (°)	116	114	116	111	114	110

Fig. 38 Unsupported M→E_{14} interactions in germylene, stannylene, and plumbylene Pd,Pt complexes

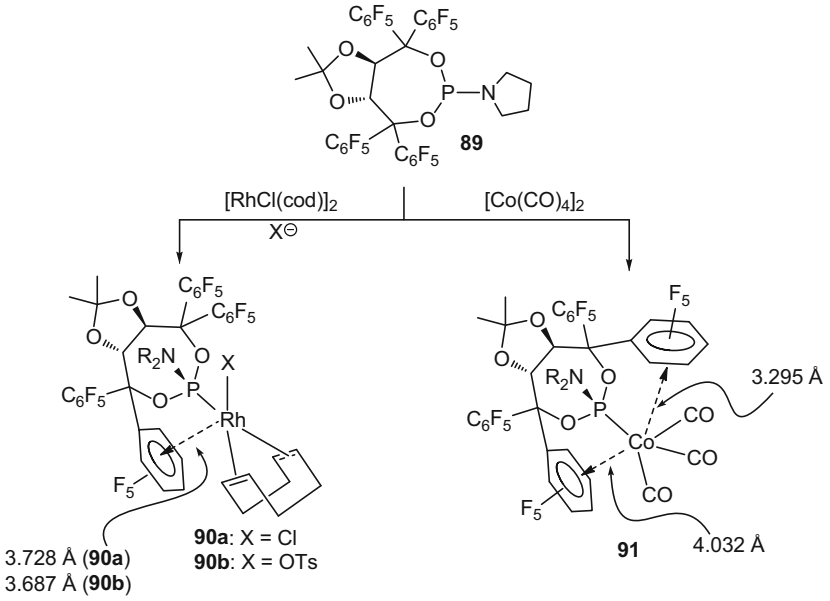

Fig. 39 Ambiphilic behavior of the phosphoramidite ligand **89** toward Rh and Co, associated M···C_6F_5(centroid) distances

Donor–acceptor 5d(Pt)→p(E_{14}) interactions probably play a major role in the bonding of **88a**–**d**, all the more so that the $E_{14}X_2$ moieties are stronger σ-acceptor ligands than NHPb.

Among group 14, M→Z interactions have so far only been substantiated unequivocally for the heavier elements, but nothing precludes carbon compounds to behave as σ-acceptor ligands. In this regard, Rovis recently reported a first hint [135]. The Rh(I) and Co(−I) complexes **90a**,**b** and **91** derived from the C_6F_5-substituted phosphoramidite **89** were prepared (Fig. 39), and unusual short contacts

between one or two C_6F_5 groups and the metal center were observed by X-ray diffraction studies (no such contacts are observed with the related Ph-substituted ligand). Electron-deficient arenes such as C_6F_6 are known to interact with Lewis bases. These interactions are non-covalent but essentially electrostatic in nature. Electrostatic potential maps calculated by DFT suggest similar situations in complexes **90** and **91**, with the metals as electron-rich centers, and ligand **89** was proposed to act as an ambiphilic L,Z ligand. If these M→C_6F_5 interactions induce a flow of electron density from the metal to the ligand, their nature is very different from that of all other M→Z interactions, in which the covalent contribution is important. Note also that the C_6F_5-substituted ligand and associated M→C_6F_5 interactions were found to strongly influence the product and enantioselectivity of the Rh-catalyzed cycloaddition of alkenyl isocyanates with alkynes.

4 Coordination of Heavier Group 15 Elements as Lewis Acids

Compounds of the group 15 elements, in particular amines, pyridines, and phosphines, are widely used as L-type ligands in transition metal chemistry. Comparatively, Z-type coordination is extremely rare, but here also the ability of the heavier elements (Sb and Bi) to form hypervalent species by coordination of Lewis bases was exemplified with electron-rich metal fragments (based on Ni, Pd, Pt, and Au).

Limberg reported in 2012 Bi analogs of our diphosphine borane, silane, and stannane complexes (Scheme 25) [136]. The gold complex **93** adopts distorted square-planar geometry and displays rather short Au···Bi contact (2.998 Å, $r = 1.06$). According to NBO calculations, donation from the lone pair at Bi to Au is weak [ΔE_{NBO} 6s(Bi)→6s(Au) = 5 kcal/mol], and d(Au)→6p (Bi) backdonation prevails ($\Delta E_{NBO} = 12$ kcal/mol) (Fig. 40, left). The diphosphine chlorobismuthine ligand **92** was also coordinated to Pt(II). The ensuing complex **94** adopts square-pyramidal environment, with the two phosphines in *cis* configuration

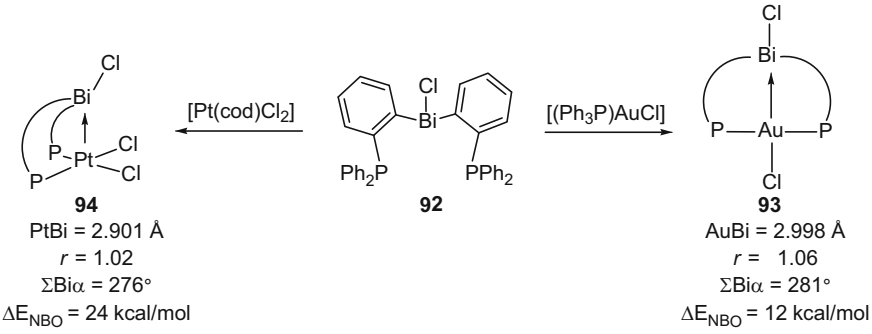

94
PtBi = 2.901 Å
r = 1.02
ΣBiα = 276°
ΔE_{NBO} = 24 kcal/mol

92

93
AuBi = 2.998 Å
r = 1.06
ΣBiα = 281°
ΔE_{NBO} = 12 kcal/mol

Scheme 25 Coordination of a diphosphine chlorobismuthine **92** to Au and Pt

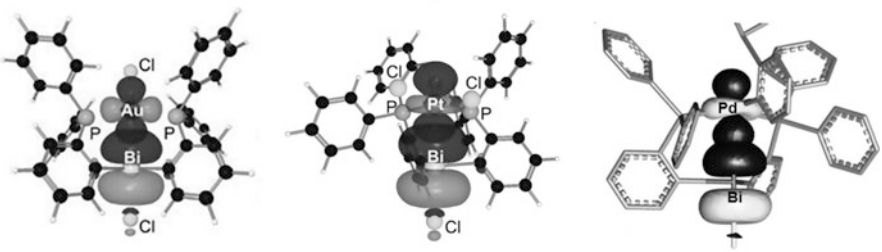

Fig. 40 Superposition of the donor (Au,Pt,Pd-centered) and acceptor (Bi-centered) NBO orbitals accounting for the TM→Bi interaction in **93** (*left*), **94** (*middle*), and **96** (*right*)

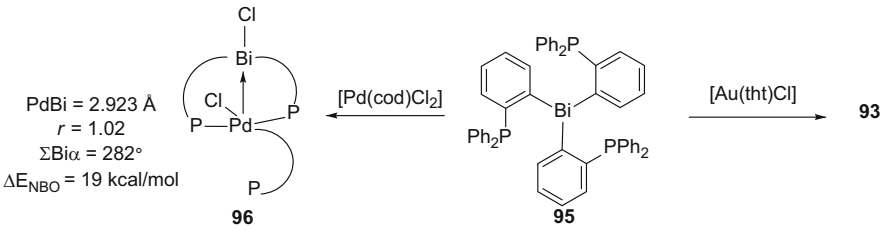

Scheme 26 M→Bi interactions arising from the reaction of a triphosphine bismuthine **95** with Au (I) and Pd(II) chlorides

and the Bi center at the apical position. The Pt···Bi distance is short (2.901 Å, $r = 1.02$) and the chlorine at Bi sits in *trans* position to Pt (the Bi is in seesaw geometry) so that to optimize the overlap between the d_z2(Pt) and σ*(Bi–Cl) orbitals. Coordination of Bi as a Z-type ligand was again supported by DFT, and relatively strong 5d(Pt)→6p(Bi) interaction was found by NBO ($\Delta E_{NBO} = 24$ kcal/mol) (Fig. 40, middle).

Concomitantly, Gabbaï prepared a triphosphine bismuthine **96**. Reaction with gold and palladium chloride precursors led in both cases to chlorobismuthine complexes (Scheme 26) [137]. With gold, one of phosphine arm at Bi was exchanged for Cl, leading to the same complex **93** than that obtained by Limberg (along with the dinuclear [*o*-$Ph_2P(C_6H_4)Au]_2$ complex). With [Pd(cod)Cl_2], the third phosphine arm is transferred to palladium and the original complex **96** is formed. The Pd center sits in a square-pyramidal environment (octahedral if the weak interaction with the third *o*-phenylene phosphine group is considered). In this case, the diphosphine chlorobismuthine is coordinated in a *trans* fashion, but again, the Bi occupies the apical position, with the chlorine atom *trans* to the metal. NBO calculations revealed a bonding situation analogous to that encountered in **93** and **94** complexes, with a relatively strong 4d(Pd)→6p(Bi) interaction ($\Delta E_{NBO} = 19$ kcal/mol) (Fig. 40, right).

Soon after, Gabbaï extended the variety of M→E_{15} interactions to antimony and reported a series of diphosphine and triphosphine–Sb complexes [138]. Gold complexes **97a**,**b** analogous to **93** were prepared, and the influence of the substituent at

Sb (Cl *vs* Ph) was investigated (Fig. 41) [138]. In line with the higher Lewis acidity of Sb vs Bi, antimony binds more strongly to gold in **97a** than bismuth in **93** ($\Delta E_{NBO} = 24$ vs 15 kcal/mol for analogous iPr$_2$P complexes). Replacement of the chlorine at Sb for a phenyl group reduces the Lewis acidity and the Au···Sb distance increases (from 2.794 to 2.867 Å). In the mean time, the 5d(Au)→5p (Sb) interaction weakens ($\Delta E_{NBO} = 9$ kcal/mol) and becomes of same magnitude than 5s(Sb)→6s(Au) donation ($\Delta E_{NBO} = 9$ kcal/mol).

A peculiar and very interesting feature of the stibine complexes is their ability to participate in redox processes, leading to profound change in coordination behavior. Indeed, reaction of complexes **97a**,**b** with *o*-chloranil induced two-electron oxidation of Sb (Scheme 27), which becomes hexacoordinate (octahedral geometry) [138]. This transformation is accompanied by a noticeable shortening of the Au···Sb distance (2.683 Å in **98b**), and now, a covalent σ(Au–Sb) bond strongly polarized toward Sb (84%) is found by NBO/NLMO.

Similar observations were made on gold complexes deriving from the related triphosphine-stibine ligand **99** (Scheme 28) [139]. The third phosphine arms do not

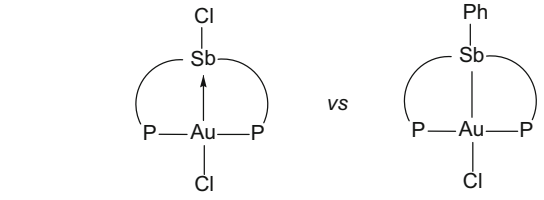

	97a	**97b**
AuSb (Å)	2.794	2.867
r	1.02	1.04
ΣSbα	282°	290°
ΔE_{NBO} (kcal/mol)	24	9

Fig. 41 Au→Sb interactions arising from the coordination diphosphine stibines

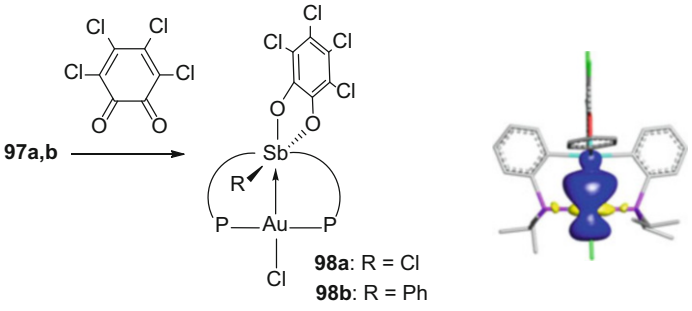

Scheme 27 Two-electron oxidation of the stibine gold complexes **97a**,**b** (*left*), NLMO associated with the Au–Sb interaction in the resulting complex **98b** (*right*)

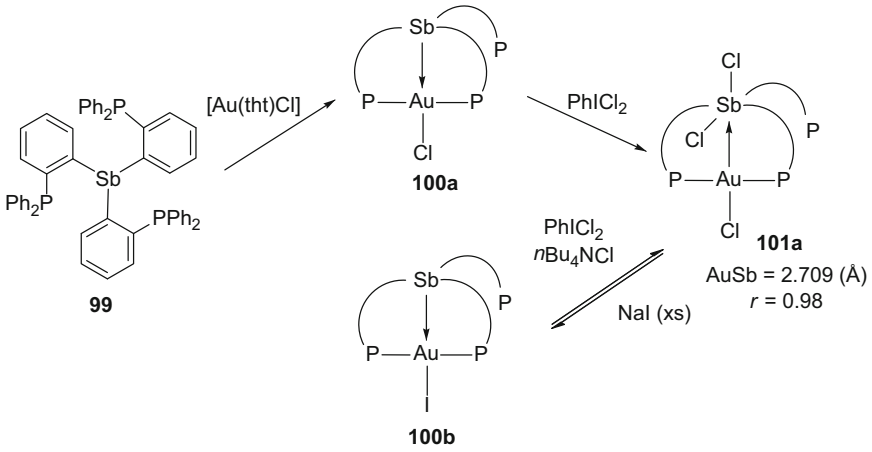

Scheme 28 Reversible two-electron oxidation and reversible *Umpolung* of the stibine gold complexes **100a** and **100b**

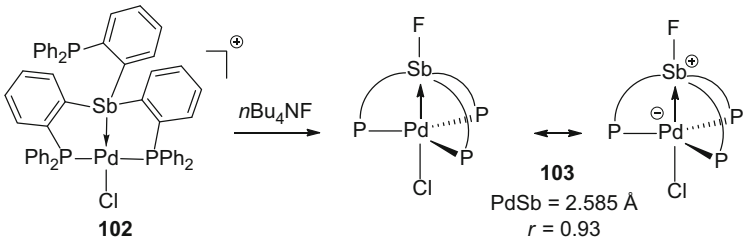

Scheme 29 Diphosphine stibine and fluoride-induced *Umpolung* in Pd–Sb bonding

play a major role in coordination here (it remains pendant in all complexes), but the absence of electronegative substituent at Sb makes the stibine more Lewis basic than Lewis acidic. Accordingly, Sb→Au interaction dominates in complex **100a**. The Sb center is readily oxidized by $PhICl_2$ to give complex **101a** (the Au···Sb distance shortens and Au→Sb interactions now prevail by NBO). Remarkably, the redox process proved to be reversible and complexes **101a** and **100b** could be interconverted using NaI/$PhICl_2$, *n*-Bu_4NCl.

Gabbaï then showed that besides redox processes, the Sb center of stibine complexes can also react with fluoride anions, inducing again formal *Umpolung* in Pd–Sb bonding [140]. Typically, the cationic Pd complex **102** readily reacts with *n*-Bu_4NF to give **103** (Scheme 29). The fluoride binds to Sb and the coordination of antimony changes from tetrahedral to trigonal-bipyramidal. The resulting pentacoordinate Sb compound is best described as a metallastiborane or as stibonium stabilized by Pd→Sb interaction. This fluoride-induced *Umpolung* behavior was also observed with related triphosphine-stibine Pd complexes (the

third phosphine arm remains pendant in the cationic complex **102** but coordinates to Pd in **103**). In the case of Pt complexes, mono and double addition of fluoride to Sb were observed starting from a dicationic triphosphine-stibine isonitrile species [141].

Original diphosphine–Sb Pt complexes were also isolated [142]. Reaction of the diphosphine stibine ligand with $[Pt(SEt_2)_2Cl_2]$ led to complex **105**, with a covalent Pt–Sb bond and formal insertion of Sb into one of the Pt–Cl bond (Scheme 30). Oxidation of Sb with *o*-chloranil followed by Cl to F exchange afforded compound **106**, which is best described as a Pt(II) complex with a stiborane coordinated as a Z-type ligand. This view is supported by NBO calculations: d(Pt)→σ* (Sb) interactions are found for **106** at the second-order perturbation level (sum of delocalization energies $\Delta E_{NBO} = 60$ kcal/mol).

Triphosphine Sb Ni complexes were prepared too (Scheme 31), and L-, X-, and Z-type coordination were authenticated, showing the unique versatility and adaptability of antimony [143]. Complex **107** is a classical stibine complex (NBO shows a lp(Sb)→Ni interaction with $\Delta E_{NBO} = 53$ kcal/mol), both Ni and Sb being in distorted tetrahedral environments. Two-electron oxidation with $PhICl_2$ gives **108** (additions of the chlorine atoms to Sb and Ni). The complex adopts a three-blade paddle wheel structure with a central covalent Ni–Sb bond (X-type behavior of the Sb fragment) polarized toward Ni (58%). Treatment of **108** with catechol, triethylamine, and cyclohexylisonitrile afforded complex **109**. CyNC coordinates

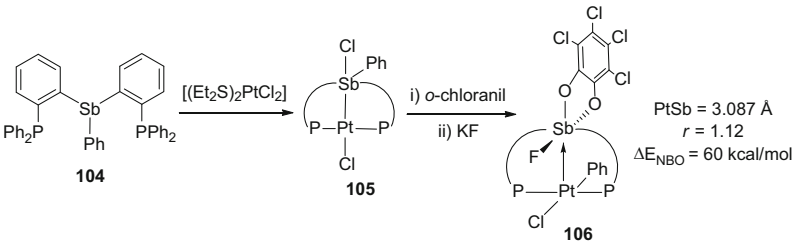

Scheme 30 Preparation of diphosphine–Sb Pt complexes

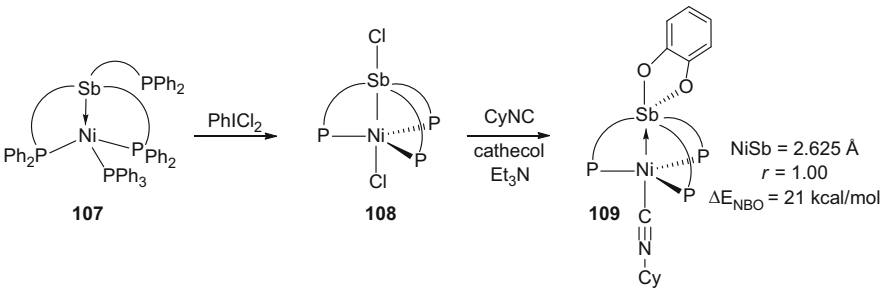

Scheme 31 L-, X-, and Z-type coordination of antimony in triphosphine–Sb Ni complexes

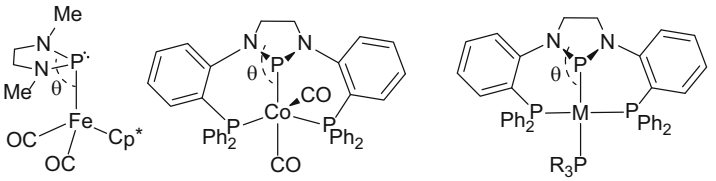

	110	**111**	**112a**	**112b**	**112c**
M	Fe	Co	Pd	Pt	Pt
R	/	/	Me	Me	Ph
MP (Å)	2.340 Å	2.239 Å	2.253	2.261	2.260
r	0.98	0.96	0.91	0.93	0.93
ΣPα (°)	313	303	326	324	319
θ (°)	119°	114°	131	143	126

Fig. 42 Phosphenium complexes with pyramidal P centers, unsupported and supported M→P^+ interactions

Ni *trans* to Sb, while the catecholate has displaced the two chlorine atoms and is bonded to Sb. This results in an hexacoordinate Sb center, a square-pyramidal stiborane moiety coordinating to Ni as a Z-type ligand. This bonding picture is corroborated by NBO analyses which show donor–acceptor 3d(Ni)→σ*(Sb) and 3d (Ni)→5p (Sb) interactions (sum of delocalization energies $\Delta E_{NBO} = 21$ kcal/mol).

The possible involvement of M→Z interactions in phosphenium (>P^+) complexes featuring pyramidal P centers has also been invoked [144]. Such a situation was first reported by Paine in the iron complex **110** (Fig. 42) [145]. As for the NHPb complexes **87**, the metal strongly deviates from the NHP^+ ring (by $\theta = 119°$), and the phosphenium was proposed to act as an electron-acceptor ligand via its 3p (P) empty orbital. In addition, Thomas recently investigated the coordination of tridentate ligands featuring a central NHP^+ moiety and two phosphine sidearms [146, 147]. In the ensuing Co and Pd/Pt complexes **111** and **112a–c** (Fig. 42), the M–P^+ axis deviates from the NHP^+ plane by θ 114–131°. However, NBO studies rather identify covalent M–P bonds with about the same contributions of the metal and phosphorus atoms. This supports strong electron transfer from M to P and thus significant contribution to the bonding of the phosphido form with formal two-electron oxidation of the metal (see the conclusion for a discussion of the bonding situation).[7]

[7] The geometry around P in phosphenium complexes can be trigonal planar or pyramidal. Planar phosphenium complexes feature MP bonds with double-bond character and can be assimilated to Fischer/Schrock-type carbene complexes. Pyramidal phosphenium complexes feature single MP bonds with a stereochemical active lone pair at P. Their bonding situation can correspond to phosphenium Z-type complexes or phosphido complexes without π(P→M) donation. The difference between the two resides in the nature of the σ interaction/bond between P and M.

5 Coordination of Heavier Group 16 Elements as Lewis Acids

5.1 $M \rightarrow SO_2$ Complexes

As mentioned in the introduction, SO_2 complexes were among the first TM→LA species to be unequivocally authenticated [4]. Compared with other Lewis acid ligands, SO_2 is remarkable in that it features ambiphilic character, and *S*-coordination can be associated with either L- and Z-type behavior (Fig. 43). This aspect has been discussed in detail in our previous review on Z-type ligands [12], and the coordination properties of SO_2 have been discussed in several reviews [148–150]. Only key aspects and selected examples will thus be recalled here.

The coordination of SO_2 as L- or Z-type ligand to transition metals is schematically depicted in Fig. 43 [12]. It results from the electronic structure of SO_2, which features a lone pair at S (in the SO_2 plane) and a low-energy allyl-type LUMO centered at S. This gives SO_2 the possibility to adapt its coordination mode to the metal fragment, and Z-type behavior is typically met with electron-rich d^8 and d^{10} systems (representative examples are depicted in Fig. 44). The coordination mode of SO_2 is easily tracked by the geometry around S. L-type coordination proceeds in the plane of SO_2 and thus S retains its planar geometry. In contrast, Z-type coordination involves the 3p(S) orbital and induces pyramidalization of the S environment as a result of $sp^2 \rightarrow sp^3$ rehybridization. The author is invited to refer to recent reviews by Mingos for general discussions on ambivalent/ambiphilic

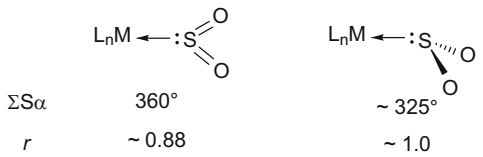

Fig. 43 L- and Z-type coordination of SO_2, main associated features

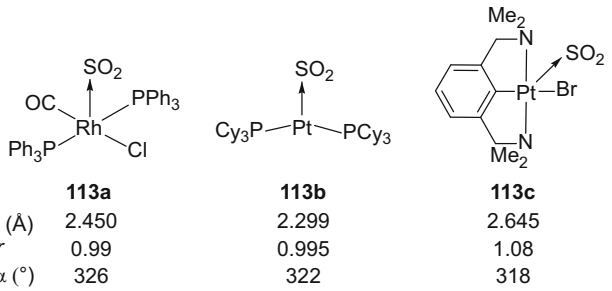

	113a	113b	113c
MS (Å)	2.450	2.299	2.645
r	0.99	0.995	1.08
ΣSα (°)	326	322	318

Fig. 44 Selected examples of Z-type SO_2 complexes

ligands with such symmetry signatures [151, 152] (for a recent comprehensive theoretical study of SO_2 complexes, see [153]). Several other features are characteristic and diagnostic of the coordination mode of SO_2. In particular, M···SO_2 distances are usually shorter for L-type vs Z-type complexes (*r* increases from ~0.88 to ~1.0). Infrared (IR) spectroscopy is also informative, when X-ray data are not available. Z-type complexes usually display lower frequency SO stretching modes, ν_s and ν_{as} appearing around 1040 and 1200 cm^{-1}, respectively. M→SO_2 interactions are also generally weaker than M←SO_2 interactions, and the binding of SO_2 as Z-type ligand is actually often reversible, a property of interest for gas detection applications (Pt NCN pincer complexes display remarkable properties for that) [154].

5.2 *Complexes with M→Te Interactions Supported by Phosphine Sidearms*

The chelation approach developed extensively with Z-type ligands based on the group 13–15 elements has also been applied to a heavier group 16 element, namely, tellurium. Accordingly, a few complexes have been reported to feature telluronium moieties (TeR_3^+) coordinated as Z-type ligands to group 10 metals (Pd,Pt).

The first such complex was prepared from the diphosphine telluroether ligand **114** (Scheme 32) [155]. Reaction with $[PtCl_2(SEt_2)_2]$ gives the cationic complex **115** (analogous to the Sb/Pd complex **102**). Oxidation with $PhICl_2$ then affords the neutral species **116** in which Pt is hexacoordinate with the two phosphines in *cis* arrangement. The Te center is four-coordinate and adopts seesaw geometry with Cl in *trans* position to Pt. The Pt···Te distance slightly elongates from **115** to **116** (from 2.528 to 2.635 Å), while the contribution of Te in the associated NLMO increases from 39% to 63%. This *Umpolung* of the Pt–Te interaction is reminiscent of those observed in Sb complexes and can be formally associated with a change from L/X- to Z-type coordination of tellurium. Another interesting feature of

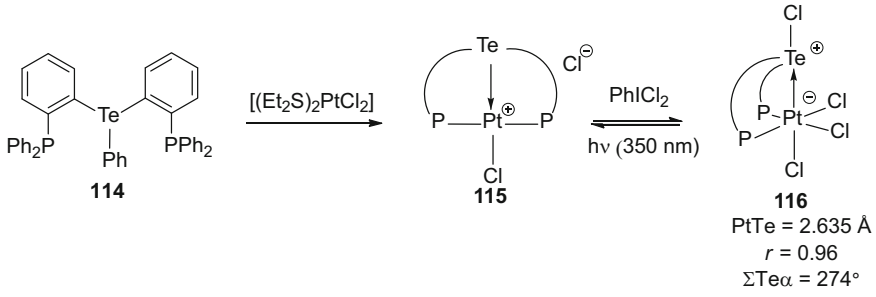

Scheme 32 Preparation of diphosphine-Te Pt complexes

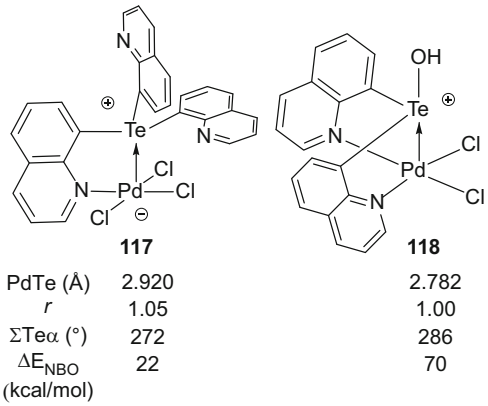

Fig. 45 Quinoline complexes featuring Pd→Te^+ interactions

complex **116** is its ability to reductively eliminate Cl_2 and gives back **115** under UV irradiation (λ 350 nm) in the presence of a radical trap.

In another study, Gabbaï employed quinoline as donor buttress and prepared the Pd telluronium complexes **117** and **118** (Fig. 45) [156]. Here, Pd→Te interaction is supported by one or two quinoline moieties. In both complexes, the Te center adopts distorted seesaw geometry with a quinoline or the hydroxy group about *trans* to Pd. The Pd center is in square-pyramidal geometry, with Te at the apical position. NBO analyses support the description of complexes **117** and **118** as Pd(II) species with telluroniums coordinated as Z-type ligands [significant d(Pd)→σ*(Te–X) interactions are identified, $\Delta E_{NBO} = 22$ and 70 kcal/mol].

6 Conclusion

Since the early 2000s, studies on TM→LA interactions have flourished and the concept of Z-type ligands has progressed spectacularly. The coordination of Lewis acids to transition metals is no longer considered as a chemical curiosity, and over 200 complexes featuring M→Z interactions have been characterized crystallographically. Polyfunctional chelating ligands with preformed or in situ generated Lewis acid moieties have played a major role in this field. They enable to control the way Lewis acids interact with metal fragments.

Limited to a few complexes involving simple Lewis acids and unsupported M→Z interactions until the 1990s, the scope of TM→LA complexes has been greatly enlarged and now includes a broad variety of Lewis acids (based on all the group 13 elements B, Al, Ga, In but also on the heavier group 14–16 elements) and transition metals (all group 8–11 metals).

Our knowledge on the nature and magnitude of M→Z interactions has considerably advanced, and the influence of different parameters (nature of the transition

metal and of the Lewis acid, topology of the complex, etc.) has been delineated. Descriptors enabling to substantiate the presence of M→Z interactions and to compare them have also been identified. This includes spectroscopic data, in particular NMR chemical shifts (for B, Si, Sn-based Lewis acids) and geometric features derived from X-ray diffraction analyses (the distance between M and Z, in its normalized value *r*, and the geometry around the Lewis acid). Considerable insight can also be gained computationally. DFT methods have proved to accurately and efficiently describe M→Z complexes. The optimized geometries usually match nicely those determined crystallographically and can be used as a predictive tool (when suitable crystals are not accessible). In addition, Molecular Orbital and Natural Bond Orbital analyses shed light into the bonding situation. Donor–acceptor M→Z interactions are commonly identified by NBO, and the corresponding delocalization energy provides a measure of their strength. When atoms-in-molecules analyses locate bond critical points between M and Z, the corresponding electron density is also a useful probe. In addition, the degree of TM to LA electron transfer can be estimated by computing and comparing the charge distributions in LA-bonded and LA-free complexes.

The preparation and characterization of a large number of TM→LA complexes has stimulated intense, sometimes contradictory, discussions about the very nature and best description of M→Z interactions.[8] Most representative of this debate are the two papers published back-to-back by Hill and Parkin in 2006 [157, 158], proposing two different formalisms for metal borane complexes (Fig. 46). One corresponds to a metal fragment interacting with a borane without strongly perturbing the nominal TM and LA fragments, while the other corresponds to a different fragmentation, with transfer of two-electron from M to B and thus 2e oxidation of the metal center. At this point, it is important to note that these two forms are extreme bonding situations related to different extents of electron transfer from the metal atom to the boron center. The bonding in TM→LA complexes must really be considered as a continuum between these two limit situations. The position of a given complex in this continuum depends on the magnitude of the M→B interaction and of the associated electron transfer. Note that the electronegativities of the involved elements also come into play here and impact the degree of M→Z electron transfer (for a discussion on the difficulty and ambiguity of assigning oxidation states in complexes featuring TM and ligating atoms of similar electronegativities, see [160]).

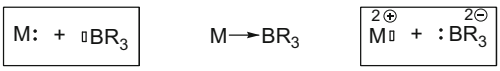

Fig. 46 Limit description for M→BR_3 complexes, extreme situation for a bonding continuum

[8] For discussions on the description of M→Z complexes, see [101] and [157–159].

The bonding in TM→LA complexes and the degree of electron transfer can be analyzed computationally via MO, NBO, and AIM calculations. Decomposition analyses also provide a useful method to identify the best fragmentation for TM→LA complexes and to assess the interaction between the fragments. Accordingly, the best description of TM→LA complexes corresponds to the lowest energy interaction (concept of minimum-energy rupture) [161] among the different conceivable fragmentations (two electrons on the TM, two electrons on the LA, or one electron on each).

It is important to stress here the difference that may exist between the nature of the TM→LA bond and the way it is generated (the two shared electrons do not remind where they are coming from). The coordination of Lewis acids is generally associated with weak interactions and small electron transfers. But it is not necessarily the case, and one should keep in mind that the classification of a complex as a M→Z species refers to its bonding not to the way it is prepared. Think about the reaction of a proton (the simplest Lewis acid) with a metal fragment leading to an hydride complex. This is an obvious case in which a Lewis acid (a nominal Z-type fragment) is converted into an X-type ligand upon coordination.

Most of the Lewis acid complexes discussed in this chapter feature relatively weak M→Z interactions compared to M-X and L→M interactions, with small electron transfer from M to Z. In our opinion, the M→Z formalism should be reserved to such complexes for which the best description is that of a weak donor–acceptor interaction between the nominal M and Z fragments.

Besides the fundamental interest associated with the structure and bonding of TM→LA complexes, the coordination of σ-acceptor ligands offers new interesting perspectives in reactivity. In particular, the presence of Lewis acids at transition metals opens new reaction pathway involving both the metal and the σ-acceptor ligand. The first results obtained in this area have been recently reviewed [107, 162].

Despite the spectacular progress achieved over the last 15 years, the study of Z-type ligands clearly remains in its infancy. It makes no doubt that the field will continue to develop. The variety and bonding analysis of M→Z interactions will further progress, and catalytic applications based on the cooperative activation of strong bonds with TM→LA complexes will certainly raise.

References

1. Shriver DF (1970) Acc Chem Res 3:231–238
2. Pearson RG (1985) Chem Rev 85:41–49
3. Angelici RJ (1995) Acc Chem Res 28:51–60
4. King RB (1967) Adv Chem Ser 62:203–220
5. Green MLH (1995) J Organomet Chem 500:127–148
6. Burlitch JM, Leonowicz ME, Petersen RB, Hughes RE (1979) Inorg Chem 18:1097–1105
7. Muir KW, Ibers JA (1969) Inorg Chem 8:1921–1928
8. Hill AF, Owen GR, White AJP, Williams DJ (1999) Angew Chem Int Ed 38:2759–2761

9. Kuzu I, Krummenacher I, Meyer J, Armbruster F, Breher F (2008) Dalton Trans 5836–5865
10. Fontaine FG, Boudreau J, Thibault MH (2008) Eur J Inorg Chem 2008:5439–5454
11. Bouhadir G, Amgoune A, Bourissou D (2010) Adv Organomet Chem 58:1–106
12. Amgoune A, Bourissou D (2011) Chem Commun 47:859–871
13. Braunschweig H, Dewhurst RD, Schneider A (2010) Chem Rev 110:3924–3957
14. Braunschweig H, Dewhurst RD (2011) Dalton Trans 40:549–558
15. Owen GR (2012) Chem Soc Rev 41:3535–3546
16. Amgoune A, Bouhadir G, Bourissou D (2013) Top Curr Chem 334:281–311
17. Kameo H, Nakazawa H (2013) Chem Asian J 8:1720–1734
18. Pandey KK (2009) Coord Chem Rev 253:37–55
19. Emslie DJH, Cowie BE, Kolpin KB (2012) Dalton Trans 41:1101–1117
20. Bauer J, Braunschweig H, Dewhurst RD (2012) Chem Rev 112:4329–4346
21. Braunschweig H, Gruss K, Radacki K (2007) Angew Chem Int Ed 46:7782–7784
22. Braunschweig H, Gruss K, Radacki K (2008) Inorg Chem 47:8595–8597
23. Bauer J, Braunschweig H, Brenner P, Kraft K, Radacki K, Schwab K (2010) Chem Eur J 16:11985–11992
24. Bauer J, Braunschweig H, Damme A, Gruss K, Radacki K (2011) Chem Commun 47:12783–12785
25. Bauer J, Bertermann R, Braunschweig H, Gruss K, Hupp F, Kramer T (2012) Inorg Chem 51:5617–5626
26. Goedecke C, Hillebrecht P, Uhlemann T, Haunschild R, Frenking G (2009) Can J Chem 87:1470–1479
27. Braunschweig H, Dewhurst RD, Hupp F, Kaufmann C, Phukan AK, Schneider C, Ye Q (2014) Chem Sci 5:4099–4104
28. Bauer J, Braunschweig H, Radacki K (2012) Chem Commun 48:10407–10409
29. Shriver DF (1963) J Am Chem Soc 85:3509–3510
30. Johnson MP, Shriver DF (1966) J Am Chem Soc 88:301–304
31. Scott RN, Shriver DF, Vaska L (1968) J Am Chem Soc 90:1079–1080
32. Lehman DD, Shriver DF (1974) Inorg Chem 13:2203–2207
33. Parshall GW (1964) J Am Chem Soc 86:361–364
34. Braunschweig H, Wagner T (1994) Chem Ber 127:1613–1614
35. Braunschweig H (1998) Angew Chem Int Ed 37:1786–1801
36. Bauer J, Braunschweig H, Dewhurst RD, Radacki K (2013) Chem Eur J 19:8797–8805
37. Braunschweig H, Radacki K, Rais D, Seeler F (2004) Organometallics 23:5545–5549
38. Braunschweig H, Brenner P, Müller A, Radacki K, Rais D, Uttinger K (2007) Chem Eur J 13:7171–7176
39. Bauer J, Braunschweig H, Kraft K, Radacki K (2011) Angew Chem Int Ed 50:10457–10460
40. Braunschweig H, Fuss M, Radacki K, Uttinger K (2009) Z Anorg Allg Chem 635:208–210
41. Kameo H, Sakaki S (2015) Chem Eur J 21:13588–13597
42. Foreman MRS, Hill AF, Owen GR, White AJP, Williams DJ (2003) Organometallics 22:4446–4450
43. Rudolf GC, Hamilton A, Orpen AG, Owen GR (2009) Chem Commun 553–555
44. Crossley IR, Foreman MRS, Hill AF, Owen GR, White AJP, Williams DJ, Willis AC (2008) Organometallics 27:381–386
45. Foreman MRS, Hill AF, White P, Williams DJ (2004) Organometallics 23:913–916
46. Figueroa JS, Melnick JG, Parkin G (2006) Inorg Chem 45:7056–7058
47. Crossley IR, Foreman MRS, Hill AF, White AJP, Williams DJ (2005) Chem Commun 221–223
48. Crossley IR, Hill AF, Willis AC (2006) Organometallics 25:289–299
49. Crossley IR, Hill AF, Humphrey ER, Willis AC (2005) Organometallics 24:4083–4086
50. Landry VK, Melnick JG, Buccella D, Pang K, Ulichny JC, Parkin G (2006) Inorg Chem 45:2588–2597

51. Lopez-Gomez MJ, Connelly NG, Haddow MF, Hamilton A, Orpen AG (2010) Dalton Trans 39:5221–5230
52. Mihalcik DJ, White JL, Tanski JM, Zakharov LN, Yap GPA, Incarvito CD, Rheingold AL, Rabinovich D (2004) Dalton Trans 1626–1634
53. Crossley IR, Hill AF (2004) Organometallics 23:5656–5658
54. Crossley IR, Hill AF, Willis AC (2008) Organometallics 27:312–315
55. Crossley IR, Hill AF (2008) Dalton Trans 201–203
56. Pang K, Quan SM, Parkin G (2006) Chem Commun 5015–5017
57. Senda S, Ohki Y, Hirayama T, Toda D, Chen JL, Matsumoto T, Kawaguchi H, Tatsumi K (2006) Inorg Chem 45:9914–9925
58. Pang K, Tanski JM, Parkin G (2008) Chem Commun 1008–1010
59. Crossley IR, Hill AF, Willis AC (2005) Organometallics 24:1062–1064
60. Crossley IR, Hill AF, Willis AC (2010) Organometallics 29:326–336
61. Blagg RJ, Charmant JPH, Connelly NG, Haddow MF, Orpen AG (2006) Chem Commun 2350–2352
62. Blagg RJ, Adams CJ, Charmant JPH, Connelly NG, Haddow MF, Hamilton A, Knight J, Orpen AG, Ridgway BM (2009) Dalton Trans 8724–8736
63. Owen GR, Hugh G, Charmant JPH, Hamilton A, Saithong S (2010) Dalton Trans 39:392–400
64. Owen GR, Gould PH, Hamilton A, Tsoureas N (2010) Dalton Trans 39:49–52
65. Zech A, Haddow MF, Othman H, Owen GR (2012) Organometallics 31:6753–6760
66. Dyson G, Zech A, Rawe BW, Haddow MF, Hamilton A, Owen GR (2011) Organometallics 30:5844–5850
67. Nuss G, Saischek G, Harum BN, Volpe M, Gatterer K, Belaj F, Mösch-Zanetti NC (2011) Inorg Chem 50:1991–2001
68. Nuss G, Saischek G, Harum BN, Volpe M, Belaj F, Mösch-Zanetti NC (2011) Inorg Chem 50:12632–12640
69. Anju RS, Roy DK, Mondal B, Yuvaraj K, Arivazhagan C, Saha K, Varghese B, Ghosh S (2014) Angew Chem Int Ed 53:2873–2877
70. Roy DK, Mondal B, Anju RS, Ghosh S (2015) Chem Eur J 21:3640–3648
71. Roy DK, De A, Panda S, Varghese B, Ghosh S (2015) Chem Eur J 21:13732–13738
72. Tsoureas N, Haddow MF, Hamilton A, Owen GR (2009) Chem Commun 2538–2540
73. Tsoureas N, Hamilton A, Haddow MF, Harvey JN, Orpen AG, Owen GR (2013) Organometallics 32:2840–2856
74. Tsoureas N, Bevis T, Butts CP, Hamilton A, Owen GR (2009) Organometallics 28:5222–5232
75. Bontemps S, Bouhadir G, Gu W, Mercy M, Chen CH, Foxman B, Maron L, Ozerov O, Bourissou D (2008) Angew Chem Int Ed 47:1481–1484
76. Sircoglou M, Bontemps S, Bouhadir G, Saffon N, Miqueu K, Gu W, Mercy M, Chen CH, Foxman BM, Maron L, Ozerov OV, Bourissou D (2008) J Am Chem Soc 130:16729–16738
77. Sircoglou M, Saffon N, Miqueu K, Bouhadir G, Bourissou D (2013) Organometallics 32:6780–6784
78. Sircoglou M, Mercy M, Saffon N, Coppel Y, Bouhadir G, Maron L, Bourissou D (2009) Angew Chem Int Ed 48:3454–3457
79. Derrah EJ, Sircoglou M, Mercy M, Ladeira S, Bouhadir G, Miqueu K, Maron L, Bourissou D (2011) Organometallics 30:657–660
80. Kameo H, Hashimoto Y, Nakazawa H (2012) Organometallics 31:3155–3162
81. Kameo H, Hashimoto Y, Nakazawa H (2012) Organometallics 31:4251–4258
82. Moret ME, Peters JC (2011) Angew Chem Int Ed 50:2063–2067
83. Moret ME, Peters JC (2011) J Am Chem Soc 133:18118–18121
84. Fong H, Moret ME, Lee Y, Peters JC (2013) Organometallics 32:3053–3062
85. Anderson JS, Moret ME, Peters JC (2013) J Am Chem Soc 135:534–537
86. Anderson JS, Cutsail GE, Rittle J, Connor BA, Gunderson WA, Zhang L, Hoffman BM, Peters JC (2015) J Am Chem Soc 137:7803–7809

87. Comba P, Schiek W (2003) Coord Chem Rev 238–239:21–29
88. Broda H, Tuczek F (2014) Angew Chem Int Ed 53:632–634
89. Anderson JS, Rittle J, Peters JC (2013) Nature 501:84–87
90. Suess DLM, Tsay C, Peters JC (2012) J Am Chem Soc 134:14158–14164
91. Gunderson WA, Suess DLM, Fong H, Wang X, Hoffmann CM, Cutsail GE III, Peters JC, Hoffman BM (2014) J Am Chem Soc 136:14998–15009
92. Del Castillo TJ, Thompson NB, Suess DLM, Ung G, Peters JC (2015) Inorg Chem 54:9256–9262
93. Moret ME, Zhang L, Peters JC (2013) J Am Chem Soc 135:3792–3795
94. Rudd PA, Liu S, Gagliardi L, Young VG, Lu CC (2011) J Am Chem Soc 133:2072
95. Rudd PA, Planas N, Bill E, Gagliardi L, Lu CC (2013) Eur J Inorg Chem 2013:3898–3906
96. Cammarota RC, Lu CC (2015) J Am Chem Soc 137:12486–12489
97. Bontemps S, Gornitzka H, Bouhadir G, Miqueu K, Bourissou D (2006) Angew Chem Int Ed 45:1611–1614
98. Bontemps S, Sircoglou M, Bouhadir G, Puschmann H, Howard JAK, Dyer PW, Miqueu K, Bourissou D (2008) Chem Eur J 14:731–740
99. Conifer CM, Law DJ, Sunley GJ, White AJP, Britovsek GJP (2011) Organometallics 30:4060–4066
100. Kameo H, Nakazawa H (2012) Organometallics 31:7476–7484
101. Sircoglou M, Bontemps S, Mercy M, Saffon N, Takahashi M, Bouhadir G, Maron L, Bourissou D (2007) Angew Chem Int Ed 46:8583–8586
102. Inagaki F, Matsumoto C, Okada Y, Maruyama N, Mukai C (2015) Angew Chem Int Ed 54:818–822
103. Sircoglou M, Bouhadir G, Saffon N, Miqueu K, Bourissou D (2008) Organometallics 27:1675–1678
104. Sircoglou M, Bontemps S, Mercy M, Miqueu K, Ladeira S, Saffon N, Maron L, Bouhadir G, Bourissou D (2010) Inorg Chem 49:3983–3990
105. Harman WH, Peters JC (2012) J Am Chem Soc 134:5080–5082
106. Harman WH, Lin TP, Peters JC (2014) Angew Chem Int Ed 53:1081–1086
107. Devillard M, Bouhadir G, Bourissou D (2015) Angew Chem Int Ed 54:730–732
108. Schindler T, Lux M, Peters M, Scharf LT, Osseili H, Maron L, Tauchert ME (2015) Organometallics 34:1978–1984
109. Suess DLM, Peters JC (2013) J Am Chem Soc 135:4938–4941
110. Nesbit MA, Suess DLM, Peters JC (2015) Organometallics 34:4741–4752
111. Suess DLM, Peters JC (2013) J Am Chem Soc 135:12580–12583
112. Cowie BE, Emslie DJH (2014) Chem Eur J 20:16899–16912
113. Cowie BE, Tsao FA, Emslie DJH (2015) Angew Chem Int Ed 54:2165–2169
114. Bontemps S, Bouhadir G, Miqueu K, Bourissou D (2006) J Am Chem Soc 128:12056–12057
115. Barnett BR, Moore CE, Rheingold AL, Figueroa JS (2014) J Am Chem Soc 136:10262–10265
116. Devillard M, Nicolas E, Ehlers AW, Backs J, Mallet-Ladeira S, Bouhadir G, Slootweg JC, Uhl W, Bourissou D (2015) Chem Eur J 21:74–79
117. Devillard M, Nicolas E, Appelt C, Backs J, Mallet-Ladeira S, Bouhadir G, Slootweg JC, Uhl W, Bourissou D (2014) Chem Commun 50:14805–14808
118. Grobe J, Krummen N, Wehmschulte R, Krebs B, Laege M (1994) Z Anorg Allg Chem 620:1645–1658
119. Grobe J, Wehmschulte R, Krebs B, Laege M (1995) Z Anorg Allg Chem 621:583–596
120. Grobe J, Lutke-Brochtrup K, Krebs B, Lage M (2007) Z Naturforsch 62b:55–65
121. Gualco P, Lin TP, Sircoglou M, Mercy M, Ladeira S, Bouhadir G, Perez LM, Amgoune A, Maron L, Gabbai FP, Bourissou D (2009) Angew Chem Int Ed 48:9892–9895
122. Gualco P, Mercy M, Ladeira S, Coppel Y, Maron L, Amgoune A, Bourissou D (2010) Chem Eur J 16:10808–10817

123. Kameo H, Kawamoto T, Bourissou D, Sakaki S, Nakazawa H (2015) Organometallics 34:1440–1448
124. Gualco P, Mallet-Ladeira S, Kameo H, Nakazawa H, Mercy M, Maron L, Amgoune A, Bourissou D (2015) Organometallics 34:1449–1453
125. Wagler J, Brendler E (2010) Angew Chem Int Ed 49:624–627
126. Wagler J, Hill AF, Heine T (2008) Eur J Inorg Chem 4225–4229
127. Brendler E, Wächtler E, Heine T, Zhechkov L, Langer T, Pöttgen R, Hill AF, Wagler J (2011) Angew Chem Int Ed 50:4696–4700
128. Truflandier LA, Brendler E, Wagler J, Autschbach J (2011) Angew Chem Int Ed 50:255–259
129. Autschbach J, Sutter K, Truflandier LA, Brendler E, Wagler J (2012) Chem Eur J 18:12803–12813
130. Kano N, Yoshinari N, Shibata Y, Miyachi M, Kawashima T, Enomoto M, Okazawa A, Kojima N, Guo JD, Nagase S (2012) Organometallics 31:8059–8062
131. Heitmann D, Pape T, Hepp A, Mück-Lichtenfeld C, Grimme S, Hahn FE (2011) J Am Chem Soc 133:11118–11120
132. Braunschweig H, Damme A, Dewhurst RD, Hupp F, Jimenez-Halla JO, Radacki K (2012) Chem Commun 48:10410–10412
133. Hupp F, Ma M, Kroll F, Jimenez-Halla JO, Dewhurst RD, Radacki K, Stasch A, Jones C, Braunschweig H (2014) Chem Eur J 20:16888–16898
134. Braunschweig H, Celik MA, Dewhurst RD, Heid M, Hupp F, Sen SS (2015) Chem Sci 6:425–435
135. Dalton DM, Rappe AK, Rovis T (2013) Chem Sci 4:2062–2070
136. Tschersich C, Limberg C, Roggan S, Herwig C, Ernsting N, Kovalenko S, Mebs S (2012) Angew Chem Int Ed 51:4989–4992
137. Lin TP, Ke IS, Gabbaï FP (2012) Angew Chem Int Ed 51:4985–4988
138. Ke IS, Gabbaï FP (2013) Inorg Chem 52:7145–7151
139. Wade CR, Gabbaï FP (2011) Angew Chem Int Ed 50:7369–7372
140. Wade CR, Ke IS, Gabbai FP (2012) Angew Chem Int Ed 51:478–481
141. Jones JS, Wade CR, Gabbaï FP (2015) Organometallics 34:2647–2654
142. Ke IS, Jones JS, Gabbaï FP (2014) Angew Chem Int Ed 53:2633–2637
143. Jones JS, Wade CR, Gabbaï FP (2014) Angew Chem Int Ed 53:8876–8879
144. Rosenberg L (2012) Coord Chem Rev 256:606–626
145. Hutchins LD, Duesler EN, Paine RT (1982) Organometallics 1:1254–1256
146. Pan B, Xu Z, Bezpalko MW, Foxman BM, Thomas CM (2012) Inorg Chem 51:4170–4179
147. Pan B, Bezpalko MW, Foxman BM, Thomas CM (2011) Organometallics 30:5560–5563
148. Mingos DMP (1978) Transit Met Chem 3:1–15
149. Ryan RR, Kubas GJ, Moody DC, Eller PG (1981) Struct Bond 46:47–100
150. Hill AF (1994) Adv Organomet Chem 36:159–227
151. Mingos DM (2014) J Organomet Chem 751:153–173
152. Mingos DM (2015) Coord Chem Rev 293–294:2–18
153. Li J, Rogachev AY (2015) Phys Chem Chem Phys 17:1987–2000
154. Albrecht M, Lutz M, Spek AL, van Koten G (2000) Nature 406:970–973
155. Lin TP, Gabbaï FP (2012) J Am Chem Soc 134:12230–12238
156. Lin TP, Gabbaï FP (2013) Angew Chem Int Ed 52:3864–3868
157. Hill AF (2006) Organometallics 25:4741–4743
158. Parkin G (2006) Organometallics 25:4744–4747
159. Karen P (2015) Angew Chem Int Ed 54:4716–4726
160. Pauling L (1948) J Chem Soc 1461–1467
161. Haaland A (1989) Angew Chem Int Ed Engl 28:992–1007
162. Bouhadir G, Bourissou D (2015) Chem Soc Rev 45:1065–1079

Index